Dissertation

zur Erlangung des Doktorgrades

der Naturwissenschaften

der Fakultät für Biologie

der Ludwig-Maximilians-Universität München

Chloride regulatory mechanisms

and their influence on neuronal excitability

vorgelegt von

Ilka Rinke

München, Oktober 2010

Erstgutachter: Prof. Alexander Borst

Zweitgutachter: PD Dr. Lars Kunz

Tag der mündlichen Prüfung: 14. Dezember 2010

Die vorliegende Arbeit wurde zwischen Juli 2007 und Oktober 2010 am

Max-Planck Institut für Neurobiologie in Martinsried durchgeführt.

Ehrenwörtliche Versicherung:

Ich versichere hiermit ehrenwörtlich, dass ich die Dissertation mit dem Titel „Chloride regulatory mechanisms and their influence on neuronal excitability" selbständig und ohne unerlaubte Beihilfe angefertigt habe. Ich habe mich dabei keiner anderen als der von mir ausdrücklich bezeichneten Hilfen und Quellen bedient.

Erklärung:

Hiermit erkläre ich, dass ich mich nicht anderweitig einer Doktorprüfung ohne Erfolg unterzogen habe. Die Dissertation wurde in ihrer jetzigen oder ähnlichen Form bei keiner anderen Hochschule eingereicht und hat noch keinen sonstigen Prüfungszwecken gedient.

München, Oktober 2010

Ilka Rinke

Meinen Eltern

Maritta und Bernd Rinke

x

CONTENTS

ABBREVIATIONS

ACSF	artificial cerebro spinal fluid
AE3	the anion exchanger three
Ae3$^{-/-}$	the anion exchanger three knockout
AMPA	α-amino-3-hydroxyl-5-methyl-4-isoxazole-propionate
ATP	adenosine-5`-triphosphate
CA	*cornu Ammonis*
$[Ca^{2+}]_i$	intracellular calcium concentration
CBS	cystathionine-b-synthase
CCC	cation-chloride cotransporter
Cl^-	chloride ion
$[Cl^-]_i$	intracellular chloride concentration
CLC	voltage-gated chloride channel family
ClC-2	voltage-gated chloride channel two
Clcn2$^{-/-}$	voltage-gated chloride channel two knockout
DG	dentate gyrus
DGC	dentate gyrus granule cells
DRG	dorsal root ganglion
EC	Entorhinal Cortex
E_x	the reversal potential of a given ionic conductance
EPSC	excitatory postsynaptic current
EPSP	excitatory postsynaptic potential
GABA	γ-aminobutyric acid
GABA$_A$	γ-aminobutyric acid receptor type A
GDP	giant depolarizing potential
GluR	glutamate receptor subunit

IPSC	inhibitory postsynaptic current
IPSP	inhibitory postsynaptic potential
KCC2	the potassium-sodium-chloride cotransporter two
KO	knockout
NBQX	2,3-dihydroxy-6-nitro-7-sulfamoyl-benzo[f]quinoxaline-2,3-dione
NKCC1	the sodium-potassium-chloride cotransporter one
Nkcc1$^{-/-}$	the sodium-potassium-chloride cotransporter one knockout
NMDA	N-methyl-D-aspartic acid
PKA	protein kinase A
PKC	protein kinase C
PP	perforant path
PPR	paired-pulse ratio
PTX	picrotoxin
R_N	neuronal input resistance
SC	Schaffer Collateral
SGK	serine-threonine protein kinase
TTX	tetrodotoxin
V_m	neuronal membrane potential
WT	wildtype

LIST OF FIGURES

3   MANUSCRIPT II

4   MANUSCRIPT III

5   GENERAL DISCUSSION

SUMMARY

The chloride concentration in neurons is in general established by the precise functional expression of the sodium-potassium-chloride cotransporter one (NKCC1) and the potassium-chloride cotransporter two (KCC2). NKCC1 raises the intracellular chloride concentration, while KCC2 extrudes chloride. The intracellular chloride concentration determines the strength and direction of γ-aminobutyric acid (GABA) receptor-mediated transmission. In general, the intracellular chloride concentration in neurons is low and causes GABA-mediated inhibition. However, the intracellular chloride concentration in immature neurons is high leading to GABAergic depolarization, which can cause excitation.

The effects of excitatory GABA signaling in early development is still unclear. It has been speculated that excitatory GABA, causing general depolarization in neurons, has profound effects on neuronal activity and neuronal maturation. Therefore, I studied in collaboration with Carsten Pfeffer the development of the hippocampal network during the early phase of postnatal development under conditions when excitatory GABA action is abolished. Here, sodium-potassium-chloride cotransporter one (NKCC1) knockout mice ($Nkcc1^{-/-}$) were used to reduce the intracellular chloride concentration in immature neurons. Young CA1 pyramidal neurons of $Nkcc1^{-/-}$ mice showed diminished GABAergic depolarization. I found that this reduction was sufficient to cause a delay in the maturation of glutamatergic and GABAergic synapses. This suggests that GABAergic excitation during early postnatal development, increasing the network activity, facilitates the maturation of synaptic networks.

GABAergic depolarization in $Nkcc1^{-/-}$ mice was reduced but not completely abolished; suggesting that additional chloride loading mechanisms might exist. As the anion-exchanger three (AE3) was proposed to contribute to chloride accumulation, AE3 knockout ($Ae3^{-/-}$) mice were also studied. I could not detect any changes in intracellular chloride concentration after loss of AE3 at postnatal day one (P1). However at P5, the disruption of AE3 affected the early network activity pattern, indicating an effect of reduced intracellular chloride concentration. These data showed that NKCC1 establishes high intracellular chloride concentration in neurons providing the basis for GABAergic excitation. The role of AE3 is still not clear; it might contribute to the chloride accumulation in neurons.

In addition to the function of chloride transporters, chloride conductive channels are likely to modulate the intracellular chloride concentration, and therefore could influence neuronal excitability. Especially ClC-2 has been suggested to contribute to chloride extrusion. I investigated

the functional role of the voltage-gated chloride channel ClC-2. As specific blockers for ClC-2 are not available, I used ClC-2 knockout (*Clcn2$^{-/-}$*) mice. It has been proposed that ClC-2 constitutes a pathway for chloride extrusion to maintain the inhibitory action of GABA in mature neurons. My data provide direct evidence that ClC-2 mediates fast chloride extrusion preventing chloride accumulation. Chloride extrusion by ClC-2 seemed to be important especially in adult hippocampal pyramidal neurons where GABA$_A$ receptor activation occurs in high frequency bursts. Interestingly, the chloride-conductance of ClC-2 occurs first in the second postnatal week of developing mice, suggesting that ClC-2 is important in fully developed neurons, but might not be important in immature neurons.

Surprisingly, neurons in *Clcn2$^{-/-}$* mice have a very high membrane resistance compared to WT animals, indicating that ClC-2 is active during the resting membrane potential. This might be a general feature of neurons, as I recorded the chloride conductance of ClC-2 in various neuron types. I showed that the resting conductance of ClC-2 affects resting membrane properties, which determine the neuronal excitability. As a consequence, the loss of ClC-2 increases the excitability of a neuron; however, it does not cause hyperexcitation of the hippocampal network. Even more, the network excitability is reduced in ClC-2 KO mice in comparison to the WT. This reduction is caused by an increased inhibition. I found that ClC-2 expressing interneurons increased their inhibitory action onto pyramidal cells after loss of ClC-2.

Taken together, my data reveal that ClC-2 plays a dual role in adult neurons. First, ClC-2 contributes a fast mechanism to extrude chloride after chloride accumulation. Second, ClC-2 provides the chloride leak conductance under resting conditions. The loss of ClC-2 leads to a higher excitability of the neuron due to a strongly increased membrane resistance. Importantly, hyperexcitability of the neuronal network is circumvented by a parallel enhanced inhibition, which can explain the absence of an epileptic phenotype in mice.

1   GENERAL INTRODUCTION

Neurons communicate through chemical and electrical signals to process information, providing the fundamental basis for perception, learning and behavior. The electrochemical gradients of different ionic conductances across the cellular membrane and the action of various neurotransmitters determine the electrophysiological properties of a neuron. The neuronal membrane is primarily permeable for ions of sodium, potassium, calcium and chloride. Whether these ions pass the membrane depends on the function of transmembrane ion channels. These channels allow the passive diffusion of the electrical charges along the electrochemical gradient and the chemical potential of the given ion. The maintenance of the ionic concentration gradient is necessary to ensure electrical signaling and information processing from one neuron to another.

In contrast to the intracellular concentrations of sodium, potassium and calcium, the intracellular concentration of chloride changes during development determining the neuronal response to the transmitter γ-aminobutyric acid (GABA) or glycine. In early development, chloride is high and leads to GABA-mediated excitation. In adult neurons, the chloride concentration is low and results in GABA-mediated inhibition. Altered chloride homeostasis caused by dysfunction of chloride regulating mechanisms can cause several human inherited diseases, for example myotonia (Koch et al., 1992), cystic fibrosis (Quinton, 1983), Dent`s disease (Lloyd et al., 1996) or epilepsy (Cohen et al., 2002). Therefore, it is important to investigate chloride regulating mechanisms, which are potential targets for pharmacological treatments.

1.1   Regulation of the intracellular chloride concentration

In early postnatal development, chloride is accumulated intracellularly (Fig. 1), ranging between 25-40 mM (e.g., Balakrishnan et al., 2003; Yamada et al., 2004; Sipila et al., 2006; Achilles et al., 2007), such that the chloride reversal potential (E_{Cl}) is positive relative to the resting membrane potential of the neuron. Under these conditions, chloride ions flow outward through GABA- or glycine receptors. Consequently, young neurons depolarize resulting in excitation of these neurons. Conversely, after fully maturation the intracellular chloride concentration is low, approximately 5 mM (e.g., Khirug et al., 2008; Tyzio et al., 2008). Then, E_{Cl} is negative to the resting membrane potential and chloride ions flow inward as a response to GABA or glycine. Under these conditions, the cell hyperpolarizes resulting in inhibition. However, small changes in the

intracellular chloride concentration can shift E_{Cl} in the near of the resting membrane potential with profound consequences for the neuronal response to GABA. An E_{Cl} in the near of the resting membrane potential causes shunting inhibition. This form of inhibition is mediated by the conductance of $GABA_A$ or glycine receptors, which changes the membrane resistance but not the membrane potential, and thereby shunts the incoming excitatory inputs. I will discuss about changes in the intracellular chloride concentration and its effects on GABA signaling further in Chapter 5.
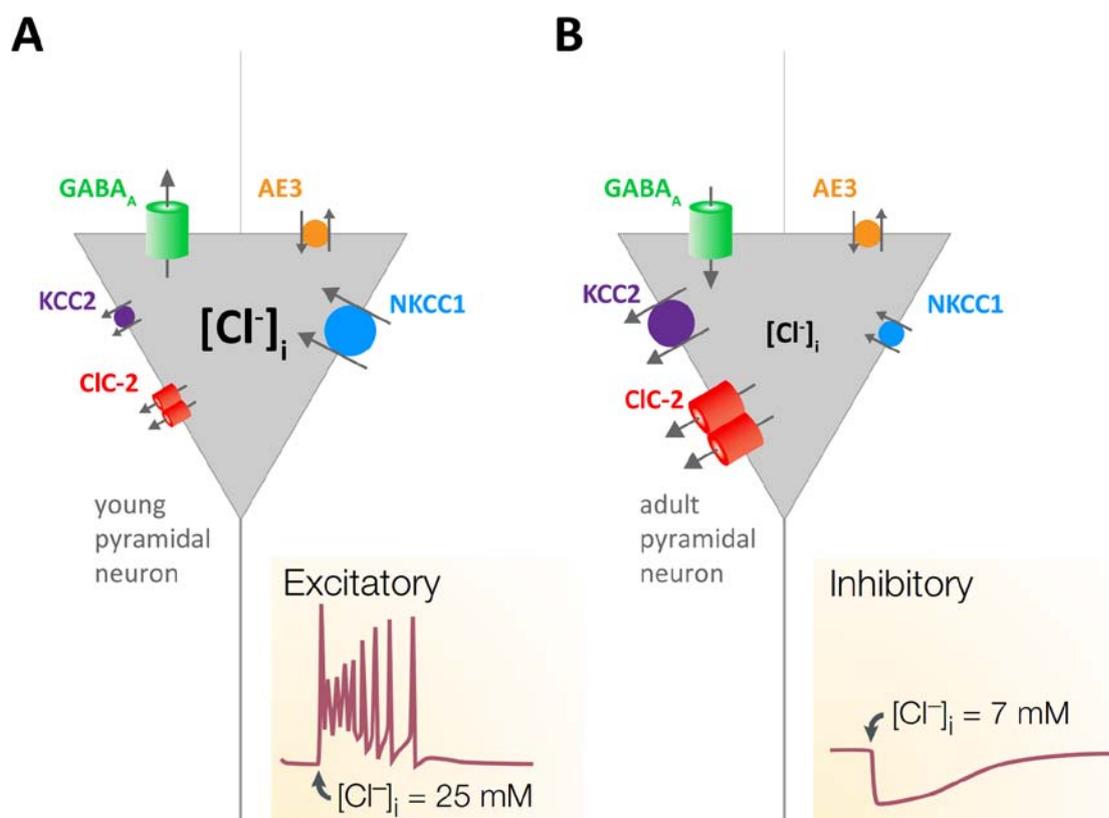
Figure 1: Developmental regulation of intracellular chloride concentration.
A and **B**, The Na-K-Cl cotransporter NKCC1 transports chloride into the neuron, the K-Cl cotransporter KCC2 and the voltage-gated chloride channel ClC-2 mediate chloride extrusion. Additionally, neurons exchange anions, e.g. through the anion exchanger 3 (AE3). **A**, In young neurons, NKCC1 establish a high intracellular chloride concentration $[Cl^-]_i$, which is required for an excitatory response to the transmitter GABA (inset). **B**, Later on, chloride extrusion mechanisms such as through KCC2 and ClC-2 dominate to maintain a low $[Cl^-]_i$ to ensure an inhibitory response to GABA (inset). GABA, γ-amino butyric acid; $GABA_A$, GABA receptor type A. Modified from Ben-Ari, Nature Reviews Neuroscience (2002).

1.1.1   Cation-Chloride cotransporters

The intracellular chloride concentration is established by cation-chloride cotransporters (CCC) and anion exchangers (AE). The CCC family consists of nine members encoded by the genes Slc12a1-9 (for review see Gamba, 2005). The sodium-potassium-chloride cotransporter one (NKCC1) and two (NKCC2) use the sodium gradient to transport chloride and potassium across the plasma membrane. The sodium-chloride cotransporter (NCC) uses the same gradient for the cotransport with chloride. The potassium-chloride cotransporters one to four (KCC1-4) use the potassium gradient with the cotransport of chloride.

The physiological function of CCCs remains to be investigated. CCCs are proposed to determine the intracellular chloride concentration of both neurons and glia. NKCC1 and KCC2 play a pivotal role in establishing intracellular chloride concentration, and hence determine the neuronal response to GABA and glycine. The functional expression of NKCC1 and KCC2 has important implications for neuronal development, sensory perception, neuronal excitability, and the response to neuronal injury.

1.1.1.1   The sodium-potassium-chloride cotransporter 1 (NKCC1)

NKCC1 was cloned from a shark`s rectal gland (Xu et al., 1994) and from a renal tubular cell line (Delpire et al., 1994). NKCC1 loads the cell with chloride, internalizing one sodium, one potassium, and two chloride in electroneutral coupled fashion (Payne et al., 2003). The binding and release of ions from the cotransporter occurs in a strictly ordered sequence: sodium binds first from outside the cell followed by one chloride, then potassium and finally the second chloride ion (Lytle et al., 1998). NKCC1 does not need adenosine-5`-triphosphate (ATP) to operate but uses the electrochemical gradient for sodium and potassium produced by sodium-potassium-ATPase. The developmental expression pattern of NKCC1 in CNS neurons is hard to assess. Several studies report that neuronal NKCC1 expression decreases during postnatal development (Hubner et al., 2001b; Yamada et al., 2004), in contrast to these findings others observed a developmental increase of expression NKCC1 messenger ribonucleic acid (mRNA) and protein (Clayton et al., 1998a; Mikawa et al., 2002).

Functionally, NKCC1 plays an important role in both young and mature central neurons (for review, see Russell, 2000; Hubner et al., 2001b; Khirug et al., 2008). High expression of NKCC1 in immature neurons plays a pivotal role in maintaining high intracellular chloride concentration

(e.g., Rohrbough and Spitzer, 1996; Fukuda et al., 1998b; Wang et al., 2002; Payne et al., 2003; Yamada et al., 2004; Dzhala et al., 2005). For example, NKCC1 is the main chloride-uptake mechanism responsible for GABA-mediated depolarizing currents mediated by postsynaptic and extrasynaptic receptors in developing hippocampal and neocortical neurons (Achilles et al., 2007; Sipilä et al., 2006; Yamada et al., 2004).

1.1.1.2 The potassium-chloride cotransporter 2 (KCC2)

KCCs extrude chloride from neurons using the electrochemical gradient for potassium established by the primary active sodium-potassium-ATPase. KCC2 was first identified in the brain with specific localization in neurons (Payne et al., 1996). KCC2 is expressed in mature neurons and its late expression underlies the developmental changes in chloride extrusion (Rivera et al., 1999; Hubner et al., 2001b; Wang et al., 2002; Stein et al., 2004a; Yamada et al., 2004). A functional inactive form of KCC2 is expressed in immature neurons in the auditory brain stem (Balakrishnan et al., 2003) and primary cortical cultures (Khirug et al., 2005). Therefore, the expression pattern throughout development does not necessarily imply functional activity. Interestingly, a previous study by Li and coworkers (2007) demonstrated a morphogenic role of KCC2 in dendritic spine formation (Li et al., 2007), independent of the well-established contribution of KCC2 in lowering the intracellular chloride concentration (Payne et al., 1996; Rivera et al., 1999; Hubner et al., 2001b; Payne et al., 2003).

Altered intracellular chloride homeostasis resulting from dysfunction of NKCC1 and/or KCC2 can cause hypoexcitability or hyperexcitability of neurons. The accompanied change in the reversal potential for GABA (E_{GABA}) results in the pathogenesis of ischemic seizures, neonatal seizures, temporal lobe epilepsy, and intractability in epilepsy associated with mesial temporal sclerosis, neuropathic pain or developmental malfunctions. Hence, CCCs are potential targets for drugs in various neurological disorders that are characterized by impaired cellular chloride homeostasis (Kahle et al., 2008).

1.1.2   Chloride channels

Chloride channels are involved in cell volume regulation, transepithelia transport and the regulation of electrical excitability of nerve and muscles (for review, see Jentsch et al., 2002). Four chloride channel families have been established: 1) Ligand-gated anion channels are plasma membrane channels, which are activated by GABA and glycine (for review, see Ben-Ari et al., 2007). 2) Cystic fibrosis transmembrane conductance regulator (CFTR) (Kerem et al., 1989) requires the activity of cAMP-dependent protein kinase A (PKA), protein kinase C (PKC), and a high ATP/ADP ratio to achieve maximal activity (Anderson et al., 1991; Jia et al., 1997; for review, see Gadsby and Nairn, 1999; Seibert et al., 1999; Yamazaki et al., 1999). 3) Voltage-gated chloride channels are activated by transmembrane voltage (for review, see Jentsch et al., 2002). 4) Calcium-activated chloride channels include Bestrophins (Sun et al., 2002; for review, see Hartzell et al., 2008) and TMEM16/anoctamins (Galindo and Vacquier, 2005; Caputo et al., 2008; Schroeder et al., 2008; Yang et al., 2008).

Chloride channels mediate passive chloride transport along the chloride concentration gradient capable to modulate chloride homeostasis and neuronal excitability. In contrast to the well characterized $GABA_A$ and glycine receptors, the function of voltage-gated chloride channels is not entirely clear. In kidney and muscles the function of voltage-gated chloride channels is fully understood; however, in neurons their role is still primarily elusive and remains to be investigated.

1.1.2.1   Voltage-gated chloride channels

Voltage-gated chloride channels of the CLC family are proposed to contribute to cellular chloride signaling. For example, several studies (Staley, 1994; Staley et al., 1996; Ben-Ari, 2002) suggested that the voltage-gated chloride channel ClC-2 expressed in neurons constitutes part chloride extrusion. A chloride conductance with similar properties of ClC-2 is activated at membrane potentials more negative to E_{Cl}, so that chloride ions only flow outward through ClC-2 (Staley et al., 1994).

The CLC chloride channel family was initially described after cloning of the voltage-gated chloride channel ClC-0 from the electric organ of the marine electric ray *Torpedo marmorata* (Jentsch, 1990). The CLC gene family is highly conserved and their members are present in pro- and eukaryotes. In mammals, nine different CLC subtypes were identified (Fig. 2), which differ

according to tissue distribution and subcellular location. Only four of the nine mammalian CLC chloride channels are real channels (ClC-1, -2, -Ka, and -Kb). All intracellular CLCs might be Cl^-/H^+ exchangers as shown for endosomal ClC-4 and ClC-5 (Accardi and Miller, 2004; Picollo and Pusch, 2005; Scheel et al., 2005). Some CLCs such as ClC-2, ClC-6 and ClC-7 are ubiquitously expressed (Thiemann et al., 1992); others, like both ClC-K subtypes, ClC-3, ClC-4 and ClC-5 are often found in kidney, and ClC-1 is exclusively expressed in skeletal muscles (Steinmeyer et al., 1991a).

	expression	function	mouse model
ClC-1	skeletal muscle	stabilizing V_m	myotonia congenita
ClC-2	broad	transepithelia transport intra-/extracellular ion homeostasis ?	degeneration retina/testes leukodystrophy
ClC-Ka	kidney, ear	transepithelia transport	diabetes
ClC-Kb			
ClC-3	broad (brain, kidney, liver...)	acidification of synaptic vesicles, endosomes	degenration retina/ hippocampus
ClC-4	broad (brain, kidney, muscle...)	?	
ClC-5	kidney	acidification of endosomes	defect in renal endocytosis, proteinuria, hyperphosphaturia
ClC-6	neurvous system	acidification of late endosomes ?	NCL
ClC-7	broad	acidification of osteoclast resorption lacuna, regulation of lysosomal Cl, pH?	osteopetrosis, retinal degenration, NCL

Figure 2: The mammalian CLC supergene family of chloride channels.

Overview about the expression and physiological functions of the CLC subtypes as well as human and mouse pathologies after disruption of the genes encoding for respective ClC subtypes. V_m, membrane potential; Cl, chloride; NCL, neuronal ceroid lipofuscinosis. Modified from Jentsch, Crit Rev Biochem Mol Biol (2008).

Gating

CLCs function as homodimers (Lorenz et al., 1996; Weinreich and Jentsch, 2001; Scholl et al., 2006), with each monomer acting independently as single protopore conductance (Fig. 3 A). The gating process to open each of this protopores independently is fast and distinct from the slow common gating process to open and close the pores simultaneously (Miller and White, 1980). The CLC channel gating can be modulated by intracellular (Lobet and Dutzler, 2006) and extracel-

lular chloride (Pusch et al., 1999; Niemeyer et al., 2003) and pH (Yusef et al., 2006; Pusch and Zifarelli, 2009; Zifarelli and Pusch, 2009, 2010). Chloride dependent gating has been observed for ClC-1 and ClC-2 (Rychkov et al., 1998; Pusch et al., 1999; Niemeyer et al., 2003). The voltage-dependent gating of CLC channels and the exchange coupling of protons to chloride depends on a glutamate side chain, which apparently blocks the access of extracellular anions to their binding site (Dutzler et al., 2003; Accardi and Miller, 2004).
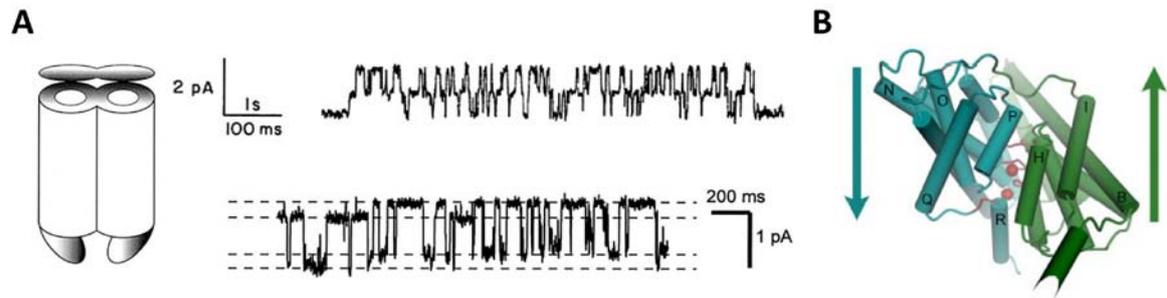
Figure 3: Gating and structure of CLC proteins.

A, Double barrel structure and gating of CLC channels. *Left*: A simple model of a CLC channel. The dimer has two largely independent pores, which can be gated individually and closed by a common gate. *Right*: Single-channel recording of the native ClC-0 (*above*) and a ClC-0/ClC-2 concatemer (*below*). These recordings support the double barrel model. **B**, Dimeric structure of a ClC subunit derived from crystal structure of the bacterial homologue EcClC. One CLC subunit consists of two similar halves (green and blue), which are orientated in opposite direction. Each subunit exhibit in total 18 α-helices (green and blue), 17 cross the plasma membrane either in full length or partly, one is located outside the plasma membrane. The anion selective regions are indicated by the red balls. Adapted from Dutzler et al., Nature (2002).

Crystal structure

The crystal structure of bacterial CLCs revealed 17 transmembrane helices and several anion binding sites (Fig. 3 B) (Dutzler et al., 2002). All eukaryotic and some prokaryotic CLC proteins have large cytoplasmic C-termini that contain two CBS domains (Bateman, 1997; Ponting, 1997). These domains are named after cystathionine-b-synthase, an enzyme with a similar domain. CBS domains are proposed to be important for the regulation of transport activity (Estevez et al., 2004) and intracellular targeting (Schwappach et al., 1998). Moreover, the N-terminus for example of the chloride channel ClC-2 determine the open probability of the channel (Grunder et al., 1992).

The voltage-gated chloride channel 2 (ClC-2)

The voltage-gated chloride channel ClC-2 was found in neurons, epithelia and heart (Thiemann et al., 1992). In the CNS, ClC-2 is highly expressed in pyramidal cells of hippocampus and cortex, in purkinje cells of cerebellum (Smith et al., 1995; Clayton et al., 1998b) as well as in glia (Sik et al., 2000). Trafficking and targeting of the ClC-2 protein to the cell surface is mediated by interaction of the CBS domains with several proteins; e.g. nucleotides like ATP *in vitro* (Scott *et al.*, 2004). This suggests that CBS domains of ClC-2 may act as energy sensors. Indeed, the kinetics of ClC-2 gating may be slightly changed by intracellular ATP (Niemeyer *et al.*, 2004). The trafficking of ClC-2 is additionally controlled by interaction with protein phosphatase-1 (Furukawa et al., 2002), retrograde dynein (Dhani et al., 2003) and chaperon Hsp90 (Hinzpeter et al., 2006).

Functionally, ClC-2 mediates an inward rectifying chloride conductance with a single channel conductance of about 3 pS (Weinreich and Jentsch, 2001). This channel opens slowly upon hyperpolarization, mild extracellular acidification and osmotic cell swelling (Grunder et al., 1992; Thiemann et al., 1992; Jordt and Jentsch, 1997; Zuniga et al., 2004). ClC-2 channel gating requires the N-terminal cytoplasmic region (Grunder et al., 1992; Jordt and Jentsch, 1997; Zuniga et al., 2004). The deletion of the N-terminus leads to constitutively open channels with an ohmic behavior. ClC-2 gating is also influenced by the intracellular chloride concentration. When raised, the ClC-2 voltage-dependence shifts to more positive potentials, resulting in an opening of the channel (Pusch et al., 1999; Niemeyer et al., 2003). Beyond that, ClC-2 gating is modulated by cholesterol (Hinzpeter et al., 2007) and by the redox status of the cell (Huber et al., 2004).

Several studies proposed that protein kinases can regulate ClC-2 channel activity (Madison et al., 1986; Fritsch and Edelman, 1996; Furukawa et al., 2002; Palmada et al., 2004). For example, activation of PKC by phorbol esters caused an almost total abolition of a chloride conductance as described for ClC-2 in hippocampal pyramidal cells (Madison et al., 1986). However, this could not be observed in heterologous expression systems. ClC-2 activity expressed in *Xenopus* oocytes could be inhibited by injection of cell-cycle dependent protein kinases (Furukawa et al., 2002). Coexpression of SGK1-3 and the related kinase PKB with ClC-2 in *Xenopus* oocytes increased the channel function (Palmada et al., 2004).

In heterologous expression systems, ClC-2 has been shown to be activated by cell swelling (Grunder et al., 1992; Furukawa et al., 1998), and therefore might play a role in cell volume regulation (Furukawa et al., 1998).

ClC-2 is activated upon hyperpolarization and depends on intracellular chloride concentration (Pusch et al., 1999; Niemeyer et al., 2003). Therefore, ClC-2 was also proposed to modulate the intracellular chloride concentration by providing a chloride extrusion pathway in neurons (Staley *et al.*, 1996).

ClC-2 has also been implicated in the regulation of extracellular ion concentration. For example in mice, disruption of ClC-2 leads to degeneration of germ cells and photoreceptors (Bosl et al., 2001; Nehrke et al., 2002). This effect is possibly attributed to impaired chloride transport across supporting epithelia. Moreover, ClC-2 knockout mice ($Clcn2^{-/-}$) exhibit vacuolation of the white matter of the brain, manifested as leukoencephalopathy (Blanz et al., 2007). This finding suggests that ClC-2 may contribute to potassium siphoning from the extracellular space. Thereby, potassium is removed from the small clefts between neurons and astrocytes and is equilibrated finally with the blood. Interestingly, ClC-2 was detected in astrocytic endfeet that contact the endothelium of brain capillaries (Sik *et al.*, 2000; Blanz *et al.*, 2007), indicating that ClC-2 regulates the exchange of potassium and is needed to neutralize the electrical currents that are associated with potassium uptake or release by glial cells.

The chloride conductance of ClC-2 is active at resting membrane potential (Madison et al., 1986; Staley et al., 1996). Therefore, ClC-2 might constitute a leak conductance, which could affect the membrane resistance, and hence could influence the excitability of neurons. If so, the loss of ClC-2 would increase the excitability, which can cause diseases like epilepsy. However, $Clcn2^{-/-}$ mice displayed no lower susceptibility for seizures when challenged by different proconvulsive agents and did not cause epilepsy (Bosl et al., 2001; Blanz et al., 2007). The data presented in this thesis provide a plausible explanation why the disruption of ClC-2 does not lead to hyperexcitability of neuronal networks.

Disruption of CLCs and associated pathophysiology

In mammals, CLC proteins mediate chloride flux across cellular membranes in most cell types and participate in maintenance of resting membrane potential. Plasma membrane chloride channels play an important role in damping muscle excitability (Steinmeyer et al., 1991a). ClC-1 contributes to membrane repolarization and stabilizes the membrane voltage in skeletal muscle. Experimental block of the chloride conductance mediated by ClC-1 facilitated muscle hyperexcitability, manifested as myotonia (Steinmeyer et al., 1991b). Moreover, plasma membrane expressed CLCs mediate transepithelial transport (Simon et al., 1997; Birkenhager et al., 2001; Bosl et al., 2001; Estevez et al., 2001; Blanz et al., 2007). As previously mentioned, the loss of ClC-2 in mice causes the degeneration of testes and photoreceptors of the retina due to the impairment

of the ion transport across associated epithelia (Bosl et al., 2001). In addition, vacuolation of the white matter of the brain in *Clcn2^{-/-}* mice might be secondary caused by changes in extracellular ion concentration (Blanz et al., 2007). In addition, ClC-K channels are essential for the transepithelia transport of chloride in kidney (Adachi et al., 1994) as well as for potassium secretion into scala media of the inner ear (Estevez et al., 2001).

Other CLC proteins localize mainly to the endosomal-lysosomal system where they may facilitate luminal acidification or regulate luminal chloride concentration (Li et al., 2002; Zhao et al., 2007). ClC-3 and ClC-5 for example affect the luminal acidification of vesicles by neutralizing proton pump currents (Gunther et al., 1998; Stobrawa et al., 2001). ClC-5 expression is restricted to kidney; human mutation in gene encoding ClC-5 were associated with Dent`s disease and kidney stones (Fisher et al., 1994; Wrong et al., 1994). Disruption of ClC-6 in mice as well as in humans can cause neuronal ceroid lipofuscinosis (NCL) (Poet et al., 2006). Human heterozygote mutations in *CLCN7* gene entail osteopetrosis (Kornak et al., 2001). In addition, ClC-7 KO mice also display a typical biochemical and morphological features of NCL, a subtype of lysosomal storage disease (Kasper et al., 2005).

1.1.2.2 Ligand-gated chloride channels

Ligand-gated chloride channels contribute to chloride signaling in neurons. The transmitter GABA binds to its receptors and opens intrinsic anion channels. This leads to passive diffusion of anions, depending on their electrochemical gradient. In adult neurons, the net anion flux is inward, so that negative charges accumulate intracellularly. This results in a hyperpolarization of the neuron, a principle mechanism of synaptic inhibition. In contrast, in early development, the net anion flux is outward, so that GABAergic transmission is mostly excitatory. Excitatory GABA action might be critical for the development of the brain (for review see Ben-Ari, 2002; Owens and Kriegstein, 2002).

Fast GABAergic transmission is mediated by ionotropic $GABA_A$ receptors and $GABA_C$ receptors. $GABA_A$ receptors constitute a heteropentamer, permeable primarily to chloride and to a lesser extent to bicarbonate (Bormann et al., 1987). In mammals, 18 $GABA_A$ receptor subunits (α_{1-6}, β_{1-3}, γ_{1-3}, δ, ϵ_{1-3}, θ, π) have been identified so far (Jacob et al., 2008). This reflects the large diversity of subunit assembly to a functional channel, which is further increased by alternative splicing. The subunit composition defines the physiological and pharmacological properties of the receptor, its expression throughout the brain and its subcellular targeting. The most abundantly expressed $GABA_A$ receptor complex contains two α-, two β- and one γ-subunit (McKernan

and Whiting, 1996). However, the expression of other possible receptor complex and their sub-cellular distribution remains to be investigated.

GABA$_A$ receptors are also permeable for bicarbonate, which functions as a significant carrier of depolarizing current across GABA$_A$ receptors (Kaila and Voipio, 1987). Hence, the reversal potential of GABA$_A$ receptor-mediated responses differs from E_{Cl} to more positive values (Kaila and Voipio, 1987).

1.2 GABAergic transmission

Usually, the intracellular chloride concentration is low. Hence, GABA mediates inhibitory synaptic transmission by extrusion of chloride through GABA$_A$ receptors. Inhibition is not necessarily a result of hyperpolarization. The reduction of excitation without affecting the membrane potential reflects also an inhibitory effect, referred to "shunting" inhibition. Shunting inhibition relies on an increased conductance through activated GABA$_A$ receptors. When E_{GABA} is in the near or slightly above the resting membrane potential (Alger and Nicoll, 1979; Andersen et al., 1980; Gulledge and Stuart, 2003) the activation of GABA$_A$ receptors reduces the depolarizing effects of concurrently activated excitatory currents in the dendrite by decreasing the membrane resistance and dendritic space constant (Barrett and Grill 1974; Koch et al. 1983; Qian and Sejnowski 1990; Rall 1964).

1.2.1 GABA$_B$ receptor-mediated inhibitory synaptic transmission

Beside the inhibitory synaptic transmission through GABA$_A$ channels, GABA can also activate metabotropic GABA$_B$ receptors. GABA$_B$ receptors functions through G_i and G_0 coupled proteins (Misgeld et al., 1995; Bettler et al., 2004). Functional GABA$_B$ receptors contain two different subunits (B1 and B2), the only two subunits, which have been identified so far (Bowery and Brown, 1997; Kaupmann et al., 1997; Pfaff et al., 1999; Schwarz et al., 2000). They exert late inhibitory action on both presynaptic and postsynaptic neuronal membrane through different mechanisms. On the presynaptic site, GABA$_B$ receptors inhibit voltage-gated calcium channels, decreasing neurotransmitter release (Scholz and Miller, 1991; Mintz and Bean, 1993; Poncer et al., 1997). On the postsynaptic site, GABA$_B$ receptor-mediated signaling activates potassium channels, which generally hyperpolarize the membrane towards the equilibrium potential of potassium ions (below −70 mV) (Dutar and Nicoll, 1988; Luscher et al., 1997). These potassium

potentials typically produce less change in membrane conductance than GABA$_A$ potentials, but are strongly inhibitory because they keep the membrane potential further from the spike threshold (McCormick, 1989). Activation of GABA$_B$ receptors can also modulate cAMP production and in turn the action of ion channels and proteins, which are targets of cAMP (Simonds, 1999).

1.2.2   GABAergic signaling during early neuronal development

In the developing brain, the intracellular chloride concentration is high, due to high activity of NKCC1. Hence, GABA acts excitatory, which leads to an increase of the intracellular calcium concentration $[Ca^{2+}]_i$ by activation of voltage-gated calcium channels (e.g. Yuste and Katz, 1991; Leinekugel et al., 1995; Fukuda et al., 1998b; Eilers et al., 2001). The depolarization is sufficient to remove the voltage dependent magnesium block from NMDA receptors (Leinekugel et al., 1997), the primary source for glutamatergic excitatory postsynaptic currents in immature neurons, which sustain the increase of $[Ca^{2+}]_i$. Moreover, as GABA acts excitatory, so called spontaneous giant depolarizing potentials (GDPs) occur (Ben-Ari et al., 1989). GDPs are slow network oscillations, which are present in all brain structures (Garaschuk et al., 2000). In the hippocampus, GDPs are observed in the vast majority of neurons, including CA3 and CA1 pyramidal cells, granule cells and interneurons (Leinekugel et al., 1995; Khazipov et al., 1997a; Leinekugel et al., 1997; Leinekugel et al., 1998; Lamsa et al., 2000; Leinekugel et al., 2002). GDPs occur during the first postnatal week in mouse hippocampus and they disappear when GABA shifts from acting excitatory to inhibitory later in development (Ben-Ari et al., 1989). Driven by GABAergic depolarization and glutamate, GDPs together with the activation of NMDAR allow the generation of large calcium oscillations. As a consequence, the raise in $[Ca^{2+}]_i$ triggers calcium-dependent second-messenger pathways, which provide the signaling to influence many processes of brain development like neuronal migration and growth, synaptogenesis, synapses maturation and modification of synaptic connections (for review, see Owens and Kriegstein, 2002).

1.3   Hippocampus

The term hippocampus was derived from the Greek word for sea horse and was initially formed by the anatomist Aranzius (1587). Later, de Garengeot coined this structure *cornu Ammonis* (Latin "horn of the Ram"). Until today, de Garengeot's nomenclature survives in the proper subdivision of the hippocampus: CA1, CA2 and CA3. The hippocampus belongs to the limbic system and is typically called hippocampal formation including the dentate gyrus, the hippocampus, the subiculum, and the entorhinal cortex (Fig. 4).
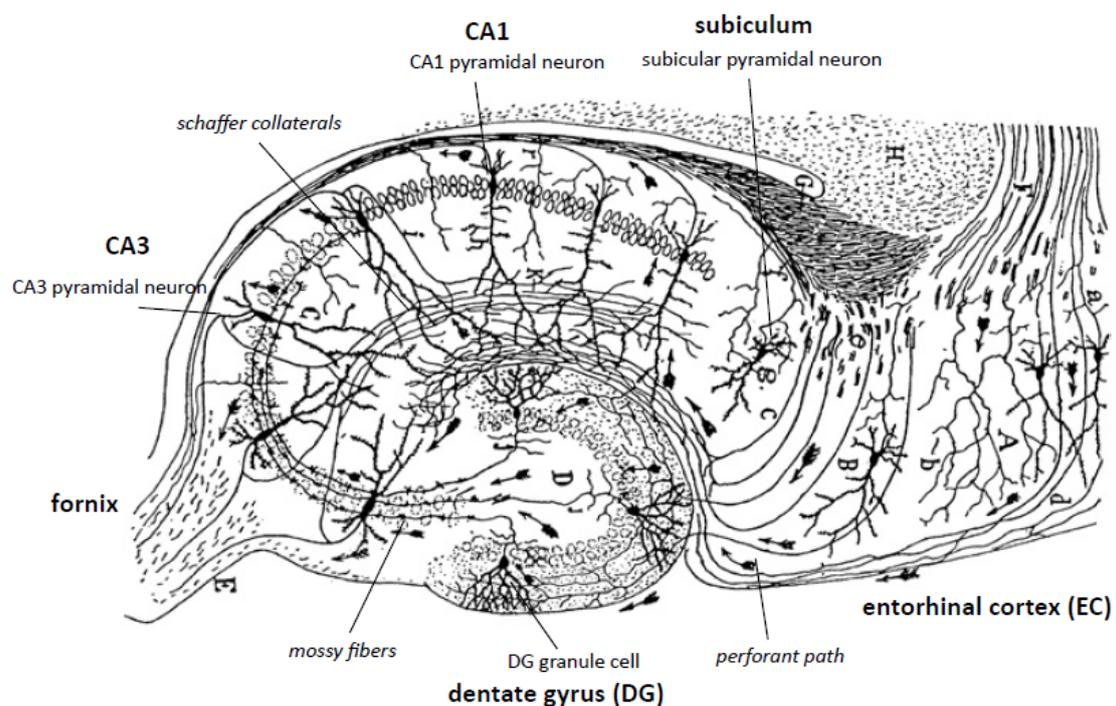
Figure 4: Neuronal organization and synaptic pathways of the hippocampal formation.
From the entorhinal cortex (EC), the lateral perforant path projects to granule cells of the dentate gyrus (DG), which send mossy fiber projections onto CA3 pyramidal neurons that in turn innervate through Schaffer collaterals CA1 pyramidal neurons. CA1 pyramidal neurons project to the subiculum and back to the EC. The drawing of a transversal slice of rodent hippocampus is adapted from Ramón y Cajal, 1911.

The entorhinal cortex (EC) is the main relay station of the hippocampus, getting input from the hippocampus und providing the output to many other parts of the brain. Incoming informations propagates from the EC via the perforant path to granule cells of the dentate gyrus (DG).

The granule cells project mossy fibers onto CA3 pyramidal cells, whose Schaffer collateral axons form synapses with CA1 pyramidal neurons of the ipsi- and contralateral hemisphere. Finally, the information propagates to the subiculum and back to the EC. Each of these layers also contains complex intrinsic circuitry and extensive longitudinal connections.

The hippocampus is important for learning and memory as well as spatial navigation. The fundamental role of the hippocampus in long-term memory was revealed by a prominent study of Henry Gustav Molaison (known as patient H.M.) (Scoville and Milner, 1957). The patient suffered from severe epilepsy and underwent surgical destruction of the hippocampus to treat epilepsy; thereby, he lost the ability for storing informations over a long time.

The hippocampus has been studied extensively as part of the brain system responsible for spatial memory and navigation. The spatial navigation theory was originally established by the discovery of neurons in the rat hippocampus that activity related to the rat's location within its environment, whereupon these cells were called "place cells" (O'Keefe and Dostrovsky, 1971).

1.3.1   Hippocampal pathology

Hippocampal pathology is associated with several neurophysiological and -psychological disorders. For example, hippocampal atrophy and changes in synaptic organization and connectivity has been observed in Schizophrenia (Harrison, 2004). As the hippocampus exhibit a central role in memory storage, hippocampal deterioration can cause age-related declines in memory and disorientation, both first symptoms of Alzheimer`s disease. People with extensive hippocampal damage may experience amnesia - the inability to form or retain new memories. The hippocampus is also region prone to epileptic seizures. In comparison to other brain regions epileptic seizures in the hippocampus were elicited in response to smaller stimulus intensities. Moreover, loss of neurons in several hippocampal fields reflects a hallmark feature of the neuropathology of temporal lobe epilepsy. Impairments of chloride regulating mechanisms and hence changes in GABAergic transmission are implicated in seizures (e.g. Cossart et al., 2001; Cohen et al., 2002; Huberfeld et al., 2007; Munoz et al., 2007; Fritschy, 2008).

1.3.2   Pyramidal cells

In mammalian brain, pyramidal neurons are found in the cerebral cortex, the hippocampus and the amygdala. The name derived from the triangular shape of their soma. Pyramidal neurons contain a single axon that projects into the alveus. CA1 pyramidal cell axons extensively branch

and send collaterals to various targets within and outside the hippocampus. Within the hippocampus, they do not establish local connections, but project to subicular neurons.

The dendritic trees of the pyramidal cell descend from the basis (basal dendrite) and the apex (apical dendrites) of the soma. The single apical dendrite bifurcates in a tuft further away from the soma. In comparison to the apical dendrite the basal dendritic tree is much shorter, consists of three to five primary dendrites, which extensively branch close to the soma.

CA1 pyramidal cell dendrites contain thousands of spines that constitute the postsynaptic target zone for most glutamatergic synapses. The density of dendritic spines is highest in stratum radiatum and oriens and lower in stratum lacunosum-moleculare. Dendritic spines are absent on the soma and proximal dendrite. In total, pyramidal cells receive between 1,000 to 30,000 synaptic inputs through their dendrites (Klausberger and Somogyi, 2008). Excitatory synaptic inputs of multiple sources target exclusively the pyramidal cell dendrites, inhibitory inputs through GABAergic interneurons target dendrites, axon and soma.

1.3.3 Interneurons

GABA producing neurons are distributed throughout the whole brain of mouse, rat, cat, monkey and human. In cortical areas GABAergic neurons are interneurons, which represent a class of local neurons of large diversity.

The heterogeneity in morphology and connectivity of local circuit neurons reflects the huge complexity of possible interaction and in turn activity patterns within cortical areas. Interneurons form intricate circuits with principal cells and play a pivotal role in network oscillations shaping the activity of the CNS and memory-related plasticity in the hippocampal formation. They provide the main inhibitory source for principal cells and temporally modulate target cell excitability.

Hippocampal interneuron subtypes show large diversity. They are distinct by their laminar distribution within region of CA1, afferent and efferent connections, by their innervations of different subcellular domains of pyramidal cells and their expression of specific biochemical markers (Fig. 5) (Klausberger and Somogyi, 2008).

Based on morphology, specific interneuron types are distinguished by the dendritic and axonal processes, such as basket cell, horizontal cells or stellate cells. Moreover, the somato-dendritic location and target domains of their axonal projections can often predict interneuron subtype-specific contributions to the active network. Stratum oriens–lacunosum molecular cells (O–LM cells) project their axons to pyramidal cell distal dendrites of the stratum lacunosum-

moleculare. A basket cell soma, located within stratum oriens, projects its axon to the pyramidal neuron soma and the proximal dendrites. A bistratified cell sends its axon to both basal and apical dendrites in stratum oriens and radiatum. Axo-axonic interneurons innervate exclusively the axon initial segment of the target neuron. Interneurons that innervate pyramidal neuron somata regulate the local generation of sodium dependent action potentials, by contrast, interneurons that innervate the dendritic part influence voltage-gated currents, shunt excitatory inputs and regulate calcium dependent action potentials (McBain and Fisahn, 2001).
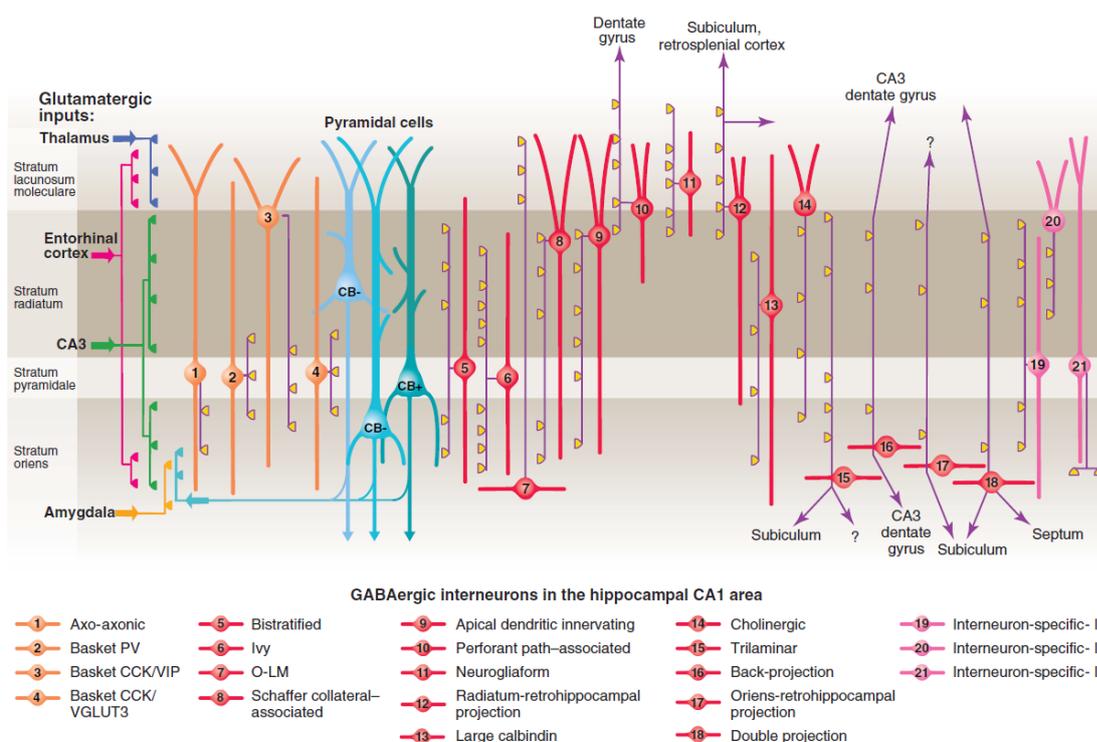
Figure 5: Interneuron diversity in the CA1 region of the hippocampus.

Klausberger and Somogyi classified 21 interneuron subtypes according to somatodendritic and axonal location, afferent and efferent connections and expression of neurochemical markers. Interneurons, which innervate the axons and somata of pyramidal neurons (blue) are depicted in orange, interneurons mainly innervate other interneurons are pink. Interneuron axons are purple with their main synaptic terminations in yellow. CB, calbindin; CCK, cholecystokinin; O-LM, oriens lacunosum molecular; PV, parvalbumin; VIP, vasoactive intestinal peptide; VGLUT3, vesicular glutamate transporter 3. Adapted from Klausberger and Somogyi, Science (2008).

Unique among all interneuron subclasses is the expression of GABA and the GABA-synthesizing enzymes GAD65 or GAD67. But, interneurons differ in the expression of additional neurochemical markers, such as calcium-binding proteins (parvalbumin, calretinin, and calbindin), or neuromodulators such as reelin, somatostatin, neuropeptide Y, nitric oxide synthase, and vasoactive intestinal peptide.

In contrast to the uniform principal cells in any of the hippocampal subfields, the afferent and efferent connectivity of interneurons shows great variation (Ramon y Cajal, 1893, 1911; Lorente de Nó, 1934). Within the hippocampal circuitry, interneurons receive excitatory input from several intrinsic and extrinsic sources (Lacaille et al., 1987; Freund and Buzsaki, 1996). Parvalbumin and calretinin interneurons are activated both in a feedforward manner by Schaffer collaterals and by entorhinal fibers and thalamic afferents from the nucleus reunions, as well as in a feedback manner by local CA1 recurrent collaterals. Calbindin cells are activated primarily in a feedforward manner receiving input from Schaffer collateral afferents in stratum radiatum.

Different classes of interneurons vary also in their firing properties and hence, in the time point of releasing GABA to distinct subcellular domains of their target cell. Therefore, the spatiotemporal interaction between pyramidal cells and different interneuron subtypes determine synchronous network oscillation pattern such as theta- and gamma oscillations as well as sharp-wave ripples, which play an important role in several behavioral states, cognitive processes and during sleep.

1.4   Aims of the thesis

NKCC1 establishes high intracellular chloride providing the basis for GABAergic excitation. The effect of excitatory GABA signaling in immature neurons is not entirely clear. Several studies speculated that GABAergic excitation is important for neuronal activity and maturation of synaptic networks in early development. In a collaborating project of Carsten Pfeffer, I studied the functional consequences of impaired GABAergic excitation in early development of mice hippocampus (Pfeffer et al., 2009). Therefore, NKCC1 knockout (*Nkcc1$^{-/-}$*) and AE3 knockout (*Ae3$^{-/-}$*) mice were used to reduce the intracellular chloride concentration, which consequently should result in a reduction of GABAergic excitation. I recorded from AE3 deficient mice to determine the equilibrium potential of chloride. Moreover, I investigated the effect of reduced GABAergic excitation on the maturation of GABAergic synapses after loss of NKCC1. Therefore, I measured miniature inhibitory postsynaptic currents (mIPSCs) of young CA1 pyramidal neurons.

Beside chloride transporters, chloride channels are likely to regulate the intracellular chloride concentration. Here, I wanted to investigate the functional role of the voltage-gated chloride channel ClC-2 (Rinke et al., 2010). As there are no specific blockers for ClC-2 available, I used ClC-2 knockout (*Clcn2$^{-/-}$*) mice. It was proposed that ClC-2 lowers the cytoplasmic chloride concentration of mature neurons after chloride accumulation, which occurs after intense GABA$_A$ receptor activation (Staley, 1994; Staley et al., 1996; Ben-Ari, 2002). I tested this hypothesis in CA1 pyramidal cells of mice.

The chloride conductance of ClC-2 activates upon hyperpolarization. It does not display any time-dependent inactivation and will be still open during subsequently brief depolarization as it closes very slowly. Hence, it was proposed that ClC-2 is open at the resting membrane potential, and thereby constituting part to the leak conductance in neurons. Leak conductances determine resting membrane properties. Therefore, I wanted to analyze the resting membrane properties such as the resting membrane potential and the membrane resistance in neurons lacking ClC-2 with current-clamp recordings.

If the conductance of ClC-2 affects resting membrane properties, ClC-2 should have an influence on the neuronal excitability. Changes in the excitability of a single neuron should also lead to changes in the excitability of the entire network. By the use of various experimental paradigms, I wanted to investigate the excitability of single neurons and of the hippocampal network.

2 MANUSCRIPT I

NKCC1-Dependent GABAergic Excitation Drives Synaptic Network Maturation during Early Hippocampal Development

[1]Max Delbrück Centrum für Molekulare Medizin (MDC) and Leibniz Institut für Molekulare Pharmakologie (FMP), D-13125 Berlin, Germany, [2]Zentrum für Molekulare Neurobiologie Hamburg (ZMNH), Universität Hamburg, D-20251 Hamburg, Germany, [3]Max Planck Institut für Neurobiologie, D-82152 Martinsried, Germany, and [4]Klinik für Hals-, Nasen- und Ohrenheilkunde, [5]Institut für Humangenetik, [6]Institut für Anatomie, Universitätsklinikum Hamburg-Eppendorf, D-22529 Hamburg, Germany, and [7]Institut für Klinische Chemie, Friedrich Schiller Universität Jena, D-07747 Jena, Germany

Gramicidin-perforated-patch clamp recordings were performed by Damien Keating. Carsten Pfeffer performed and analyzed the calcium-imaging experiments, the recordings of giant depolarizing potentials as well as Western blots. York Rudhard and Gabriele Rune performed immunocytochemical stainings. Ilka Rinke performed electrophysiological recordings with gramicidin in Ae3$^{-/-}$ animals and electrophysiological recordings of mIPSCs in Nkcc1$^{-/-}$ mice and analyzed the data. Valentin Stein and Carsten Pfeffer performed and analyzed electrophysiological recordings. Moritz Hentschke quantified mRNA expression pattern. Christian Hübner and Valentin Stein wrote the manuscript.

2.1   Abstract

A high intracellular chloride concentration in immature neurons leads to a depolarizing action of GABA that is thought to shape the developing neuronal network. We show that GABA-triggered depolarization and calcium (Ca^{2+}) transients were attenuated in mice deficient for the Na–K–2Cl cotransporter NKCC1. Correlated Ca^{2+} transients and giant depolarizing potentials (GDPs) were drastically reduced and the maturation of the glutamatergic and GABAergic transmission in CA1 delayed. Brain morphology, synaptic density, and expression levels of certain developmental marker genes were unchanged. The expression of lynx1, a protein known to dampen network activity, was decreased. In mice deficient for the neuronal $Cl^-/HCO3^-$ exchanger AE3, GDPs were also diminished. These data show that NKCC1-mediated Cl^- accumulation contributes to GABAergic excitation and network activity during early postnatal development and thus facilitates the maturation of excitatory and inhibitory synapses.

2.2   Introduction

The development and maturation of the brain involve cellular proliferation and migration, followed by dendritic and axonal outgrowth, synapse formation, and circuit refinement. Whereas the first events are mainly genetically determined, the latter processes are believed to depend on intrinsic spontaneous and later on extrinsically evoked neuronal activity (Katz and Shatz, 1996; Khazipov and Luhmann, 2006). GABA, the main inhibitory neurotransmitter of the mature central nervous system (CNS), is the main excitatory agonist in the immature brain (Ben-Ari et al., 1989) and is thought to be important for brain development (Hanse et al., 1997; Leinekugel et al., 1997; Ben-Ari, 2002; Owens and Kriegstein, 2002). GABA dependent depolarization can lead to network-driven, spontaneous giant depolarizing potentials (GDPs), which drive the correlated activity of large ensembles of pyramidal neurons in the developing hippocampus (Khazipov et al., 1997; Leinekugel et al., 1997; Garaschuk et al., 1998; Ben-Ari, 2002). The ensuing opening of voltage-gated calcium channels results in Ca^{2+} oscillations, which may trigger neuronal growth and synaptogenesis. GDPs disappear around the second postnatal week with decreasing neuronal $[Cl^-]_i$ (Garaschuk et al., 1998) that results from the increasing expression of the K–Cl cotransporter KCC2 (Rivera et al., 1999; Stein et al., 2004). Disruption of *Kcc2* in mice leads to hyperexcitability and perinatal death because of impaired synaptic inhibition in spinal cord and

brainstem (Hübner et al., 2001b). Conversely, premature lowering of $[Cl^-]_i$ by overexpressing KCC2 in *Xenopus* tectal neurons blocks the normal developmental increase in AMPA receptor-mediated retinotectal transmission (Akerman and Cline, 2006). Using *in utero* electroporation, KCC2 was expressed prematurely in rat ventricular progenitors and cortical neurons (Cancedda et al., 2007), resulting in a marked impairment of morphological maturation.

The mechanisms contributing to intracellular chloride accumulation in immature neurons are insufficiently characterized. The Na–K–2Cl cotransporter NKCC1, which uses the inwardly directed sodium gradient to raise $[Cl^-]_i$, shows a decreasing neuronal expression during postnatal development (Clayton et al., 1998; Hübner et al., 2001a). Inhibition of Na–K–2Cl cotransport by bumetanide causes a hyperpolarizing shift of the GABA reversal potential in rat neocortical neurons (Yamada et al., 2004) and in hippocampal neurons (Dzhala et al., 2005; Sipilä et al., 2006). Likewise, in dorsal root ganglion neurons, which normally maintain high levels of NKCC1 but do not express KCC2, disruption of *Nkcc1* abolishes GABA-induced depolarization (Sung et al., 2000). Small interfering RNA-mediated knock-down of NKCC1 in the developing cortex entailed profound morphological and developmental changes in single neurons (Wang and Kriegstein, 2008).

We used Nkcc1-knock-out (KO) (*Nkcc1*$^{-/-}$) mice (Pace et al., 2000) to examine the role of NKCC1 in the regulation of $[Cl^-]_i$ and the developing neuronal network in the immature hippocampus. Diminished GABAergic excitation in *Nkcc1*$^{-/-}$ mice resulted in reduced and less correlated spontaneous network activity. We further show that the neuronal anion exchanger AE3 also influences early network activity. Whereas we did not detect morphological defects, we observed a delayed maturation of glutamatergic and GABAergic synapses in *Nkcc1*$^{-/-}$ mice. Our results demonstrate the importance of GABAergic excitation for early network development and suggest a homeostatic control of network excitability by nicotinergic mechanisms.

2.3 Materials and Methods

Mice. The generation of *Nkcc1*$^{-/-}$ and *Ae3*$^{-/-}$ mice used in this study has been described previously (Pace et al., 2000; Hentschke et al., 2006). Studies were performed on a C57Bl6 (NKCC1) or a mixed 129-SVJ/C57Bl6 (AE3) background, respectively, using littermates as controls. Genotyping was performed on tail biopsy DNA by PCR using standard protocols. For *Nkcc1* the sense-primer F1 (GCA AAT ATC TCA GGT GAT CTT GC) and the antisense primers R1 (GAG TTC TGT TGC TAC TTC TGA AC) and R2 (CTA AAG CGC ATG CTC CAG ACT GCC) were used in a single PCR mix. The

primer pair F1/R1 amplified a ~ 600 bp band for the wild-type allele and the primer pair F1/R2 a ~ 200 bp band for the targeted allele. For *Ae3* the sense-primer F1′ (GCC ACC AGG GGA ATG ACA AGC CCG) and the antisense primers R1′ (CTG GAG ACC TGG GGG TTG GGC TAA) and R2′ (TCT CTA GAC ACC TAG CTC CCA ACA) were used in a single PCR mix, F1′/R1′ yielding a ~ 800 bp amplicon in the knockout and the primer pair F1′/R2′ a ~ 400 bp wild-type allele. Experiments were approved by the Ministry of Science and Public Health of Hamburg and Berlin, Germany. Experimenters were blinded to the genotype.

Expression analysis. Total hippocampal RNA was extracted from P1, P5 and P15 *Nkcc1*^{-/-} and wild-type littermates using Trizol (Invitrogen) reagent and the High Pure RNA purification kit (Qiagen). RNA was transcribed into cDNA using the SuperScript II cDNA kit (Invitrogen) with random hexamers. Real-time PCR was performed using the 7900 HT cycler from Applied Biosystems and the SYBR green Power PCR master mix (Applied Biosystems) and normalized to GAPDH and HPRT. An initial denaturation step (10 min at 95°C) was followed by 40 cycles with 2 steps: 95°C for 15 s, followed by 60°C for 60 s. Each sample was amplified in triplicate and gave consistent results in two independent experiments. The value of one P1 animal, the calibrator, was set to 1. All other amplicons are shown as x-fold of the calibrator. Contamination with genomic DNA was negligible. Primers are listed in Supplementary Table 1.

Affymetrix GeneChip Mouse Expression Array 430A and TEST chips were used for expression analysis. Total hippocampal RNA was extracted from 3 *Nkcc1*^{-/-} and 3 control mice at P5 using Trizol reagent (Invitrogen) followed by the High Pure RNA purification kit (Qiagen). First strand cDNA was synthesized using T7-Oligo(dT)24 Primer (Ambion) and Superscript II (Invitrogen) following the manufacturers′ instructions. Second strand synthesis was accomplished using *E. coli* DNA ligase, *E. coli* DNA polymerase I, *E. coli* RNase H and T4 DNA polymerase (all from Invitrogen) according to the manufacturers′ instructions. cDNA was then extracted using phenol-chloroform-isoamylalcohol + EDTA and precipitated with NH_4OAc and EtOH, washed twice with 80% EtOH, dried and dissolved in H_2O. Biotin-labeled cRNA was synthesized with the RNA labeling kit (ENZO). RNA and cDNA quality were controlled at all stages. Labeled cRNA was checked on TEST chips before hybridizing chip A according to the Affymetrix protocol. Chip data were analyzed using the RMA xpress software (Bolstad BM et al., Bioinformatics, 2003; Version: 0.4.1 Release) followed by t-test evaluation (cut off P > 0.05). *In situ* hybridization was performed as described elsewhere (Hübner et al., 2001a).

Slice electrophysiology. Brains were removed from decapitated mice and placed directly into chilled artificial cerebrospinal fluid (ACSF) containing (mM): 119 NaCl, 2.5 KCl, 4 CaCl$_2$, 1.3 MgSO$_4$, 2.7 MgCl$_2$, 1 NaH$_2$PO$_4$, 26 NaHCO$_3$, and 11 glucose (unless otherwise indicated), which was gassed continuously with 95% O$_2$/5% CO$_2$ (carbogen). From P1 to P7 brains were cut horizontally 350 μm thick with a vibratome (Leica). In case of 2-week-old mice, we cut transverse hippocampal slices. After equilibration in gassed ACSF at 32 ºC for at least 45 minutes, slices were placed into a bath chamber, and continuously superfused with carbogen-gassed ACSF at room temperature (22-24 ºC) at a rate of 2-3 ml/min. Pyramidal CA1 and CA3 neurons were visualized using differential interference contrast infrared video microscopy.

The GABA reversal potential was determined in P1 CA1 pyramidal neurons in the presence of TTX (0.5 μM) to block voltage-gated Na$^+$ channels and exclude network effects. GABA (100 μM) was bath applied. Electrodes (Clark Electromedical) (5-8 MΩ) were filled with a solution containing (mM): 140 KCl, 2 MgCl$_2$, 10 Hepes, 5 EGTA at pH 7.4. Pipettes were dipped into this solution for several seconds and then back-filled with the same solution containing gramicidin (Sigma) (10 μg/ml). The chloride reversal potential was measured using a voltage ramp from +20 mV to -100 mV at a rate of 150 mV/s after stepping the membrane from a holding potential of 60 to +20 mV for 80 ms. Recordings were performed with an Axopatch 200A amplifier and analyzed with pClamp 8.0 (Axon Instruments).

Field EPSPs were recorded in the stratum radiatum of CA1 of P15 mice in the presence of 100 μM picrotoxin (PTX, Sigma) using a MultiClamp 700A amplifier (Axon Instruments). Recording and stimulation electrodes were filled with ASCF containing (mM): NaCl 119, KCl 2.5, CaCl$_2$ 2.5, MgSO$_4$ 1.3, NaH$_2$PO$_4$ 1, NaHCO$_3$ 26.2, Glucose 11. Inputs from CA3 to CA1 were severed to prevent propagation of epileptiform activity.

To measure the AMPA/NMDA ratio, whole cell patch recordings were performed with 3-5 MΩ glass electrodes filled with an internal solution containing (mM): 150 CsGluconate, 8 NaCl, 2 MgATP, 10 HEPES, 0.2 EGTA, 0.1 spermine, and 5 QX314 (Tocris), pH 7.2. Ratios of AMPA to NMDA currents in CA1 pyramidal cells were obtained by evoking eEPSCs with a monopolar glass electrode. AMPA eEPSCs were recorded at −70 mV, the NMDA component was recorded at +40 mV, the current being taken 70 ms after stimulus. Spontaneous miniature EPSCs (mEPSC) were recorded at -70 mV in the presence of TTX (0.5 μM), PTX (100 μM), and 50 mM sucrose in ACSF to increase the events frequency. mEPSCs were analyzed off line with customized software using a threshold of 5 pA. Spontaneous miniature IPSCs (mIPSCs) were recored at -70mV in ACSF in the presence of 0.5 μM TTX and 20μM NBQX. The pipette solution contained in mM: 90 CsCl, 20 CsGluconate, 8 NaCl, 2 MgCl2, 2QX314, 10 HEPES, 1 EGTA.

For extracellular measurements of spontaneous activity (GDPs), P5 and P10 slices were recorded at 32°C in ACSF containing 4.5 mM KCl. 3-5 MΩ glass electrodes filled with ACSF were placed into the CA3 stratum pyramidale. Extracellular voltage changes were recorded using a MultiClamp 700A amplifier (Axon Instruments). Voltage changes were analyzed offline with Clampfit (Axon Instruments) using a threshold of 0.01 mV and visual event control.

Calcium imaging. Animals were decapitated, their brains removed and placed directly into chilled artificial cerebrospinal fluid (ACSF) containing (mM): 125 NaCl, 4.5 KCl, 1.25 NaH_2PO_4, 26 $NaHCO_3$, 2 $CaCl_2$, 1 $MgCl_2$, and 20 Glucose gassed continuously with carbogen. 300µm horizontal slices were equilibrated in gassed ACSF at 32ºC for at least 45 minutes and then loaded with the Ca^{2+}-sensitive dye fura-2 AM (15 µM; Molecular Probes) in ACSF for 30 min at 37 ºC. Fura-2 was excited using a multiple wavelength monochromator (Polychrome IV, TILL Photonics) and the emitted light filtered at a wavelength of 510 nm using a bandpass filter. Images were obtained using a 40x water immersion objective fitted to a CCD camera (Imago) on an upright microscope (Olympus, BXWI50) at a 0.5 Hz rate. To record responses to either GABA (100µM) or glutamate (100µM), TTX (0.5µM) was added to the superfusion buffer (ACSF) to block network effects. Analysis was performed with the TILLvisION software (version 4.0, TILL Photonics) for user-defined individual pyramidal cell somata. $[Ca^{2+}]_i$ was expressed as the ratio of fura-2 fluorescence intensity at 340 nm divided by that at 380 nm. $[Ca^{2+}]_i$ changes in response to GABA or glutamate were calculated by subtracting the average $[Ca^{2+}]_i$ of five consecutive images before agonist application from the peak fluorescence in response to these drugs (Δ340/380).

Spontaneous CA1 Ca^{2+} events were recorded in ACSF at 32 °C (without TTX; continuously gassed with carbogen) for 500s at 2Hz sampling rate using a 40x water immersion objective (Olympus) lens. The change in $[Ca^{2+}]_i$ for individual cells was calculated.

To analyze the network of spontaneously active neurons, we adopted a method described by (Schwartz et al., 1998). Changes in fluorescence in multiple cells were analyzed with a program written in MatLab (The Mathworks). The onset of each calcium transient for every cell was determined by the following algorithm.

To correct for baseline drifts, we high-pass filtered the raw data in the following way. Each recording was separated into 10 segments of 50 seconds. The value corresponding to the lower 10% percentile of each segment was used as the baseline of the segment. This baseline value was placed in the middle of the respective segment. These points were fitted with a ´spline´ function, which was then subtracted from the recording.

As biologically significant increases of intracellular Ca^{2+} are characterized by a fast rise-time, we used the 1st derivative of the baseline-corrected fluorescence trace to detect 'Ca^{2+} events'. We determined the noise level of the recording to define a threshold for event detection in a two step process. In the first step we calculated the mean (MV1) and the standard deviation (SD1) of the 1st derivative for each cell. As these values include all Ca^{2+} events, a threshold based on this standard deviation would be larger than necessary and might lead to false negatives. In particular, apparent noise levels and hence detection criteria would depend on the frequency of Ca^{2+}-events in the recording, which would pose a problem when comparing KO and WT slices (the latter showing higher activity). Therefore, we minimized the influence of Ca^{2+} events on the detection threshold by excluding values above a first threshold (T1 = MV1 + 1.64 * SD1; (note that the mean value of the 1st derivate is almost zero)) to calculate a second mean (MV2) and second standard deviation (SD2). Time points at which values exceeded a threshold based on MV2 and SD2 (T2 = MV2 + 3.09 * SD2) were defined as Ca^{2+} events. Thus, Ca^{2+}-induced fluorescence continuously increasing over several time points will be interpreted as a series of Ca^{2+}-events, whereas a 'plateau' will just yield a single event at the beginning.

To test whether the coincidence of 'Ca^{2+}-events' (as determined by the above procedure) of different cells was due to some form of coupling, we compared our data to the coincidence expected by chance if neurons fire randomly and independently. This is commonly done by Monte Carlo simulations (Schwartz et al., 1998). These, however, are slow as they need a high number of simulations (N ~ 1000) to give reliable results. Since speed is a critical factor in the analysis of large networks we developed an analytical method to calculate probabilities of coinciding events. This method is illustrated below. In contrast to Monte Carlo simulations, which are only valid for a specific parameter set (Aguilo et al., 1999), our analytical model allows us to calculate the number of coincident events expected by chance independent of event rate and recording length. We then defined a correlation index I_{corr} as the ratio of coincidences found in a specific set of cell pairs to that expected by chance for the same parameters. In other words, if the number of coincidences is equal to that expected by chance the correlation index equals one, and increases with a larger event correlation.

For two given time series of length N, the number of events shall be n, m≤0m, n ≤ N in each trace, and n≥ m. In this case the maximum of possible coincidences is m. The probability for M coinciding events is given by:

$$\text{Prob}_M(N,n,m) = p_{m-M+1,M+1} \frac{F(N-n, m-M)F(n, M)}{F(N, m)} \qquad 0 \leq M \leq m$$

using the Pascal matrix P with elements $p_{i,j}$ and

$$F(x,n) = \begin{cases} 1 & i<1 \\ \prod_{i=1}^{n}\left(x-(i-1)\right) & i \geq 1 \end{cases}$$

The resulting distribution is known as hypergeometric distribution (Feller, 1968). We verified this specific numerical model against a Monte Carlo simulation (MCS). We obtained equivalent results when using sufficiently large sample sizes (N ≥ 10000 MCS runs). This enabled us to calculate the significance for coinciding events, and also yielded a relative measure for coincidence. For two randomly chosen cells (i, j) of a set of cells with M coinciding events the synchronous activity is described by the matrix element:

$$ci_{i,j}(N,n,m) = \begin{cases} 0 & n,m = 0 \\ \dfrac{M}{E(N,n,m)} & n,m \neq 0 \end{cases}$$

Where E is the expectancy value

$$E(N,n,m) = \sum_{M=0}^{m} Prob_{M}(N,n,m) \cdot M \qquad \text{for } m \leq n$$

This symmetric matrix is then used to calculate the correlation index I_{corr} by averaging the triangular elements (i≠j) and scaling with the number of elements (= number of possible cell pairs).

$$I_{corr} = \frac{1}{\sum_{i=1,i<j}^{NC} 1} \cdot \sum_{i=1,i<j}^{NC} c_{i,j}$$

I_{corr} represents the statistical average interaction in the observed set and describes the characteristics for a given number of cells (NC). Hence the number of possible cell pairs [N = $(NC^2-NC)/2$] may differ from set to set, averages of experiments with differing numbers of cells have to be weighted with the number of pairs.

We analyzed 12 KO and 9 WT slices at P2 and 35 KO and 33 WT slices at P4. The median of observed cells per set were n = 52 (27-88, KO) vs. n = 56 (35-117, WT) at P2 and n = 49 (30-81, KO) vs. n = 49 (22-86, WT) at P4. All recorded cells of one experiment (slice) were used for the analysis, leading to an average number of pairs of >1300 contributing to the index I_{corr}.

Details on the methods and routines in MatLab (The Mathworks) will be made available upon request.

Western blot analysis. Hippocampi were dissected from P1, P5, and P15 $Nkcc1^{-/-}$ and WT mice. Tissues were homogenized in lysis buffer (20 mM Tris, 140 mM NaCl, 5 mM EDTA, 1 % Triton X-100, pH 7.4) supplemented with a commercial protease inhibitor cocktail (Complete, Roche). Debris was pelleted by centrifugation at 1,000 g for 10 min. The protein concentration of the supernatant was determined and 20 μg of total protein per lane were separated on 8.5% to 15% SDS-polyacrylamide gels, followed by a transfer to PVDF membranes. These blots were incubated with respective primary antibodies and rabbit anti-actin or mouse anti-tubulin (both 1:2000, Sigma) as a loading control. Detection used a peroxidase-coupled anti IgG-antibody (Roche) and a chemoluminescence kit (Renaissance, DuPont). Quantification of Western blots was performed using a camera detection system (ChemiSmart 5000/ChemiCapt, PeqLab) allowing for linear signal integration. Band intensities were quantified using ImageJ software (NIH, USA). Intensity values were normalized to tubulin levels. The following primary antibodies were used: rabbit anti-KCC2 1:500 (Hübner et al., 2001b); mouse anti-GluR2 (1:500, Chemicon); mouse anti-gephyrin (1:500, Synaptic Systems); mouse anti-GAD 65/67 (1:500, Biotrend), mouse anti-Synaptophysin (1:1000, Sigma), rabbit anti-lynx1 (1:100) (Ibañez-Tallon et al., 2002), rabbit anti-GluR4p842 (1:1000) (Esteban et al., 2003), rabbit anti-GluR4 (1:1000), rabbit anti-GluR1 (1:1000), rabbit anti-GluR1p831 (1:1000), rabbit anti-GluR1p845 (1:1000, all from Millipore), rabbit anti-AE3 (1:200; epitop: H2N-CLLRKRREREQTKVEM-CONH2, purified with standard procedures against the peptide).

Morphological studies. For light microscopy, brains were dissected and fixed at 4°C for 6 h in 4% PFA in phosphate buffered saline (PBS). The barrel-cortex of P5 mice was stained for cytochrome oxidase as described (Iwasato et al., 2000). Nissl stainings were performed on 5 μm paraffin tissue sections. Immunohistological stainings were done on freely floating 50 μm cryosections. In brief, sections were blocked with 5% normal goat serum (NGS), 0.25% Triton X-100 in 0.1 M phosphate buffer (PB). Dilutions of primary and secondary fluorescence-labeled antibodies were applied in 0.1 M PB with 5% NGS and 0.25% Triton X-100. Sections were mounted on gelatinized

glass slides, coverslipped with Fluoromount, and visualized using confocal microscopy (Leica TCS SP2). The following primary antibodies were used: rabbit anti-KCC2 (1:500) (Hübner et al., 2001b), mouse anti-Map2 (1:1000, Chemicon), rabbit anti-synaptophysin (1:1000, Synaptic Systems), mouse anti-reelin (1:1000, gift of A. Goffinet), mouse anti-GAD65/67 (1:1000, Biotrend), mouse anti-synaptophysin (1:1,000, Sigma), guinea pig anti-vGlut1 (1:500, Chemicon), rabbit anti-Snap25 (1:500, Synaptic Systems), rabbit anti-GABA$_A$ α1 (1:500, Upstate), rabbit anti-GABA$_A$ α3 (1:500, Sigma), rabbit anti-GluR4 (1:1000, Millipore). Secondary antibodies were goat-anti-rabbit 488 and goat-anti-mouse 546 (both Molecular Probes), each used at 1:1000. Nuclei were stained with TOTO-3 (Molecular Probes) 1:2000. Biocytin filling and electron microscopic techniques are given in Supplementary Methods.

Biocytin filling was done as described (Current protocols in neuroscience (2004) 1.12.1-1.12.10) using the whole cell patch-clamp technique. Briefly, P7 animals were decapitated and brain slices prepared as described above. CA1 neurons were patched using DIC visual control. After sealing and whole cell access, Neurobiotin (Vector Labs) (2.5% in internal solution containing in mM: 150 CsGluconate, 8 NaCl, 2 MgATP, 10 HEPES, 0.2 EGTA, pH 7.2) filling was done for 10-15 minutes. The slices were fixed in 4% PFA/PBS at 4°C overnight and Neurobiotin visualized using 488-coupled streptavidin (Molecular Probes). Stack images were taken with a confocal microscope (Leica TCS SP2). After dendritic reconstruction, apical dendritic length and branching points were determined with NeuronJ (Application of ImageJ, Rasband, W.S., ImageJ, U. S. National Institutes of Health, Bethesda, Maryland, USA, http://rsb.info.nih.gov/ij/, 1997-2007). For the Sholl analysis of dendritic complexity (Sholl, 1953), crossings of apical dendrites with a grid of concentric circles spaced 5 μm and centered on the soma were counted.

For electron microscopy, four P4 and four P8 hippocampi per genotype were fixed in 1% glutaraldehyde and 1% paraformaldehyde in 0.1 M PB, postfixed in 1% OsO$_4$ for 30 min, dehydrated in graded ethanol using 1% uranyl acetate in 70% ethanol for 30 min, and embedded in Epon 820 (Serva). Blocks were trimmed to contain only the stratum pyramidale and radiatum of the CA1 region. Thin sections were cut on a Reichert-Jung OmU3 ultramicrotome. Ultrathin sections were stained with uranyl acetate followed by lead citrate. Hippocampi were evaluated for the density of synapses. The spine synapse density was calculated using unbiased stereological methods as described previously (Prange-Kiel et al., 2004). Briefly, pairs of consecutive serial ultrathin sections were cut and collected on Formvar-coated single grids. The sections contained the upper and middle third of the CA1 stratum radiatum. Photographs were made at a magnification of 6,600x with the observer blinded to the genotype. Areas occupied by interfering structures, such as large dendrites or blood vessels were excluded. To obtain a comparable measure of synaptic

numbers, unbiased for possible changes in synaptic size, the disector technique was used (Sterio, 1984). The density of spine synapses of pyramidal cell dendrites was calculated with the help of a reference grid superimposed on the EM prints. Only those spine synapses were counted that were present on the reference section but not on the look-up section. The disector volume was calculated by multiplying the unit area of the reference grid by the distance (0.09 μm) between the upper faces of the reference and the look up section. At least 10 neuropil fields were photographed on each electron microscopic grid. With at least two grids from each slice, containing at least two pairs of consecutive ultrathin sections, each slice provided a minimum of 20 neuropil fields.

2.4   Results

NKCC1-dependent chloride accumulation is important for excitatory GABA responses in P1 hippocampal pyramidal neurons

In situ hybridization of hippocampal sections showed that neuronal NKCC1 expression decreased from P1 to P15 in the CA1 and CA3 regions and in the dentate gyrus (supplemental Fig. S1A–H, available at www.jneurosci.org as supplemental material). Quantitative reverse transcription (RT)-PCR using RNA extracted from dissected hippocampi revealed a decline of NKCC1 mRNA levels from P1 to P15 by almost 50% (supplemental Fig. S1I, available at www.jneurosci.org as supplemental material), whereas the amount of the KCC2 message more than doubled during the same period (supplemental Fig. S1J, available at www.jneurosci.org as supplemental material). Expression levels of KCC2 did not differ between the WT and the NKCC1 KO hippocampus (supplemental Fig. S1J, available at www.jneurosci.org as supplemental material).

To determine whether NKCC1 contributes to GABAergic excitation by accumulating chloride into early postnatal neurons, GABA reversal potentials were measured using gramicidin perforated patch-clamp recordings. Resting membrane potentials of P1 CA1 hippocampal pyramidal cells were unaltered in $Nkcc1^{-/-}$ neurons (-63.4 ± 2.4 vs -67.8 ± 2.3 mV in the WT; p = 0.21, t test; WT, six cells from four mice; $Nkcc1^{-/-}$, nine cells from five mice). In the presence of GABA, the reversal potential shifted to -46.9 ± 3.1 mV in WT but only to -57.6 ± 1.9 mV in $Nkcc1^{-/-}$ neurons (Fig. 1*A*,*B*). The lower GABA-induced depolarization of $Nkcc1^{-/-}$ neurons [5.8 ± 0.7 mV ($Nkcc1^{-/-}$) vs 20.9 ± 2.2 mV (WT); p < 0.05, t test] indicates a decrease of $[Cl^-]_i$, caused by the loss of the chloride cotransporter NKCC1. Depolarization of neurons can evoke a Ca^{2+} response, which is mainly caused by the activation of voltage-gated calcium channels (Yuste and Katz, 1991). We recorded

changes in the fluorescence of the Ca^{2+} indicator fura-2 as an indirect measure of the depolariza-tion induced by GABA. WT pyramidal neurons responded rapidly to GABA (100 µM) with a tran-sient Ca^{2+} signal of 1.03 ± 0.03 [$F_{340/380}$ (peak) - $F_{340/380}$ (baseline)]. This signal was approximately threefold larger than that evoked in $Nkcc1^{-/-}$ preparations (0.31 ± 0.02). The response to the exci-tatory neurotransmitter glutamate, in contrast, was not affected by the loss of NKCC1 (Fig. 1*C–E*; supplemental Fig. S2*A,C*, available at www.jneurosci.org as supplemental material). Hence cal-cium imaging provided additional support for a role of NKCC1 in early GABA-mediated excitation. This finding motivated us to use $Nkcc1^{-/-}$mice as a model to study the role of GABA-mediated neuronal activity in the developing brain.
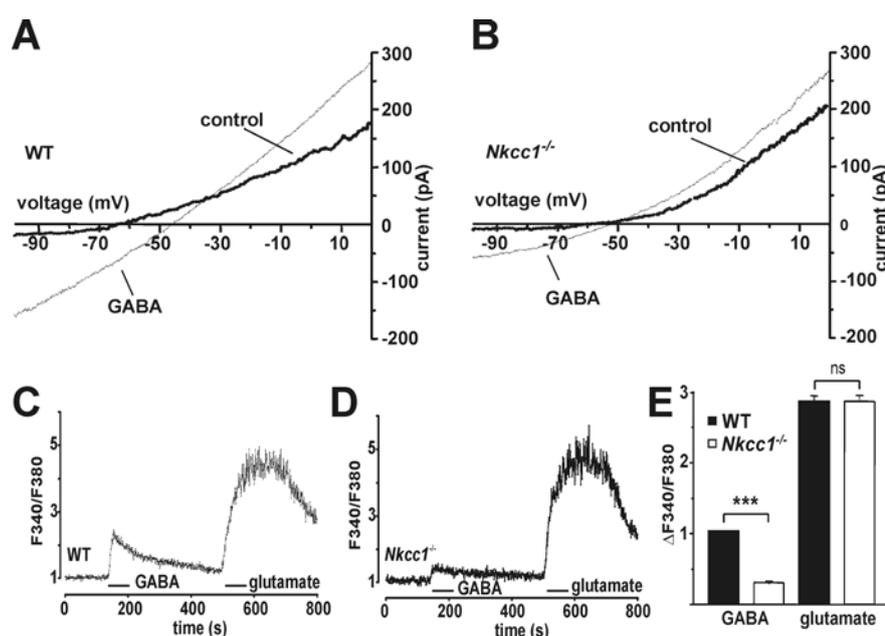
Figure 1: GABA-induced depolarization in hippocampal CA1 neurons depends on NKCC1.

A,**B**, Representative current–voltage traces of hippocampal pyramidal CA1 neurons (P1) from both WT (**A**) and $Nkcc1^{-/-}$ (**B**) mice using gramicidin-perforated patch clamping before and during appli-cation of 100 µM GABA. **C–E**, Reduced Ca^{2+} entry in response to GABA, but not glutamate, in $Nkcc1^{-/-}$ CA1 neurons at P1. **C,D**, Typical fura-2 fluorescence traces indicative of intracellular calcium of a single WT (**C**) and $Nkcc1^{-/-}$ (**D**) CA1 neuron sequentially exposed to GABA (100 µM) and glutamate (100 µM) for 60 s each. The ratio of fluorescence at 340 and 380 nm, which increases with $[Ca^{2+}]_i$, is given. **E**, Ca^{2+} responses as indicated by mean changes in fura-2 fluorescence in response to GABA and glutamate in WT (filled bars) and $Nkcc1^{-/-}$ (open bars) P1 CA1 neurons (WT: 108 cells, 6 record-ings, 5 mice; $Nkcc1^{-/-}$: 141 cells, 7 recordings, 5 mice). The asterisks indicate significance (***p < 0.001, *t* test). Error bars indicate SEM.

Spontaneous Ca²⁺ transients are reduced in number and are less correlated in hippocampal slices of *Nkcc1⁻/⁻* mice at P2 and P4

The depolarizing action of GABA is critical for neuronal network activity during the first week after birth (Leinekugel et al., 1997; Garaschuk et al., 1998). To investigate the role of NKCC1-dependent Cl⁻ accumulation in spontaneous network activity, Ca²⁺ signals from fura-2 fluorescence traces (Fig. 2A) were quantified in the CA1 region of WT and *Nkcc1⁻/⁻* hippocampal slices. Data were reduced to 'Ca²⁺ events' at the time point at which the rate of the fluorescence increase exceeded a certain threshold (for details see Methods) (supplemental Fig. S3A,B, available at www.jneurosci.org as supplemental material). The frequency of Ca²⁺ events per neuron increased in WT from P2 (12.5 ± 0.5 events per 1000 s) to P4 (18.3 ± 0.6 events per 1000 s). In *Nkcc1⁻/⁻* animals, Ca²⁺ events were significantly reduced at P2 (7.1 ± 0.3 events / 1000 s) and did not increase with time (P4: 7.1 ± 0.4 events/1000 s) (Fig. 2B).
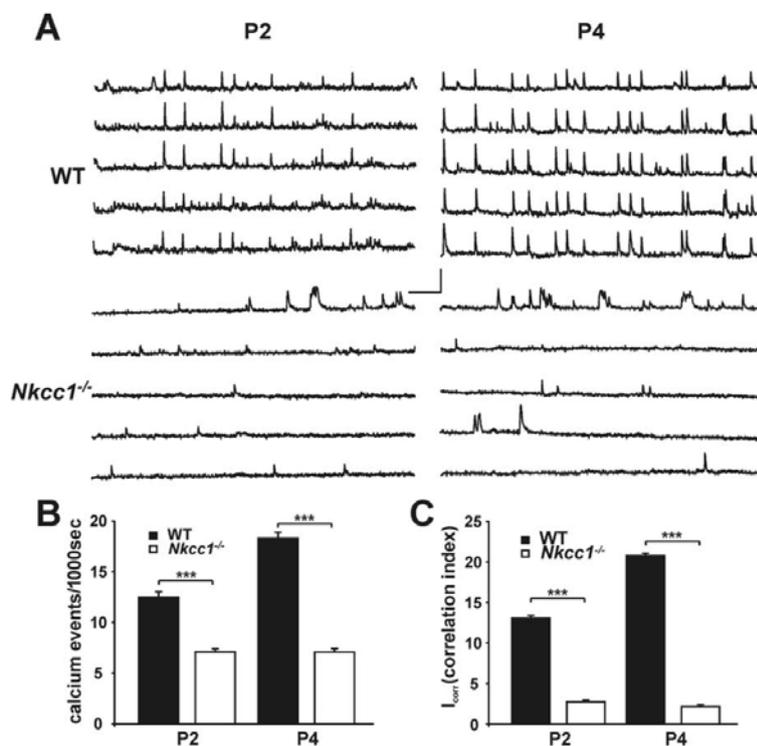
Figure 2: Correlated network activity is present in WT, but not in *Nkcc1⁻/⁻* hippocampal slices.
A, Representative recordings of fura-2 fluorescence indicative of [Ca²⁺]ᵢ changes in single neurons in WT and *Nkcc1⁻/⁻* slices at P2 and P4. Most Ca²⁺ events in WT slices occur simultaneously in many neurons, whereas they are reduced in number and mostly lack correlation in *Nkcc1⁻/⁻* slices. Calibration: horizontal, 50 s; vertical, 0.15 F_{340}/F_{380}. **B,C**, Quantification of the number of calcium events (**B**) and of correlated activity (**C**) at P2 and P4 shows highly significant reduction in *Nkcc1⁻/⁻* slices (open bars) (P2: 3 mice per genotype, 6 slices per genotype; P4: 3 mice per genotype, 5 slices per genotype; p < 0.001, t-test). Error bars indicate SEM.

To compare the degree of synchronous Ca^{2+} activity between different CA1 pyramidal neurons independent of overall activity, we developed an algorithm to determine a correlation index I_{corr}. Values of $I_{corr} > 1$ indicate a correlation greater than that achieved by chance alone. As illustrated in Fig. 2C, the correlation index was drastically decreased in *Nkcc1^-/-* slices at both P2 [I_{corr} = 13.1 ± 0.3 (WT), I_{corr} = 2.7 ± 0.2 (*Nkcc1^-/-*)] and at P4 [I_{corr} = 20.8 ± 0.3 (WT), I_{corr} = 2.1 ± 0.3 (*Nkcc1^-/-*)]. Thus NKCC1 plays a pivotal role in correlated network activity.

Frequency and amplitudes of GDPs are reduced in *Nkcc1^-/-* and *Ae3^-/-* mice at P5

GDPs of the early postnatal hippocampus are known to depend on GABA (Leinekugel et al., 1997; Ben-Ari, 2002; Sipilä et al., 2005). In mice, GDPs are observed in the first postnatal week and gradually disappear after P10 (Crepel et al., 2007). We measured GDPs at P5 by extracellular recordings of spontaneous activity in the CA3 stratum pyramidale. GDP frequencies and amplitudes were significantly reduced, but not abolished in *Nkcc1^-/-* mice at P5 (Fig. 3A–C; supplemental Fig. S4A, available at www.jneurosci.org as supplemental material). At P10 GDP frequency had decreased and the difference between genotypes had vanished (supplemental Fig. S5, available at www.jneurosci.org as supplemental material).

As GABA was still slightly depolarizing in P1 pyramidal neurons of *Nkcc1^-/-* mice (Fig. 1E), we hypothesized that transporters other than NKCC1 may also raise $[Cl^-]_i$ and contribute to the generation of GDPs. The neuronal anion-exchanger AE3 is expressed early in development (Hentschke et al., 2006) and is predicted to elevate $[Cl^-]_i$ above electrochemical equilibrium. However, GABA reversal potentials and GABA evoked Ca^{2+} responses of CA1 neurons did not differ between *Ae3^-/-* and WT mice at P1 (supplemental Figs. S2B,D,S6, available at www.jneurosci.org as supplemental material), suggesting that Cl^- accumulation by AE3 is insignificant compared to that by NKCC1 at that early time point. However, at P5, when AE3 protein levels had increased compared to P1 (supplemental Fig. S7I, available at www.jneurosci.org as supplemental material), disruption of AE3 decreased GDP frequency and amplitudes (Fig. 3A-D; supplemental Fig. S4B, available at www.jneurosci.org as supplemental material).
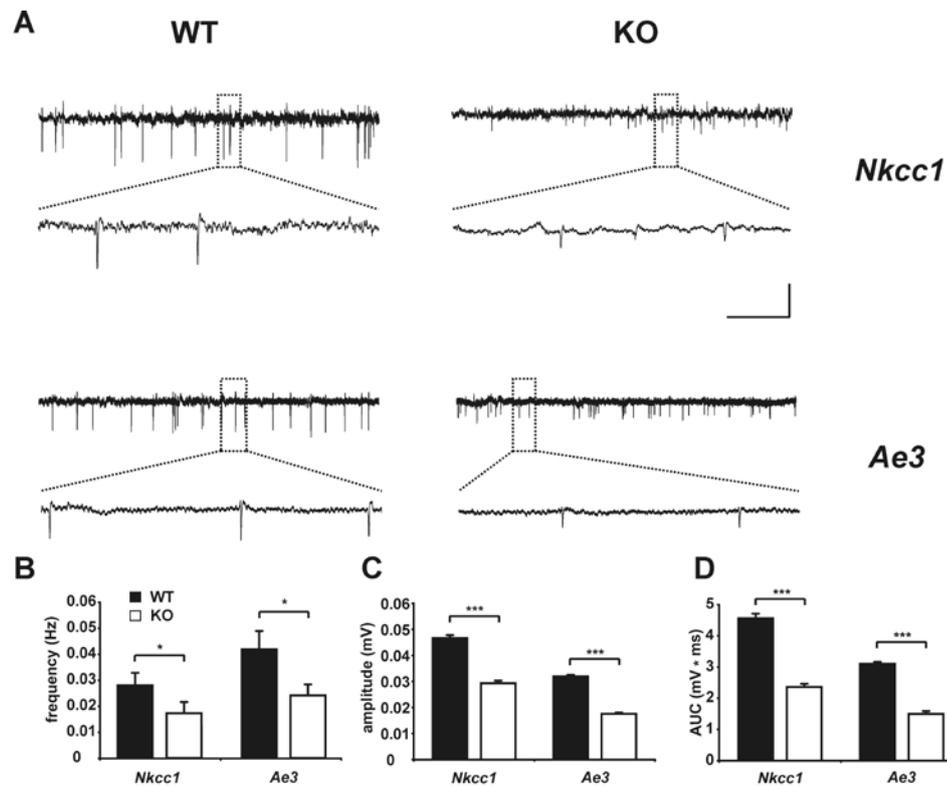
Figure 3: Reduced spontaneous electrical activity in CA3 of *Nkcc1*$^{-/-}$ and *Ae3*$^{-/-}$ hippocampal slices.

 A, Representative extracellular recordings in CA3 stratum pyramidale of P5 *Nkcc1* and *Ae3* WT and KO slices. Framed parts are shown as enlargements below original trace. Quantification of frequency (**B**), amplitude (**C**) and area under curve (AUC) (**D**) of single spontaneous electrical events are shown for Nkcc1 and Ae3 WT and KO slices. Asterisks indicate significant difference (*$p < 0.05$, ***$p < 0.001$, *t* test) (NKCC1: WT: 3 mice, 15 slices; KO: 3 mice, 19 slices; AE3: WT: 3 mice, 11 slices; KO: 3 mice, 12 slices). Different WT levels may be attributable to differences in genetic background of NKCC1 and AE3 mouse lines (see Materials and Methods). Error bars indicate SEM.

No gross structural alterations are evident in *Nkcc1*$^{-/-}$ brains

As GABA$_A$-receptor dependent depolarization has been implicated in the migration and differentiation of neuronal precursor cells (Owens and Kriegstein, 2002), we performed Nissl stainings of neocortical (Fig. 4A,B) and hippocampal sections (Fig. 4C,D) at P5. Gross brain structure appeared unaltered in *Nkcc1*$^{-/-}$ mice with regard to both layering and estimated neuron density. We did neither detect changes in the refinement of the somatosensory barrel cortex at P5, a structure known to depend on neuronal activity (Iwasato et al., 2000; Lu et al., 2003) (Fig. 4E,F). Neither the quantification by electron microscopy of spine synapses per μm^3 in the stratum radiatum of the CA1 region at P4 and P8 (Fig. 4L), nor the reconstruction of individual P7 CA1 pyramidal neurons (Fig. 4G-K) revealed significant structural changes in *Nkcc1*$^{-/-}$ brains. In addition,

hippocampal sections were stained for marker proteins such as GABA$_A$-receptor subunits α1 (Fig. 4M,N) and α3 (supplemental Fig. S8W,Z, available at www.jneurosci.org as supplemental material), glutamic acid decarboxylase (GAD) (a presynaptic marker of GABAergic synapses) (supplemental Fig. S8V,Y, available at www.jneurosci.org as supplemental material), the vesicular glutamate transporter vGlut1 (a presynaptic protein of glutamatergic synapses) (Fig. 4O,P; supplemental Fig. S8Q-T, available at www.jneurosci.org as supplemental material) and the neuronal KCl-co-transporter KCC2 (supplemental Fig. S8A-H,U,X, available at www.jneurosci.org as supplemental material). None of these or other stainings (supplemental Fig. S8, available at www.jneurosci.org as supplemental material) indicated significant differences between WT and *Nkcc1$^{-/-}$* brains, neither at P1 nor at P7.
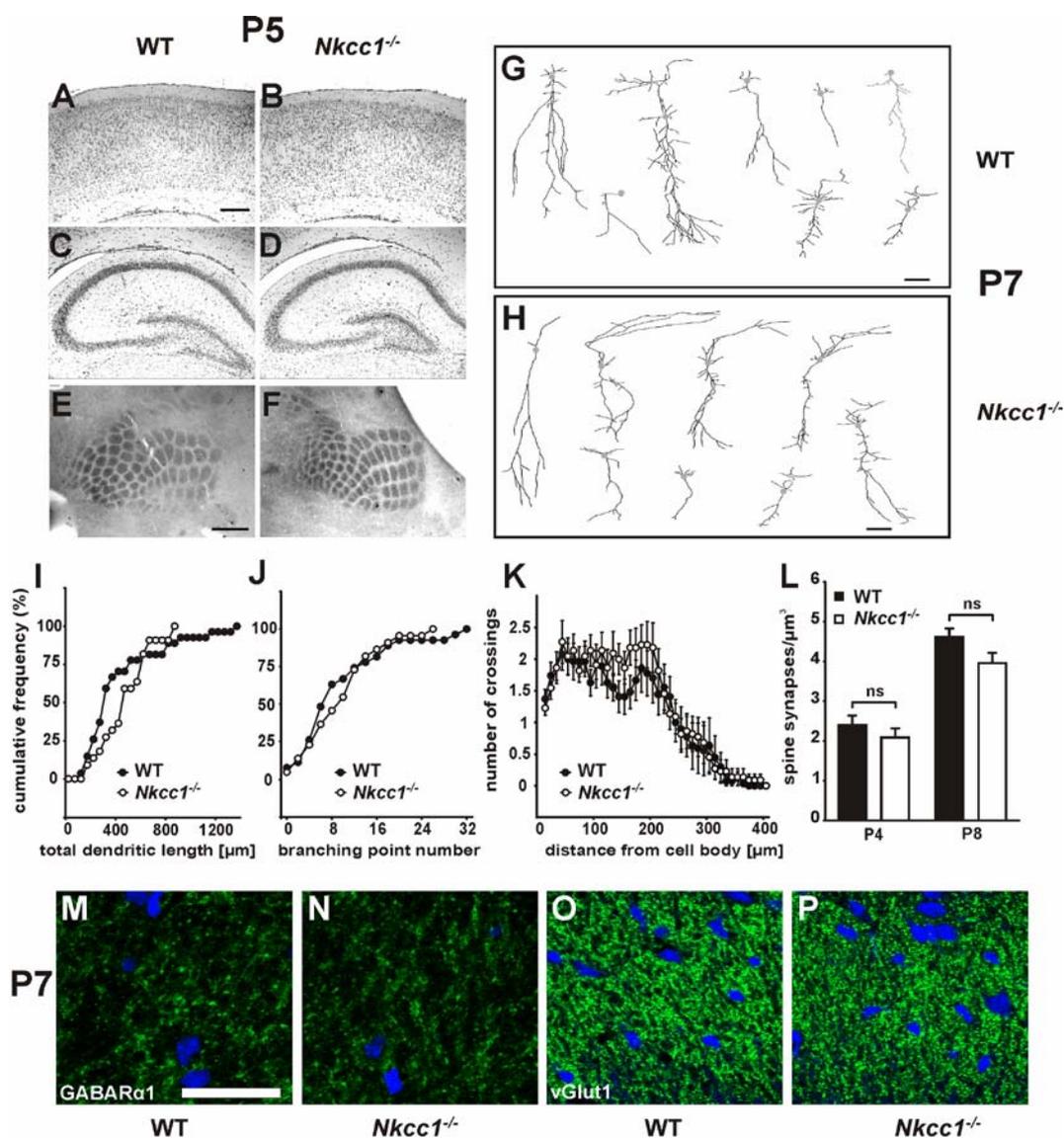
Figure 4: Gross morphology is intact in *Nkcc1^-/-* brain.

A–D, No obvious changes were detected in the layering of the cortex (**A**, **B**) and the hippocampus (**C**, **D**) in Nissl-stained sections. E, **F**, Analysis of the barrel cortex at P5 of WT (**E**) and *Nkcc1^-/-* mice (**F**) did not reveal any differences in sections stained for cytochrome oxidase. **G,H**, Two-dimensional projection of three-dimensional reconstruction of representative biocytin-filled P7 CA1 pyramidal neurons of WT (**G**) and *Nkcc1^-/-* (**H**) mice. Quantification of total dendritic length (**I**), branching point number (**J**), and Sholl test of dendritic complexity (**K**) revealed no major differences between WT and *Nkcc1^-/-* mice (WT: 5 mice, 27 cells; *Nkcc1^-/-*: 7 mice, 22 cells). **L**, Spine synapse numbers were unchanged in the stratum radiatum of CA1 neurons at P4 and P8 in *Nkcc1^-/-* (white bars) compared with WT (black bars) (4 mice per age and genotype). Error bars indicate SEM. Immunocytochemistry (**M–P**) of GABA$_A$ receptor subunit α1 (**M**, **N**) and vesicular glutamate transporter vGLUT1 (**O**, **P**) showed comparable staining of P7 stratum radiatum in WT (**M**, **O**) and *Nkcc1^-/-* (**N**, **P**) slices. Cell nuclei are stained in blue. Scale bars: (in **A**) **A–D**, 200 μm; (in **E**) **E**, **F**, 500 μm; (in G) G, H, 20 μm; (inM) **M**, **N**, 20 μm; (inM) **O**, **P**, 35 μm. Statistical analysis was as follow: total dendritic length: p > 0.05, Kolmogorov–Smirnov test; branching point number: p > 0.05, Kolmogorov–Smirnov test; Sholl test, p > 0.05, *t* test for individual data points; synapse number: p > 0.05, *t* test.

The maturation of excitatory and inhibitory synapses is delayed in CA1 pyramidal cells at P7

The absence of gross morphological abnormalities in *Nkcc1^-/-* animals did not exclude a functional deficit in synaptic transmission. To test basal synaptic transmission, we compared the size of the presynaptic fiber volley (input) with the slope of the excitatory postsynaptic field potential (output) in the stratum radiatum of CA1. No differences were found between genotypes at P15, a time point after the GABA-switch in that region (Stein et al., 2004b) (supplemental Fig. S9A, available at www.jneurosci.org as supplemental material). Paired-pulse facilitation at 40 ms and 100 ms pulse interval (150 ms not shown) was not significantly altered either, excluding a major presynaptic defect at this time point (supplemental Fig. S9B, available at www.jneurosci.org as supplemental material).

During early postnatal development, excitatory hippocampal synapses contain mainly NMDA receptors and lack AMPA receptors (Durand et al., 1996; Tyzio et al., 1999). To examine the maturation of excitatory synaptic transmission, the relative contribution of CA1 AMPA versus NMDA receptors was measured at the end of the first postnatal week, when NKCC1 is rapidly replaced by KCC2 in the WT, and at P15, when KCC2 plays the major role in neuronal chloride homeostasis. Whereas the AMPA/NMDA ratio was unaltered at P15, it was reduced in *Nkcc1^-/-* slices at P7 to 1.3 ± 0.1 (*Nkcc1^-/-*) versus 1.8 ± 0.1 in WT (Fig. 5A). To understand the basis of the reduction of the AMPA/NMDA ratio, we evaluated mEPSCs.
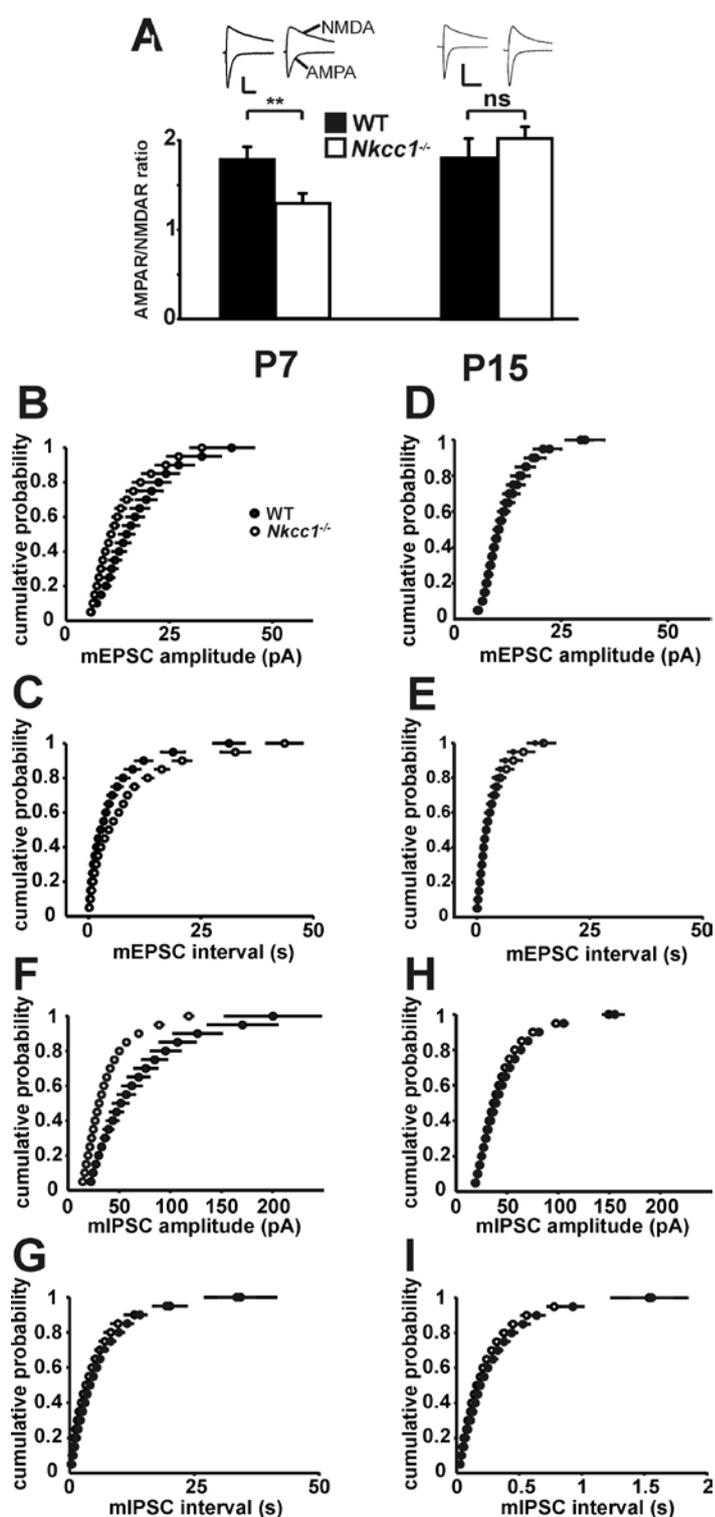
Figure 5: Delayed maturation of glutamatergic and GABAergic synapses in *Nkcc1⁻ᐟ⁻* CA1 neurons.

A, AMPA/NMDA ratio is reduced in *Nkcc1⁻ᐟ⁻* CA1 neurons at P7 but not at P15 (P7: 5 mice per genotype; WT, 25 cells; KO, 26 cells; P15: 3 mice per genotype; WT, 8 cells, KO, 10 cells; mean SEM). Representative current traces for WT and *Nkcc1⁻ᐟ⁻* CA1 neurons at P7 and P15 are shown above. Stimulation artifacts were omitted for clarity. Calibration: P7: vertical, 40 pA; horizontal, 50 ms; P15: vertical, 100 pA; horizontal, 100 ms. **B**, **C**, mEPSCs are reduced in amplitude (**B**) and frequency (**C**) at P7, but not at P15 (**D**, **E**) in *Nkcc1⁻ᐟ⁻* CA1 neurons as shown in cumulative distribution plots (3 mice per age and genotype; P7: WT, 10 cells; KO, 11 cells; P15: WT, 9 cells; KO, 10 cells; P7: amplitude, $p < 0.005$; interval, $p < 0.005$; P15: amplitude, $p > 0.1$; interval, $p > 0.1$; Kolmogorov–Smirnov test). **F**, **G**, In *Nkcc1⁻ᐟ⁻* CA1 neurons, mIPSCs are reduced in amplitude (**F**) but not frequency (**G**) at P7, whereas they were unchanged at P15 (**H**, **I**) as shown in cumulative distribution plots (3 mice per age and genotype; P7: WT, 8 cells; KO, 16 cells; P15: WT, 23 cells; KO, 30 cells; P7: amplitude, $p < 0.0005$; interval, $p > 0.1$; P15: amplitude, $p > 0.1$; interval, $p > 0.1$; Kolmogorov–Smirnov test). The asterisks indicate significance (**$p < 0.01$, *t* test).

Similar to the changes in AMPA/NMDA ratio, mEPSC amplitudes and frequencies were reduced at P7 (Fig. 5B,C), but not at P15 (Fig. 5D,E), indicating a delay in the maturation of excitatory synapses in the absence of NKCC1. Similar to mEPSCs, the amplitudes of mIPSCs of *Nkcc1*^{-/-} CA1 pyramidal neurons were reduced at P7. This difference had vanished at P15. mIPSC frequencies were unchanged throughout (Fig. 5F–I). These results indicate an influence of NKCC1 on the maturation of GABAergic synapses.

AMPA receptors are the major source of CA1 postsynaptic glutamatergic depolarization in the adult brain (Bredt and Nicoll, 2003). Phosphorylation of specific serines of GluR1 and GluR4 is important for their regulated postsynaptic insertion (Boehm and Malinow, 2005). We therefore analyzed the phosphorylation state of GluR1 and GluR4 with phosphospecific antibodies. GluR1 phosphorylation at serines 831 and 845 was not significantly altered betweenWTand *Nkcc1*^{-/-} hippocampus at P5 and P15 (supplemental Fig. S7E,F, available at www.jneurosci.org as supplemental material). In contrast, GluR4 phosphorylation at serine 842 was moderately, but significantly decreased compared with WT at P5 (Fig. 6A) and drastically increased at P15 (Fig. 6B). At both time points, total amounts of GluR1, GluR2, and GluR4 did not differ between the genotypes neither on protein (Fig. 6A,B; supplemental Fig. S7A–C,E,F, available at www. jneurosci.org as supplemental material) nor on RNA levels (supplemental Fig. S10, available at www.jneurosci.org as supplemental material). In the hippocampal formation, GluR4 mainly localized to GABAergic interneurons at P15 in WT and *Nkcc1*^{-/-} animals (supplemental Fig. S11, available at www.jneurosci.org as supplemental material). The decrease in S842 phosphorylation of GluR4 in the hippocampus of young *Nkcc1*^{-/-} animals might be a consequence of the decreased and mostly uncorrelated neuronal activity (Fig. 2) and may underlie the observed decreased AMPA/NMDA ratio at P7 (Fig. 5A).

To determine whether changes in spontaneous neuronal activity in *Nkcc1*^{-/-} hippocampi may also induce more global changes, we analyzed the phosphorylation states of the transcriptional regulator CREB (cAMP-responsive element binding protein), which plays a key role in changing glutamatergic transmission in long-term plasticity, and of the upstream ERK1/2 (extracellular signal-regulated kinases 1/2).We could not detect significant differences between the genotypes in the phosphorylation states of these proteins, neither at P5 nor at P15 (supplemental Fig. S7G,H, available at www.jneurosci.org as supplemental material).
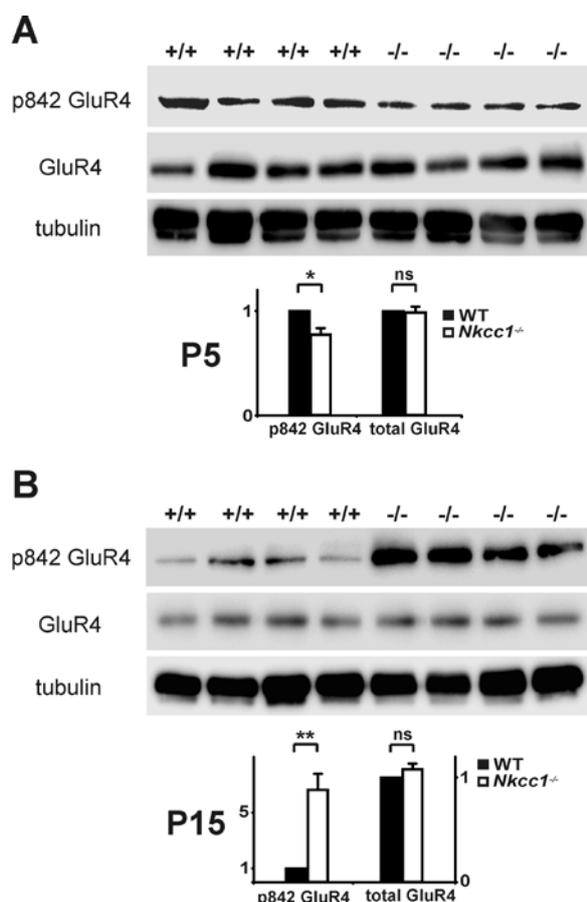
Figure 6: Differential GluR4 phosphorylation during development.

A,B, Compared with WT, in the *Nkcc1*^{-/-} hippocampus serine 842 of GluR4 is less phosphorylated at P5 (**A**) and more phosphorylated at P15 (**B**). Quantification of total and phosphorylated (at serine 842) GluR4 is shown below the respective Western blots (normalized to tubulin ± SEM; P5: n = 12 animals per genotype, P15: n = 4 animals per genotype). The asterisks indicate significance (*p < 0.05, **p < 0.01, t test).

lynx1, a modulator of network activity, is decreased in the developing *Nkcc1*^{-/-} hippocampus

The changes in spontaneous activity in the *Nkcc1*^{-/-} hippocampus prompted us to look for alterations in expression levels of activity-dependent genes, genes important for GABAergic function, and genes involved in postsynaptic glutamatergic transmission (supplemental Figs. S7A–D, S10, available at www.jneurosci.org as supplemental material). Except for Olig1 (Fig. 7A), a transcription factor important for oligodendrocyte function and for neural precursor cell differentiation (Ross et al., 2003), no significant changes in the expression of genes enumerated in supplemental Figure S10 (available at www.jneurosci.org as supplemental material) were found by either quantitative RT-PCR or Western blot analysis. We also performed a chip-based comparison of the transcriptome of WT and *Nkcc1*^{-/-} hippocampus at P5. Differentially expressed transcripts (verified by RT-PCR) were the transcriptional regulator Id4, which is important for neural progenitor proliferation and differentiation (Yun et al., 2004; Bedford et al., 2005), the cell cycle-associated gene G0s2 (Russell and Forsdyke, 1991), the gene encoding the neurofilament heavy chain, as well as lynx1 (Fig. 7A, B; supplemental Fig. S12, available at www.jneurosci.org as supplemental material). Lynx1 is a membrane-anchored protein that interacts with nicotinic acetylcholine receptors (nAChRs) and thereby influences neuronal excitability (Ibanez-Tallon et al.,
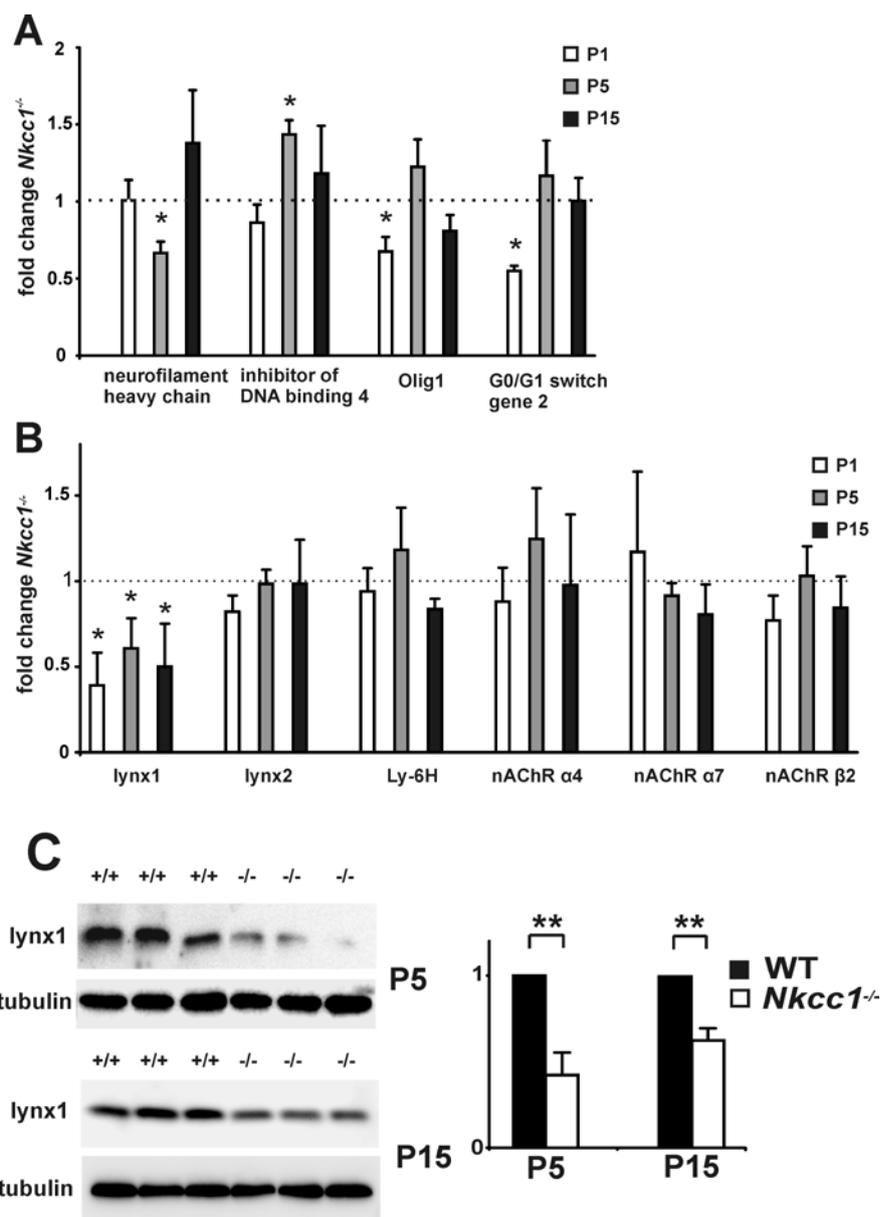
Figure 7: Transcriptional changes in *Nkcc1*$^{-/-}$ hippocampus.

A, Quantification of quantitative RT-PCR (qRT-PCR) of neurofilament heavy chain, Id4, G0s2 (found in gene chip analysis), and Olig1 (found in independent screen) at different ages during development (normalized to WT ± SEM; n = 3 animals per genotype and age). **B**, lynx1 mRNA is downregulated in the *Nkcc1*$^{-/-}$ hippocampus at different ages during early development as assessed by qRT-PCR, whereas nicotinic receptor subunits α4, α7, α2, and lynx1-related genes (lynx2, Ly-6H) are unaffected (normalized to WT ± SEM; n = 3 animals per genotype). **C**, Lynx1 protein is downregulated in the *Nkcc1*$^{-/-}$ hippocampus at P5 and P15. Quantifications are shown to the right of Western blots (normalized to tubulin ± SEM; 6 animals per genotype and age). The asterisks indicate significance (*p < 0.05, **p < 0.01, *t* test).

2002; Miwa et al., 2006). Lynx1 was downregulated both at the mRNA (P1, P5, P15) (Fig. 7B) and at the protein level (P5 and P15) (Fig. 7C). In contrast, expression levels of lynx2 and Ly-6H (Fig. 7B), proteins related to lynx1 and expressed in the hippocampus (Dessaud et al., 2006), were unchanged. The abundance of the transcripts encoding the α7, α4, and β2 subunits onAChRs, known targets of lynx1 that are expressed in the early hippocampus, were not changed either (Fig. 7B). In conclusion, the expression of a small subset of genes involved in cell differentiation, proliferation, and network excitability were changed in the absence of NKCC1.

2.5   Discussion

Chloride accumulation via NKCC1 significantly contributes to GABA dependent depolarization early in development

The excitatory action of GABA on immature neurons is a consequence of active chloride accumulation. The Na-K-2Cl co-transporter NKCC1, a chloride loader, is expressed early during neuronal differentiation (Hübner et al., 2001a). Application of bumetanide, a NKCC1 inhibitor, shifted the GABA reversal potential by -10 mV in P1-P3 cortical neurons (Yamada et al., 2004) and by -13 to -18 mV in CA3 pyramidal cells (Dzhala et al., 2005; Sipilä et al., 2006). In a genetic approach we used $Nkcc1^{-/-}$ mice to examine the role of NKCC1 in determining $[Cl^-]_i$ and in brain maturation. The GABA reversal potential was shifted by approximately -10 mV in $Nkcc1^{-/-}$ pyramidal cells, identifying NKCC1 as a major chloride loader in these neurons. GABA was still depolarizing and could trigger Ca^{2+} transients by opening voltage-dependent Ca^{2+}-channels (Yuste and Katz, 1991; Owens et al., 1996) in the absence of NKCC1. At P1 the anion exchanger AE3 is expressed at low levels in the hippocampus and did not contribute to chloride loading in CA1 cells in the presence of NKCC1. However, we cannot exclude that it raises Cl^- in the absence of this major Cl^- loader. At P5, expression levels of AE3 are higher and disruption of AE3 led to a decrease in GDPs. This decrease in GDP frequency suggests an effect of diminished intracellular chloride. An increased HCO_3^- efflux through $GABA_A$ receptors owed to an increase in cellular HCO_3^- (another possible outcome of the AE3 KO) should rather lead to an increase in excitability and hence GDPs. The unchanged steady-state intracellular pH in $Ae3^{-/-}$ neurons (Hentschke et al., 2006) makes it unlikely that AE3 influences GDPs by changing pH-dependent conductances.

Network-driven calcium events and GDPs are diminished in *Nkcc1$^{-/-}$* mice

Long-lasting elevations of intracellular calcium concentration can be observed in the early hippo-campus. The underlying mechanisms change during hippocampal development (Garaschuk et al., 1998; Crepel et al., 2007). At late embryonic stages, small ensembles of neurons show calcium events which depend strongly on voltage-gated Ca^{2+}-channels, but not on $GABA_A$-receptors. Around birth, long lasting gap junction-mediated calcium plateaus appear. They disappear grad-ually during the following days, while the number of calcium elevations driven by GDPs increases with ongoing hippocampal maturation and increasing synaptic connectivity. GDPs are population discharges that mainly originate in the CA3 subfield and propagate to CA1, thereby affecting the entire hippocampal network (Menendez de la Prida et al., 1998). They depend on synaptic transmission and involve both the action of glutamate and of depolarizing GABA, gradually dis-appearing in parallel to the GABA-switch during the second postnatal week (Ben-Ari et al., 1989; Sipilä et al., 2005). As glutamatergic synapses between CA3 and CA1 neurons are initially purely NMDA receptor-based (Durand et al., 1996; Tyzio et al., 1999), GABA-induced depolarization may be needed to facilitate glutamatergic transmission by weakening the voltage-dependent Mg^{2+}-block of NMDA receptors (Leinekugel et al., 1997). In *Nkcc1$^{-/-}$* mice, extracellular GDPs in CA3 were indeed diminished in amplitude and frequency. The relative lack of synchronicity of calcium events in the *Nkcc1$^{-/-}$* hippocampus at P2 and P4 suggests that the electrical synchroniza-tion of large neuronal ensembles depends on depolarizing GABA at that developmental stage. Both recurrent glutamatergic connections between pyramidal neurons (Miles and Wong, 1983; Sipilä et al., 2006) as well as synchronous activation of interneurons that excite multiple target neurons via excitatory GABA transmission (Khazipov et al., 1997b; Garaschuk et al., 1998) were proposed as mechanisms for synchronization. Our results favor the latter mechanism and show that the generation and propagation of early network activity critically depends on high $[Cl^-]_i$ that is established by NKCC1. At P10, when in the WT the chloride loader NKCC1 is largely replaced by the chloride extruder KCC2, GDPs in *Nkcc1$^{-/-}$* hippocampi were indistinguishable from the WT.

Delayed maturation of glutamatergic and GABAergic transmission in *Nkcc1$^{-/-}$* mice

Correlated spiking of pre- and postsynaptic neurons can result in strengthening or weakening of glutamatergic synapses, depending on the temporal order of spiking. Pairing of GDPs with Schaf-fer collateral stimulation can enhance the efficacy of these glutamatergic synapses (Mohajerani et al., 2007). Therefore, the observed decrease in coincident activity in *Nkcc1$^{-/-}$* hippocampus might change glutamatergic transmission between the Schaffer collaterals and CA1 neurons.

Indeed, evoked AMPA eEPSCs in CA1 were decreased compared to NMDA eEPSCs at P7. Moreover, the amplitudes and frequencies of spontaneous mEPSCs were diminished in *Nkcc1$^{-/-}$* mice at that time. The decreased frequency is most likely caused by poor detection of small events, rather than a decrease in synapse number. This interpretation is corroborated by our observation that the number of synaptic spines is unchanged in the KO compared to WT.

These change in excitatory synaptic transmission may result from a differential insertion of receptors into the postsynaptic membrane rather than from differential transcription (Malenka and Bear, 2004). Indeed, we did not detect differences between the genotypes in mRNA and protein levels of different GluR subunits, neither at P5 nor at P15. We suggest that the decreased S842 phosphorylation of GluR4 observed at P5 is a consequence of the decreased and largely uncorrelated electrical activity of the *Nkcc1$^{-/-}$* hippocampus. Because phosphorylation may stimulate the incorporation of glutamate receptors into silent synapses (Zhu et al., 2000; Esteban et al., 2003), such a mechanism could explain the decrease in AMPA/NMDA ratio in P7 *Nkcc1$^{-/-}$* hippocampus. No differences in GluR1 phosphorylation were detected, consistent with the predominant role of GluR4 in activity-dependent maturation of silent synapses (Zhu et al., 2000).

The changes in glutamatergic transmission disappear at P15 when NKCC1 expression in pyramidal neurons has declined in favor of KCC2 and when GDPs do not differ anymore between genotypes. The impressive increase in phosphorylation of GluR4 at S842 in P15 *Nkcc1$^{-/-}$* hippocampus was not associated with a changed AMPA/NMDA ratio of pyramidal cells, quite in contrast to the correlation between decreased GluR4 phosphorylation and decreased AMPA/NMDA ratio at earlier time points. This difference can be explained by the shift in expression pattern of GluR4 from pyramidal cells to interneurons in adult hippocampus (Fig. S11) (Kullmann and Lamsa, 2007). The increased GluR4 phosphorylation therefore probably occurs in interneurons, rather than in pyramidal cells that were studied electrophysiologically.

The maturational delay also extended to GABAergic synapses, with mIPSC amplitudes being lower in *Nkcc1$^{-/-}$* mice at P7, but not at P15. Similar to the amplitude changes observed for mEPSCs, these amplitude changes may result from changes in the numbers of postsynaptic receptors. Compared to mEPSCs, mIPSCs have much larger amplitudes under our recording conditions. Therefore, fewer events escaped detection in the KO, the result being that we measured similar frequencies to WT.

The shift of the GABA reversal potential in *Nkcc1$^{-/-}$* pyramidal cells (Fig. 1) was not associated with an increase of KCC2 transcript and protein levels (Fig. 1B, Fig. S7D). Together with previous work (Ludwig et al., 2003; Titz et al., 2003; Wojcik et al., 2006), our results do not support a role

of depolarizing GABA in inducing KCC2 expression, an effect previously reported in cultured neurons (Ganguly et al., 2001).

Expression analysis of *Nkcc1*^{-/-} hippocampus

Genome-wide expression analysis revealed a downregulation of lynx1 in *Nkcc1*^{-/-} hippocampus at P1, P5 and P15. Lynx1, a membrane-tethered protein, reduces the agonist sensitivity of nicotinic acetylcholine receptors and accelerates their desensitization, thereby decreasing neuronal excitation (Ibañez-Tallon et al., 2002; Miwa et al., 2006). A downregulation of lynx1 should increase neuronal excitability, thereby partially compensating for the diminished GABAergic excitation in *Nkcc1*^{-/-} mice. Thus, our data suggest a previously unrecognized role of lynx1 in early network homeostasis.

No obvious defects in brain morphology of *Nkcc1*^{-/-} mice

Despite of the trophic effects of depolarizing GABA on neurite extension, neuronal migration, differentiation, and synaptogenesis (Komuro and Rakic, 1998; Ben-Ari, 2002), no morphological alterations were observed in *Nkcc1*^{-/-} hippocampal neurons, which displayed normal dendritic length, branching, and spine synapse density. However, inducing a hyperpolarizing GABA-response by prematurely expressing KCC2 in a subpopulation of rat ventricular neuronal progenitor cells impaired their dendritic arborization (Cancedda et al., 2007). These differences might be explained by the fact that GABA was still slightly depolarizing in *Nkcc1*^{-/-} neurons. Additionally, one must distinguish between manipulations of individual neurons within a normally developing network and manipulations of the global network as in our study. Indeed, the number of functional synapses in developing cultured neurons was reduced when their electrical activity was suppressed individually, but not when all neurons were uniformly suppressed (Burrone et al., 2002). Similarly, expression of short hairpin RNAs against NKCC1 in just a small subset of newborn granular neurons or ventricular neuronal progenitor cells changed synapse formation and dendritic development (Ge et al., 2006; Wang and Kriegstein, 2008).

    We also identified differences in mRNA levels of Olig1 and Id4, transcription factors with a role in brain development (Ross et al., 2003; Yun et al., 2004; Bedford et al., 2005), as well as of the cell cycle related gene G0s2 (Russell and Forsdyke, 1991). Those findings suggest that GABAergic excitation may influence early transcriptional processes involved in cell proliferation and differentiation, even though we did not detect changes in hippocampal architecture.

In summary, our analysis showed a major role of NKCC1-dependent Cl$^-$-accumulation in the excitatory action of GABA. *Nkcc1* disruption severely affected early spontaneous electrical activity and transiently delayed the maturation of glutamatergic and GABAergic synapses without, however, leading to detectable morphological changes. Our work focusing on the role of NKCC1 in early network activity further suggests that future studies addressing the role of lynx1 in early network homeostasis may be warranted.

Acknowledgements

2.6   References

Aguilo A, Schwartz TH, Kumar VS, Peterlin ZA, Tsiola A, Soriano E, Yuste R (1999) Involvement of cajal-retzius neurons in spontaneous correlated activity of embryonic and postnatal layer 1 from wild-type and reeler mice. J Neurosci 19:10856-10868.

Bartos M, Vida I, Jonas P (2007) Synaptic mechanisms of synchronized gamma oscillations in inhibitory interneuron networks. Nat Rev Neurosci 8:45-56.

Bedford L, Walker R, Kondo T, van Cruchten I, King ER, Sablitzky F (2005) Id4 is required for the correct timing of neural differentiation. Dev Biol 280:386-395.

Ben-Ari Y (2002) Excitatory actions of gaba during development: the nature of the nurture. Nat Rev Neurosci 3:728-739.

Ben-Ari Y, Cherubini E, Corradetti R, Gaiarsa JL (1989) Giant synaptic potentials in immature rat CA3 hippocampal neurones. J Physiol 416:303-325.

Blanz J, Schweizer M, Auberson M, Maier H, Muenscher A, Hubner CA, Jentsch TJ (2007) Leukoencephalopathy upon disruption of the chloride channel ClC-2. J Neurosci 27:6581-6589.

Bosl MR, Stein V, Hubner C, Zdebik AA, Jordt SE, Mukhopadhyay AK, Davidoff MS, Holstein AF, Jentsch TJ (2001) Male germ cells and photoreceptors, both dependent on close cell-cell interactions, degenerate upon ClC-2 Cl(-) channel disruption. Embo J 20:1289-1299.

Brumback AC, Staley KJ (2008) Thermodynamic regulation of NKCC1-mediated Cl- cotransport underlies plasticity of GABA(A) signaling in neonatal neurons. J Neurosci 28:1301-1312.

Burrone J, O'Byrne M, Murthy VN (2002) Multiple forms of synaptic plasticity triggered by selective suppression of activity in individual neurons. Nature 420:414-418.

Cancedda L, Fiumelli H, Chen K, Poo MM (2007) Excitatory GABA action is essential for morpho-logical maturation of cortical neurons in vivo. J Neurosci 27:5224-5235.

Carvalho TP, Buonomano DV (2009) Differential effects of excitatory and inhibitory plasticity on synaptically driven neuronal input-output functions. Neuron 61:774-785.

Chenoy-Marchais D (1982) A Cl- conductance activated by hyperpolarization in Aplysia neurones. Nature 299:359-361.

Chesnoy-Marchais D (1983) Characterization of a chloride conductance activated by hyperpolari-zation in Aplysia neurones. The Journal of physiology 342:277-308.

Combi R, Grioni D, Contri M, Redaelli S, Redaelli F, Bassi MT, Barisani D, Lavitrano ML, Tredici G, Tenchini ML, Bertolini M, Dalpra L (2009) Clinical and genetic familial study of a large co-hort of Italian children with idiopathic epilepsy. Brain Res Bull 79:89-96.

Crepel V, Aronov D, Jorquera I, Represa A, Ben-Ari Y, Cossart R (2007) A parturition-associated nonsynaptic coherent activity pattern in the developing hippocampus. Neuron 54:105-120.

D'Agostino D, Bertelli M, Gallo S, Cecchin S, Albiero E, Garofalo PG, Gambardella A, St Hilaire JM, Kwiecinski H, Andermann E, Pandolfo M (2004) Mutations and polymorphisms of the CLCN2 gene in idiopathic epilepsy. Neurology 63:1500-1502.

Daoudal G, Debanne D (2003) Long-term plasticity of intrinsic excitability: learning rules and mechanisms. Learn Mem 10:456-465.

Durand GM, Kovalchuk Y, Konnerth A (1996) Long-term potentiation and functional synapse induction in developing hippocampus. Nature 381:71-75.

Dzhala VI, Talos DM, Sdrulla DA, Brumback AC, Mathews GC, Benke TA, Delpire E, Jensen FE, Staley KJ (2005) NKCC1 transporter facilitates seizures in the developing brain. Nat Med 11:1205-1213.

Esteban JA, Shi SH, Wilson C, Nuriya M, Huganir RL, Malinow R (2003) PKA phosphorylation of AMPA receptor subunits controls synaptic trafficking underlying plasticity. Nat Neurosci 6:136-143.

Everett K et al. (2007) Linkage and mutational analysis of CLCN2 in childhood absence epilepsy. Epilepsy research 75:145-153.

Ganguly K, Schinder AF, Wong ST, Poo M (2001) GABA itself promotes the developmental switch of neuronal GABAergic responses from excitation to inhibition. Cell 105:521-532.

Garaschuk O, Hanse E, Konnerth A (1998) Developmental profile and synaptic origin of early network oscillations in the CA1 region of rat neonatal hippocampus. J Physiol 507 219-236.

Ge S, Goh EL, Sailor KA, Kitabatake Y, Ming GL, Song H (2006) GABA regulates synaptic integra-tion of newly generated neurons in the adult brain. Nature 439:589-593.

Goldstein SA, Bockenhauer D, O'Kelly I, Zilberberg N (2001) Potassium leak channels and the KCNK family of two-P-domain subunits. Nat Rev Neurosci 2:175-184.

Grunder S, Thiemann A, Pusch M, Jentsch TJ (1992) Regions involved in the opening of ClC-2 chloride channel by voltage and cell volume. Nature 360:759-762.

Haug K et al. (2009) Retraction: Mutations in CLCN2 encoding a voltage-gated chloride channel are associated with idiopathic generalized epilepsies. Nature genetics 41:1043.

Hentschke M, Wiemann M, Hentschke S, Kurth I, Hermans-Borgmeyer I, Seidenbecher T, Jentsch TJ, Gal A, Hübner CA (2006) Mice with a targeted disruption of the Cl^-/HCO_3^- exchanger AE3 display a reduced seizure threshold. Mol Cell Biol 26:182-191.

Honore E (2007) The neuronal background K2P channels: focus on TREK1. Nat Rev Neurosci 8:251-261.

Hübner CA, Lorke DE, Hermans-Borgmeyer I (2001a) Expression of the Na-K-2Cl-cotransporter NKCC1 during mouse development. Mech Dev 102:267-269.

Hübner CA, Stein V, Hermans-Borgmeyer I, Meyer T, Ballanyi K, Jentsch TJ (2001b) Disruption of KCC2 reveals an essential role of K-Cl cotransport already in early synaptic inhibition. Neuron 30:515-524.

Huguenard JR, Alger BE (1986) Whole-cell voltage-clamp study of the fading of GABA-activated currents in acutely dissociated hippocampal neurons. J Neurophysiol 56:1-18.

Ibañez-Tallon I, Miwa JM, Wang HL, Adams NC, Crabtree GW, Sine SM, Heintz N (2002) Novel modulation of neuronal nicotinic acetylcholine receptors by association with the endogenous prototoxin lynx1. Neuron 33:893-903.

Iwasato T, Datwani A, Wolf AM, Nishiyama H, Taguchi Y, Tonegawa S, Knopfel T, Erzurumlu RS, Itohara S (2000) Cortex-restricted disruption of NMDAR1 impairs neuronal patterns in the barrel cortex. Nature 406:726-731.

Jentsch TJ, Stein V, Weinreich F, Zdebik AA (2002) Molecular structure and physiological function of chloride channels. Physiol Rev 82:503-568.

Jordt SE, Jentsch TJ (1997) Molecular dissection of gating in the ClC-2 chloride channel. Embo J 16:1582-1592.

Khazipov R, Leinekugel X, Khalilov I, Gaiarsa JL, Ben-Ari Y (1997) Synchronization of GABAergic interneuronal network in CA3 subfield of neonatal rat hippocampal slices. J Physiol 498 763-772.

Klausberger T, Somogyi P (2008) Neuronal diversity and temporal dynamics: the unity of hippocampal circuit operations. Science 321:53-57.

Komuro H, Rakic P (1998) Orchestration of neuronal migration by activity of ion channels, neurotransmitter receptors, and intracellular Ca^{2+} fluctuations. J Neurobiol 37:110-130.

Kullmann DM, Lamsa KP (2007) Long-term synaptic plasticity in hippocampal interneurons. Nat Rev Neurosci 8:687-699.

Leinekugel X, Medina I, Khalilov I, Ben-Ari Y, Khazipov R (1997) Ca^{2+} oscillations mediated by the synergistic excitatory actions of GABA(A) and NMDA receptors in the neonatal hippocampus. Neuron 18:243-255.

Ling DS, Benardo LS (1995) Activity-dependent depression of monosynaptic fast IPSCs in hippocampus: contributions from reductions in chloride driving force and conductance. Brain research 670:142-146.

Lu HC, She WC, Plas DT, Neumann PE, Janz R, Crair MC (2003) Adenylyl cyclase I regulates AMPA receptor trafficking during mouse cortical 'barrel' map development. Nat Neurosci 6:939-947.

Ludwig A, Li H, Saarma M, Kaila K, Rivera C (2003) Developmental up-regulation of KCC2 in the absence of GABAergic and glutamatergic transmission. Eur J Neurosci 18:3199-3206.

Madison DV, Malenka RC, Nicoll RA (1986) Phorbol esters block a voltage-sensitive chloride current in hippocampal pyramidal cells. Nature 321:695-697.

Malenka RC, Bear MF (2004) LTP and LTD: an embarrassment of riches. Neuron 44:5-21.

Marder CP, Buonomano DV (2003) Differential effects of short- and long-term potentiation on cell firing in the CA1 region of the hippocampus. J Neurosci 23:112-121.

McCarren M, Alger BE (1985) Use-dependent depression of IPSPs in rat hippocampal pyramidal cells in vitro. J Neurophysiol 53:557-571.

Menendez de la Prida L, Bolea S, Sanchez-Andres JV (1998) Origin of the synchronized network activity in the rabbit developing hippocampus. Eur J Neurosci 10:899-906.

Miles R, Wong RK (1983) Single neurones can initiate synchronized population discharge in the hippocampus. Nature 306:371-373.

Miwa JM, Stevens TR, King SL, Caldarone BJ, Ibañez-Tallon I, Xiao C, Fitzsimonds RM, Pavlides C, Lester HA, Picciotto MR, Heintz N (2006) The prototoxin lynx1 acts on nicotinic acetyl-choline receptors to balance neuronal activity and survival in vivo. Neuron 51:587-600.

Mladinic M, Becchetti A, Didelon F, Bradbury A, Cherubini E (1999) Low expression of the ClC-2 chloride channel during postnatal development: a mechanism for the paradoxical depo-larizing action of GABA and glycine in the hippocampus. Proc Biol Sci 266:1207-1213.

Mohajerani MH, Sivakumaran S, Zacchi P, Aguilera P, Cherubini E (2007) Correlated network activity enhances synaptic efficacy via BDNF and the ERK pathway at immature CA3 CA1 connections in the hippocampus. Proc Natl Acad Sci U S A 104:13176-13181.

Nehrke K, Arreola J, Nguyen HV, Pilato J, Richardson L, Okunade G, Baggs R, Shull GE, Melvin JE (2002) Loss of hyperpolarization-activated Cl(-) current in salivary acinar cells from Clcn2 knockout mice. The Journal of biological chemistry 277:23604-23611.

Obata K, Oide M, Tanaka H (1978) Excitatory and inhibitory actions of GABA and glycine on em-bryonic chick spinal neurons in culture. Brain research 144:179-184.

Owens DF, Kriegstein AR (2002) Is there more to GABA than synaptic inhibition? Nat Rev Neuros-ci 3:715-727.

Owens DF, Boyce LH, Davis MB, Kriegstein AR (1996) Excitatory GABA responses in embryonic and neonatal cortical slices demonstrated by gramicidin perforated-patch recordings and calcium imaging. J Neurosci 16:6414-6423.

Pace AJ, Lee E, Athirakul K, Coffman TM, O'Brien DA, Koller BH (2000) Failure of spermatogenesis in mouse lines deficient in the Na(+)-K(+)-2Cl(-) cotransporter. J Clin Invest 105:441-450.

Prange-Kiel J, Rune GM, Leranth C (2004) Median raphe mediates estrogenic effects to the hip-pocampus in female rats. Eur J Neurosci 19:309-317.

Ross SE, Greenberg ME, Stiles CD (2003) Basic helix-loop-helix factors in cortical development. Neuron 39:13-25.

Russell L, Forsdyke DR (1991) A human putative lymphocyte G0/G1 switch gene containing a CpG-rich island encodes a small basic protein with the potential to be phosphorylated. DNA Cell Biol 10:581-591.

Saint-Martin C, Gauvain G, Teodorescu G, Gourfinkel-An I, Fedirko E, Weber YG, Maljevic S, Ernst JP, Garcia-Olivares J, Fahlke C, Nabbout R, LeGuern E, Lerche H, Christophe Poncer J, De-pienne C (2009) Two novel CLCN2 mutations accelerating chloride channel deactivation are associated with idiopathic generalized epilepsy. Hum Mutat 30:397-405.

Schwartz TH, Rabinowitz D, Unni V, Kumar VS, Smetters DK, Tsiola A, Yuste R (1998) Networks of coactive neurons in developing layer 1. Neuron 20:541-552.

Sholl DA (1953) Dendritic organization in the neurons of the visual and motor cortices of the cat. Journal of anatomy 87:387-406.

Sik A, Smith RL, Freund TF (2000) Distribution of chloride channel-2-immunoreactive neuronal and astrocytic processes in the hippocampus. Neuroscience 101:51-65.

Sipilä ST, Huttu K, Soltesz I, Voipio J, Kaila K (2005) Depolarizing GABA acts on intrinsically bursting pyramidal neurons to drive giant depolarizing potentials in the immature hippocampus. J Neurosci 25:5280-5289.

Sipilä ST, Schuchmann S, Voipio J, Yamada J, Kaila K (2006) The cation-chloride cotransporter NKCC1 promotes sharp waves in the neonatal rat hippocampus. J Physiol 573:765-773.

Smith RL, Clayton GH, Wilcox CL, Escudero KW, Staley KJ (1995) Differential expression of an inwardly rectifying chloride conductance in rat brain neurons: a potential mechanism for cell-specific modulation of postsynaptic inhibition. J Neurosci 15:4057-4067.

Staff NP, Spruston N (2003) Intracellular correlate of EPSP-spike potentiation in CA1 pyramidal neurons is controlled by GABAergic modulation. Hippocampus 13:801-805.

Staley K (1994) The role of an inwardly rectifying chloride conductance in postsynaptic inhibition. J Neurophysiol 72:273-284.

Staley K, Smith R, Schaack J, Wilcox C, Jentsch TJ (1996) Alteration of GABAA receptor function following gene transfer of the CLC-2 chloride channel. Neuron 17:543-551.

Stein V, Hermans-Borgmeyer I, Jentsch TJ, Hübner CA (2004b) Expression of the KCl cotransporter KCC2 parallels neuronal maturation and the emergence of low intracellular chloride. J Comp Neurol 468:57-64.

Sterio DC (1984) The unbiased estimation of number and sizes of arbitrary particles using the disector. J Microsc 134:127-136.

Stobrawa SM, Breiderhoff T, Takamori S, Engel D, Schweizer M, Zdebik AA, Bosl MR, Ruether K, Jahn H, Draguhn A, Jahn R, Jentsch TJ (2001) Disruption of ClC-3, a chloride channel expressed on synaptic vesicles, leads to a loss of the hippocampus. Neuron 29:185-196.

Stogmann E, Lichtner P, Baumgartner C, Schmied M, Hotzy C, Asmus F, Leutmezer F, Bonelli S, Assem-Hilger E, Vass K, Hatala K, Strom TM, Meitinger T, Zimprich F, Zimprich A (2006) Mutations in the CLCN2 gene are a rare cause of idiopathic generalized epilepsy syndromes. Neurogenetics 7:265-268.

Thiemann A, Grunder S, Pusch M, Jentsch TJ (1992) A chloride channel widely expressed in epithelial and non-epithelial cells. Nature 356:57-60.

Thompson SM, Gahwiler BH (1989) Activity-dependent disinhibition. I. Repetitive stimulation reduces IPSP driving force and conductance in the hippocampus in vitro. J Neurophysiol 61:501-511.

Titz S, Hans M, Kelsch W, Lewen A, Swandulla D, Misgeld U (2003) Hyperpolarizing inhibition develops without trophic support by GABA in cultured rat midbrain neurons. J Physiol 550:719-730.

Tyzio R, Represa A, Jorquera I, Ben-Ari Y, Gozlan H, Aniksztejn L (1999) The establishment of GABAergic and glutamatergic synapses on CA1 pyramidal neurons is sequential and correlates with the development of the apical dendrite. J Neurosci 19:10372-10382.

Tyzio R, Minlebaev M, Rheims S, Ivanov A, Jorquera I, Holmes GL, Zilberter Y, Ben-Ari Y, Khazipov R (2008) Postnatal changes in somatic gamma-aminobutyric acid signalling in the rat hippocampus. The European journal of neuroscience 27:2515-2528.

Wang DD, Kriegstein AR (2008) GABA regulates excitatory synapse formation in the neocortex via NMDA receptor activation. J Neurosci 28:5547-5558.

Wojcik SM, Katsurabayashi S, Guillemin I, Friauf E, Rosenmund C, Brose N, Rhee JS (2006) A shared vesicular carrier allows synaptic corelease of GABA and glycine. Neuron 50:575-587.

Yamada J, Okabe A, Toyoda H, Kilb W, Luhmann HJ, Fukuda A (2004) Cl⁻ uptake promoting depolarizing GABA actions in immature rat neocortical neurones is mediated by NKCC1. J Physiol 557:829-841.

Yun K, Mantani A, Garel S, Rubenstein J, Israel MA (2004) Id4 regulates neural progenitor proliferation and differentiation in vivo. Development 131:5441-5448.

Yuste R, Katz LC (1991) Control of postsynaptic Ca^{2+} influx in developing neocortex by excitatory and inhibitory neurotransmitters. Neuron 6:333-344.

Zhu JJ, Esteban JA, Hayashi Y, Malinow R (2000) Postnatal synaptic potentiation: delivery of GluR4-containing AMPA receptors by spontaneous activity. Nat Neurosci 3:1098-1106.

Zuniga L, Niemeyer MI, Varela D, Catalan M, Cid LP, Sepulveda FV (2004) The voltage-dependent ClC-2 chloride channel has a dual gating mechanism. The Journal of physiology 555:671-682.

2.7   Supplemental material

NKCC1-Dependent GABAergic Excitation Drives Synaptic Network Maturation During Early Hippocampal Development

by

Carsten Pfeffer, Valentin Stein, Damien J. Keating, Hannes Maier, Ilka Rinke, York Rudhard, Moritz Hentschke, Gabriele Rune, Thomas J. Jentsch and Christian A. Hübner

Supplementary Table 1:

Sequence 5´ > 3´	Gene
CATGCCAGCAAAGCACCAT	AE3 forward
AGAAGTGCAATGCAGCCCA	AE3 reverse
CCGCCAAACCCAATGTGAT	Arc forward
TGCTTGGACACTTCGGTCAAC	Arc reverse
GCTGAAGGCGTGCGAGTATTA	BDNF ex4 forward
GAGTCTTTGGTGGCCGATATG	BDNF ex4 reverse
GGAATGGTGAAGACCGTGTCA	cFOS forward
CCCTTCGGATTCTCCGTTTCT	cFOS reverse
GCTTGTCGATTGCTCAGCTCA	Chrna4 forward
TCCCAGCGCAGTTTGTAGTCA	Chrna4 reverse
CTTTGCTGGTATTCTTGCTGCC	Chrna7 forward
ATCTCAGCCACAAGCAGCATG	Chrna7 reverse
GGAAGCCTGAGGATTTCGACA	Chrnb2 forward
AGACTTCGTACATGCCGTCAGC	Chrnb2 reverse
CCCGACAATGAGCAAACGTAC	Dopamine β-Hydroxylase forward
TTGGAAGACCTCCATGTGGTG	Dopamine β-Hydroxylase reverse
TTAAGGCCGGTGACTGACAGAG	G0S2 forward
TCCCAGACCCCTTAGGTGATCT	G0S2 reverse
GCGACCAAAATTCAGGCTAGC	GAP43 forward
TTCTCCACACCATCAGCAACG	GAP43 reverse
TTGAAGGCAATGACCGCTATG	GluR1 forward
TTTGCCGTCGCTGACAATC	GluR1 reverse
ACCTGGATTCCAAAGGCTACG	GluR2 forward
CCAACAGGCCTTGTTCATTCA	GluR2 reverse
CATTGAGCAGAGAAAGCCGTG	GluR3 forward

CGTTCCTAATGCTGAGCCTT	GluR3 reverse
AACCTCCCAATGAGTTTGGCA	GluR4 forward
ATACGCCTCCAACAATCCGAC	GluR4 reverse
TGCCTGCAGTGCGATATGAA	Id4 forward
GATAACGTGCTGCAGGATCTCC	Id4 reverse
TTGGCGCAAGATGCTAAAGAG	Itp3R forward
CCCGGAGATTTCATTGATGG	Itp3R reverse
TCGTTAAGCGGCACTTTTTCTC	Ly-6H forward
GCCCCGTTGCACAAATCTT	Ly-6H reverse
CCACACGAACTTACTTCACCCC	Lynx1 forward
AGATGCATGCTTGGAATAGCCA	Lynx1 reverse
CGTAAATTGCACCGTGAACGT	Lynx2 forward
AAGCAATGAGACAGGCTGCTG	Lynx2 reverse
AAACGCAAGATGACCAAGGC	NeuroD2 forward
TCGATCTTGGACAGCTTCTGC	NeuroD2 reverse
TACAGAAAGCTCCTGGAAGGC	Neurofilament heavy chain forward
TTATGTGCGTGGATATGGAGG	Neurofilament heavy chain reverse
TCCTCAGTCAGCCATACCCAAA	NKCC1 forward
ATCCCGAACAACACACGAACC	NKCC1 reverse
TCGAGGATACCAGATGTCCACC	NR1 forward
CCTCTTTGCATGTGCCATCAC	NR1 reverse
TGTTGATGTTCCCGCCTTTG	NR4A1 forward
ATGCGATTCTGCAGCTCTTCC	NR4A1 reverse
TGGCGGAAGACAAATGCAG	NRSF forward
TCCGGATGTGATGCACAAACT	NRSF reverse
TTGGAACCTGGAACCATGGAC	N-Tubulin b3 forward
ATAGTGCCCTTTGGCCCAGTT	N-Tubulin b3 reverse
TGTTGATGTTCCCGCCTTTG	Nur77 forward
ATGCGATTCTGCAGCTCTTCC	Nur77 reverse
TCCCACCTGTTTAGAGCCAGAA	Olig1 forward
CGATGCTCACGGATACGAGAAT	Olig1 reverse
TCAGGAGACACCGTCTTTTGG	SynGAP forward
AACGTAGCCAGCCTTGTCCTT	SynGAP reverse
CAAATGGCCTCCCTCTCATCA	TNFalpha forward
TTGGTGGTTTGCTACGACGTG	TNFalpha reverse
CCTGCGGCACATAAATTTCAC	TrkB-Receptor forward
AACGGATTACCCGTCAGGATC	TrkB-Receptor reverse
CTTCACAATCGAGTTCGGCCT	Tryptophan Hydroxylase 2 forward
CCTTGTCGGAAAGAGCATGCT	Tryptophan Hydroxylase 2 reverse
ACATTTGCCCAGTTCTCCCAG	Tyrosine Hydroxylase forward
CCCAAACTCCACAGTGAACCA	Tyrosine Hydroxylase reverse
AGGCCGAGATGCAATTGATGT	Zif268 forward
TCAGCAGCATCATCTCCTCCA	Zif268 reverse
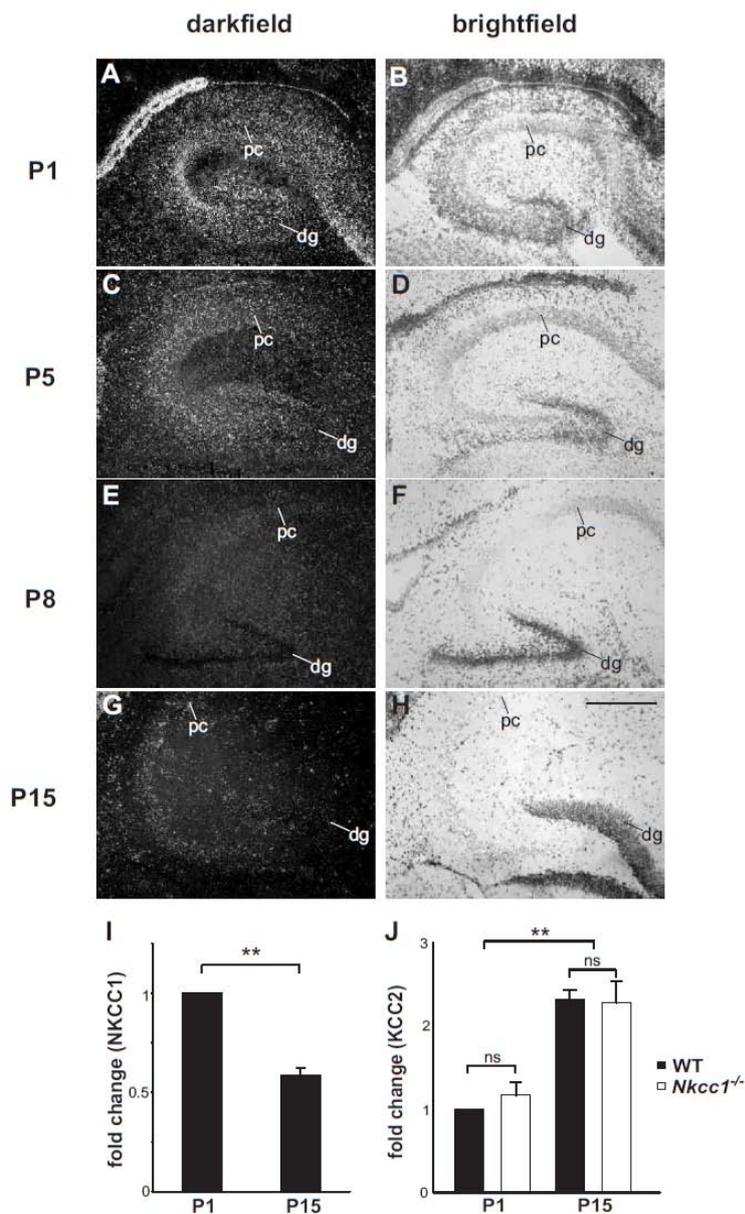
Figure S1: *In-situ* hybridization for *Nkcc1* transcripts in the developing hippocampus.

(A,C,E,G) Darkfield photomicrographs reveal a decrease of *Nkcc1* transcripts from postnatal day (P) 1 (P1) to P15. Signals in G most likely correspond to glial cells. Hybridization signals appear white in darkfield (sense controls gave no signal). (B,D,F,H) Photomicrographs of Giemsa-stained coronal brain sections at P1, P5, P8 and P15 corresponding to darkfield photomicrographs. (I) Nkcc1 transcript levels in the hippocampus decrease from postnatal day 1 (P1) to P15. Levels were determined by quantitative RT PCR, and normalized to those of hypoxanthine guanine phosphoribosyl transferase (HPRT), and to the WT values at P1 (mean ± SEM, n = 3 animals). (J) Kcc2 transcripts increased during the same period and did not change in *Nkcc1*$^{-/-}$ mice (n = 3 animals per genotype). Scale bar in (H) corresponds to 50 µm for (A-H); pc: pyramidal cell layer; dg: dentate gyrus. Asterisks (**) indicate significance (p < 0.01, t-test).
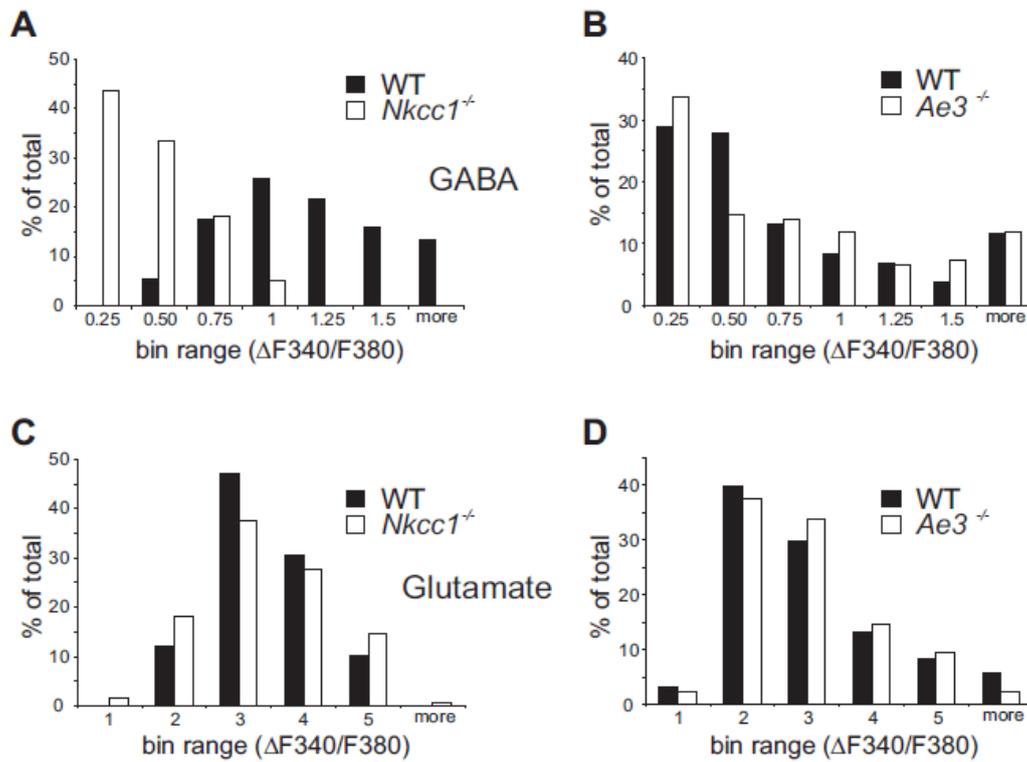
Figure S2: KO of *Nkcc1* but not of *Ae3* reduces the amplitude of GABA induced calcium elevations in CA1 neurons at P1.

(**A,B,C,D**) Histogram plots show amplitude distribution of Calcium elevations of WT (black bars) and KO (white bars) slices disrupted for *Nkcc1* (**A,C**) and *Ae3* (**B,D**) after GABA (**A,B**) and glutamate (**C,D**) application. (Nkcc1: WT 5 mice, 6 recordings, 108 cells; KO 5 mice, 7 recordings, 141 cells; Ae3: WT 3 mice, 7 recordings, 136 cells; KO 3 mice, 5 recordings, 191 cells). Different WT distributions may be due to differences in genetic background of NKCC1 and AE3 mouse lines (see methods/mice).
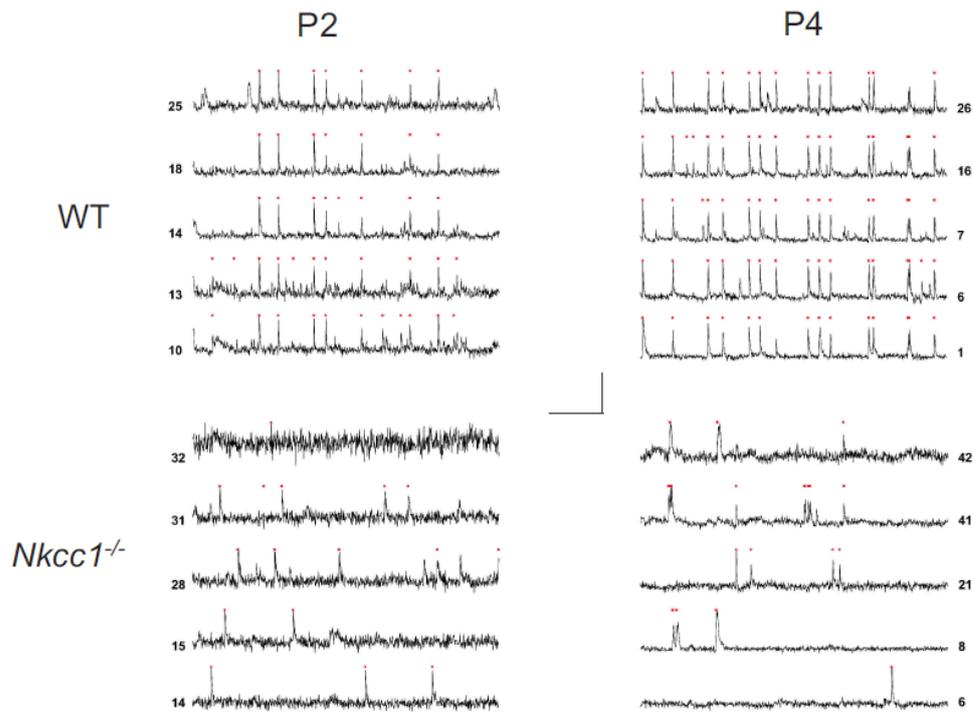
Figure S3A: Detection of spontaneous calcium transients.

Representative recordings from P2 and P4 WT and *Nkcc1*^{-/-} slices (also shown in Fig. 2A). Calcium transients that were identified by a mathematical routine (Suppl. Methods) are marked by red dots. Detection parameters were conservatively chosen to underestimate rather than to overestimate spike rates and synchronous events. Missed events were rare (< 10 %) while events that were erroneously assigned as calcium transients by the routine were minimized (< 2 %). Numbers assigned to each trace correspond to cells in the respective raster plot diagram (Fig. S3B). Scale bars: horizontal 100 s; vertical 0.15 F_{340}/F_{380}.
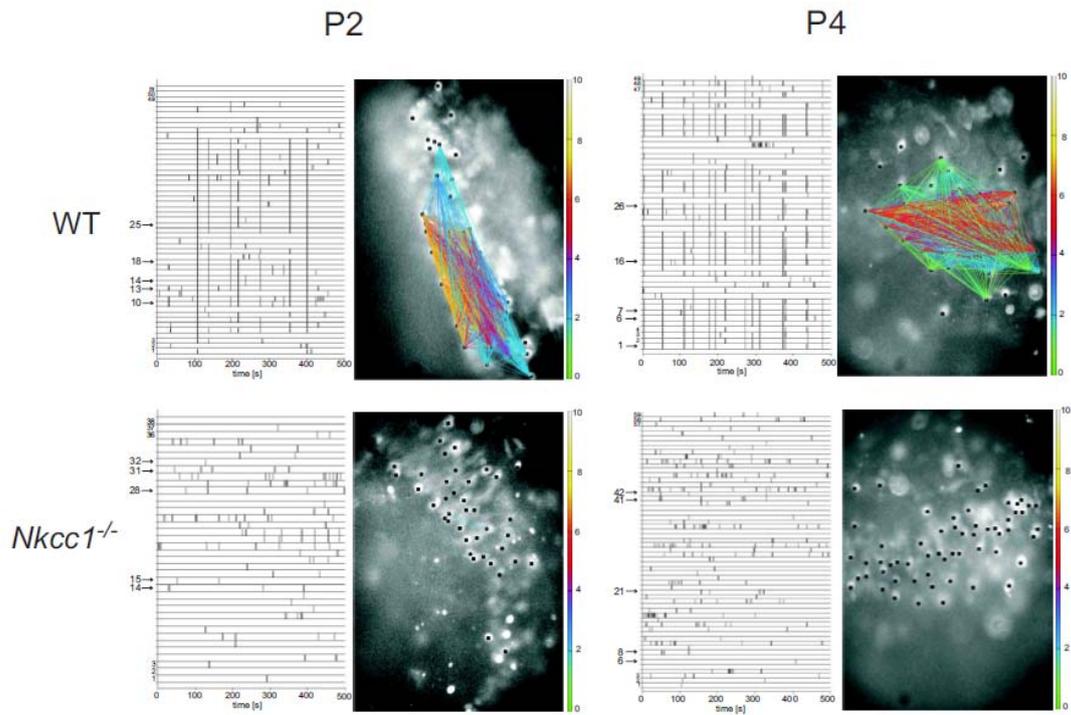
Figure S3B: Raster plot and correlation representation of individual calcium recordings.

The fura-2 loaded slice is shown at t=0 in each panel. Individual cells that were analyzed during the subsequent 500 s period are marked by black squares. On the left side of each panel the individual cellular calcium events of these cells, detected by the mathematical routine, are represented by vertical black lines. Each cell is represented by a white bar, bordered by horizontal black lines. The numbers with arrows refer to the traces displayed in Fig. S3A. Cells showing correlated activity are connected by a colored line in the right image of each panel. Color codes right to the image indicate strength of correlated activity by representing the number of synchronous events only for those cell pairs with significant (p<.001) synchronicity. WT cells show correlated activity all over the recorded area, while *Nkcc1*^{-/-} cells do not.
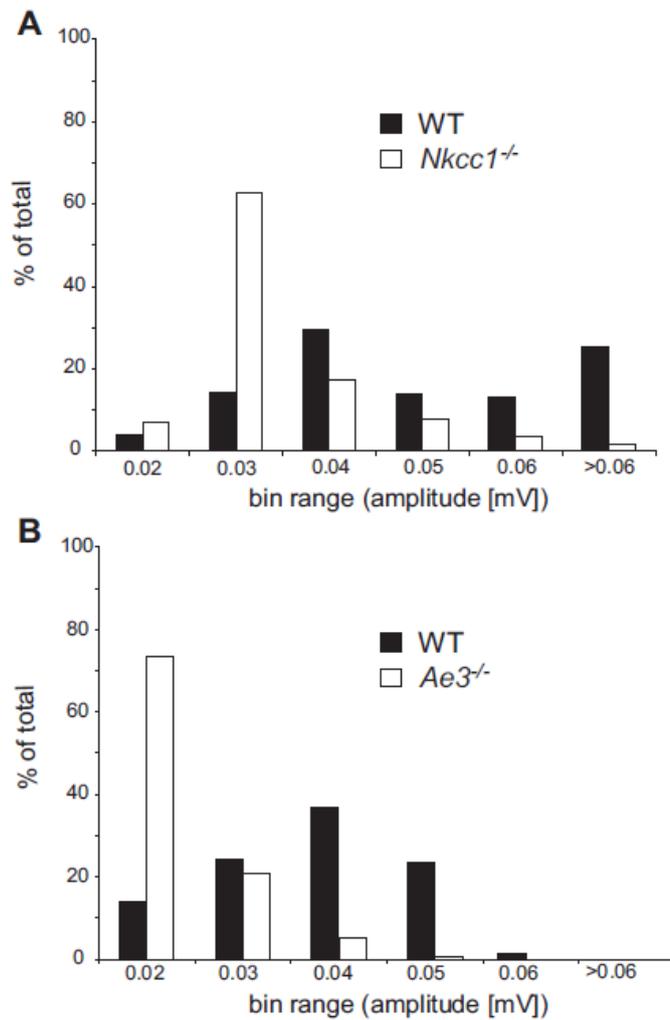
Figure S4: KO of *Nkcc1* or *Ae3* reduces the amplitudes of GDPs.

Histogram plots show amplitude distribution of GDPs of WT (black bars) and KO (white bars) slices disrupted for *Nkcc1* (**A**) and *Ae3* (**B**) (3 animals per genotype; Nkcc1: WT 15 slices, 331 GDP events; KO 19 slices, 115 GDP events; Ae3: WT 11 slices, 384 GDP events; KO 12 slices, 193 GDP events). Different WT distributions may be due to differences in genetic background of NKCC1 and AE3 mouse lines (see methods/mice).
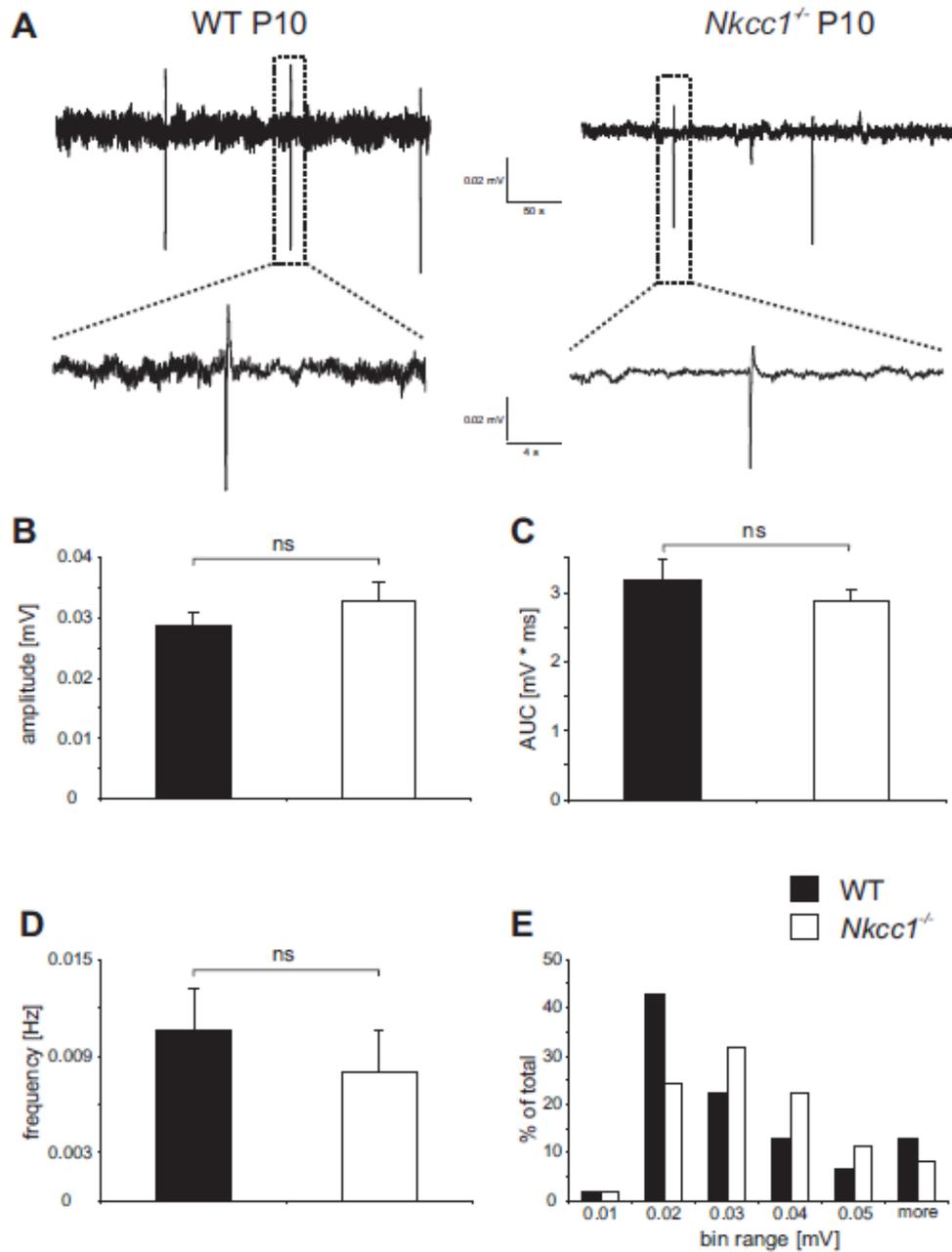
**Figure S5: GDPs at P10 were unchanged between WT and *Nkcc1*$^{-/-}$ animals.**

(**A**) representative traces showing typical GDPs in WT and *Nkcc1*$^{-/-}$ at p10. (**B,C,D,E**) Quantification of GDPs revealed unchanged amplitude (**B**), area under curve (**C**), frequency (**D**) and histogram plot distribution of the amplitude (**E**) of WT (black bar) and *Nkcc1*$^{-/-}$ (open bar) animals (3 animals per genotype; WT: 14 slices, *Nkcc1*$^{-/-}$: 17 slices; WT: 107 GDPs, *Nkcc1*$^{-/-}$: 98 GDPs). Scale bars are shown for the respective traces in (**A**).
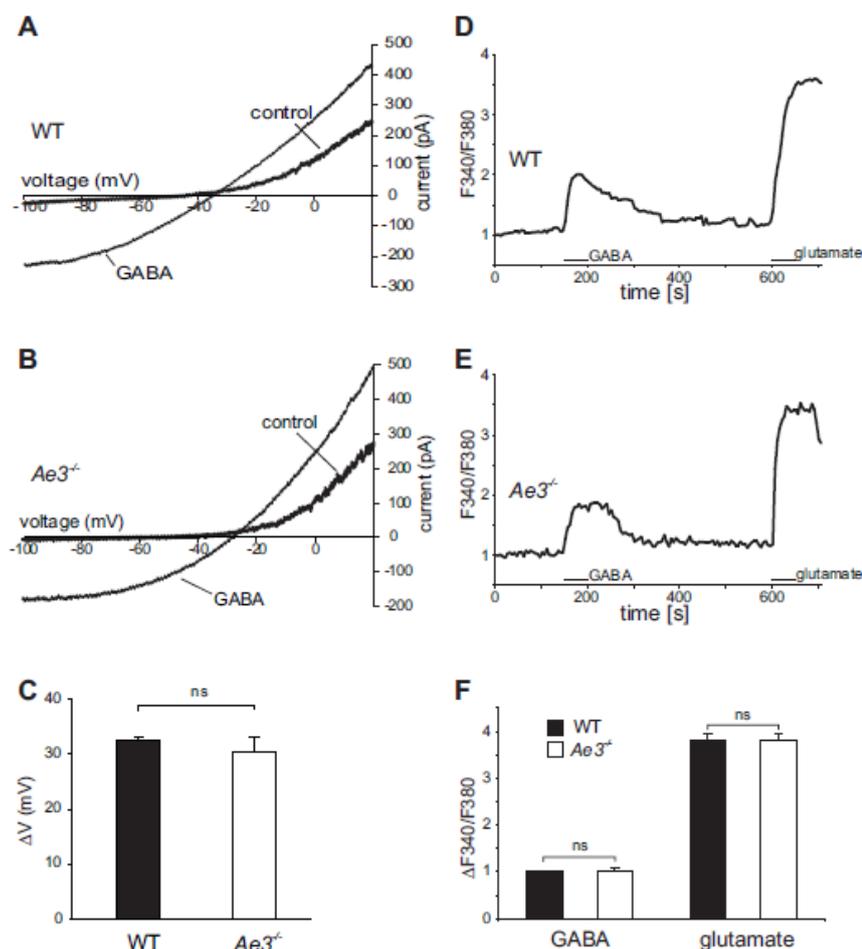
Figure S6: GABA-induced depolarization in hippocampal CA1 neurons does not depend on AE3 at P1.

(**A,B**) Representative current-voltage traces of hippocampal pyramidal CA1 neurons (P1) from both WT (**A**) and *Ae3$^{-/-}$* (**B**) mice using gramicidin-perforated patch-clamp recordings before and during application of 100 μM GABA. (**C**) Mean shift in reversal potential (mean ± SEM) upon application of 100 μM GABA in voltage clamp mode does not differ significantly between WT and *Ae3$^{-/-}$* CA1 neurons (WT: 6 cells from 3 mice, mean ± SEM = 20.2mV ± 4.6mV; *Ae3$^{-/-}$*: 10 cells from 6 mice, mean ± SEM = 23.4mV ± 3.3mV; p>0.5, t-test). (**D,E,F**) Ca^{2+} entry in response to GABA and glutamate in *Ae3$^{-/-}$* CA1 neurons at P1. (**D,E**) Typical fura-2 fluorescence traces indicative of intracellular calcium of a single WT (**D**) and *Ae3$^{-/-}$* (**E**) CA1 neuron sequentially exposed to GABA (100 μM) and glutamate (100 μM) for 50 s each. The ratio of fluorescence at 340 nm and 380 nm, which increases with [Ca^{2+}]$_i$, is given. (**F**) Ca^{2+} responses as indicated by mean (± SEM) changes in fura-2 fluorescence in response to GABA and glutamate in WT (filled bars) and *Ae3$^{-/-}$* (empty bars) P1 CA1 neurons normalized to WT GABA (WT: 136 cells, 7 recordings, 3 mice, GABA: normalized to 1, Glutamate: mean ± SEM = 3.80 ± 0.14; *Ae3$^{-/-}$*: 191 cells, 5 recordings, 3 mice; GABA: mean ± SEM = 1.01 ± 0.08, Glutamate: mean ± SEM = 3.79 ± 0.17; t-test GABA: p > 0.5, t-test Glutamate: p>0.5).
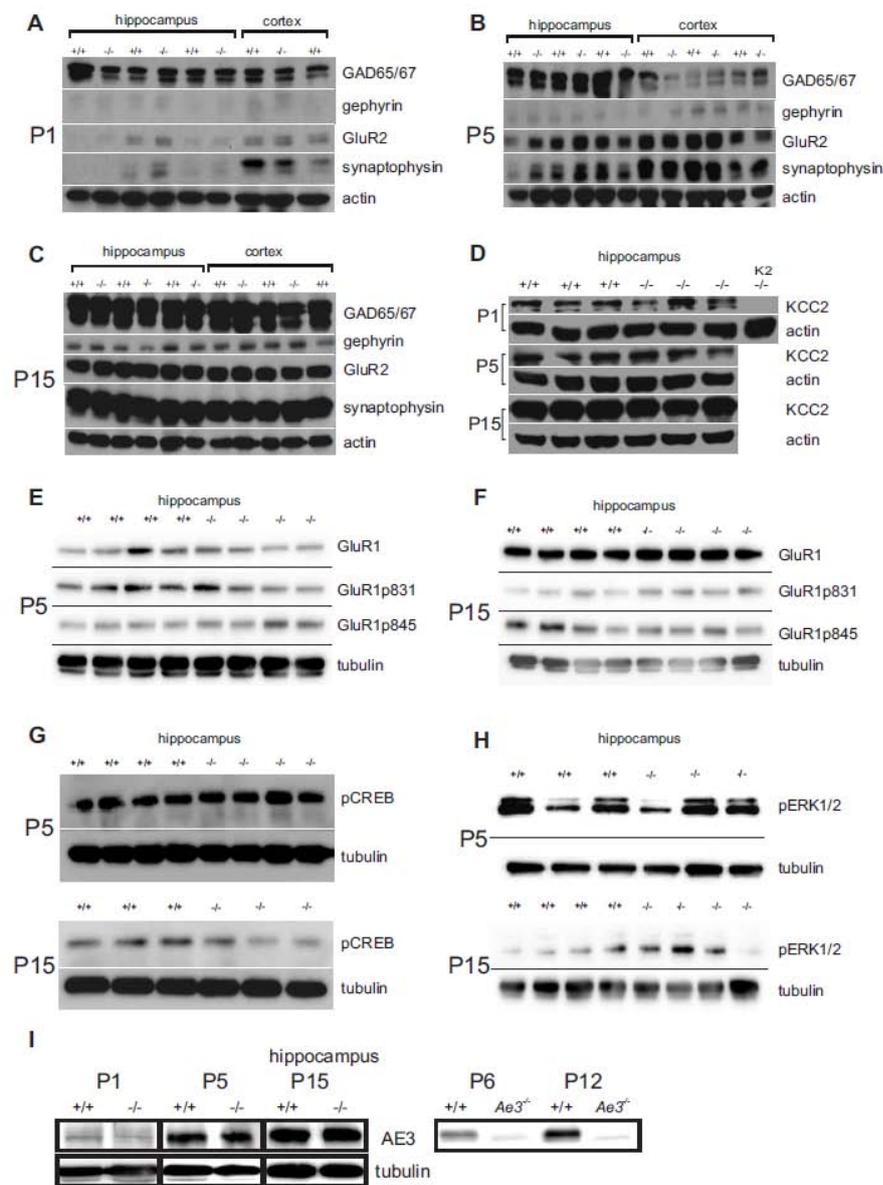
Figure S7: Normal pre- and postsynaptic marker protein levels in the *Nkcc1*$^{-/-}$ hippocampus.

(**A,B,C,D**) Hippocampal protein levels of glutamic acid decarboxylase (GAD) 65/67, gephyrin, the AMPA receptor subunit GluR2 and synaptophysin quantified by Western blots did not differ between genotypes at P1 (**A**), P5 (**B**), and P15 (**C**). Hippocampal KCC2 protein levels (**D**) were unchanged in *Nkcc1*$^{-/-}$ mice at P1, P5, and P15 (right lane labeled with K2$^{-/-}$ represents KCC2 KO control). Levels of hippocampal GluR1 and GluR1 phosphorylated at serines 831 or 845 did not differ significantly between genotypes at P5 (**E**) and P15 (**F**). Phosphorylated CREB (pCREB) and phosphorylated ERK1/2 (pERK1/2[p42/44 MAPK]) did not differ significantly between genotypes at P5 and P15 (**G,H**) either. (**I**) The anion exchanger AE3 shows developmental upregulation from P1 to P15 in the hippocampus. No expression level differences could be detected between WT and N*kcc1*$^{-/-}$ animals. Specificity of the antibody is shown with *Ae3*$^{-/-}$ and WT hippocampal tissue at P6 and P12.
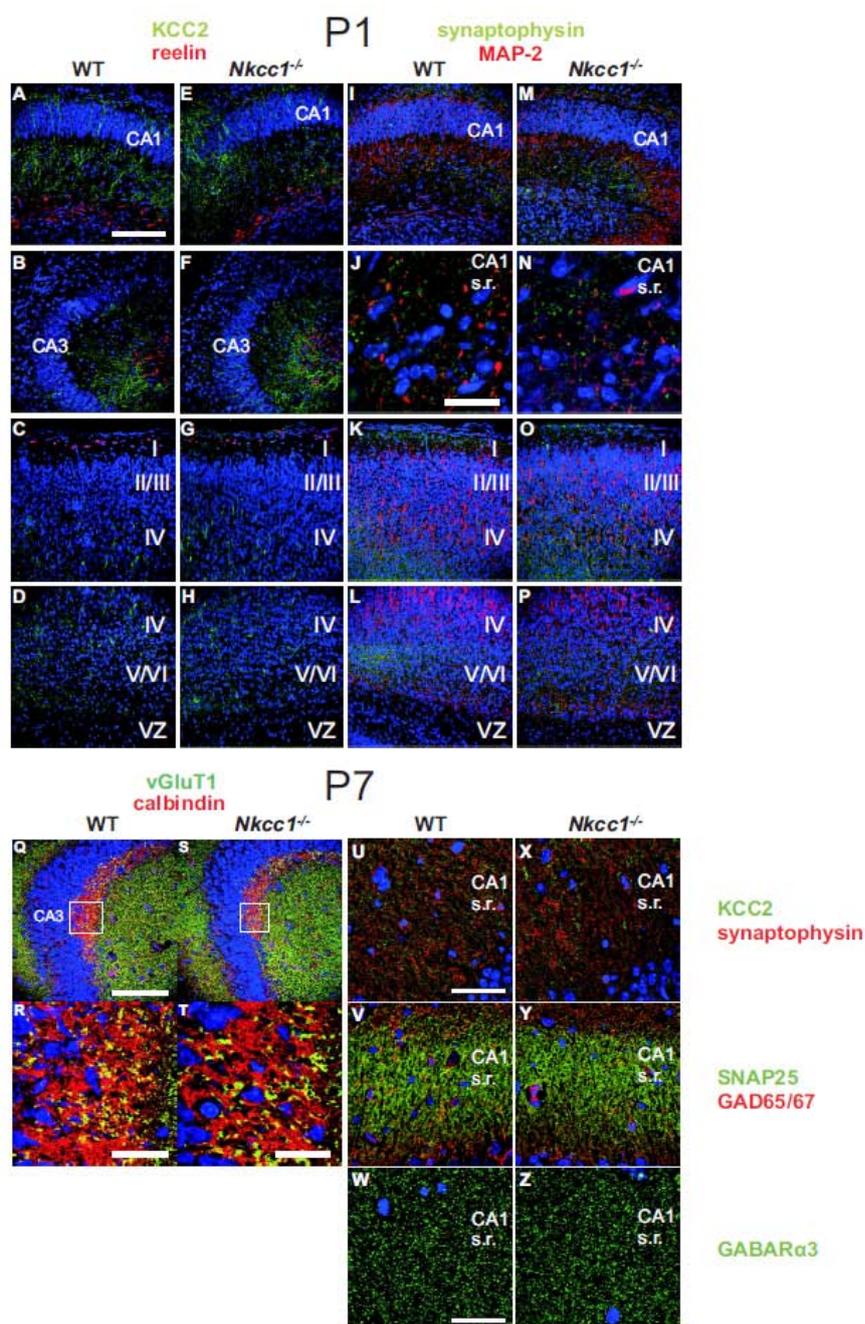
Figure S8: Immunofluorescence analysis of selected marker proteins in the hippocampus and cortex of *Nkcc1*$^{-/-}$ mice.

(**A-H**) Double staining for KCC2 (green) and reelin (red) in hippocampus (**A,B,E,F**) and cortex (**C,D,G,H**) of P1 WT (**A,B,C,D**) and *Nkcc1*$^{-/-}$ (**E,F,G,H**) mice. (**I-P**) Synaptophysin (green) and microtubule associated protein 2 (MAP-2) (red) in hippocampus (I,J,M,N) and cortex (**K,L,O,P**) of WT (**I,J,K,L**) and *Nkcc1*$^{-/-}$ (**M,N,O,P**) animals at P1. (**Q-T**) Staining for vGluT1 (green) and calbindin (red) of the projection (mossy fibers) from dendate gyrus cells to CA3 neurons. Squares in (**Q**) and (**S**) appear enlarged in (**R**) and (**T**). (**U-Z**) Co-staining of KCC2 with synaptophysin (**U,X**), of the

presynaptic marker synaptosome-associated protein of 25 kDa (SNAP25) with and glutamic acid decarboxylase GAD65-67 (**V,Y**) and staining for the GABA$_A$-receptor subunit α3 (**W,Z**) in CA1 stratum radiatum of WT (**U,V,W**) and *Nkcc1*$^{-/-}$ (**X,Y,Z**) mice. Nuclei stained by TOTO-3 are shown in blue. Scale bars: (**A**) 100 μm (**A-P** without **J,N**), (**J**) 23 μm for (**J,N**), (**Q**) 100 μm for (**Q,S**), (**R**) 21 μm, (**T**) 15 μm, (**U**) 35 μm for (**U,V,X,Y**) and in (**W**), 20 μm for (**W,Z**). No difference between WT and *Nkcc1*$^{-/-}$ sections is seen in any of the panels.
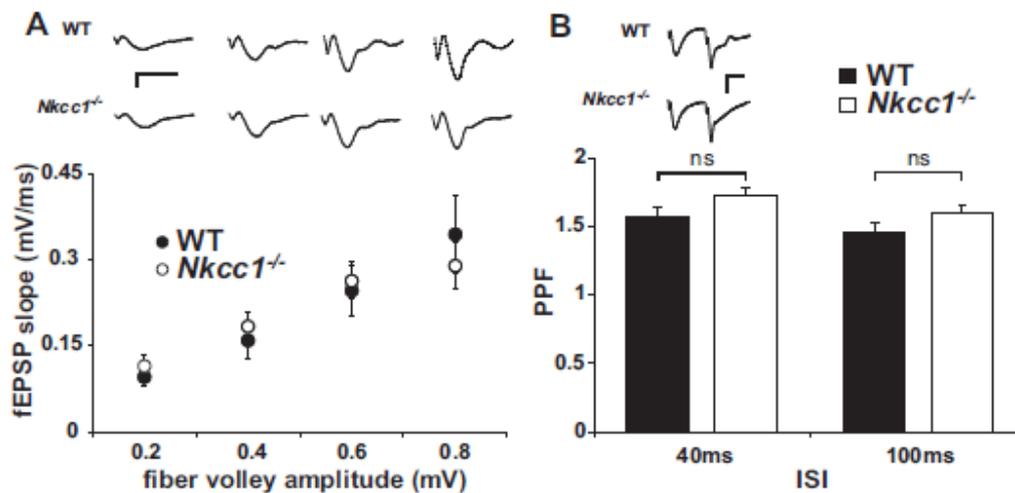
Figure S9: Glutamatergic neurotransmission in P15 brain slices.

(**A**) Field excitatory postsynaptic potentials (fEPSP) of WT and *Nkcc1*$^{-/-}$ slices in CA1 stratum radiatum show intact glutamatergic transmission (mean ± SEM, WT: 6 slices, 3 mice; KO: 7 slices, 3 mice; t-test: p>0.1). Representative sample traces for the given fiber volley amplitudes (0.2, 0.4, 0.6, 0.8 mV) are displayed above. Stimulation artifacts were omitted for clarity. (**B**) Paired pulse facilitation (PPF) in the CA1 stratum radiatum at inter stimulus intervals (ISI) of 40 ms and 100 ms, respectively (mean ± SEM, WT: 6 slices, 3 mice; KO: 7 slices, 3 mice; t-test: p>0.1). Representative sample traces are shown above. Stimulation artifacts were omitted for clarity. Scale bars: (**A**): horizontal 10 ms, vertical 0.4 mV; (**B**): horizontal 20 ms, vertical 0.4 mV. No significant difference between WT and *Nkcc1*$^{-/-}$ transmission is detectable in either test paradigm.

qRT-PCR quantification of selected genes in *Nkcc1$^{-/-}$* vs WT:

Gene	P1 KO vs. WT (%)	SEM(%)	P5 KO vs. WT (%)	SEM(%)	P15 KO vs. WT (%)	SEM(%)
Na-K-2Cl Cotransporter 1 (NKCC1)	0.1	0.0	0.3	0.1	1.5	0.4
Activity-regulated gene 3.1 protein homolog (Arg3.1/Arc)	125.1	48.8	96.2	16.2	100.4	15.1
V-Fos FBJ Murine Osteosarcoma Viral Oncogene Homolog (cFos)	75.1	26.5	108.8	6.4	90.1	8.6
Early Growth Response 1 (Egr1,Zif268)	91.8	19.9	102.8	9.1	97.4	21.0
Dopamine b-Hydroxylase (DbH)	101.8	15.9	119.5	28.6	106.0	60.7
Tryptophan Hydroxylase 2 (TrpH2)	78.1	13.0	78.2	2.7	78.8	11.4
Tyrosine Hydroxylase (TH)	135.4	24.4	72.5	18.4	109.5	38.6
Synaptic RAS-GTPase-Activating Protein 1 (SynGap)	82.7	10.6	108.9	9.8	93.5	12.0
Nuclear Receptor Subfamily 4, A, 1 (NR4A1)	101.3	14.9	95.2	10.9	87.4	23.0
Growth Associated Protein 43 (GAP43)	110.0	11.5	90.2	9.2	101.1	2.9
Neurogenic Differentiation 2 (NeuroD2)	100.6	1.7	101.7	9.4	83.6	1.8
Neuron Restrictive Silencing Factor (NRSF)	92.5	4.5	90.6	11.5	137.7	2.7
N-Tubulin	84.6	11.0	78.1	6.0	94.8	3.3
Tumor Necrosis Factor alpha (TNFalpha)	110.9	23.2	97.8	24.4	113.8	4.5
Brain Derived Neurotrophic Factor (BDNF) exon4	96.5	27.7	118.7	31.9	100.4	31.9
Tyrosine Kinase Receptor B (TrkB)	82.9	11.3	95.5	6.7	77.8	10.8
Inositol 1,4,5-TriPhosphat Receptor 3 (Itp3R)	94.5	19.3	103.4	32.6	106.7	11.0
Glutamate Receptor subunit 1 (GluR1)	88.2	32.0	84.7	20.4	120.3	7.6
Glutamate Receptor subunit 2 (GluR2)	101.4	19.7	84.9	12.7	105.1	32.7
Glutamate Receptor subunit 3 (GluR3)	106.7	24.4	76.1	21.3	129.5	21.8
Glutamate Receptor subunit 4 (GluR4)	107.6	11.2	88.1	4.4	110.4	19.9
NMDA Receptor subunit 1 (NR1)	127.5	29.3	97.5	24.6	73.0	37.3
Anion Exchanger 3 (AE3)	69.9	3.5	124.7	20.4	98.0	24.8

Figure S10: Quantification of expression levels of selected genes relevant for transcription, development, and neurotransmission as assessed by qRT-PCR at P1, P5 and P15.

The percentage of WT transcription (± SEM) is given. Quantification of at least 3 animals per genotype per time point. No significant differences were observed.
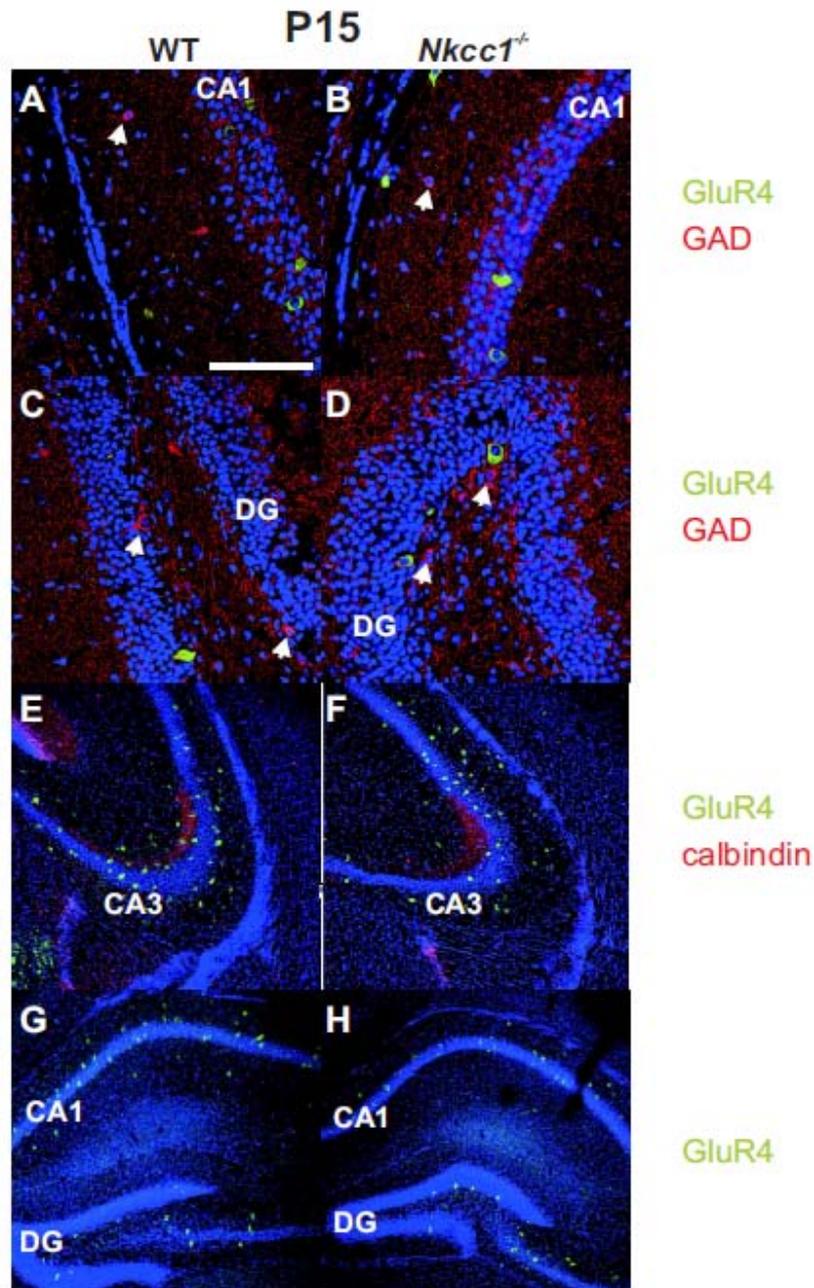
Figure S11: Normal localization of GluR4 in interneurons of the hippocampus.

(**A,B,C,D**) GluR4 (green) is localized to GAD (red) positive GABAergic interneurons in CA1 (**A,B**) and dentate gyrus (**C,D**) of P15 WT (**A,C**) and $Nkcc1^{-/-}$ mice. Not all GABAergic interneurons express GluR4 (white arrows). (**E,F,G,H**) The overall quantity and distribution of GluR4 (green) is similar between WT (**E,G**) and $Nkcc1^{-/-}$ (**F,H**) hippocampus. Calbindin (red) stains the mossy fibers and outlines the hippocampal CA3 region. Scale bar: in (**A**) for (**A-D**) 500µm; for (**E-H**) 125µm.

A   genes upregulated in *Nkcc1^{-/-}* on gene chips at P5:

Probesets	RefSeq Transcript ID	Fold Change	Gene Title
1450928_at	NM_031166	1.54	Inhibitor of DNA binding 4
1423259_at	NM_031166	1.53	Inhibitor of DNA binding 4
1455886_at	NM_007619	1.46	Casitas B-lineage lymphoma
1452671_s_at	NM_027400	1.40	lectin, mannose-binding, 1
1450042_at	NM_007492	1.40	aristaless related homeobox gene (Drosophila)
1428282_at	NM_178337	1.37	tubulin-specific chaperone e
1427902_at	NM_175229	1.37	serine/arginine repetitive matrix 2
1423760_at	NM_001039150	1.37	CD44 antigen
1426968_a_at	NM_133832	1.36	retinol dehydrogenase 10 (all-trans)
1428467_at	NM_001003898	1.35	TAR DNA binding protein
1452114_s_at	NM_010518	1.35	insulin-like growth factor binding protein 5
1448199_at	NM_133971	1.35	ankyrin repeat domain 10
1420836_at	NM_026232	1.35	solute carrier family 25, member 30
1419286_s_at	NM_009879	1.35	intraflagellar transport 81 homolog (Chlamydomonas)
1452036_a_at	NM_011605	1.34	thymopoietin
1427084_a_at	NM_024275	1.33	mitogen-activated protein kinase kinase kinase kinase 5
1416700_at	NM_028810	1.33	Rho family GTPase 3
1424135_at	NM_026274	1.33	ring finger and SPRY domain containing 1
1451289_at	NM_019978	1.32	doublecortin and calcium/calmodulin-dependent protein kinase-like 1
1416814_at	NM_011585	1.32	cytotoxic granule-associated RNA binding protein 1
1426985_s_at	NM_176836	1.30	RIKEN cDNA 2810485I05 gene
1451980_at	NM_145398	1.30	CAS1 domain containing 1
1431921_a_at	NM_009282	1.30	stromal antigen 1

B   genes downregulated in *Nkcc1^{-/-}* on gene chips at P5:

Probesets	RefSeq Transcript ID	Fold Change	Gene Title
1421653_a_at	XM_001004859	0.52	immunoglobulin heavy chain (J558 family)
1433809_at	NM_007840	0.61	DEAD (Asp-Glu-Ala-Asp) box polypeptide 5
1418636_at	NM_012051	0.64	ets variant gene 3
1425902_a_at	NM_019408	0.65	nuclear factor of kappa light polypeptide gene enhancer in B-cells 2, p49/p100
1422904_at	NM_018881	0.65	flavin containing monooxygenase 2
1455115_a_at	NM_177638	0.65	crumbs homolog 3 (Drosophila)
1425866_a_at	NM_148927	0.65	pleckstrin homology domain containing, family A member 4
1434137_x_at	NM_026918	0.65	RIKEN cDNA 1810010M01 gene
1422377_at	NM_053227	0.65	vomeronasal 1 receptor, B4
1427576_at	--	0.68	immunoglobulin kappa chain variable 28 (V28)
1424847_at	NM_010904	0.70	neurofilament, heavy polypeptide
1427734_a_at	XM_001002206	0.70	Down syndrome cell adhesion molecule-like 1
1460167_at	NM_138600	0.70	aldehyde dehydrogenase family 7, member A1
1422403_at	NM_008334	0.70	interferon alpha
1419383_at	NM_009115	0.72	S100 protein, beta polypeptide, neural
1450196_s_at	NM_030678	0.72	glycogen synthase 1, muscle
1437686_x_at	NM_009986	0.73	cut-like 1 (Drosophila)
1449499_at	NM_010455	0.73	homeo box A7
1431227_at	NM_027149	0.73	RIKEN cDNA 2310040A13 gene
1434932_at	NM_001024837	0.73	adenosine deaminase, RNA-specific, B1
1420170_at	NM_022410	0.73	myosin, heavy polypeptide 9, non-muscle
1448700_at	NM_008059	0.73	G0/G1 switch gene 2
1455910_at	NM_027910	0.73	kelch domain containing 3
1427824_at	--	0.73	--
1420663_at	NM_009565	0.73	Vzinc finger and BTB domain containing 7B
1448041_at	NM_011277	0.74	ring finger protein 2
1421500_at	NM_009293	0.74	steroid sulfatase
1419426_s_at	NM_011124	0.74	chemokine (C-C motif) ligand 21
1421453_at	NM_021566	0.74	junctophilin 2
1418411_at	NM_015821	0.74	F-box and leucine-rich repeat protein 8
1426970_a_at	NM_023738	0.74	ubiquitin-activating enzyme E1-like
1452528_a_at	NM_008699	0.74	NK2 transcription factor related, locus 3 (Drosophila)
1448043_x_at	NM_011277	0.75	ring finger protein 2
1424651_at	NM_144932	0.75	cDNA sequence BC021611
1453389_a_at	NM_018825	0.75	SH2B adaptor protein 2
1422404_x_at	NM_008334	0.75	interferon alpha
1421167_at	NM_015804	0.75	ATPase, class VI, type 11A
1417283_at	NM_011838	0.75	Lyl/neurotoxin 1

Figure S12: Comparative expression profiling of the P5 hippocampus.

(**A**) Genes up-regulated in the P5 *Nkcc1^{-/-}* hippocampus. (**B**) Genes down regulated in the P5 *Nkcc1^{-/-}* hippocampus. Affymetrix probe set numbers, ID's for the corresponding RefSeq, a short gene description and the calculated fold change are displayed. Genes underlined in red were further assessed by qRT-PCR.

3   MANUSCRIPT II

ClC-2 voltage gated channels constitute part of the background conductance and assist chloride extrusion

This chapter was published in March 2010 by Ilka Rinke, Judith Artmann and Valentin Stein in The Journal of Neuroscience, Vol. 30(13) pp. 4776-4786.

Max Planck Institute of Neurobiology

Ilka Rinke performed the electrophysiological experiments, biocytin stainings and analyzed the data. Judith Artmann performed the electrophysiology recordings concerning properties of ClC-2 currents. Valentin Stein wrote the programs to analyze the data. Ilka Rinke and Valentin Stein conceived the experiments and wrote the manuscript.

3.1   Abstract

The function of voltage gated chloride channels in neurons is largely unknown. The voltage gated chloride channel ClC-2 mediates a chloride current in pyramidal cells of the hippocampus. We directly show that ClC-2 assists chloride extrusion after high chloride load. Furthermore, the loss of this chloride channel leads to a dramatic increase of the input resistance of CA1 pyramidal cells, making these cells more excitable. Surprisingly, basal synaptic transmission, as judged from recordings of field EPSPs, was decreased. This difference was eliminated when GABAergic inhibition was blocked. Recordings from hippocampal interneurons revealed ClC-2-mediated currents in a subset of these cells. An observed increase in GABAergic inhibition could thus be explained by an increase in the excitability of interneurons, caused by the loss of ClC-2. Together, we suggest a dual role for ClC-2 in neurons, providing an additional efflux pathway for chloride and constituting a substantial part of the background conductance, which regulates excitability. In ClC-2 knock-out mice an increased inhibition seemingly balances the hyperexcitability of the network and thereby prevents epilepsy.

3.2   Introduction

Aside from the ligand-gated $GABA_A$ receptors, voltage gated chloride channels are expressed in the hippocampus (Jentsch et al., 2002). In contrast to the well characterized $GABA_A$ receptors, the function of voltage gated chloride channels in neurons is still largely elusive. They have been suggested to be involved in regulating chloride homeostasis (Staley et al., 1996), excitability (Madison et al., 1986), and acidification of synaptic vesicles (Stobrawa et al., 2001).

One of the voltage gated chloride channels expressed in neurons is ClC-2. ClC-2 is an almost ubiquitously expressed chloride channel of the CLC family of chloride channels and transporters. ClC-2 is activated by negative membrane voltage, cell swelling, a rise in intracellular chloride concentration, or mild extracellular acidification (Grunder et al., 1992; Thiemann et al., 1992; Jordt and Jentsch, 1997; Zuniga et al., 2004). The loss of ClC-2 in mice has profound effects leading to testicular and retinal degeneration (Bosl et al., 2001). Recently, in aged knock-out (KO) animals, a spongiform vacuolation of the white matter in the central nervous system was reported, which might be related to defective oligodendrocyte function (Blanz et al., 2007).

Although, currents with properties similar to ClC-2 have been described in neurons (Chenoy-Marchais, 1982; Madison et al., 1986; Staley, 1994), the molecular identity and the function of this current remain unclear. ClC-2 has been proposed to participate in lowering the cytoplasmic chloride concentration $[Cl^-]_i$ of neurons (Staley, 1994; Staley et al., 1996; Ben-Ari, 2002). Chloride extrusion is primarily mediated by the neuron specific potassium chloride co-transporter 2 (KCC2); however, additional mechanisms might play an important role under conditions of high chloride load. The large conductance of ClC-2 makes it well suited for this purpose (Staley et al., 1996). In addition, if this conductance is active at resting membrane potential it should contribute to the membrane resistance (Madison et al., 1986). Both actions are such that loss of ClC-2 should lead to increased neuronal excitability, which could cause diseases like epilepsy. However, the disruption of ClC-2 in mice did not entail epilepsy (Bosl et al., 2001; Nehrke et al., 2002; Blanz et al., 2007). This has been controversial, as mutations in the gene encoding ClC-2 in humans have been linked to epilepsy (D'Agostino et al., 2004; Everett et al., 2007).

Here we investigate the role of ClC-2 in hippocampal pyramidal cells. We found that ClC-2, mediates a chloride current, is involved in chloride extrusion, and constitutes a substantial part of the background conductance in hippocampal neurons. The loss of ClC-2 leads to a dramatic increase of the input resistance of CA1 pyramidal cells, thereby increasing excitability. Surprisingly, basal synaptic transmission decreased in field recordings, which was dependent on GABAergic inhibition. We show that a subset of interneurons display a characteristic ClC-2-mediated current. The loss of ClC-2 in interneurons leads to an increase of excitability of interneurons resulting in an increased inhibition of principal neurons, thereby reducing overall network excitability. Our data suggest a dual role for ClC-2 in neurons, regulating excitability via the membrane resistance and providing an additional efflux pathway for chloride.

3.3 Materials and Methods

Mice: The generation of ClC-2 knockout mice was described elsewhere (Bosl et al., 2001). Both, male and female mice were used for all experiments.

Slice preparation: Animals were anesthetized with Isoflurane (Baxter), and decapitated. Brains were removed quickly, and chilled in carbogen (95% O_2; 5% CO_2) gassed artificial cerebro spinal fluid (ACSF) containing (in mM): 130.9 NaCl; 2.75 KCl; 1.43 $MgSO_4$; 2.5 $CaCl_2$; 1.1 NaH_2PO_4; 28.82 $NaHCO_3$ and 11.1 D-glucose with an osmolarity of 315-325 mosm/l. Hippocampal slices (400 µM)

were cut either horizontally (P1-P8) or transversally (P9-P20) with a vibratome (VT1200S, Leica). Prior to recording slices were kept for 30 min at 32°C and subsequently stored at room temperature in ACSF continuously gassed with carbogen.

Electrophysiology: All recordings were performed using a Multiclamp 700B amplifier (Molecular Devices, Sunnyvale, CA). Data were digitized using a Digidata 1322A (Molecular Devices, Sunnyvale, CA). Pipettes (3-5 MΩ) were pulled from borosilicate glass (Science Products, Hofheim, Germany). Inputs from CA3 to CA1 were severed to prevent propagation of epileptiform activity. Liquid junction potentials were calculated with the liquid junction potential assistant of pClamp. Membrane potentials were corrected by 15 mV.

Extracellular recordings: Field EPSPs were recorded in the stratum radiatum of CA1 of P15 - P20 mice. Recording and stimulation electrodes were filled with ASCF.

Whole cell recordings: Whole cell recordings were obtained from CA1 pyramidal cells or interneurons, which were visualized using differential interference contrast infrared video microscopy.

ClC-2 currents: chloride currents were recorded with high chloride pipette solution containing (in mM): 90 CsCl; 20 CsGluconate; 8 NaCl; 2 $MgCl_2$; 10 HEPES; 1 EGTA, and 2 QX314 (Alomone Labs, Israel); pH 7.2; 290 mosm/l. Extracellular recording solution contained (in mM): 70 NaCl; 2.5 KCl, 16 $MgSO_4$, 26.2 $NaHCO_3$; 11 Glucose; 30 Tetraethylammonium-chloride, 10 CsCl; supplemented with 200 nM tetrodotoxin (TTX) to block APs. In some recordings 50 µM ZD7288 (Ascent Scientific) was added to block the hyperpolarization-activated inward current (I_h). Interneurons were identified as such by their location, morphology, and posthoc biocytin staining. Recordings were not obtained from any specific type of interneuron. ClC-2 chloride currents were evoked by stepping the membrane potential from -10 mV to -120 mV for 4 s (see Fig. 1F). ClC-2-mediated currents were calculated as the difference of the inward current at the beginning and the end of the voltage step.

Chloride transport: GABA evoked chloride currents were recorded at the soma in response to pressure application of GABA (100 µM) in ACSF to the apical dendrites 50 – 100 µm from the soma (5 - 15 ms, 5 psi) using a pneumatic drug ejector (NPI, Tamm, Germany). Cells were clamped to -70 mV. Recordings were performed with a low chloride intracellular solution containing (in mM): 150 K-methylsulphonate, 4 KCl, 4 NaCl, 4 MgATP, 0.4 Mg GTP and 10 HEPES. To estimate chloride transport, $[Cl^-]_i$, was transiently increased and the rate at which $[Cl^-]_i$ returned to baseline was determined. For experimental protocol also see Fig. 2. Charges of GABA evoked currents were normalized to the absolute sum of the charges of the baseline and the first test

pulse, as the rate of decay depends on the baseline charge and the effective loading, which is given by the first test pulse. To obtain time constants curves were fitted with a mono exponential function.

Chloride accumulation: Recording conditions were the same as for chloride transport experiments. Trains of IPSCs were synaptically evoked by repetitive stimulation at different frequencies (0.5 Hz, 1 Hz, 2 Hz and 5 Hz) with a monopolar stimulation electrode placed nearby the recorded pyramidal cell. The depression was calculated as the ratio of the 10th to the 1st eIPSC.

Excitatory synaptic transmission: Whole cell patch recordings were obtained in ASCF supplemented with picrotoxin (PTX) (100 μM) to block GABA$_A$ receptors. Glass electrodes were filled with an internal solution containing (mM): 150 CsGluconate, 8 NaCl, 2 MgATP, 10 HEPES, 0.2 EGTA, 0.1 spermine, and 5 QX314, pH 7.2. Ratios of AMPA to NMDA currents in CA1 pyramidal cells were obtained by evoking AMPA eEPSCs at -70 mV and NMDA eEPSC at +40 mV, the current being taken 70 ms after stimulus. Paired pulse facilitation was determined as the ratio of the AMPA EPSC of the second pulse to the AMPA EPSC of the first pulse with an inter stimulus interval of 40 ms. mEPSC were recorded at -70 mV in ACSF supplemented with of TTX (0.2μM), PTX (100 μM), and trichiormethiazide (TCM) (250 μM) to increase mEPSC frequency.

Inhibitory synaptic transmission: Inhibitory postsynaptic currents were recorded at -70 mV holding potential using a high chloride internal solution containing (in mM) 90 CsCl; 20 CsGluconate; 8 NaCl; 2 MgCl$_2$; 10 HEPES; 1 EGTA, and 2 QX314; pH 7.2; 290 mosm/l. sIPSCs were recorded in ASCF supplemented with NBQX (10 μM) to block AMPA receptors. To isolate mIPSC, ACSF was additionally supplemented with TTX (0.2 μM) to block action potentials. IPSCs were evoked with a stimulation electrode placed 100 μm away from the soma of the recorded cell. The position of the stimulation electrode was adjusted such that the smallest stimulus (5 pA) elicited a current smaller than 40 pA. Paired pulse ratio was determined as the ratio of the IPSC amplitude of the second pulse to the IPSC amplitude of the first pulse with an inter stimulus interval of 50 ms.

Current clamp recordings: Pipette solutions contained (in mM) 150 K-methylsulphonate, 4 KCl, 4 NaCl, 4 MgATP, 0.4 Mg GTP and 10 HEPES. AP threshold was determined using the first derivative of single APs. I/O functions: A series of EPSPs were evoked at various stimulus intensities covering a range from subthreshold to supramaximal. EPSP slopes were measured between 20 % and 80 % of the peak. I/O functions were generated by binning the EPSP slopes and plotting the bin center against the percentage of successful action potentials in the respective bin. Data was fitted with an asymmetric sigmoid function:

Y = (1/(1+exp((EC50 + (1/HillSlope)*Log((2^(1/S))-1) -X)*HillSlope))^S).

The threshold, the EPSP slope that yields an AP 50 % of the times, was defined as the EC50 value of this fit (threshold). The gain was determined as the Hill slope.

Biocytin staining: For interneuron identification intracellular solution was supplemented with biocytin (0.2 %, Molecular Probes). To morphologically characterize biocytin filled neurons, slices were fixed in 4 % paraformadehyde (PFA in 0.1 M phosphate-buffered saline (PBS), pH 7.3) for at least 30 minutes at RT. After washing with PBS (3 x 10 min) endogenous peroxidase was blocked by 3 % hydrogen peroxide (H_2O_2) for 15 minutes. Following additional washing with PBS (5 x 10 min), cell membranes were permeabilized in 0.4 % Triton in 0.1 M PBS. Subsequently, slices were incubated with Avidin and biotinylated horseradish peroxidase macromolecular complex (Vectastain ABC reagent, Vector Laboratories, Burlingame, CA) overnight at 4 °C. Afterwards, slices were washed with PBS (5 x 10 min) and then incubated in 0.7 mg/ml 0.1 M PBS Diaminobenzidin (DAB, Serva Electrophoresis, Heidelberg, Germany) at RT in the dark. After 25 minutes pre-incubation, 0.03 % H_2O_2 was added resulting in a brown reaction product. Slices were again washed (5 x 10 min PBS and 1 x 10 min dH$_2$O), and embedded in Mowiol 4-88 mounting medium (Roth, Karlsruhe, Germany).

Data Analysis: All data were analyzed using Clampfit 10.2 (Molecular Devices, Sunnyvale, CA), Prism 5 (GraphPad, La Jolla, CA), and Matlab (The Mathworks, Natick, MA). mEPSCs, sIPSCs, mIPSCs were analyzed offline with customized software using a threshold of 5 pA (mEPSCs) and 15 pA (m/sIPSCs). Data are presented as means ± SEM. Differences between groups were tested using the Student's t-test (when normally distributed), the Mann-Whitney test (when not normally distributed) or the Kolmogorov-Smirnov test, as indicated. P values are reported in the text and significance was set as $p < 0.05$, for Kolmogorov-Smirnov test the significance level was 0.01; in Figures (*) represents $p < 0.05$, (**) $p < 0.01$, (***) $p < 0.001$. N represents the number of cells examined. For mini analysis histograms were derived from 150 – 200 events per cell. Averaged cumulative distributions were calculated from normalized histograms. As the K-S test is only appropriate for testing data against a continuous distribution, 25 events were randomly chosen from each cell and a continuous cumulative probability functions was calculated from these events.

3.4   Results

CA1 neurons show ClC-2 mediated currents.

We first characterized the properties of the hyperpolarization activated chloride current in CA1 pyramidal neurons. ClC-2 currents were isolated by blocking potassium and sodium conductances. The currents obtained showed the characteristic slow activation at negative membrane potentials and a pronounced inward rectification. Wash in of 50 µM ZD7288 had no effect on the slowly developing inward current, excluding the possibility that the obtained currents are mediated by I_h (WT: 556 ± 50 pA; +ZD7288: 595 ± 44 pA, n = 9, p < 0.05, t-test) (Fig. 1A). When heterologously expressed in *Xenopus* oocytes, ClC-2 is activated by acidic extracellular pH (Jordt and Jentsch, 1997) and, in contrast to non-CLC chloride channels, has a lower permeability for iodide than for chloride (Thiemann et al., 1992). Both of these properties are conserved in the currents obtained from CA1 pyramidal cells. Lowering the extracellular pH from 7.2 to 6.5 increased ClC-2 currents by 64 % (pH 7.2: 783 ± 132 pA; pH 6.5: 1285 ± 115 pA, n = 7, p < 0.05, t-test) (Fig. 1B). Substituting the extracellular anion chloride with iodide reduced ClC-2 currents to 33 % (Cl^-: 812 ± 146 pA; I^-: 269 ± 78 pA, n = 8, p < 0.05, t-test) (Fig. 1C). In the absence of specific ClC-2 antagonists, we recorded from CA1 neurons of ClC-2 KO (*Clcn2$^{-/-}$*) animals. Under the same conditions, we did not observe a voltage gated chloride current (KO: 11 ± 2 pA, n = 23) (Fig. 1D, E). These data clearly show that the observed chloride conductance is mediated by ClC-2, and allowed us to use *Clcn2$^{-/-}$* animals to study the function of ClC-2 in neurons.
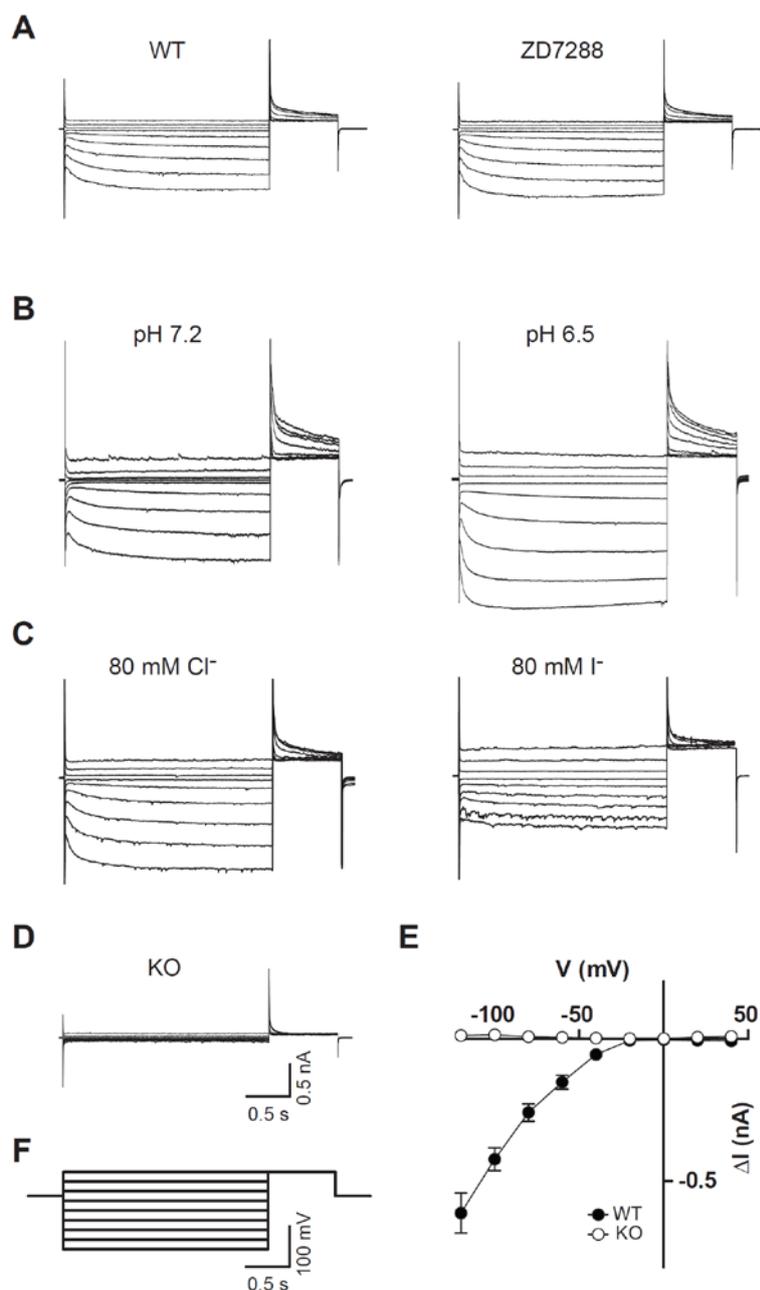
Figure 1: Properties of ClC-2 currents in CA1 pyramidal cells CA1 pyramidal cells show ClC-2 mediated currents.

Currents were elicited by voltage steps of 4 s from a holding potential of -10 mV to values between 40 mV and -120 mV in steps of -20 mV followed by a test pulse of +40 mV for 2 s, as illustrated in F. **A**, The slowly developing inward current is not blocked by the specific I_h inhibitor ZD7288. **B**, ClC-2 currents in CA1 pyramidal cells are activated by acid extracellular pH. **C**, Currents obtained in CA1 neurons show a lower permeability for iodide, which is typical for ClC chloride channels. **D**, Under the same recording conditions as in WT mice, no currents were elicited from *Clcn2*$^{-/-}$ animals. **E**. Current - voltage plot of steady state currents from WT (closed symbols) and KO (open symbols). **F**, Voltage step protocol used for evoking ClC-2 currents. Error bars represent SEM in all graphs. Note, symbol size might occlude error bars.

Does ClC-2 assist chloride extrusion?

One of the proposed functions of ClC-2 is a role in rapid extrusion of chloride after GABA$_A$ receptor activation (Smith et al., 1995; Staley et al., 1996). ClC-2 is an inwardly rectifying chloride conductance (Thiemann et al., 1992) that activates at membrane potentials more negative than E$_{Cl}$, so that chloride can flow out, but not in through ClC-2 (Staley, 1994; Smith et al., 1995). Because the conductance of ClC-2 is large and does not display time-dependent inactivation, it is well suited to stabilize E$_{Cl}$ near resting membrane potential (Staley et al., 1996).

To test whether chloride is extruded via ClC-2 under conditions of high $[Cl^-]_i$, we measured outward chloride transport by transiently elevating $[Cl^-]_i$ and monitoring as it returned to baseline (Brumback and Staley, 2008). Briefly, the cell was clamped to resting membrane potential using a low chloride intracellular solution. After recording an outward baseline response by pressure applying GABA to the dendrite, the cell was depolarized to -15 mV for 6 seconds. During this depolarization another GABA application caused a large chloride influx, thereby increasing $[Cl^-]_i$ in the small compartment of the dendrite. To measure chloride transport, we stepped the membrane voltage back to resting membrane potential and pressure applied GABA. Shortly after loading, when $[Cl^-]_i$ is high, the test currents showed a strong chloride efflux (inward current), indicating the successful loading of the cell. We repeated this seven times with increasing delays between the loading and test application (Illustration of experimental protocol shown in Fig. 2A). GABA evoked currents returned more slowly toward baseline in *Clcn2$^{-/-}$* animals compared to WT (*Clcn2$^{+/+}$*) (Fig. 2B, C). To quantify the time course of chloride extrusion, charges of GABA evoked currents were normalized to the absolute sum of the baseline and the first test pulse. Fitting the time courses with a mono-exponential function show a significant difference in the decay kinetics (WT: τ = 1.8 s, N = 13; KO: τ = 2.9 s, N = 11; p < 0.0001, Mann-Whitney) (Fig. 2C).

It has been reported that repetitive activation of GABA$_A$ receptors reduces IPSC amplitude, at least in part due to chloride accumulation (McCarren and Alger, 1985; Huguenard and Alger, 1986; Thompson and Gahwiler, 1989a; Ling and Benardo, 1995). If ClC-2 quickly extrudes chloride, chloride should accumulate more strongly in cells lacking ClC-2 after synaptic activation of GABA$_A$ receptors, leading to a greater reduction of IPSC amplitudes (Fig. 2D - F). We tested this by synaptically evoking IPSCs at 0.5, 1, 2, and 5 Hz, while cells were clamped at -70 mV with a low chloride internal. Indeed, at 0.5 Hz and 1 Hz IPSC amplitudes were significantly decreased in KO animals (0.5 Hz: WT 29.8 ± 4.7 %, N = 11, KO 41.1 ± 2.1 %, N = 14, p < 0.05; 1 Hz: WT 35.5 ± 3.9 %, N = 15, KO 49.8 ± 2.8 %, N = 14, p < 0.01, t-test) (Fig. 2D - F). At higher frequencies, we did not observe significant differences between WT and KO (2 Hz: WT 42.4 ± 3.5 % N = 14, KO 48.9 ±

4.3 %, N = 15, p > 0.05; 5 Hz: WT 58.1 ± 4.0 %, N = 8, KO 57.5 ± 4.9 %, N = 9, p > 0.05, t-test), consistent with the idea that the reduction of presynaptic release is the main cause for the depression at higher frequencies (Ling and Benardo, 1995). These experiments demonstrate that ClC-2 accelerates chloride extrusion if the cell is strongly loaded with chloride.
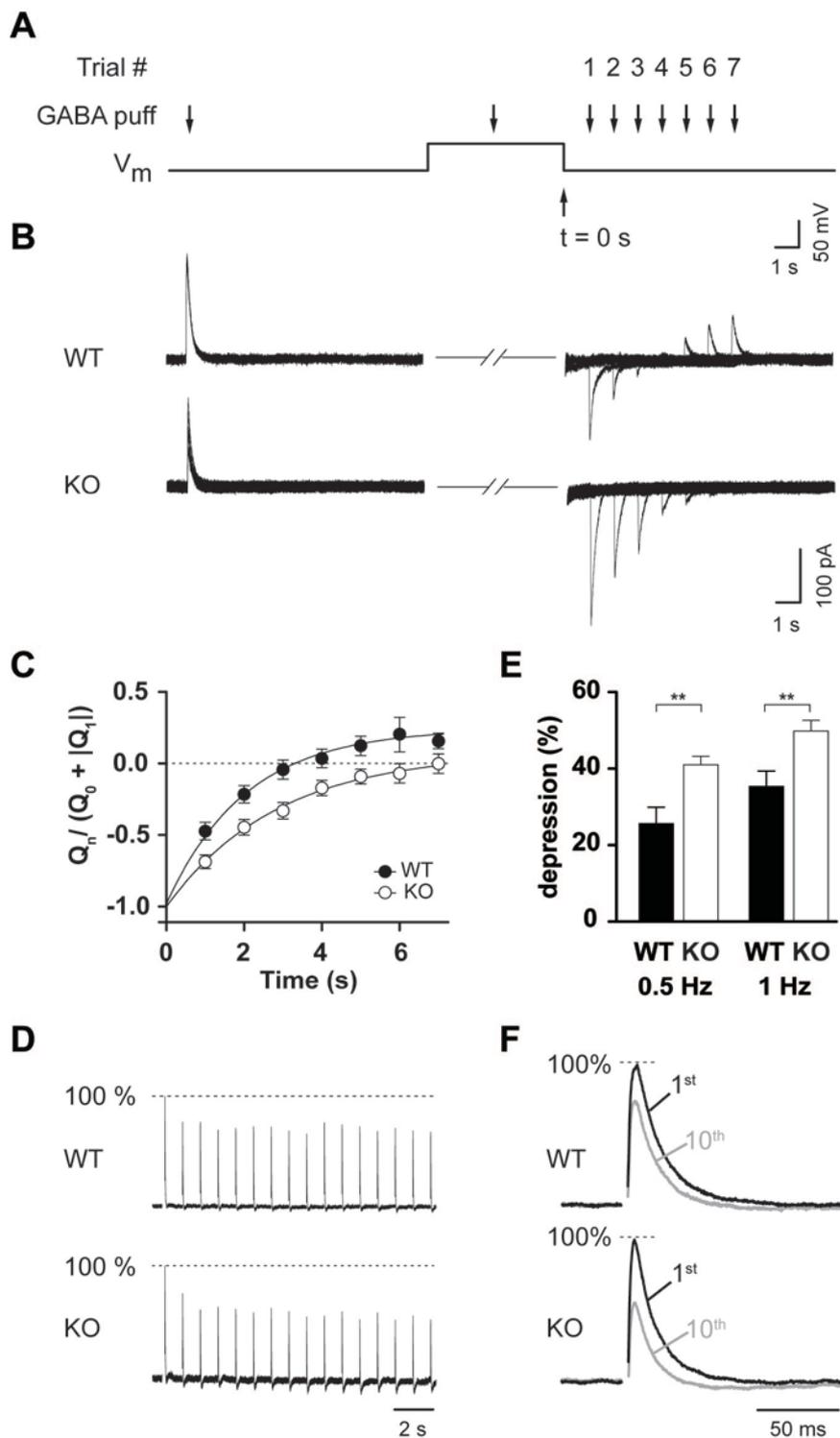
Figure 2: Chloride is extruded quickly via ClC-2

A, Experimental protocol, a first GABA puff elicited a baseline chloride current, thereafter V_m was depolarized to -15 mV for 6 s. 3 s into the voltage step, $[Cl^-]_i$ was increased by a second GABA puff. V_m was then stepped back to resting membrane potential, and a third GABA application evoked a test current. Seven trials of GABA puffs with increasing delays between load and test pulse were performed. **B**, Sample traces for WT (top) and KO (bottom) show a much slower return to steady state conditions in the KO. Note, currents during depolarization are omitted for clarity. **C**, Average returns to steady state. Charges were normalized to the absolute sum of the baseline and first evoked trial. Decay kinetics of WT (closed circles) were significantly faster than for KO (open circles). See material and methods for detailed description of analysis. **D**, Sample traces for WT (top), and KO (bottom) of normalized IPSCs, dotted line indicates 100% of the baseline. Stimulus artifacts have been omitted for clarity. **E**, Repetitive activation of GABA$_A$ receptors leads to a chloride accumulation, reducing the driving force and thereby leading to a depression of evoked IPSCs. At 0.5 and 1Hz, $Clcn2^{-/-}$ showed a stronger depression than $Clcn2^{+/+}$. **F**, Normalized sample traces of the first and 10th stimulus for WT (top) and KO (bottom). Stimulus artifacts have been omitted for clarity. Closed symbols represent WT, open symbols represent KO in all graphs. Error bars represent SEM in all graphs.

ClC-2-mediated currents are not seen at early postnatal ages

In the early stages of development, E_{Cl} is positive relative to the resting membrane potential and GABA acts as an excitatory neurotransmitter (Obata et al., 1978). In hippocampal pyramidal cells, GABAergic responses undergo a switch from excitatory to inhibitory during the first postnatal week (Stein et al., 2004a). This process is primarily mediated by the differential up- and down regulation of the cation-chloride co-transporters KCC2 and NKCC1. To investigate whether ClC-2 is functional during this period, we recorded chloride currents at postnatal day one (P1), P5, P8, P10, and P15 from WT CA1 pyramidal cells (Fig. 3A, B). Functional ClC-2 expression could only be observed from P8 onwards. At P10 it reached levels indistinguishable from later time points (P1: 4 ± 3 pA, N = 13; P5: 3 ± 2 pA, N = 20; P8: 60 ± 14 pA, N = 18; P10: 797 ± 76 pA, N = 21; P15: 648 ± 74 pA, N = 33, ANOVA). This functional expression profile parallels the switch from high to low intracellular chloride (Stein et al., 2004a), compatible with the idea of providing an efflux pathway for chloride that assists chloride extrusion.
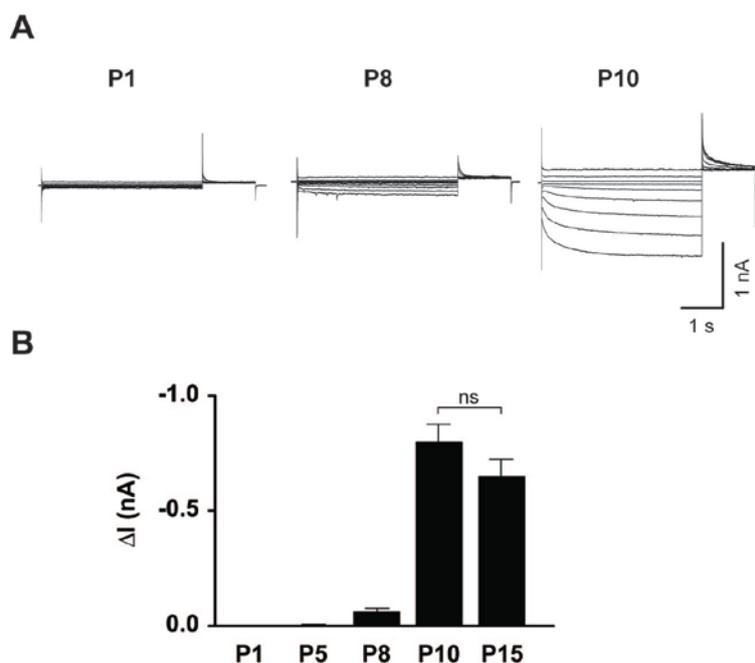
Figure 3: ClC-2-mediated currents are not seen at early postnatal ages

A, Sample traces of ClC-2 currents at P1 (left), P8 (middle), and P10 (right). **B**, Average currents at different postnatal stage. No currents were observed at P1 and P5. After P10 the amplitude does not signify-cantly change.

ClC-2 constitutes a substantial part of the background conductance

Because ClC-2 is active at resting membrane potential, it could contribute to the background conductance and affect the membrane resistance (Madison et al., 1986). This would directly influence the excitability of the neuron. In current clamp recordings (Fig. 4A), we observed a strong increase in membrane resistance in KO animals (WT: 160 ± 10 MΩ, N = 17, KO: 286 ± 15 MΩ, N = 16, p < 0.0001, t-test) (Fig. 4B). In addition, the voltage difference between resting membrane potential and action potential threshold was significantly decreased in $Clcn2^{-/-}$ animals (WT: 27.7 ± 1.3 mV, N = 17, KO: 20.1 ± 1.0 mV, N = 16, p < 0.0001, t-test). In turn, the same current injected elicited more action potentials (Fig. 4A, B). In contrast to the potassium leak conductance, loss of ClC-2 did not significantly alter the resting membrane potential (WT: -77.8 ± 1.0 mV, N = 17, KO: -75.4 ± 1.1 mV, N = 16, p > 0.05, t-test), possibly because E_{Cl} is close to resting membrane potential (Tyzio et al., 2008). Furthermore, the sag ratio (WT: 0.7 ± 0.1, N = 17, KO: 0.8 ± 0.1, N = 16, p > 0.05, t-test) were not different between genotypes. These data clearly show that ClC-2 constitutes a significant part of the background conductance. The loss of ClC-2 leads to an increase of the input resistance, thereby increasing the excitability of the neuron.
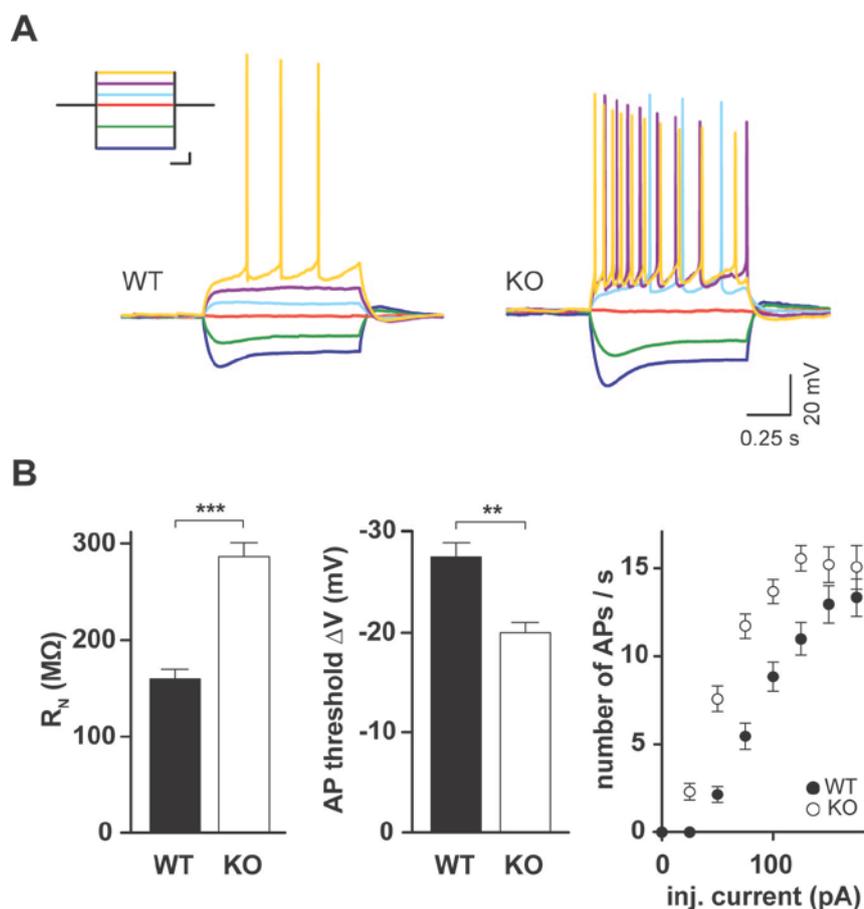
Figure 4: Intrinsic membrane properties of *Clcn2$^{-/-}$* pyramidal neurons are altered.

A, Sample traces of current clamp recordings. Inset shows the current step protocol, same colors indicate same injected currents, dark blue -100 pA, green -50 pA, red 0 pA, light blue 25 pA, magenta 50 pA, yellow 75 pA. Scale bar for inset 250 ms, 25 pA. **B**, Comparison of input resistance (left), AP threshold (middle), and number of APs generated at various current injections (right). Closed symbols represent WT, open symbols represent KO. Error bars represent SEM in all graphs.

Network gain is reduced in fEPSP recordings

The strong effects on input resistance should lead to a higher excitability of the hippocampal network and possibly seizures. By contrast, epilepsy or higher seizure susceptibility has not been observed in *Clcn2$^{-/-}$* mice (Bosl et al., 2001; Nehrke et al., 2002; Blanz et al., 2007). One possible explanation is a reduction of synaptic transmission, which would compensate for the increased excitability of the postsynaptic neuron. Therefore, we tested basal synaptic transmission with extracellular field recordings, as these do not affect [Cl$^-$]$_i$. In addition, extracellular recordings are well suited to determine the network properties, as the signals are sampled from many neurons,

including interneurons. Here we compared the size of the presynaptic fiber volley (input) with the slope of the field EPSP (output) in stratum radiatum. Much to our surprise, the slope of the I/O curve (network gain) of synaptic transmission was strongly reduced in *Clcn2*$^{-/-}$ animals (Fig. 5A, C). In contrast, no difference between WT and KO was observed in the presence of picrotoxin (PTX) (Fig. 5B, D). These data suggest loss of ClC-2 leads to a change in the inhibitory microcircuit of the CA1.
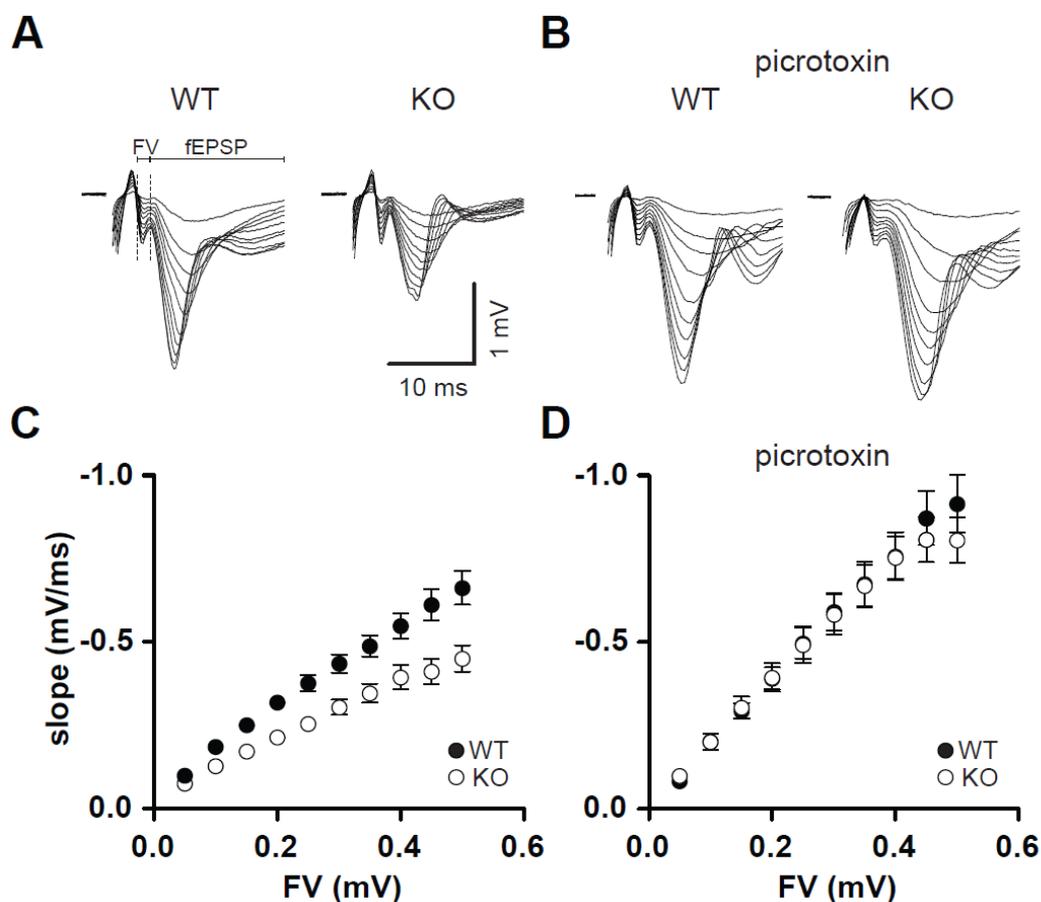
Figure 5: Network gain is reduced in ClC-2 KO animals.

A and **B**, Sample traces of extracellular field recordings for WT and KO in the absence (**A**) and presence (**B**) of picrotoxin. **C**, Input-output curve for basal synaptic transmission in hippocampal slices from WT (closed symbols) and KO (open symbols) mice. fEPSPs were recorded at a range of stimulus intensities from CA1 stratum radiatum. fEPSP slopes in the knockout mice are significantly smaller than from WT mice at every fiber volley amplitude. **D**, Input-output curve in the presence of picrotoxin to block inhibition showed no significant differences between WT and KO. The slope of the I/O curve is increased compared to conditions without PTX for both WT and KO. Error bars represent SEM in all graphs. Note, symbol size might occlude error bars.

Excitatory synaptic transmission is not impaired in *Clcn2*^{-/-} animals

To exclude changes in excitatory synaptic transmission as a cause for the reduced network gain, we studied basal synaptic transmission in more detail using whole cell patch clamp recordings. During these recordings, we noted that reduced membrane resistance resulted in significantly smaller holding current in KO cells than in WT cells (data not shown). First, we compared the α-amino-3-hydroxy-5-methyl-4-isoxazole propionic acid (AMPA) receptor and N-methyl-D-aspartate (NMDA) receptor components of excitatory postsynaptic currents (EPSC) (Fig. 6A).
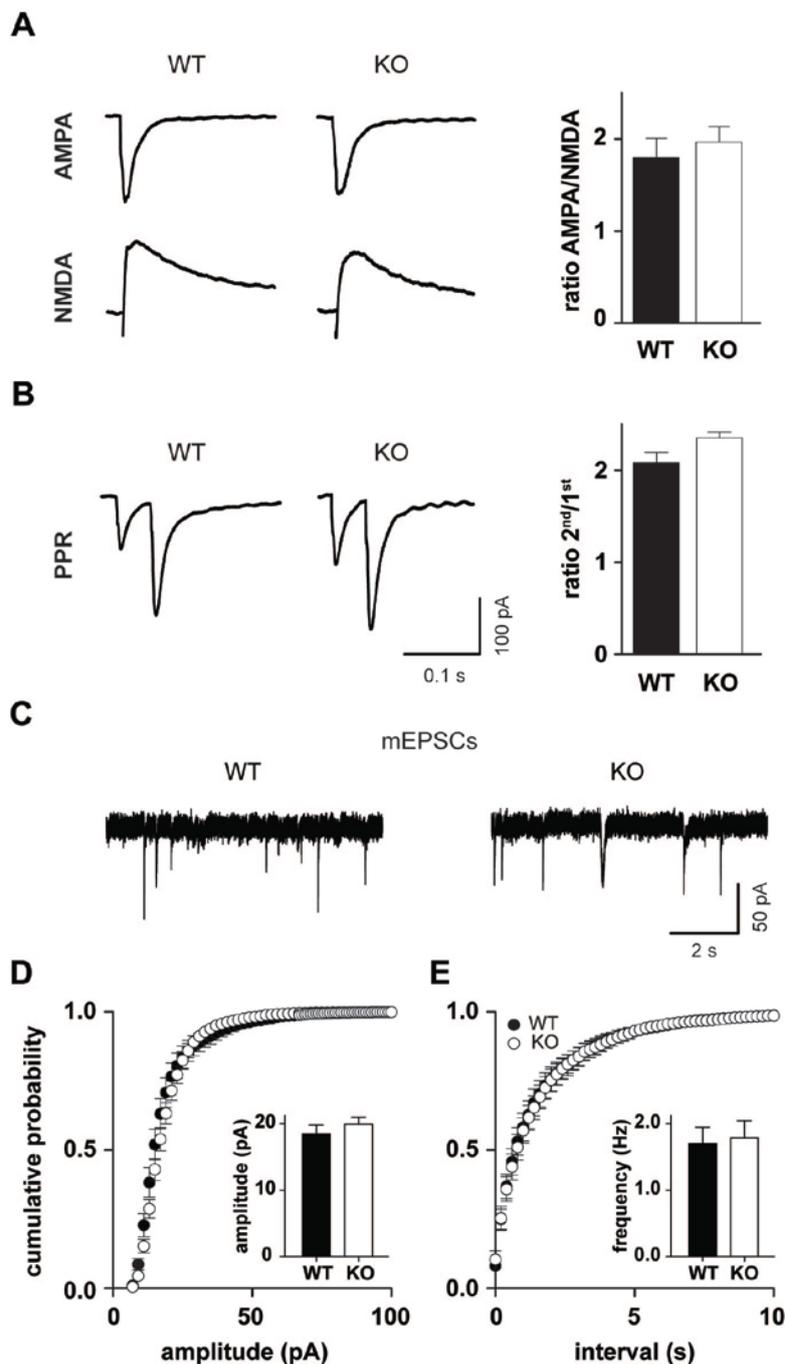
Figure 6: Excitatory synaptic transmission is not altered in *Clcn2⁻ᐟ⁻* mice.

A, Ratio of AMPA to NMDA currents is not altered. Sample traces are shown at the left. AMPA currents were recorded at -70 mV, NMDA currents we determined at +40 mV, 70 ms after the stimulus. **B**, PPR a measure for presynaptic release shows no difference between WT and KO. Sample traces are shown on the left. Stimulus artifacts have been omitted for clarity. Scale bar is the same in A and B. **C**, Sample traces for mEPSCs recordings for WT (left) and KO (right). **D**, Cumulative frequency distribution of mEPSC amplitudes (P = 1, Kolmogorov-Smirnov test, N = 18 for WT; N = 18 for KO). **E**, Cumulative frequency distribution of mEPSC frequencies (P = 1, Kolmogorov-Smirnov test, N = 18 for WT; N = 18 for KO). Error bars represent SEM in all graphs.

The AMPA/NMDA ratio was not altered (WT: 1.8 ± 0.2, N = 22; KO: 1.9 ± 0.2, N = 25; p > 0.05, Mann-Whitney). Second, the paired-pulse ratio (PPR), a measure of changes in the probability of transmitter release, was unchanged (WT: 2.1 ± 0.1, N = 16; KO: 2.1 ± 0.1, N = 24; p > 0.05, Mann-Whitney) (Fig. 6B). Additionally, we compared excitatory miniature excitatory postsynaptic currents (mEPSCs) in *Clcn2⁺ᐟ⁺* and *Clcn2⁻ᐟ⁻* mice to exclude changes in synapse number and synaptic receptor density (Fig. 6C, D). Neither mEPSC amplitude nor frequency was changed (mean mEPSC amplitude: WT: 18.5 ± 1.3 pA, N = 18; KO: 19.9 ± 1.1 pA, N = 18, p = 1; mean mEPSC frequency: WT: 1.5 ± 0.1 Hz, N = 18; KO: 1.5 ± 0.1 Hz, N =18, p = 1, KS). Together, we did not observed any difference in basal excitatory synaptic transmission between WT and KO animals, excluding a change of excitatory synapse function in KO animals as a cause for the reduction in network gain.

GABAergic inhibition is increased in *Clcn2⁻ᐟ⁻* mice

As I/O curves did not differ between WT and KO in the presence of picrotoxin (Fig. 5D), we studied inhibitory synaptic transmission in more detail. Inhibitory interneurons and pyramidal neurons form microcircuits in the hippocampus. Feed-forward inhibition is provided by excitatory inputs that activate both pyramidal cells and inhibitory interneurons (Fig. 8B). Sik and coworkers suggested by immunostaining that ClC-2 is expressed in a small subset of interneurons (Sik et al., 2000). Therefore, we tested whether interneurons show ClC-2 mediated currents. A typical ClC-2 current was detected in a subset of randomly selected interneurons (11 out of 33 neurons; avg. current: 114 ± 17 pA, N = 11) morphologically identified by biocytin filling (Fig. 7A).
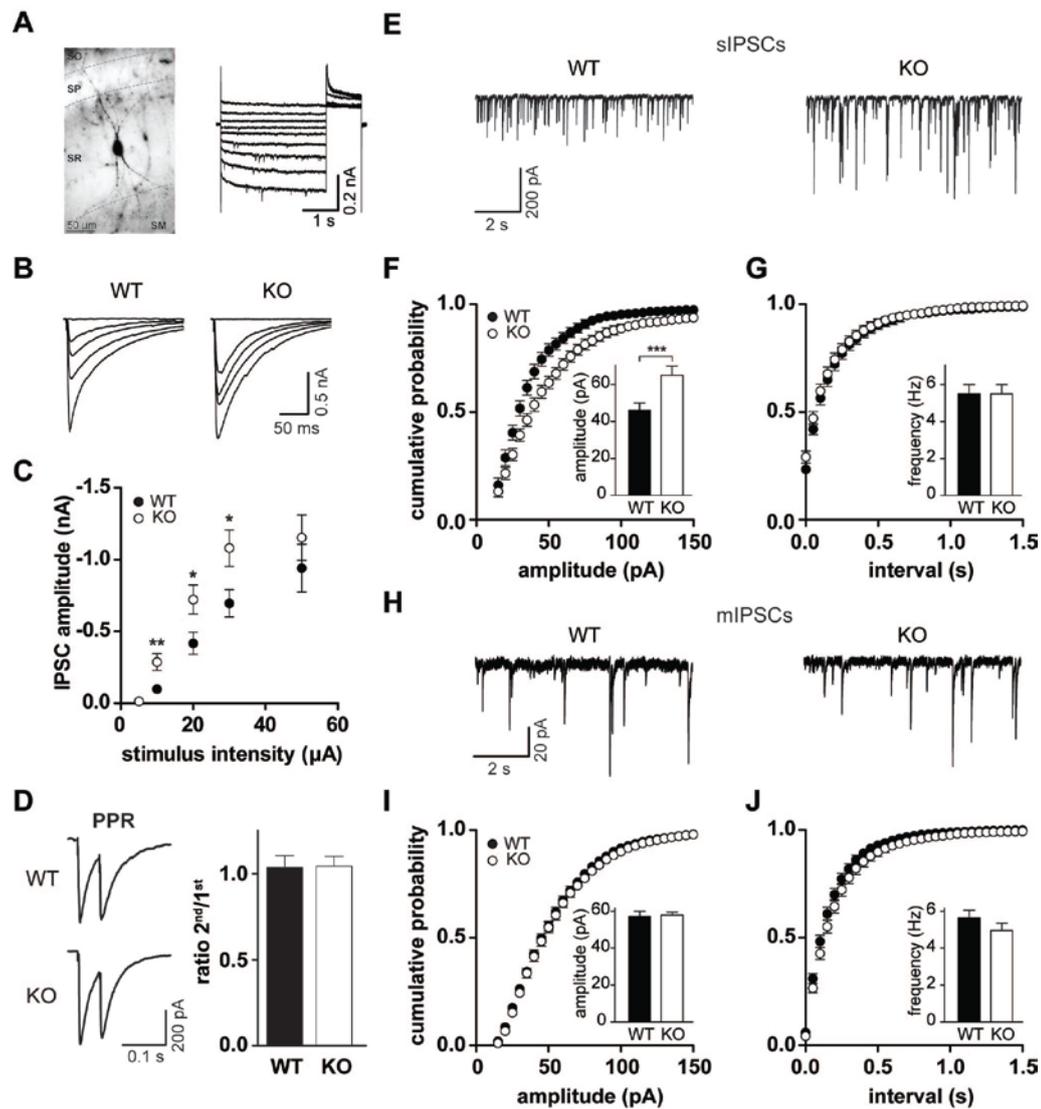
Figure 7: Loss of ClC-2 in interneurons leads to an increased inhibition.

A, ClC-2 is expressed in a subset of interneurons. Sample trace of a ClC-2 current from an interneuron identified by biocytin filling. **B, C**, Evoked IPSCs were measured as a function of the stimulus strength in CA1 pyramidal cells in response to extracellular stimulation by a microelectrode positioned nearby. Sample traces for WT (left) and KO (right) (B). Averaged data reveal an increase of IPSCs (C). **D**, Paired pulse ratio, a measure for presynaptic release shows no difference between WT and KO. Sample traces on the left. Stimulus artifacts have been omitted for clarity. **E**, Sample traces for sIPSCs recordings for WT (left) and KO (right). **F**, Cumulative frequency distribution of sIPSC amplitudes (P < 0.001, Kolmogorov-Smirnov test, N = 24 for WT; N = 24 for KO). Inset shows mean amplitude. **G**, Cumulative frequency distribution of sIPSC frequencies (P = 1, Kolmogorov-Smirnov test, N = 18 for WT; N = 18 for KO). Inset shows mean frequency. **H**, Sample traces for mIPSCs recordings for WT (left) and KO (right). **I**, Cumulative frequency distribution of mIPSC amplitudes (P = 1, Kolmogorov-Smirnov test, N = 22 for WT; N =23 for KO). Inset shows mean amplitude. **J**, Cumulative frequency distribution of mIPSC frequencies (P = 1, Kolmogorov-Smirnov test, N = 22 for WT; N = 23 for KO). Inset shows mean frequency. Error bars represent SEM in all graphs.

No ClC-2 mediated current was seen in 22 interneurons of *Clcn2^{-/-}* animals (data not shown). The large variety of interneuron types (Klausberger and Somogyi, 2008) precluded us from a more detailed analysis of interneuron membrane properties. But, if the increased GABAergic inhibition results from more excitable interneurons evoking IPSCs should be easier in KO than in WT. I/O curves for IPSCs revealed that IPSCs were significantly increased over a range of stimulus intensities (Fig. 7B, C). Only at the highest stimulus intensity this difference was not significant, consistent with the idea that the upper limit of IPSC amplitude is reached when action potentials are evoked in all recruitable interneurons (0.05 µA: WT -12 ± 3 pA, N = 10, KO -12 ± 6 pA, N = 9, p > 0.9; 0.1 µA: WT -97 ± 20 pA, N = 10, KO -286 ± 58 pA, N = 9 , p < 0.005; 0.02 µA: WT -416 ± 77 pA, N = 10, KO -720 ± 101 pA, N = 9 , p < 0.05 ; 0.3 µA: WT -694 ± 95 pA, N = 10, KO -1024 ± 124 pA, N = 9 , p < 0.05; 0.5 µA: WT -939 ± 166 pA, N = 8, KO 1152 ± 158 pA, N = 7, p > 0.4, t-test) (Fig. 7B, C). In addition, a higher excitability of inhibitory neurons should lead to an increased rate of action potential firing reflected in an increased fraction of action potential dependent sIPSCs. If our idea is correct, the average sIPSC amplitude should be increased, as the amplitudes of action potential dependent sIPSCs are bigger than the amplitudes of action potential independent mIPSCs. To test this hypothesis, we measured action potential dependent spontaneous IPSCs (sIPSC) (Fig. 7E - G). Indeed, the mean amplitude of these events was significantly increased (WT: 46 ± 4 pA, N = 24; KO: 65 ± 5 pA, N = 24, p < 0.001, KS) (Fig. 7F). The frequency of events was not changed (WT: 5.5 ± 0.5 Hz, N = 24; KO: 5.5 ± 0.5 Hz, N = 24, p = 1, KS) (Fig. 7G). To exclude changes in the number of postsynaptic receptors, and number of synapses, we recorded miniature IPSCs (mIPSC) (Fig. 7H - J). We did not detect any difference in mIPSC amplitude (Fig. 7I) and mIPSC frequency (Fig. 7J) between the two genotypes (amplitude WT: 57 ± 3 pA, N = 22; KO: 58 ± 2 pA, N = 23, p = 1; frequency WT: 5.6 ± 0.4 Hz, N = 22; KO: 4.9 ± 0.4 Hz, N =23, p = 1, KS). In addition, we recorded the paired pulse ratio (PPR) of two evoked IPSCs, to exclude changes in presynaptic release. We did not detect a difference in PPR between WT and KO, demonstrating that presynaptic release was not affected by the loss of ClC-2 (WT 1.0 ± 0.1, N = 12; KO 1.0 ± 0.1, N = 12; p > 0.4, Mann-Whitney) (Fig. 7D).

Together, the I/O curve of evoked IPSC, and the increase in sIPSC amplitude indicate that more excitable interneurons are the cause for the increased inhibition. In addition, we can exclude increased presynaptic release.

I/O function is changed in *Clcn2^(-/-)* mice

To further study this idea of increased inhibition, we examined the input-output (I/O) characteristic of CA1 pyramidal cells. We use the term neuronal I/O function to refer to the relationship between the excitatory input to a neuron and the probability it will generate an AP (Daoudal and Debanne, 2003; Marder and Buonomano, 2003; Staff and Spruston, 2003). A neuron's I/O curve, generally represented as a sigmoidal function, is characterized by two components: the threshold and the gain. Here, we define the I/O threshold as the EPSP slope that elicits a spike 50 % of the time. The gain refers to the slope of the I/O function (Carvalho and Buonomano, 2009). Carvalho and Buonomano recently described a model predicting that threshold and gain of the I/O function can be independently controlled by changes in excitatory and/or inhibitory synaptic inputs (Carvalho and Buonomano, 2009). More specifically, increased excitation shifts the threshold of the I/O function to the left, while increased inhibition shifts the threshold to the right and additionally decreases gain of the I/O function. We recorded EPSPs at various stimulus intensities and plotted the probability of generating an AP against the slope of the EPSP (Fig. 8C). Typical traces at stimulus intensities around the threshold are presented in Fig. 8A. If our idea of increased inhibition in KO mice is correct, we should see only a small difference in the I/O function of WT and KO in the absence of bicuculline, a $GABA_A$ receptor antagonist, but a stronger difference between WT and KO in the presence of bicuculline. Indeed, in the absence of bicuculline the threshold between KO and WT was not significantly different. In the presence of bicuculline the I/O function for KO neurons shifted significantly more to the left, reflecting a change in threshold (ΔWT: 2.2 ± 0.1, N = 16; ΔKO: 2.8 ± 0.1, N = 16; $p < 0.05$) (Fig. 8D, E). Compatible with the prediction by the model, the slope was also increased more in KO than in WT cells (ΔWT: 0.6 ± 0.1, N = 16; ΔKO: 0.8 ± 0.1, N = 16; $p < 0.05$) (Fig. 8A, C, E). These data clearly indicate that inhibition is strongly increased in *Clcn2^(-/-)* animals.
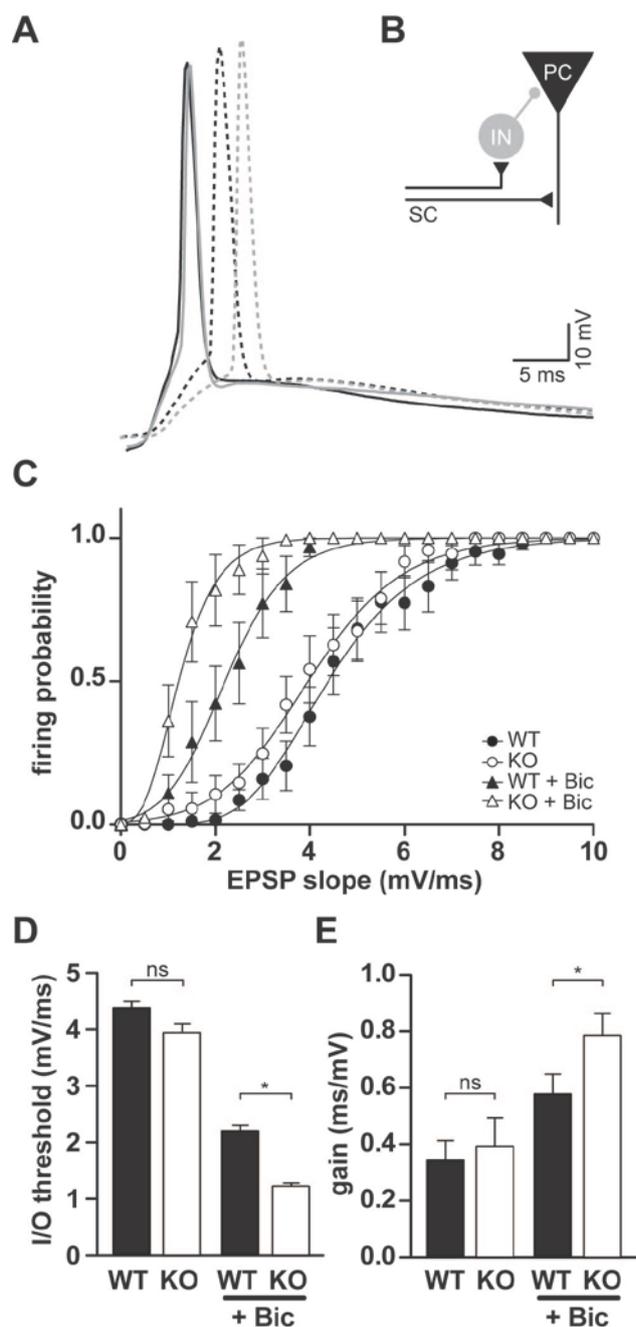
Figure 8: Feed-forward inhibition is increased in *Clcn2*^{-/-} animals.
A, sample traces of evoked EPSP in WT (black) and KO (gray) CA1 neurons in the absence (solid) and presence of bicuculline (dashed). **B**, Schematic diagram of disynaptic feed-forward inhibition. SC, Schaffer collateral; IN, interneuron; PC, pyramidal cell. **C**, Neuronal I/O function. Firing probability plotted against the EPSP slope in the absence (circles) and presence (triangles) of bicuculline for WT (closed symbols) and KO (open symbols). In the absence of bicuculline, I/O functions for WT and KO were not significantly different (N = 16 for WT; N = 16 for KO), while in the presence of bicuculline the I/O function for KO was shifted more to the left relative to WT, and had a steeper slope. **D** and **E**, Average gain and threshold for I/O functions shown in C. Error bars represent SEM in all graphs.

3.5   Discussion

Our data clearly prove that ClC-2 mediates an earlier described chloride conductance (Chesnoy-Marchais, 1983; Madison et al., 1986; Smith et al., 1995) in CA1 pyramidal cells and a subset of interneurons. In addition to the absence of this conductance in $Clcn2^{-/-}$ neurons, we observed the same biophysical properties described in heterologous expression systems such as activation by acidic pH (Jordt and Jentsch, 1997) and a higher permeability for chloride than for iodide (Thiemann et al., 1992).

We used KO mice to test whether ClC-2 is involved in chloride extrusion and if the loss of ClC-2 leads to a higher excitability. We directly demonstrated that the voltage gated chloride channel ClC-2 helps to quickly extrude chloride from neurons after chloride accumulation. More importantly, we revealed that ClC-2 contributes substantially to the background conductance, which has a strong effect on neuronal excitability by changing the input resistance. Surprisingly, fEPSP I/O curves are reduced in $ClC-2^{-/-}$ mice. Our data demonstrate this reduction is caused by an increased activity of a subset of GABAergic interneurons, which thereby decrease activity of excitatory pyramidal cells. This inhibition increase might balance over excitability and thereby prevent seizures in $ClC-2^{-/-}$ mice.

Chloride extrusion

The inhibitory effect of GABA depends on the intracellular chloride concentration, which can be changed by several transporters that couple the movement of chloride across the membrane to that of potassium, sodium, or bicarbonate. The resulting chloride gradient, which is mainly established by NKCC1 and KCC2, determines the response of a particular neuron to GABA. Importantly, however, an inhibitory outcome does not require the chloride reversal potential to be more negative than the resting membrane potential, as a major component of inhibition is mediated by shunting (Bartos et al., 2007). It has been proposed that ClC-2 plays a role in chloride homeostasis (Staley, 1994; Staley et al., 1996; Mladinic et al., 1999; Ben-Ari, 2002); however, the extrusion of chloride was thus far only indirectly shown. Here we provide direct evidence that ClC-2 mediates an efflux pathway for chloride in CA1 neurons, which normally have a low $[Cl^-]_i$. After strongly loading neurons with chloride, by pressure applying GABA during depolarization, $[Cl^-]_i$ returned to initial values more slowly in KO than in WT animals. In addition, we analyzed whether repetitive synaptic activation of $GABA_A$ receptors leads to a stronger chloride accumula-

tion in KO animals. At frequencies of 0.5 and 1 Hz, evoked IPSCs were more depressed in KO than WT animals, indicating a stronger chloride accumulation. These data clearly emphasize that ClC-2 is involved in chloride homeostasis. However, the complex nature of the interplay of chloride reversal potential, shunting inhibition and action potential threshold makes it difficult to predict whether the loss of chloride extrusion via ClC-2 results in a substantial loss of GABAergic inhibition. The effect on chloride extrusion might be more relevant under conditions of high neuronal activity, and the loss of ClC-2 might thereby increase the susceptibility to seizures.

Remarkably, typical ClC-2 currents were not seen during the first postnatal week in CA1 pyramidal cells. This functional expression profile parallels the switch from high to low intracellular chloride (Stein et al., 2004a), compatible with the idea of providing an efflux pathway for chloride, which assists chloride homeostasis.

ClC-2 contributes to the background conductance

Background (or leak) conductances are important in determining membrane resting potential and input resistance, both key components of neuronal excitability. Some of the leak conductance is mediated by the family of two pore potassium channels, which are voltage insensitive, but tightly regulated by cyclic nucleotides, noradrenaline, serotonin, pH, and GABA (for review see (Goldstein et al., 2001; Honore, 2007)). Mouse models suggest that some of these channels are involved in neurological diseases such as epilepsy and depression (Honore, 2007). While two pore potassium channels are largely voltage independent, ClC-2 opening depends on hyperpolarized membrane potentials; however, as ClC-2 closes only very slowly with depolarization, it practically does not close during the brief depolarization of an AP. Thus, the remarkable effect on membrane resistance further indicates that ClC-2 is conductive at resting conditions similar to other channels contributing to the background conductance.

Although the information on the subcellular localization of ClC-2 is limited, Sik and coworkers localized ClC-2 to perinuclear regions and apical dendrites in CA1 neurons (Sik et al., 2000). This localization is complementary with our data, demonstrating that ClC-2 contributes strongly to the leak conductance, more specifically the input resistance, thereby affecting neuronal excitability; however, as the chloride reversal potential is close to the resting membrane potential (Tyzio et al., 2008), the loss of ClC-2 does not affect the resting membrane potential. It is tempting to speculate that modulating ClC-2 by neuronal activity changing extracellular pH or the activity of PKC could regulate neuronal excitability.

Increased inhibition

Surprisingly, the network gain is reduced in *Clc2*$^{-/-}$ mice. Generally, a decrease in fEPSP I/O curves reflects a change in excitatory synaptic transmission. But, when we repeated the fEPSP recordings in the presence of picrotoxin blocking GABAergic inhibition, we did not observe any difference between the two genotypes. As AMPA / NMDA ratios, paired pulse facilitation, and mEPSCs could not account for this reduction, we excluded a change in excitatory synaptic transmission. The fEPSP I/O curves recorded in the presence of picrotoxin suggested a change in GABAergic inhibition. A subset of interneurons showed ClC-2 mediated currents; however, the large variety of interneuron subtypes did not allow for a specific characterization of membrane properties of these neurons. We showed that evoked IPSCs are bigger in *Clcn2*$^{-/-}$ animals over a range of stimulus intensities. In addition, the increase in the amplitude of action potential dependent sIPSC further supports the idea of more excitable interneurons. We did not find a change in the frequency of sIPSCs, as one could have expected. But, as only a subset of interneurons expresses ClC-2, a change in sIPSC frequency might not be detectable. As mIPSC amplitude and frequency, as well as PPR of evoked IPSCs were not altered, we can exclude a change in number of postsynaptic GABA$_A$ receptors, inhibitory synapse number, and probability of release as cause for the increased inhibition.

In a final set of recordings, we revealed that the neuron's I/O function is not altered in *Clcn2*$^{-/-}$ mice compared to *Clcn2*$^{+/+}$ mice. In contrast, in the presence of bicuculline, the threshold of neurons of *Clcn2*$^{-/-}$ mice was shifted more to the left and had a bigger gain than in *Clcn2*$^{+/+}$ mice.

Together, these experiments confirm that the loss of ClC-2 leads to an increase in neuronal inhibition in KO animals.

ClC-2 and epilepsy

Whether mutations in ClC-2 cause epilepsy or not has been controversial. Over the last years several mutations in the gene encoding for ClC-2 have been described (Stogmann et al., 2006; Everett et al., 2007; Combi et al., 2009; Saint-Martin et al., 2009); however, the paper by Haug which established the link between mutations in *CLCN2* and epilepsy has recently been retracted (Haug et al., 2009). Moreover, mutations found in humans do not lead to drastic changes in biophysical properties of ClC-2 (Blanz et al., 2007), as one might expect for a single disease causing gene. In contrast, the complete loss of ClC-2 in mice did not lead to higher seizure susceptibility (Bosl et al., 2001; Blanz et al., 2007). In addition, as discussed above, it is difficult to predict whether the loss of chloride extrusion via ClC-2 results in a substantial loss of GABAergic inhib-

tion under prolonged paroxysmal conditions that could lead to hyperexcitability. Therefore, the loss of ClC-2 might increase the susceptibility of seizures by impairing inhibition. Moreover, we cannot exclude that mutated ClC-2 proteins are trafficked differently or the interactions with other proteins are disturbed affecting the function of ClC-2.

Summary and Outlook

This work revealed an important role of ClC-2 in neuronal excitability. ClC-2 is not only expressed in pyramidal neurons but also in a subset of inhibitory interneurons. The loss of ClC-2 in interneurons increases inhibition mediated by a higher excitability of a subpopulation of interneurons. The increased inhibition might balance hyperexcitability of the network and thereby preventing epilepsy in ClC-2 knock-out mice. Together, we suggest that ClC-2 in neurons regulates excitability via the membrane resistance and provides an additional efflux pathway for chloride. The effects on membrane resistance pose the question whether ClC-2 is regulated by neuronal activity, for example by changing extracellular pH or PKC activity, thereby regulating neuronal excitability.

3.6   References

Bartos M, Vida I, Jonas P (2007) Synaptic mechanisms of synchronized gamma oscillations in inhibitory interneuron networks. Nat Rev Neurosci 8:45-56.

Ben-Ari Y (2002) Excitatory actions of gaba during development: the nature of the nurture. Nat Rev Neurosci 3:728-739.

Blanz J, Schweizer M, Auberson M, Maier H, Muenscher A, Hubner CA, Jentsch TJ (2007) Leukoencephalopathy upon disruption of the chloride channel ClC-2. J Neurosci 27:6581-6589.

Bosl MR, Stein V, Hubner C, Zdebik AA, Jordt SE, Mukhopadhyay AK, Davidoff MS, Holstein AF, Jentsch TJ (2001) Male germ cells and photoreceptors, both dependent on close cell-cell interactions, degenerate upon ClC-2 Cl(-) channel disruption. Embo J 20:1289-1299.

Brumback AC, Staley KJ (2008) Thermodynamic regulation of NKCC1-mediated Cl- cotransport underlies plasticity of GABA(A) signaling in neonatal neurons. J Neurosci 28:1301-1312.

Carvalho TP, Buonomano DV (2009) Differential effects of excitatory and inhibitory plasticity on synaptically driven neuronal input-output functions. Neuron 61:774-785.

Chenoy-Marchais D (1982) A Cl- conductance activated by hyperpolarization in Aplysia neurones. Nature 299:359-361.

Chesnoy-Marchais D (1983) Characterization of a chloride conductance activated by hyperpolarization in Aplysia neurones. The Journal of physiology 342:277-308.

Combi R, Grioni D, Contri M, Redaelli S, Redaelli F, Bassi MT, Barisani D, Lavitrano ML, Tredici G, Tenchini ML, Bertolini M, Dalpra L (2009) Clinical and genetic familial study of a large cohort of Italian children with idiopathic epilepsy. Brain Res Bull 79:89-96.

D'Agostino D, Bertelli M, Gallo S, Cecchin S, Albiero E, Garofalo PG, Gambardella A, St Hilaire JM, Kwiecinski H, Andermann E, Pandolfo M (2004) Mutations and polymorphisms of the CLCN2 gene in idiopathic epilepsy. Neurology 63:1500-1502.

Daoudal G, Debanne D (2003) Long-term plasticity of intrinsic excitability: learning rules and mechanisms. Learn Mem 10:456-465.

Everett K et al. (2007) Linkage and mutational analysis of CLCN2 in childhood absence epilepsy. Epilepsy research 75:145-153.

Goldstein SA, Bockenhauer D, O'Kelly I, Zilberberg N (2001) Potassium leak channels and the KCNK family of two-P-domain subunits. Nat Rev Neurosci 2:175-184.

Grunder S, Thiemann A, Pusch M, Jentsch TJ (1992) Regions involved in the opening of ClC-2 chloride channel by voltage and cell volume. Nature 360:759-762.

Haug K et al. (2009) Retraction: Mutations in CLCN2 encoding a voltage-gated chloride channel are associated with idiopathic generalized epilepsies. Nature genetics 41:1043.

Honore E (2007) The neuronal background K2P channels: focus on TREK1. Nat Rev Neurosci 8:251-261.

Huguenard JR, Alger BE (1986) Whole-cell voltage-clamp study of the fading of GABA-activated currents in acutely dissociated hippocampal neurons. J Neurophysiol 56:1-18.

Jentsch TJ, Stein V, Weinreich F, Zdebik AA (2002) Molecular structure and physiological function of chloride channels. Physiol Rev 82:503-568.

Jordt SE, Jentsch TJ (1997) Molecular dissection of gating in the ClC-2 chloride channel. Embo J 16:1582-1592.

Klausberger T, Somogyi P (2008) Neuronal diversity and temporal dynamics: the unity of hippocampal circuit operations. Science 321:53-57.

Ling DS, Benardo LS (1995) Activity-dependent depression of monosynaptic fast IPSCs in hippocampus: contributions from reductions in chloride driving force and conductance. Brain research 670:142-146.

Madison DV, Malenka RC, Nicoll RA (1986) Phorbol esters block a voltage-sensitive chloride current in hippocampal pyramidal cells. Nature 321:695-697.

Marder CP, Buonomano DV (2003) Differential effects of short- and long-term potentiation on cell firing in the CA1 region of the hippocampus. J Neurosci 23:112-121.

McCarren M, Alger BE (1985) Use-dependent depression of IPSPs in rat hippocampal pyramidal cells in vitro. J Neurophysiol 53:557-571.

Mladinic M, Becchetti A, Didelon F, Bradbury A, Cherubini E (1999) Low expression of the ClC-2 chloride channel during postnatal development: a mechanism for the paradoxical depolarizing action of GABA and glycine in the hippocampus. Proc Biol Sci 266:1207-1213.

Nehrke K, Arreola J, Nguyen HV, Pilato J, Richardson L, Okunade G, Baggs R, Shull GE, Melvin JE (2002) Loss of hyperpolarization-activated Cl(-) current in salivary acinar cells from Clcn2 knockout mice. The Journal of biological chemistry 277:23604-23611.

Obata K, Oide M, Tanaka H (1978) Excitatory and inhibitory actions of GABA and glycine on embryonic chick spinal neurons in culture. Brain research 144:179-184.

Saint-Martin C, Gauvain G, Teodorescu G, Gourfinkel-An I, Fedirko E, Weber YG, Maljevic S, Ernst JP, Garcia-Olivares J, Fahlke C, Nabbout R, LeGuern E, Lerche H, Christophe Poncer J, De-

pienne C (2009) Two novel CLCN2 mutations accelerating chloride channel deactivation are associated with idiopathic generalized epilepsy. Hum Mutat 30:397-405.

Sik A, Smith RL, Freund TF (2000) Distribution of chloride channel-2-immunoreactive neuronal and astrocytic processes in the hippocampus. Neuroscience 101:51-65.

Smith RL, Clayton GH, Wilcox CL, Escudero KW, Staley KJ (1995) Differential expression of an inwardly rectifying chloride conductance in rat brain neurons: a potential mechanism for cell-specific modulation of postsynaptic inhibition. J Neurosci 15:4057-4067.

Staff NP, Spruston N (2003) Intracellular correlate of EPSP-spike potentiation in CA1 pyramidal neurons is controlled by GABAergic modulation. Hippocampus 13:801-805.

Staley K (1994) The role of an inwardly rectifying chloride conductance in postsynaptic inhibition. J Neurophysiol 72:273-284.

Staley K, Smith R, Schaack J, Wilcox C, Jentsch TJ (1996) Alteration of GABAA receptor function following gene transfer of the CLC-2 chloride channel. Neuron 17:543-551.

Stein V, Hermans-Borgmeyer I, Jentsch TJ, Hubner CA (2004) Expression of the KCl cotransporter KCC2 parallels neuronal maturation and the emergence of low intracellular chloride. The Journal of comparative neurology 468:57-64.

Stobrawa SM, Breiderhoff T, Takamori S, Engel D, Schweizer M, Zdebik AA, Bosl MR, Ruether K, Jahn H, Draguhn A, Jahn R, Jentsch TJ (2001) Disruption of ClC-3, a chloride channel expressed on synaptic vesicles, leads to a loss of the hippocampus. Neuron 29:185-196.

Stogmann E, Lichtner P, Baumgartner C, Schmied M, Hotzy C, Asmus F, Leutmezer F, Bonelli S, Assem-Hilger E, Vass K, Hatala K, Strom TM, Meitinger T, Zimprich F, Zimprich A (2006) Mutations in the CLCN2 gene are a rare cause of idiopathic generalized epilepsy syndromes. Neurogenetics 7:265-268.

Thiemann A, Grunder S, Pusch M, Jentsch TJ (1992) A chloride channel widely expressed in epithelial and non-epithelial cells. Nature 356:57-60.

Thompson SM, Gahwiler BH (1989) Activity-dependent disinhibition. I. Repetitive stimulation reduces IPSP driving force and conductance in the hippocampus in vitro. J Neurophysiol 61:501-511.

Tyzio R, Minlebaev M, Rheims S, Ivanov A, Jorquera I, Holmes GL, Zilberter Y, Ben-Ari Y, Khazipov R (2008) Postnatal changes in somatic gamma-aminobutyric acid signalling in the rat hippocampus. The European journal of neuroscience 27:2515-2528.

Zuniga L, Niemeyer MI, Varela D, Catalan M, Cid LP, Sepulveda FV (2004) The voltage-dependent ClC-2 chloride channel has a dual gating mechanism. The Journal of physiology 555:671-682.

4 MANUSCRIPT III

The voltage gated chloride channel ClC-2 forms the chloride background conductance in neurons

This chapter is planned to submit by Ilka Rinke and Valentin Stein

Max Planck Institute of Neurobiology

Ilka Rinke performed the experiments and wrote the manuscript. *Ilka Rinke* and Valentin Stein conceived the experiments. Valentin Stein reviewed the manuscript.

4.1   Abstract

Neurons exhibit a resting permeability for potassium, sodium and chloride; however, the molecular identity for a chloride leak conductance is still unknown. Here, we observe a chloride conductance in principal neurons of hippocampus, cortex and cerebellum, essentially mediated by the voltage-gated chloride channel ClC-2. Current-clamp recordings revealed that the loss of ClC-2 leads to a small shift of the resting membrane potential towards more depolarized values and to a remarkable increase of the membrane resistance in pyramidal cells of CA1 and cortex. Moreover, the number of action potentials increases in all recorded subtypes of neurons lacking ClC-2. Thus, ClC-2 is proposed to provide the molecular basis for the chloride leak conductance. The ClC-2 leak conductance is present in various neuron types throughout the brain regulating neuronal excitability.

4.2   Introduction

The electrophysiological behavior of a neuron either spontaneously or to an extern stimulus is determined by the resting membrane potential and the ionic currents across the cell membrane. In the absence of an extrinsic input, leak conductances affect basal membrane properties and therefore the neuronal excitability. Under resting conditions the cell membrane is predominantly permeable to potassium, conducted through two-pore potassium channels (Goldstein et al., 2001). The resting membrane potential in mammalian neurons ranges between -60 mV and -90 mV, clearly above the equilibrium of potassium (E_K = -103 mV). This suggests additional leak conductances provided by other ions: for example leak of sodium and chloride pull the membrane towards their Nernst potentials (about +67 and -93 mV, respectively) (Goldstein et al., 2001). A non-selective, voltage-independent and not inactivating sodium channel (NALCN) has been shown to mediate the sodium leak conductance (Lu et al., 2007). Beyond that, Hodgkin and Huxley (1952) proposed a chloride conductance, which constitutes at least a small fraction to the total leak conductance of a neuron (Hodgkin and Huxley, 1952). However, the molecular basis for such a chloride leak conductance in major neuronal cell types remains to be investigated.

The voltage-gated chloride channel ClC-2 would be a suitable candidate to provide a chloride leak conductance at resting conditions. The chloride conductance mediated by ClC-2 has been

previously described in neurons and non-neuronal cells (Chesnoy-Marchais, 1983; Misgeld et al., 1986; Parker and Miledi, 1988). ClC-2 is activated by negative membrane voltage, cell swelling, a rise in intracellular chloride concentration, or mild extracellular acidification (Grunder et al., 1992; Thiemann et al., 1992; Jordt and Jentsch, 1997; Zuniga et al., 2004). ClC-2 is inwardly rectifying, with significant conductance only at membrane potentials more negative than the chloride equilibrium potential (E_{Cl}). Further, ClC-2 stabilizes the relationship between E_{Cl} and resting membrane potential independent of electroneutral chloride transport (Staley, 1994). Due to its properties, it is not surprising that ClC-2 regulates neuronal chloride homeostasis by providing a fast chloride extrusion mechanism (Rinke et al., 2010). In addition, we recently provided evidence that ClC-2 influences neuronal excitability via affecting intrinsic membrane properties in hippocampal CA1 pyramidal neurons. Because ClC-2 is active at resting membrane potential and contributes to the membrane resistance (R_N) (Madison et al., 1986), we assumed that ClC-2 constitutes a significant part to the chloride leak conductance in this particular cell type (Rinke et al., 2010).

Here we hypothesize, that ClC-2 acts as a fundamental chloride leak conductance in principal neurons of the brain. We observed ClC-2-mediated currents in neurons of hippocampal formation, cortex and cerebellum. The disruption of ClC-2 increases the input resistance in almost all of the specific types of recorded neurons, supporting our previous findings in CA1 pyramidal cells of the hippocampus (Rinke et al., 2010).

4.3   Materials and Methods

Mice: The generation of ClC-2 knockout mice (*Clcn2$^{-/-}$*) was described elsewhere (Bosl et al., 2001). Both, male and female mice of postnatal day 12 to 23 (P12-23) were used for all experiments.

Slice preparation: Animals were anesthetized with Isoflurane (Baxter), and decapitated. Brains were removed quickly, and chilled in 4°C cold, carbogen (95% O_2; 5% CO_2) gassed artificial cerebro spinal fluid (ACSF) containing (in mM): 130.9 NaCl; 2.75 KCl; 1.43 $MgSO_4$; 2.5 $CaCl_2$; 1.1 NaH_2PO_4; 28.82 $NaHCO_3$ and 11.1 D-glucose with an osmolarity of 315-325 mosm/l. Coronal slices (400 µM) were cut from Hippocampus (P12-P21), Cerebellum (P17-P21) and Cortex (P17-P23) with a vibratome (VT1200S, Leica). Prior to recording slices were kept for 30 min at 32°C and subsequently stored at room temperature in ACSF continuously gassed with carbogen.

Electrophysiology: All recordings were performed using a Multiclamp 700B amplifier (Molecular Devices, Sunnyvale, CA). Data were digitized using a Digidata 1322A (Molecular Devices, Sunnyvale, CA). Pipettes (3-5 MΩ) were pulled from borosilicate glass (Science Products, Hofheim, Germany). Inputs from CA3 to CA1 were severed to prevent propagation of epileptiform activity. Liquid junction potentials were calculated with the liquid junction potential assistant of pClamp. Membrane potentials were corrected by -15 mV.

Whole cell recordings: Whole cell recordings were obtained from pyramidal cells of CA1 hippocampus, granule cells of dentate gyrus, pyramidal cells of cortical layer II/III as well as V and purkinje cells of cerebellum. The recorded cells were visualized using differential interference contrast infrared video microscopy.

ClC-2 currents: chloride currents were recorded with high chloride pipette solution containing (in mM): 90 CsCl; 20 CsGluconate; 8 NaCl; 2 $MgCl_2$; 10 HEPES; 1 EGTA, and 2 QX314 (Alomone Labs, Israel); pH 7.2; 290 mosm/l and Alexa 594 fluorescent dye for subsequent determination of morphology. Extracellular recording solution contained (in mM): 70 NaCl; 2.5 KCl, 16 $MgSO_4$, 26.2 $NaHCO_3$; 11 Glucose; 30 Tetraethylammonium-chloride, 10 CsCl; supplemented with 200 nM tetrodotoxin (TTX) to block action potentials (APs). Neurons were identified as such by their location and morphology. ClC-2 chloride currents were evoked by stepping the membrane potential from -10 mV to -120 mV for 4 s (see Fig. 1F). ClC-2-mediated currents were calculated as the difference of the inward current at the beginning and the end of the voltage step.

Current clamp recordings: Pipette solutions contained (in mM) 150 K-methylsulphonate, 4 KCl, 4 NaCl, 4 MgATP, 0.4 Mg GTP and 10 HEPES. We recorded the voltage response to hyperpolarizing and depolarizing current injection directly into the soma of the neuron. The membrane resistance was estimated by the delta voltage (steady-state voltage – resting membrane potential) divide of the step current. The action potential (AP) threshold ΔV was determined using the first derivative of single APs. The sag ratio was calculated by steady-state voltage divided of peak voltage.

Posthoc analysis: Slices were fixed in 4 % paraformadehyde (PFA in 0.1 M phosphate-buffered saline (PBS), pH 7.3) for at least 30 minutes at RT. After washing three times for 10 minutes with PBS, slices were embedded in Fluoro-Gel mounting medium (Electron Microscopy Sciences, Hatfield). Subsequently, Alexa filled neurons were imaged with confocal microscopy.

Data Analysis: All data were analyzed using Clampfit 10.2 (Molecular Devices, Sunnyvale, CA), Prism 5 (GraphPad, La Jolla, CA), and Matlab (The Mathworks, Natick, MA). Data are presented

as means ± SEM. Differences between groups were tested using the Student's t-test (when normally distributed), the Mann-Whitney test (when not normally distributed) as indicated. P values are reported in the text and significance was set as p < 0.05; in Figures (*) represents p < 0.05, (**) p < 0.01, (***) p < 0.001. N represents the number of cells examined.

4.4   Results

ClC-2 mediated currents are present in major neuronal regions of the brain

It is known that ClC-2 is ubiquitously expressed, as revealed by northern analysis of RNA in different rat tissues (Thiemann et al., 1992). The presence of ClC-2 mRNA in various brain regions and spinal cord has been shown earlier by *in situ* hybridization (Smith et al., 1995). Functionally, the hyperpolarization activated chloride conductance mediated by ClC-2 was already well characterized in CA1 pyramidal neurons (Madison et al., 1986; Staley, 1994; Rinke et al., 2010). Now, we study and compare the functional expression of the ClC-2 mediated current in principal neuronal cell types of various brain regions.

Recorded neurons were identified by their location and morphology. ClC-2 currents were isolated by blocking potassium and sodium conductances, as described earlier (Madison et al., 1986; Rinke et al., 2010). First, we showed as a control the characteristic slow activation at negative membrane potentials and a prominent inward rectification of ClC-2 in CA1 neurons of the hippocampus, exhibiting a delta current (ΔI) of -640 ± 71 pA (n = 33) (Fig. 1A). *Posthoc* analysis of the recorded cell confirmed that the ClC-2 typical current was obtained from pyramidal cells (Fig. 1A). Furthermore, we observed such a chloride current in neurons of the dentate gyrus (Fig. 1B). The principal cells of the dentate gyrus are densely packed. The recorded cells show a small soma (~10 µm) and a monopolar dendritic tree, characteristic for granule cells of dentate gyrus (Fig. 1B). In cortex, we measured from neurons in layer II/III (Fig. 1C) and layer V (Fig. 1D). All recorded cells exhibit pyramidal cell like structures with smaller somata of the neurons in layer II/III than those of layer V (Fig. 1C and D, respectively). Recordings of neurons in both cortical layers (Fig. 1C-D) revealed a similar conductance as observed in hippocampal neurons. Moreover, we found such a conductance also in cerebellar purkinje cells (Fig. 1E). This cell type is characterized by the large reciprocating soma and a complex elaborated dendritic arbor both orientated monoplanar (Fig. 1E). The magnitude of the observed chloride current varied markedly among the diverse types of neurons (granule cells: 63 ± 5 pA, n = 24; layer II/III pyramidal cells: 207 ± 41 pA, n = 27; layer V pyramidal cells: 475 ± 49 pA, n = 30; purkinje cells: 533 ± 118 pA, n =

19; ANOVA) (Fig. 1F). Such a chloride conductance typical for ClC-2 was absent in recordings of ClC-2 knockout mice (*Clcn2*$^{-/-}$) under the same conditions (see Rinke et al., 2010). These data clearly demonstrate that the observed chloride conductance present in neurons of distinct brain regions is essentially mediated by ClC-2.
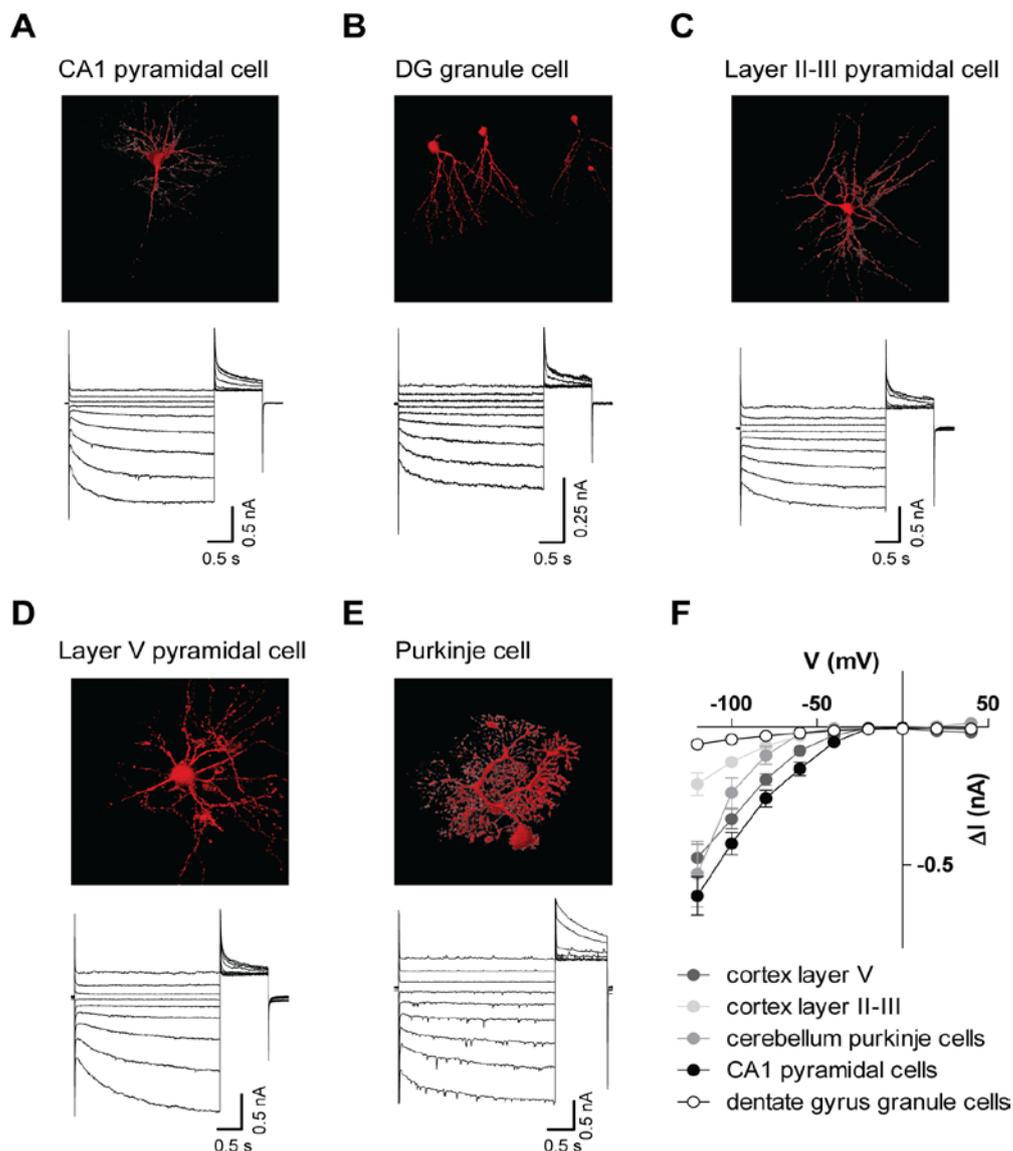
Figure 1: ClC-2 is functionally expressed in major neuronal cell types of various brain regions.
Currents were elicited by voltage steps of 4 s from a holding potential of -10 mV to values between 40 mV and -120 mV in steps of -20 mV followed by a test pulse of +40 mV for 2 s. **A**, As a control, the characteristic ClC-2 current (below) is activated by hyperpolarization and shows typical inward rectification. The 3-D reconstruction (upper panel) revealed that the observed current was obtained from CA1 pyramidal cells of hippocampus. **B-E**, ClC-2 mediated currents are also present in other major neuronal regions of the brain: granule cells of the dentate gyrus (**B**) pyramidal cells of cortical layer II/III (**C**), pyramidal cells of cortical layer V (**D**) and purkinje cells of cerebellum (**E**). **F**, Current - voltage plot of steady state currents summarized for the principal neurons of hippocam-

pus (black), dentate gyrus (white), layer II/III (light grey) and layer V (dark grey) of cortex as well as for cerebellum (middle grey). **G,** Under the same recording conditions as in WT mice, no currents were elicited from *Clcn2*$^{-/-}$ animals. Example trace was obtained from a CA1 pyramidal cell. Error bars represent SEM in all graphs. Note that the symbol size might occlude error bars.

ClC-2 affects intrinsic membrane properties in principal neuronal cell types of major regions of the brain

ClC-2 is active at the resting membrane potential. Therefore, ClC-2 should contribute substantially to the resting conductance of the membrane (Madison et al., 1986) and affect the resting membrane properties like the membrane resistance and/or resting membrane potential. With current clamp recordings (Fig. 2A, C, E), we investigate the effect of ClC-2 on intrinsic membrane properties of different neuronal cell types within major brain regions (Fig. 2).

Leak currents adjust the resting membrane potential (V_m) to their equilibrium, respectively (Goldstein et al., 2001). Here, we found a slight but significant depolarizing shift of V_m in CA1 neurons of *Clcn2*$^{-/-}$ compared to WT (WT: -62.8 ± 1.0 mV, n = 17, KO: -60.4 ± 0.6 mV, n = 16, p < 0.05, unpaired t-test) (Fig. 2B) as well as in cortical pyramidal neurons (WT: -63.6 ± 0.5 mV, n = 21, KO: -59.5 ± 1.3 mV, n = 12, p < 0.01, unpaired t-test) (Fig. 2D).

The most remarkable effect we observed on the membrane resistance (R_N). The disruption of ClC-2 led to a strong increase of R_N in CA1 pyramidal cells (WT: 151 ± 6 MΩ, n = 17, KO: 286 ± 15 MΩ, n = 16, p < 0.0001, unpaired t-test) (Fig. 2B) as well as in cortical layer V pyramidal cells in KO animals (WT: 131 ± 8 MΩ, n = 21, KO: 185 ± 8 MΩ, n = 12, p < 0.001, unpaired t-test) (Fig. 2D). Moreover, the voltage threshold (ΔV) to elicit an action potential was significantly decreased in *Clcn2*$^{-/-}$ animals both in pyramidal cells of CA1 (WT: 27.7 ± 1.3 mV, n = 17, KO: 20.1 ± 1.0 mV, n = 16, p = 0.0001, unpaired t-test) (Fig. 2B) and of cortical layer V (WT: 29.2 ± 0.9 mV, n = 21, KO: 25.2 ± 0.9 mV, n = 12, p = 0.01, unpaired t-test) (Fig. 2D). The observed effects on the resting membrane potential, the membrane resistance and the voltage threshold result in an increased number of action potentials in KO animals, elicited with same current injected (CA1 pyramidal cell: p < 0.01, cortex layer V pyramidal cell: p < 0.001, paired t-test) (Fig. 2A-D). In contrast, the resting membrane properties in cerebellar purkinje cells were not changed, neither V_m (WT: -49.8 ± 1.2 mV, n = 11, KO: -47.8 ± 1.0 mV, n = 10, p > 0.05, unpaired t-test), R_N (WT: 85.6 ± 4 MΩ, n = 11, versus KO: 94 ± 4 MΩ, n = 10, p > 0.05, unpaired t-test) nor ΔV (WT: 15.6 ± 1.4 mV, n = 11, KO: 13.8 ± 1.0 mV, n = 10, p > 0.05, unpaired t-test) differ between the genotypes (Fig. 2F). However, the number of action potentials in purkinje cells of *Clcn2*$^{-/-}$ animals was increased (p < 0.001, paired t-test) (Fig. 2E-F), similar to what we found in neurons of CA1 (Fig. 2A-B) and cortex (Fig. 2C-D)
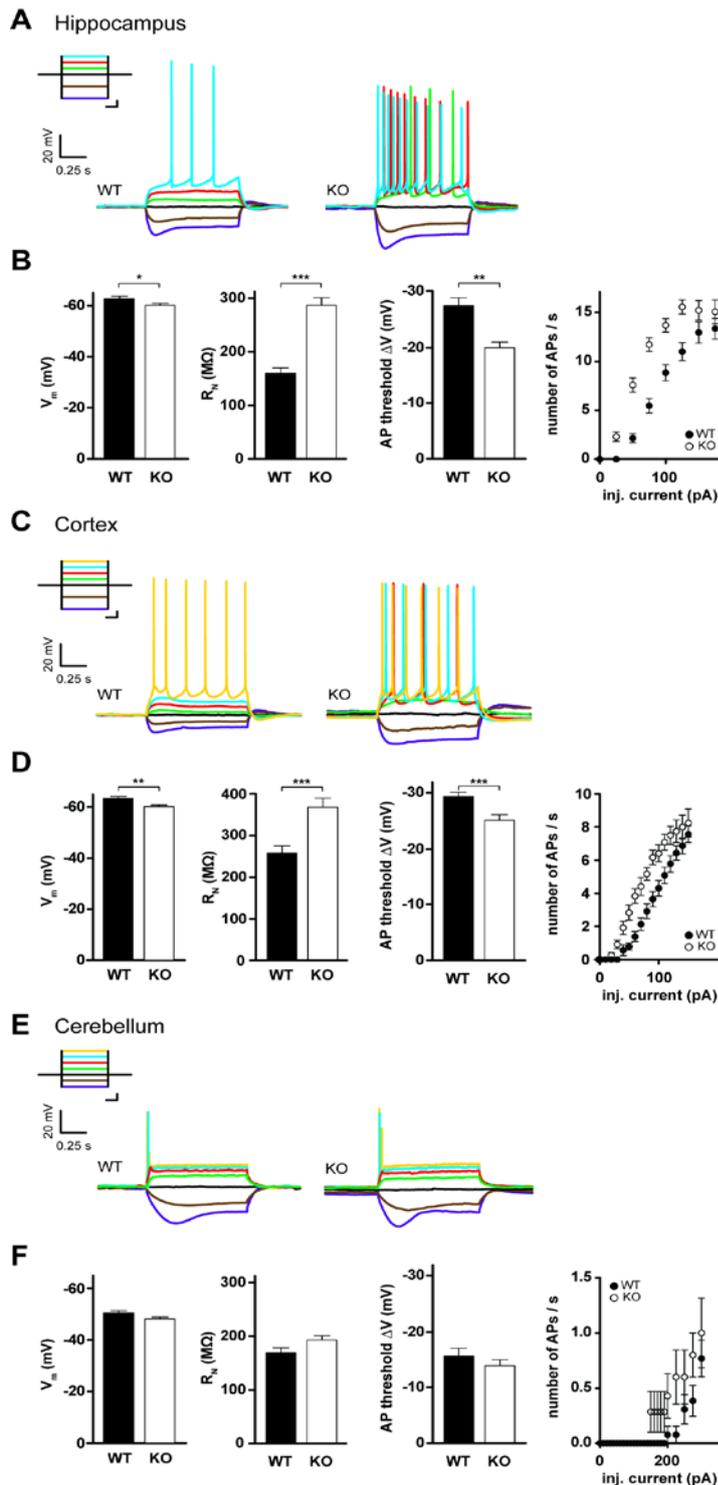
Figure 2: Intrinsic membrane properties of *Clcn2⁻ᐟ⁻* pyramidal neurons are altered.

A, C and E, Sample traces of current clamp recordings in principal cells of hippocampus **(A)**, accept as control, layer V of cortex **(C)** and of cerebellum **(E)**, comparing WT (left) and KO (right). Insets show the current step protocol, same colors indicate same injected currents for distinct cell types, respectively. Scale bar for inset 250 ms, 25 pA. **B, D and F,** Comparison of resting membrane potential (V_m) membrane resistance (R_N), action potential (AP) threshold, and number of APs generated at various current injections. Closed symbols represent WT, open symbols represent KO. Error bars represent SEM in all graphs.

Consistently for all analyzed cell subtypes, the sag ratio remained unaltered between the genotypes (CA1 pyramidal cell WT: 0.7 ± 0.1, n = 17, KO: 0.8 ± 0.1, n = 16; cortex layer V pyramidal cell WT: 1.0 ± 0.005, n = 21, KO: 0.9 ± 0.01, n = 12; purkinje cell WT: 0.8 ± 0.01, n = 11, KO: 0.8 ± 0.02, n = 10; $p > 0.05$, unpaired t-test) (data not shown). Taken together, our data clearly reveal that ClC-2 constitutes a significant part of the leak conductance, affecting resting membrane properties and thereby modulating the excitability of the neuron.

4.5   Discussion

We hypothesized that ClC-2 contributes a substantial part to the leak conductance in neurons. We found a ClC-2 mediated chloride conductance in principal neurons of major regions of the brain. Importantly, we provide direct evidence that ClC-2 affect resting membrane properties of almost all recorded cell types, thus influencing their excitability and firing behavior significantly.

ClC-2 is functionally expressed in principal cells of major regions of the brain

According to the characteristic properties as described earlier for the voltage-gated chloride channel ClC-2 (Chesnoy-Marchais, 1983; Madison et al., 1986; Smith et al., 1995), the chloride conductance, which we observed in principal neurons of major regions of the brain activated upon hyperpolarization, showed inward rectification and non-inactivating behavior. The chloride conductance is mediated by ClC-2, which was confirmed by studies of KO animals (Rinke et al., 2010). In agreement with the ClC-2 mRNA expression pattern in rat brain (Smith et al., 1995), we observed that ClC-2 functionally acts in pyramidal cells of CA1, cortical layer II/III and layer V as well as in purkinje cells of cerebellum. The magnitude of the recorded chloride conductance increased with size of the neuron, consistent with the distribution of ClC-2 mRNA, which was highest in the largest classes of neurons (Smith et al., 1995). Hence, ClC-2 expression might correlate with the size of the neuron.

In contrast to other studies (Staley, 1994; Smith et al., 1995), we detected a significant ClC-2 mediated conductance in granule cells of dentate gyrus. One first possible explanation for the difference could be that the results were obtained from different species; whilst our studies involved mice they used rats. Secondly and also considered by Smith et al. (1995), the amount of mRNA may not directly reflect the amount of protein in the cells (Smith et al., 1995), suggesting that *in situ* hybridization is not as sensitive to detect small amounts of mRNA.

ClC-2 provides the fundamental leak conductance for chloride

The intrinsic physiological properties of a neuron`s membrane such as resting membrane potential and input resistance determine the excitability of the neuron, fundamentally. These properties depend largely on the leak conductances of potassium, sodium and other ions. Potassium leak is provided by KCNK channels and two-P-domain channels (Goldstein et al., 2001). For example, Kir subunits containing channels are crucial for heart rate control (Krapivinsky et al., 1995), Kv subunits containing channels are important in skeletal muscle (Abbott et al., 2001) and

KCNQ subunit containing channels contribute to M-currents in sympathetic neurons and the central nervous system (Jentsch, 2000).

Sodium resting permeability is known to be mediated by hyperpolarization-activated cation channels (I_h) (Storm, 1987; Robinson and Siegelbaum, 2003; Brager and Johnston, 2007) and by a TTX-sensitive component (Crill, 1996). However, a widely expressed voltage-independent, non-selective cation channel formed by NALCN provides the majority of sodium leak conductance (Lu et al., 2007).

Based on experiments in the squid giant axon, the model of Hodgkin and Huxley (1952) predicts that the resting membrane potential is not only established by potassium and sodium leak conductances but also, at least to a small fraction, by a chloride leak conductance (Hodgkin and Huxley, 1952). Moreover, a computational model demonstrates that the leak conductance density, G_L, in the squid giant axon appears to be optimal for the action potential firing frequency if chloride channels are assumed (Seely and Crotty, revised 2009). In skeletal muscle, the stabilizing influence of chloride channels on the membrane potential is highly significant (Hille, 2001). The loss of ClC-1 for example leads to myotonia, an intrinsic muscle hyperexcitability (Steinmeyer et al., 1991b). Although neurons exhibit only a small proportion of resting chloride permeability, a leak chloride conductance (g_{Cl}) and unitary chloride channels are found there as well (Franciolini and Nonner, 1987; Inoue, 1988). Our data provide direct evidence that the chloride channel ClC-2 possesses characteristic properties of a leak conductance as described earlier (Goldstein et al., 2001). According to that, leak conductances should be active at resting membrane potential, instantaneous, stable and able to suppress excitation because they shift the resting membrane potential towards a potential that is negative relative to the firing threshold of nerves (Goldstein et al., 2001). Indeed, we revealed that the resting membrane potential is significantly shifted towards more depolarized values in CA1 and cortical pyramidal neurons of *Clcn2$^{-/-}$* animals compared to WT littermates. The small effect in CA1 pyramidal neurons occurred possibly because E_{Cl} is close to resting membrane potential (Tyzio et al., 2008). However, our results support that a resting activity of ClC-2 shifts the membrane potential closer to E_{Cl} and therefore would be sufficient to reduce neuronal excitability. Intriguingly, the strong effect on the membrane resistance in pyramidal neurons of CA1 and cortex substantiate that ClC-2 is conductive at resting conditions similar to the potassium and sodium channels contributing to the leak conductance.

Surprisingly, although we demonstrated the functional expression of ClC-2 in purkinje cells of the cerebellum the resting membrane potential and the membrane resistance remained unaltered after loss of ClC-2. The reason may be that purkinje cells exhibit a much larger soma and

thicker dendrites in comparison to any other neuron (beside Betz cell) in the brain. Therefore, leak provides a much smaller fraction of total conductance resulting in a much smaller effect on resting membrane properties. However, we found an increased number of action potentials in *Clcn2*$^{-/-}$ animals compared to WT animals, confirming that ClC-2 affects the excitability of purkinje cells as well.

The identification of ClC-2 mediated currents in granule cells of the dentate gyrus raises the question whether ClC-2 affects their resting membrane properties. In contrast to pyramidal cells and purkinje cells, granule cells are small and have very thin dendrites. Thus, leak induced effects on resting membrane properties would be much larger. Spruston and Johnston (1992) investigated resting membrane properties in pyramidal cells and granule cells of dentate gyrus in acute hippocampal slices of rats. They showed that membrane resistance and tau of CA1 and CA3 pyramidal cells as well as in granule cells of dentate gyrus are voltage dependent, suggesting that voltage dependent conductances close to resting membrane potential contribute to passive membrane properties. In granule cells, I_h had a small or no effect on resting membrane properties (Spruston and Johnston, 1992). Our data support that ClC-2 is a potential candidate, providing such a conductance.

To summarize, we provide the first direct evidence that the voltage-gated chloride channel ClC-2 possesses the molecular basis of a fundamental chloride leak conducter across neuron`s membrane. In addition, the ClC-2 leak conductance strongly affects the resting membrane properties. Differences in density and distribution of ClC-2 are likely to define the membrane resistance for each class of neuron, specifically. However, the functional expression of ClC-2 prevents neurons from hyperexcitability, which could cause diseases like epilepsy.

4.6   References

Abbott GW, Butler MH, Bendahhou S, Dalakas MC, Ptacek LJ, Goldstein SA. MiRP2 forms potassium channels in skeletal muscle with Kv3.4 and is associated with periodic paralysis. Cell (2001) 104:217-231.

Bosl MR, et al. Male germ cells and photoreceptors, both dependent on close cell-cell interactions, degenerate upon ClC-2 Cl(-) channel disruption. Embo J (2001) 20:1289-1299.

Brager DH, Johnston D. Plasticity of intrinsic excitability during long-term depression is mediated through mGluR-dependent changes in I(h) in hippocampal CA1 pyramidal neurons. J Neurosci (2007) 27:13926-13937.

Chesnoy-Marchais D. Characterization of a chloride conductance activated by hyperpolarization in Aplysia neurones. The Journal of physiology (1983) 342:277-308.

Crill WE. Persistent sodium current in mammalian central neurons. Annu Rev Physiol (1996) 58:349-362.

Franciolini F, Nonner W. Anion and cation permeability of a chloride channel in rat hippocampal neurons. The Journal of general physiology (1987) 90:453-478.

Goldstein SA, Bockenhauer D, O'Kelly I, Zilberberg N. Potassium leak channels and the KCNK family of two-P-domain subunits. Nat Rev Neurosci (2001) 2:175-184.

Grunder S, Thiemann A, Pusch M, Jentsch TJ. Regions involved in the opening of ClC-2 chloride channel by voltage and cell volume. Nature (1992) 360:759-762.

Hille B. Ion channels of excitable membranes, third edition. Sinauer Associates, Inc. (2001)

Hodgkin AL, Huxley AF. A quantitative description of membrane current and its application to conduction and excitation in nerve. The Journal of physiology (1952) 117:500-544.

Inoue I. Anion conductances of the giant axon of squid Sepioteuthis. Biophysical journal (1988) 54:489-494.

Jentsch TJ. Neuronal KCNQ potassium channels: physiology and role in disease. Nat Rev Neurosci (2000) 1:21-30.

Jentsch TJ. CLC chloride channels and transporters: from genes to protein structure, pathology and physiology. Crit Rev Biochem Mol Biol (2008) 43:3-36.

Jordt SE, Jentsch TJ. Molecular dissection of gating in the ClC-2 chloride channel. The EMBO journal (1997) 16:1582-1592.

Krapivinsky G, Gordon EA, Wickman K, Velimirovic B, Krapivinsky L, Clapham DE. The G-protein-gated atrial K+ channel IKACh is a heteromultimer of two inwardly rectifying K(+)-channel proteins. Nature (1995) 374:135-141.

Lu B, Su Y, Das S, Liu J, Xia J, Ren D. The neuronal channel NALCN contributes resting sodium permeability and is required for normal respiratory rhythm. Cell (2007) 129:371-383.

Madison DV, Malenka RC, Nicoll RA. Phorbol esters block a voltage-sensitive chloride current in hippocampal pyramidal cells. Nature (1986) 321:695-697.

Rinke I, Artmann J, Stein V. ClC-2 voltage-gated channels constitute part of the background conductance and assist chloride extrusion. J Neurosci (2010) 30:4776-4786.

Robinson RB, Siegelbaum SA. Hyperpolarization-activated cation currents: from molecules to physiological function. Annu Rev Physiol (2003) 65:453-480.

Smith RL, Clayton GH, Wilcox CL, Escudero KW, Staley KJ. Differential expression of an inwardly rectifying chloride conductance in rat brain neurons: a potential mechanism for cell-specific modulation of postsynaptic inhibition. J Neurosci (1995) 15:4057-4067.

Spruston N, Johnston D. Perforated patch-clamp analysis of the passive membrane properties of three classes of hippocampal neurons. J Neurophysiol (1992) 67:508-529.

Staley K. The role of an inwardly rectifying chloride conductance in postsynaptic inhibition. J Neurophysiol (1994) 72:273-284.

Storm JF. Action potential repolarization and a fast after-hyperpolarization in rat hippocampal pyramidal cells. The Journal of physiology (1987) 385:733-759.

Thiemann A, Grunder S, Pusch M, Jentsch TJ. A chloride channel widely expressed in epithelial and non-epithelial cells. Nature (1992) 356:57-60.

Tyzio R, et al. Postnatal changes in somatic gamma-aminobutyric acid signalling in the rat hippocampus. The European journal of neuroscience (2008) 27:2515-2528.

Zuniga L, Niemeyer MI, Varela D, Catalan M, Cid LP, Sepulveda FV. The voltage-dependent ClC-2 chloride channel has a dual gating mechanism. The Journal of physiology (2004) 555:671-682.

5 GENERAL DISCUSSION

The effects of excitatory GABA action early in development caused by high intracellular chloride concentration are still not clear. Therefore, I studied in collaboration with Carsten Pfeffer how the hippocampal network develops if GABA does not act excitatory during the early phase of postnatal development (Pfeffer et al., 2009). We used NKCC1 and AE3 knockout mice to reduce the intracellular chloride concentration, as these transporters are the main chloride loaders. It has been speculated that excitatory GABA action, causing a general depolarization of neurons, increases network activity, and thereby promotes the development of synaptic networks. My data provide evidence that GABAergic depolarization increases the network activity and facilitates the maturation of synaptic networks.

Besides transporters ion channels are likely involved in the modulation of intracellular chloride concentration. In the present thesis, I studied the effect of the voltage-gated chloride channel ClC-2. Previous studies had suggested that this voltage-gated chloride channel is important for fast chloride extrusion to maintain the inhibitory action of GABA in fully developed neurons. After loading neurons with high chloride concentration, I directly showed that ClC-2 indeed mediates a fast mechanism to extrude chloride (Rinke et al., 2010). I found that CA1 pyramidal neurons functionally express ClC-2 from postnatal day eight (P8) onwards suggesting that the function of ClC-2 is important only in mature neurons, but not in immature neurons. These results demonstrate that chloride extrusion by ClC-2 prevents chloride accumulation after intense GABA$_A$ receptor activation, and thus prevents from excitatory GABA action.

Somewhat unexpected, my recordings in ClC-2 KO neurons showed a strongly increased membrane resistance. The higher membrane resistance causes an increase of the neuronal excitability, which should lead to a higher excitability of the entire neuronal network. However, the excitability of the hippocampal network is reduced. The reduction is explained by an increased inhibition. I found that ClC-2 expressing interneurons within the hippocampus are also more excitable and enhance their inhibitory action onto pyramidal cells.

From my data, I conclude that ClC-2 has a dual role in neurons. First, this chloride channel provides a fast extrusion pathway for chloride after chloride accumulation, and second ClC-2 constitutes a substantial part of the leak conductance, which regulates excitability. These findings might be a general concept as I could record ClC-2 currents in various neuron types.

5.1   The intracellular chloride concentration is developmentally regulated

In immature neurons, the intracellular chloride concentration is high. In turn, the activation of GABA receptors causes depolarization. With further maturation of the neuron, the cytoplasmatic concentration of chloride decreases until GABA acts inhibitory. This change in GABA signaling is mediated by the appropriate functional expression of the chloride transporters NKCC1 and KCC2. NKCC1 is the major transport protein that accumulates intracellular chloride. KCC2 plays a pivotal role in chloride extrusion.

NKCC1 establishes high intracellular chloride concentration

It was found that NKCC1 mRNA expression is high in early development and declines from post-natal day one (P)1 to P15 in all hippocampal regions (Pfeffer et al., 2009). These data confirm previous findings in rats (Clayton et al., 1998a; Hubner et al., 2001a; Li et al., 2002; Wang et al., 2002; Dzhala et al., 2005), supporting the predominant function of NKCC1 in early postnatal development.

The chloride cotransporter NKCC1 increases the intracellular chloride concentration, and thereby shifts E_{Cl} to more positive values relative to the resting membrane potential (Misgeld et al., 1986; Zhang et al., 1991). After loss of NKCC1, the intracellular chloride concentration is lower, as we demonstrated with gramicidin perforated-patch clamp recordings (Pfeffer et al., 2009). This allowed us to use NKCC1 KO mice as a model for lowered chloride concentration in early development. However, the chloride concentration was not entirely shifted to values found in mature neurons, which suggests the existence of additional chloride loading mechanism.

The anion exchanger three contributes to intracellular chloride accumulation

There is evidence that the anion exchanger three (AE3) and NKCC1 are expressed at the same time of neuronal postnatal development (Raley-Susman et al., 1993). AE3 transports extracellular chloride into the cell, while transporting intracellular bicarbonate outward. Therefore, AE3 was proposed to contribute to intracellular chloride accumulation in hippocampal neurons (Hentschke et al., 2006).

I recorded from AE3 deficient mice to test whether the loss of AE3 has an effect on the intracellular chloride concentration. I found no changes in the intracellular chloride concentration between AE3 KO and WT animals, as judged from gramicidin perforated-patch clamp recordings at P1. However, giant depolarizing potentials (GDPs) were affected in AE3 KO animals at P5

(Pfeffer et al., 2009), indicating an effect of reduced intracellular chloride concentration. An explanation for the observed difference between P1 and P5 might be that AE3 is not functional as an anion exchanger at P1, which is also suggested by another study (Raley-Susman et al., 1993). It might be that during this time AE3 serve function as a cytoskeletal anchoring protein. The binding to other proteins could affect or modulate AE3 function as an anion exchanger (Raley-Susman et al., 1993). With further neuronal maturation, AE3 contribute to load the neuron with chloride at P5.

KCC2 lowers the intracellular chloride concentration

During development, NKCC1 down-regulation and KCC2 up-regulation lead to the decrease of the intracellular chloride concentration (Rivera et al., 1999; Gulyas et al., 2001; Hubner et al., 2001b). In hippocampal cultures and acute slices, KCC2 expression appears around birth and increased strongly after the first week of postnatal life (Zhang et al., 1991; Khirug et al., 2005). The KCC2 expression pattern parallels the neuronal differentiation and precedes the decline of E_{GABA} as demonstrated in spinal cord motoneurons and hippocampal pyramidal cells (Stein et al., 2004a).

KCC2 decreases the intracellular chloride concentration. Low intracellular chloride concentration determines the classical inhibitory response of mature neurons to GABA (Misgeld et al., 1986; Thompson and Gahwiler, 1989b; Hubner et al., 2001b). It is expected that the disruption of KCC2 function stops chloride extrusion, which in turn changes GABA-mediated signaling. To test this hypothesis, two different approaches were previously used: 1) antisense knockdown of KCC2 transfected in hippocampal cultures (Rivera et al., 1999) and 2) KCC2 knockout mice (Hubner et al., 2001b). 1) Knockdown of KCC2 in hippocampal cultures produced a shift of E_{GABA} to more depolarized values relative to the resting membrane potential. The positive shift of E_{GABA} precluded the pyramidal neurons from $GABA_A$ receptor-mediated inhibition (Rivera et al., 1999). 2) KCC2 knockout mice showed an abnormal muscle tone and defects in motor control. In addition, these mice were inable to breathe, which results in perinatal death. Spinal cord motoneurons of the KCC2 knockout animals showed GABAergic excitation accounting for the phenotype of KCC2 knockout mice (Hubner et al., 2001b). Both methods support that KCC2 is the dominant chloride extruder in neurons facilitating GABAergic inhibition.

The age of the neuron determines the chloride concentration

The time point when chloride changes from high to low intracellular concentrations and the GABA-mediated response shifts from excitation to inhibition depends on the developmental

stage of the neuron. For example, the observations in KCC2 knockout mice suggested that spinal cord motoneurons differentiate before hippocampal pyramidal neurons (Hubner et al., 2001b; Stein et al., 2004a). During the first days of postnatal development E_{GABA} was significantly higher for pyramidal neurons than for motoneurons (Stein et al., 2004a). At P8, motoneurons hyperpolarized in the presence of GABA, whereas hippocampal neurons still slightly depolarized. GABA-induced hyperpolarization in hippocampal pyramidal neurons was only observed after P14 (Stein et al., 2004a).

Even within the same brain region the time point of switching GABA signaling can differ between neuron types. For instance in the hippocampus, GABA-mediated inhibitory postsynaptic potentials occurred first around P5-6 in CA3 pyramidal neurons and around P9 in CA1 pyramidal neurons (e.g. Swann et al., 1989) indicating earlier differentiation of CA3 pyramidal neurons than those of CA1.

The maturational stage of the neuron rather than the age of the organism is important for the shift from excitation to inhibition (Ge et al., 2006). For example, as in neonates and in contrast to adult neurons, newborn dentate gyrus granule cells (DGCs) in adult hippocampus were depolarized by GABA (Ge et al., 2006). Newborn DGCs in the adult brain express high levels of NKCC1 and little KCC2. This result further supports that the sequential expression of the NKCC1 and KCC2 underlies the conversion from excitation to inhibition by GABA during neuronal maturation in the fetal brain (Ben-Ari, 2002; Owens and Kriegstein, 2002).

5.2   Functional consequences of GABAergic excitation

In immature neurons, GABAergic depolarization determines the neuronal network activity and triggers the maturation of synapses and the refinement of synaptic circuits (for review, see Owens and Kriegstein, 2002). If now GABAergic depolarization is impaired in immature neurons what will be the functional consequences? I addressed this question in the collaboration with Carsten Pfeffer. As NKCC1 is the major chloride loader providing the basis for GABAergic depolarization and excitation, we used NKCC1 KO animals to reduce the intracellular chloride concentration in immature neurons. As previously discussed, the GABAergic depolarization was only reduced but not completely abolished in these KO animals (Pfeffer et al., 2009). I found that the reduction of GABAergic depolarization leads to a delayed maturation of GABAergic and glutamatergic synapses. My data strongly suggest that immature neurons require GABAergic excitation for the development and refinement of synapses and synaptic networks.

Surprisingly, impaired GABAergic depolarization did not cause changes in the brain morphology of *Nkcc1$^{-/-}$* animals (Pfeffer et al., 2009). In contrast to our findings, short hairpin RNAs against NKCC1 expressed in newborn granular neurons or ventricular neuronal progenitor cells affected synapse formation and dendritic development (Ge et al., 2006; Wang and Kriegstein, 2008). An explanation for the observed difference might be that in *Nkcc1$^{-/-}$* animals GABA is still depolarizing and probably sufficient to trigger dendritic and axonal outgrowth, which might compensate for morphological changes.

5.3   Low intracellular chloride concentration is required for GABAergic inhibition

To circumvent hyperexcitability of neuronal networks, inhibition is necessary. Intense GABA$_A$ receptor activation loads the neuron with high chloride. Therefore, chloride-extruding mechanisms are active to prevent chloride accumulation in neurons. These mechanisms have to be very fast to prevent excitatory GABA action. KCC2 is the primary chloride extruder known at this moment. However, chloride transport by KCC2 is slow in comparison to a chloride current across a channel. I showed now for the first time that the voltage-gated chloride channel ClC-2 removes chloride from the intracellular space providing a fast mechanism for chloride extrusion (Rinke et al., 2010).

Chloride accumulation is limited by the function of ClC-2

If ClC-2 channels are open, the chloride conductance is large across the neuronal membrane. Further, ClC-2 does not display time-dependent inactivation and the channel can be still open even when the membrane repolarizes. Therefore, it was proposed that ClC-2 stabilizes E$_{Cl}$ near the resting membrane potential (Staley et al., 1996). *De novo* expression of ClC-2 in cultured embryonic DRG neurons, which have normally high intracellular chloride, produced a constitutive chloride efflux preventing from chloride accumulation. Thereby, E$_{Cl}$ was clamped at or near the resting membrane potential (Staley et al., 1996). This resulted in a large negative shift of E$_{GABA}$. Under these conditions, GABA$_A$ receptor activation increased the conductance over the membrane shunting incoming excitatory inputs (Staley et al., 1996).

Due to these previously discribed properties, it is not surprising that ClC-2 regulates neuronal chloride homeostasis by providing a fast chloride extruding mechanism (Rinke et al., 2010). My data suggest that chloride extrusion by ClC-2 is important especially in adult hippocampal pyramidal neurons where GABA$_A$ receptor activation occurs in high frequency bursts (Buzsaki et

al., 1992), and in turn would accumulate intracellular chloride very fast. A recently published study on CA1 pyramidal cells support my idea (Foldy et al., 2010). In CA1 pyramidal neurons, ClC-2 is functional at regions that receive highly active GABAergic inputs. ClC-2 selectively modulates the inhibitory postsynaptic response provided by fast spiking interneurons, and thereby prevents chloride accumulation in the postsynaptic cell (Foldy et al., 2010).

5.4   Impaired chloride homeostasis has pathophysiological consequences

Dysfunction of active chloride transport mechanisms

High intracellular chloride concentration leads to $GABA_A$ receptor-mediated depolarization that can cause excitability of the neuron. Therefore, chloride transporting proteins seem to play a key role in setting the susceptibility of neurons to epileptiform activity. NKCC1 might contribute to a lower susceptibility for seizures in neonates. Blocking NKCC1 with bumetanide lowered E_{Cl} in immature neurons, suppressed epileptiform activity in hippocampal slices *in vitro* and atte-nuated seizures in neonatal rats *in vivo* (Dzhala et al., 2005). In transgenic mice, the susceptibility to epilepsy *in vivo* and hyperexcitability *in vitro* are enhanced by down-regulation of KCC2 ex-pression (e.g. Zhu et al., 2005; Riekki et al., 2008). In humans, hippocampal slices obtained from temporal lobe epilepsy patients generated interictal activity that was attributable to depolarizing $GABA_A$ receptor-mediated transmission (Kohling et al., 1998; Cohen et al., 2002), which was re-lated to a down-regulation of KCC2. Interestingly, the interictal activity was blocked by bumeta-nide, an antagonist of NKCC1 (Huberfeld et al., 2007; Munoz et al., 2007). In summary, activation of NKCC1-mediated chloride import and/or decreased KCC2-mediated chloride export accumu-lates intracellular chloride such that E_{Cl} is above the resting membrane potential. Accordingly, GABAergic synaptic transmission becomes excitatory, and hence facilitates epileptogenesis and seizure intractability in epilepsy (for review, see Kahle et al., 2008; and Blaesse et al., 2009). However, human mutations in the genes encoding for these transporters that could cause epi-lepsy are still not found. It is likely that epilepsy is not caused by mutation of only one protein rather by mutations of genes encoding for various proteins. Therefore, it is possible that a single-gene mutation encoding for KCC2 or NKCC1 will not be detected.

Can ClC-2 cause epilepsy?

ClC-2 prevents cells from chloride accumulation and strongly affects their membrane resistance (Rinke et al., 2010). Recently, it was shown that ClC-2 is functionally expressed in postsynaptic

regions that receive GABAergic inputs from highly active inhibitory synapses (Foldy et al., 2010). The loss of ClC-2 should than lead to GABA$_A$ receptor-mediated excitation, which could cause overexcitation of the entire network. One expects now that the loss of ClC-2 could cause diseases like epilepsy. Human heterozygous mutations in the gene encoding the chloride channel ClC-2 (CLCN2) were associated with several subtypes of idiopathic generalized epilepsy (Haug et al., 2003). However, large parts of the pedigree structures and epilepsy phenotypes were different. More importantly, re-examination revealed that the reported mutations are asymptomatic, refuting the association of the two mutations with the clinical phenotypes that was originally reported. Because of the contradictions, the paper about the association of human heterozygous mutations in CLCN2 with epilepsy has been retracted (Haug et al., 2009). Moreover, several more studies found no evidence for a role of CLCN2 variants in epilepsy. These altered proteins did not lead to drastic changes in biophysical properties of ClC-2 function, as one expects for a single disease-causing gene (Niemeyer et al., 2004; Blanz et al., 2007; Jentsch, 2008). The complete loss of ClC-2 function in mice neither leads to epilepsy (Bosl et al., 2001; Nehrke et al., 2002) nor a lower susceptibility for seizures when facilitated by different proconvulsive agents (Bosl et al., 2001; Blanz et al., 2007). The results of my study represent a plausible explanation for the absence of an epileptic phenotype in *Clcn2$^{-/-}$* mice (Rinke et al., 2010). Although a single neuron showed higher excitability after loss of ClC-2, field recordings revealed a reduction in synaptic transmission at the pyramidal cell dendrites. The reduced synaptic transmission arose from increased inhibition, which is provided by interneurons also expressing ClC-2. After disruption of ClC-2, these interneurons get more excitable resulting in increased release of GABA onto pyramidal neurons, and thereby increasing postsynaptic inhibition (Rinke et al., 2010). Taken together, I provide evidence that the complete loss of ClC-2 in mice increases neuronal excitability; however, this hyperexcitability is balanced by parallel enhanced inhibiton preserving the mice from an epileptic phenotype.

5.5 The relationship between the reversal potential for chloride and the resting membrane potential

Small changes in intracellular chloride concentration can switch GABAergic signaling

The direction and magnitude of ion flow across the membrane is defined by both the concentration gradient and the membrane potential. Under physiological conditions, the chloride concentration gradient causes net chloride current when chloride-permeable channels, such as GABA$_A$

receptors, open. The reversal potential for a given ion is the membrane potential at which no net current occurs. A reversal potential of a given ion more positive than the resting membrane potential causes depolarization. A reversal potential more negative than the resting membrane potential causes hyperpolarization. In contrast to the reversal potential for sodium (+62 mV) and potassium (-103 mV) the reversal potential for chloride (E_{Cl}) is in general close to the resting membrane potential (-75 mV), so the net driving force for chloride ions is small. Under these conditions, the activation of GABA$_A$ receptors does not lead to changes in the membrane potential, because no net current will flow through these channels. Rather, the activation of GABA$_A$ receptors increases the conductance across the membrane and shunts concurrently incoming excitatory inputs.

The relationship between E_{Cl} and the intracellular chloride concentration, determined by the Nernst equation, is logarithmic (Fig. 1). Hence, even small deviations of the chloride concentration can shift the reversal potential of E_{GABA} above or in the near of the resting membrane potential causing excitation or inhibition, respectively. This is important especially in mature neurons, which have a low intracellular chloride concentration.
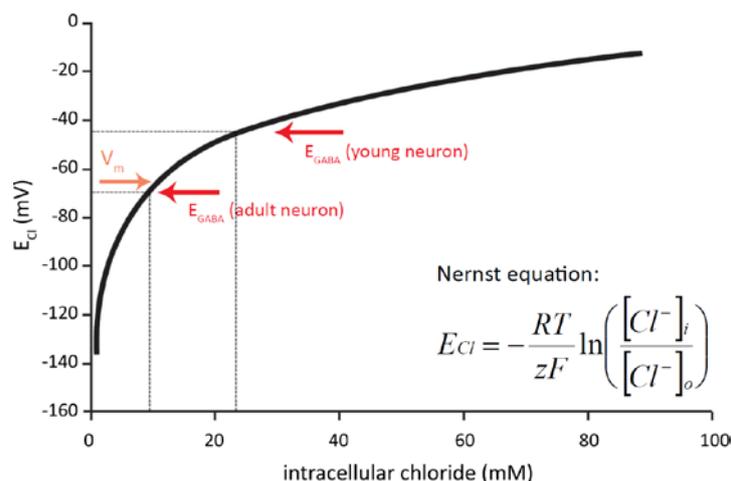

Figure 1: Nernst equation relating the reversal potential for chloride (E_{Cl}) to the intracellular chloride concentration.

At resting membrane potential slight changes of intracellular chloride (around 10 mM) are sufficient to change the neuronal response to GABA. The reversal potential for ionic conductances through GABA-channels (E_{GABA}) is assumed to equal E_{Cl}, because GABA$_A$ receptors are more permeable for chloride than for bicarbonate (Bormann et al., 1987). In young neurons E_{GABA} is at -45 mV and will decrease with further development until -70 mV in adult neurons.

GABAergic depolarization in mature neurons

As previously discussed, the intracellular chloride concentration is developmentally regulated. Hence, E_{Cl} changes during development so that $GABA_A$ receptor activation produces excitation in early development and inhibition in late development (Fig. 1). However, GABA can also produce depolarization in adult neurons. The mechanism underlying this effect might be explained by the bicarbonate permeability of $GABA_A$ receptors. Intense $GABA_A$ receptor activation collapses the electrochemical gradient for chloride more significantly than the bicarbonate gradient producing a shift in E_{GABA} toward the reversal potential for bicarbonate that is sufficient to explain the depolarizing response (Staley et al., 1995).

GABAergic depolarization in mature neurons can be excitatory. GABAergic excitation in mature neurons depends critical on the resting membrane potential as well as the location and timing of the GABAergic input related to the excitatory input (Gulledge and Stuart, 2003). E_{GABA} seems to be rather similar among different types of mature neurons (approximately -70 mV) (Ulrich and Huguenard, 1997). Hence, the resting membrane potential is the critical component determining whether GABAergic depolarization leads to excitation. The location and timing of the GABAergic input to other depolarizing inputs determines whether a neuron overcomes shunting conductances, and hence will be excited (Gulledge and Stuart, 2003; Stein and Nicoll, 2003). Excitation occurs when the time course of somatic GABA-mediated depolarization is longer than the conductance change at the soma. Hence, additional depolarizing inputs will sum with the residual somatic GABAergic depolarization. When GABA is applied onto the dendrite, the conductance change occurs locally. The dendritic GABA-mediated depolarization spreads electrotonically and reaches the soma purely excitatory with summation of additional depolarizing inputs.

5.6   How to measure the intracellular chloride concentration?

Because slight changes in intracellular chloride concentration have profound effects on the neuronal response to GABA, it is important to quantify the physiological chloride concentration of neurons. However, there are several difficulties in measuring physiological chloride concentration: invasive techniques including whole cell and intracellular sharp electrode recordings disrupt the neuronal membrane. Moreover, these methods alter the composition of cytoplasm and the activity of ionic channels. Other problems are the liquid junction potential of the pipette solution and short circuit effect of the leak through the contact between the electrode and the mem-

brane (Barry and Lynch, 1991; Spruston and Johnston, 1992; Staley and Mody, 1992). Using non-invasive techniques including gramicidin perforated patch-clamp recordings, cell-attached recordings and optic approaches preserve the cytoplasmatic environment and do not introduce leak currents.

The next three sections will give further insights into non-invasive methods to quantify the intracellular chloride concentration and the resting membrane potential.

Gramicidin perforated-patch clamp recordings

When incorporated in membranes, gramicidin forms cation-selective channels, which are impermeable for chloride. Perforated-patch clamp with gramicidin does not disturb the intracellular ion composition that can affect the chloride concentration gradient and the activity of chloride channels (Kyrozis and Reichling, 1995). I used gramicidin perforated-patch clamp because this method is non-invasive and it is conventionally used for indirect measurement of the intracellular chloride concentration monitoring changes in E_{GABA}. To calculate E_{GABA}, the current response of a cell to a voltage ramp is recorded during application of a $GABA_A$ receptor agonist. The voltage at which no net current flows represents E_{GABA} (Owens et al., 1996). Assuming E_{GABA} equals E_{Cl}, the intracellular chloride concentration is calculated by the Nernst equation.

Although gramicidin perforated-patch clamp improves the measurement of the cytoplasmatic chloride concentration, it still has several sources of error. First, the access resistance using this method is higher compared to whole-cell. This will decrease electrical access and thus decrease current resolution, and magnify series resistance error. Second, clamping the voltage of complex cells has the general problem of *space-clamp*. Constrictions at the branching points of the axon and the dendrites represent serial resistances within the cell, at which the voltage drops. Therefore, the voltage of peripheral regions can only be insuffciently contolled. Third, gramicidin perforated-patch clamp is sensitive to liquid junction potentials, modification of intracellular composition, and short-circuit effect of leak conductances (Spruston and Johnston, 1992; Staley et al., 1992). Together, these sources of errors can lead to underestimations of the resting membrane potential. As previously discussed, whether GABA acts inhibitory or excitatory depends on E_{GABA} compared to the resting membrane potential. Therefore, it is necessary to measure the resting membrane potential of the neuron accurately.

Cell-attached recordings

Cell-attached recordings of single channels provide another non-invasive method to measure the intracellular chloride concentration (Fricker et al., 1999; Verheugen et al., 1999; Tyzio et al.,

2003). Cell-attached recordings of single GABA$_A$ channels allow the measurement of the ionic driving force through GABA$_A$ channels without affect of E$_{GABA}$ or the resting membrane potential. At the reversal potential for GABA, the ionic driving force through GABA$_A$ channels is the pipette potential.

Cell-attached recordings of single NMDA channels (Leinekugel et al., 1997; Tyzio et al., 2003; Tyzio et al., 2006) or potassium channels (Fricker et al., 1999; Verheugen et al., 1999) enable the measurement of the resting membrane potential. In the cell-attached approach, the reversal potential of a conductance is used as a voltage sensor. For example, NMDA channels reverse near 0 mV (Nowak et al. 1984). Accordingly, NMDA currents should reverse their direction at a holding potential that equals the resting membrane potential (Leinekugel et al., 1997; Tyzio et al., 2003; Tyzio et al., 2006). The reversal potential for potassium across the patch is 0 mV when the pipette solution contains 155 mM potassium, which is the estimated intracellular potassium concentration (Hille, 1992). Therefore, the holding potential on the pipette at which the potassium current reverses gives a direct quantitative measure for the resting membrane potential (Fricker et al., 1999; Verheugen et al., 1999).

The major disadvantage of cell-attached recordings is that it is technically difficult to get high quality data. Especially, small conductance channels are hardly to detect because of the background noise. In addition, single channel recording is very time consuming for both acquisition and analysis. Therefore, this method is not conventionally used to estimate the intracellular chloride concentration and the resting membrane potential.

Direct measurements of intracellular chloride concentration

Measuring the intracellular chloride concentration without disturbing the intracellular ion compositions is also possible by using optical methods. This technique allows the spatial resolution of chloride concentration changes. Fluorescent chloride indicators can be loaded into neurons without disturbing the intracellular ion composition. Several studies used for example quinoline-based fluorescent dyes such as 6-methoxy-N-(3-sulphopropyl) quinolinium (SPQ), its derivative N-(ethoxycarbonylmethyl)-6-ethoxyquinolinium bromide (MQAE), or 6-methoxy-N-ethylquinolinium chloride (MEQ) to measure intracellular chloride in neurons and glia (Mansoura et al., 1999; Chub et al., 2006; Painter and Wang, 2006). Quinoliniums have low biological toxicity, are selective for chloride and insensitive to changes in pH. The main disadvantage of quinoline-based indicator dyes is the decrease of fluorescence caused by the gradual leakage of dye from the labelled cells or bleaching (Inglefield and Schwartz-Bloom, 1999; Chub et al., 2006; Painter and Wang, 2006).

Genetically encoded fluorescent proteins allow targeting of chloride-sensitive indicators to specific cell types and even to subcellular compartments. For example, the genetically encoded chloride indicator Clomeleon is a fusion protein of chloride-sensitive yellow fluorescent protein (YFP) and the chloride-insensitive cyan fluorescent protein (CFP). This construct allows fluorescence-resonance-energy-transfer (FRET)-based ratiometric measurements of intracellular chloride in neurons (Kuner and Augustine, 2000). Clomeleon is excitable by visible light, shows little bleaching, and it is not affected by other anions. However, the chloride affinity to Clomeleon is low and far from the physiological intracellular chloride concentration, which ranges in neurons between 5 and 40 mM (e.g. Balakrishnan et al., 2003; Yamada et al., 2004; Sipila et al., 2006; Achilles et al., 2007; Khirug et al., 2008; Tyzio et al., 2008). Another CFP-YFP construct with a triple mutated YFP improves the limitations of Clomeleon (Markova et al., 2008). The mutations in YFP enhance the protein sensitivity for chloride (Galietta et al., 2001).

Optic methods allow the direct measurement of intracellular chloride concentration. However, the sensitivity of chloride indicators to the intracellular chloride concentration is still low. This is of high importance as small changes in intracellular chloride concentration have profound consequences on neuronal excitability, especially in neurons that have low cytoplasmic chloride concentration. Moreover, chloride indicators can not monitor fast changes of intracellular chloride concentration that can be recorded electrophysiologically (Fukuda et al., 1998a). Simultaneous imaging and electrophysiological recordings from cultured hippocampal neurons had been shown that Clomeleon binds chloride ions only very slowly. While rapide application of GABA produces an immediate increase of the chloride current, changes in the intracellular chloride concentration reported by Clomeleon are delayed by 1 s (Kuner and Augustine, 2000).

5.7   The electrophysiological behavior of a neuron depends on resting membrane properties and ionic currents

Neurons exhibit leak conductances, which represent fixed currents at resting membrane potential determining neuronal excitability (Hodgkin and Huxley, 1952). At resting conditions, the cell membrane is predominantly permeable to potassium conducted through KCNK channels and two-P-domain channels (Goldstein et al., 2001). In addition, sodium and chloride leak conductances contribute to establish the resting membrane potential (Hodgkin and Huxley, 1952; Goldstein et al., 2001). The widely expressed voltage-independent, non-selective cation channel NALCN provides the majority of sodium leak conductance (Lu et al., 2007). In this thesis, I have

presented evidence that the voltage-gated chloride channel ClC-2 constitutes the main chloride leak conductance (Rinke et al., 2010).

ClC-2 provides chloride leak conductance

Resting permeability for chloride is best exemplified in vertebrate twitch muscles (e.g. Blatz and Magleby, 1985, 1989). In skeletal muscles, the stabilizing influence of chloride channels on the membrane potential is very important (Bretag, 1987; Steinmeyer et al., 1991b; Hille, 2001). For example, regarding human diseases such as myotonia congenita, the loss of ClC-1 chloride channel function leads to intrinsic muscle hyperexcitability (Steinmeyer et al., 1991b). Neurons exhibit also resting chloride permeability (Franciolini and Nonner, 1987; Inoue, 1988). In my thesis, I provide the first direct evidence that ClC-2 mediates the chloride leak conductance. In contrast to the voltage-independent leak conductances for potassium and sodium, the chloride conductance of ClC-2 activates upon hyperpolarization. It does not display any time-dependent inactivation and will be still open during subsequently brief depolarization. Therefore, I proposed that ClC-2 is open at resting membrane potential and exhibits similar properties like other leak conductances (Goldstein et al., 2001).

I recorded the voltage-gated chloride conductance of ClC-2 in principal neurons of major brain regions (Rinke et al., 2010) and found that the loss of ClC-2 affected resting membrane properties of CA1 pyramidal neurons, cortical pyramidal neurons, and purkinje cells of the cerebellum (Rinke et al., 2010). Importantly, the neuronal membrane resistance is higher after loss of ClC-2, in agreement with the idea that ClC-2 is active at resting conditions. Further, the higher membrane resistance increased the excitability of the neurons in *Clcn2*^{-/-} (Rinke et al., 2010). Therefore, my data provide evidence that ClC-2 is active at the resting membrane potential, and sufficient to suppress excitation of the neuron. As ClC-2 is functionally expressed in various neurons of major brain regions, I propose that the chloride leak conductance of ClC-2 is a general feature of neurons, regulating their excitability.

Leak conductance of ClC-2 affects neuronal excitability

I found that single neurons in *Clcn2*^{-/-} animals become more excitable due to the strongly increased membrane resistance. However, the network excitability was impaired (Rinke et al., 2010). Increased GABAergic inhibition rather than changes in excitatory synaptic transmission accounted for this reduction. My data showed that the activity of interneurons, which provide inhibition to the network, was affected. I found that a subset of interneurons functionally expressed ClC-2 (Rinke et al., 2010). The disruption of ClC-2 increased the excitability of interneu-

rons, resulting in increased inhibition onto CA1 pyramidal cells (Fig. 2). In summary, the chloride channel ClC-2 determines neuronal excitability, affecting resting membrane properties (Rinke et al., 2010). The cellular hyperexcitability caused by ClC-2 dysfunction is balanced in the network by increased inhibition provided by interneurons (Fig. 2).
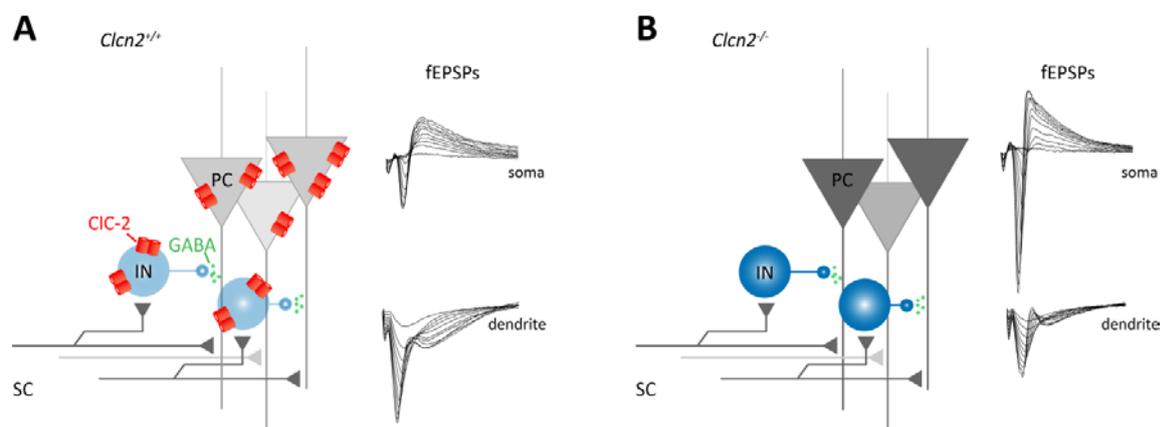

Figure 2: The functional role of ClC-2 in the mature neuronal network of CA1.

A-B, Schaffer collaterals (SC) offer excitatory synaptic input onto both CA1 pyramidal cells (grey colors) and a subset of interneurons (blue colors). These interneurons provide GABAergic inhibition onto CA1 pyramidal cells. Field excitatory postsynaptic potentials (fEPSPs) reflect the population discharges in the somatic and dendritic region of CA1. **A**, In WT ($Clcn2^{+/+}$), ClC-2 (red) is functionally expressed in CA1 pyramidal neurons and in a subset of interneurons. ClC-2 prevents the neurons from hyperexcitability primarily by constituting leak conductance across neuronal membrane. **B**, After loss of ClC-2 ($Clcn2^{-/-}$), CA1 pyramidal cells and interneurons get more excitable because of an increased membrane resistance. The hyperexcitability of CA1 pyramidal cells (somatic fEPSP) is balanced by increased inhibition onto pyramidal cell dendrites (dendritic fEPSPs) provided by higher excitable interneurons.

Until today, chloride leak conductances in neurons have usually been ignored, because neurons exhibit only a small proportion of chloride leak conductances in comparison to skeletal muscles (Bretag, 1987; Steinmeyer et al., 1991b; Hille, 2001). However, it is clear that chloride leak conductances play several important roles in neuronal function. Leak conductances influence the resting membrane properties and suppress the neuronal excitability because they shift the resting membrane potential towards a potential that is negative relative to the firing threshold of neurons (Goldstein et al., 2001). In squid giant axons, it has been shown that the firing rate of the axon is optimal, if the leak current is assumed to be chloride or some combination of ions whose overall reversal potential is approximately E_{Cl} (Seely and Crotty, 2010). Moreover, leak conductances are subject to modulation by second messengers and other substances

(Krapivinsky et al., 1995; Jentsch, 2000; Goldstein et al., 2001), which could potentially provide a means of regulating the integrative properties of the cell.

Why was ClC-2 not taking into account providing a leak conductance? The major problem is that there is no specific pharmacology to block the conductance of ClC-2 and one has to use ClC-2 KO animals to resolve the function of this channel. Without specific pharmacology, it was not possible to isolate the chloride leak conductance by ClC-2 under resting conditions, and therefore, it has never been shown before directly that ClC-2 is active at resting membrane potential. The ClC-2 KO mice are already several years available, but why they were not used is not clear. Moreover, previous studies focussed on studying the role of ClC-2 in regulating the intra- and extracellular ion homeostasis and simply were not asking for another role. As previously discussed, ClC-2 provides a fast mechanism to extrude chloride (Rinke et al., 2010) preventing from chloride accumulation after intense GABA$_A$ receptor activation. Even for us, it was somewhat unexpected that ClC-2 has a second role as chloride leak conductance.

5.8   Outlook

My data suggest a dual role for ClC-2 in neurons. First, this chloride channel mediates fast extrusion of chloride after chloride accumulation, and second ClC-2 constitutes the chloride leak conductance in neurons, which regulates excitability. These findings might be a general concept as I could record ClC-2 currents in various neuron types. However, several questions remain to be addressed. First, I observed the chloride conductance of ClC-2 in some interneurons (Rinke et al., 2010). Up to now, it is not clear, which type of interneurons express this channel. Second, it is unclear, which subcellular regions functionally express ClC-2. Finally, the leak conductance by ClC-2 affects neuronal excitability. Therefore, it would be interesting to know how the function of ClC-2 can be altered to regulate the excitation of neurons.

Which class of interneurons expresses ClC-2?
There are several difficulties to identify the interneurons expressing ClC-2. First, a purely immunohistochemical approach combining several protein markers (see chapter 1.3.3) is not possible since a specific antibody targeting ClC-2 is not available. Hence, ClC-2 can only be functionally identified. However, the electrophysiological conditions to record the ClC-2 current exclude recordings of the firing properties of an interneuron at the same time. The chloride conductance of ClC-2 is recorded with a pipette solution containing high intracellular chloride, cesium to block

potassium conductances, and QX314 to block action potentials. But the firing properties of interneurons can only be analyzed with physiological pipette solution containing low chloride and no blockers of ionic conductances. Furthermore, interneurons itself are highly diverse in morphology, local connectivity, expression of various neurochemical markers and electrophysiological properties (Freund and Buzsaki, 1996; Maccaferri and Lacaille, 2003; Klausberger, 2009), which complicates the definition of a certain interneuron subtype.

It would be interesting whether the presence of ClC-2 in interneurons correlates with a specific property of such an interneuron, defining a specific interneuron class. Future studies could combine electrophysiological recordings with for example immunohistochemistry to resolve the interneuron subtype expressing ClC-2. Once a specific interneuron type expressing ClC-2 is identified, one could generate a conditional mutant line that allow disruption of the temporal pattern of GABA signaling to circumvent compensatory mechanisms that arise in non-conditional mutants such as in *Clcn2*$^{-/-}$ animals.

Which subcellular regions express ClC-2?

Producing an own antibody against ClC-2, one study demonstrated the subcellular distribution of ClC-2 in the rat hippocampus. ClC-2 immunoreactivity occurred in dendrites, axon initial segments and somata, usually within or adjacent active zones of GABAergic synapses, but it can also be found in transport vesicles or multivesicular bodies. Moreover, the end feet of astrocytes in the neuropil and around small blood vessels are strongly immunoreactive for ClC-2, and have a characteristic laminar distribution in the hippocampus (Sik et al., 2000). However, a specific antibody against a ClC-2 antigen is still not commercialized.

Is ClC-2 modulated by physiological activity?

ClC-2 mediates a chloride leak conductance, which strongly affects the input resistance and hence the neuronal excitability (Rinke et al., 2010). Therefore, it would be highly interesting to know how the function of ClC-2 can be altered to regulate the excitation of neurons. One possibility is the modulation of ClC-2 channel function by protein kinase C (PKC). For example, a chloride conductance similar to that mediated by ClC-2 is blocked after activation of PKC by phorbol esters (Madison et al., 1986). My preliminary data in CA1 pyramidal neurons show that phorbolester PDBu blocks the ClC-2 chloride conductance. So far, it is not known, whether PKC phosphorylates ClC-2 directly and in turn alters its single channel conductance or voltage dependence, or whether PKC affects the phosphorylation state of a ClC-2 associated proteins. A physiological mechanism to activate PKC is provided by metabotropic glutamate receptors and the

underlying second-messenger pathway. The activation of metabotropic glutamate receptors that are coupled to G-protein leads to the activation of phospholipase C (PLC), which hydrolyzes phosphatidylinositol-4,5-bisphosphate (PIP2) releasing inositoltriphosphate (IP3) and diacylglycerol (DAG). In addition, intracellular calcium concentration increases due to the activation of IP3 receptors, which release calcium from internal stores. Phosphatidylserine only or in combination with diacylglycerol and/or calcium activates PKC.

The functional expression of ClC-2 can also be modulated by several other kinases and phosphatases (Madison et al., 1986; Fritsch and Edelman, 1996; Furukawa et al., 2002; Palmada et al., 2004; Denton et al., 2005; Klaus et al., 2009). Activation of protein kinase A (PKA), cyclin-dependent kinase p34cdc2/cyclin B and PI3-kinase have been shown to regulate the function of ClC-2 at the cell surface (Grunder et al., 1992; Fritsch and Edelman, 1996; Bali et al., 2001; Zheng et al., 2002; Cuppoletti et al., 2004).

In addition, the functional expression of ClC-2 has been shown to be modulated by metabolic stress. For example, replacement of intracellular ATP by adenosine-5`-monophosphate (AMP) in HEK cells expressing human ClC-2 accelerated the rate of channel opening (Niemeyer et al., 2004). Moreover, metabolic stress induced by ATP depletion enhanced the number of ClC-2 channels expressed on the surface by affecting the endocytic pathway that ClC-2 undergoes during trafficking (Dhani et al., 2003). Therefore, the modulation of vesicle retrieval from or insertion of ClC-2 into the plasma membrane are potential targets to regulate ClC-2 channel function (Dhani et al., 2003). ClC-2 interacts with motor protein dynein decreasing the functional expression of ClC-2 at the cell surface (Dhani et al., 2003).

Together, these studies suggest numerous possibilities to modulate ClC-2. In turn, the excitability of a ClC-2 expressing neuron can be controlled by the function of the chloride leak conductance provided by ClC-2.

6 BIBLIOGRAPHY

Abbott GW, Butler MH, Bendahhou S, Dalakas MC, Ptacek LJ, Goldstein SA (2001) MiRP2 forms potassium channels in skeletal muscle with Kv3.4 and is associated with periodic paralysis. Cell 104:217-231.

Accardi A, Miller C (2004) Secondary active transport mediated by a prokaryotic homologue of ClC Cl- channels. Nature 427:803-807.

Achilles K, Okabe A, Ikeda M, Shimizu-Okabe C, Yamada J, Fukuda A, Luhmann HJ, Kilb W (2007) Kinetic properties of Cl uptake mediated by Na+-dependent K+-2Cl cotransport in immature rat neocortical neurons. J Neurosci 27:8616-8627.

Adachi S, Uchida S, Ito H, Hata M, Hiroe M, Marumo F, Sasaki S (1994) Two isoforms of a chloride channel predominantly expressed in thick ascending limb of Henle's loop and collecting ducts of rat kidney. The Journal of biological chemistry 269:17677-17683.

Aguilo A, Schwartz TH, Kumar VS, Peterlin ZA, Tsiola A, Soriano E, Yuste R (1999) Involvement of cajal-retzius neurons in spontaneous correlated activity of embryonic and postnatal layer 1 from wild-type and reeler mice. J Neurosci 19:10856-10868.

Anderson MP, Berger HA, Rich DP, Gregory RJ, Smith AE, Welsh MJ (1991) Nucleoside triphosphates are required to open the CFTR chloride channel. Cell 67:775-784.

Balakrishnan V, Becker M, Lohrke S, Nothwang HG, Guresir E, Friauf E (2003) Expression and function of chloride transporters during development of inhibitory neurotransmission in the auditory brainstem. J Neurosci 23:4134-4145.

Bali M, Lipecka J, Edelman A, Fritsch J (2001) Regulation of ClC-2 chloride channels in T84 cells by TGF-alpha. American journal of physiology 280:C1588-1598.

Barry PH, Lynch JW (1991) Liquid junction potentials and small cell effects in patch-clamp analysis. The Journal of membrane biology 121:101-117.

Bartos M, Vida I, Jonas P (2007) Synaptic mechanisms of synchronized gamma oscillations in inhibitory interneuron networks. Nat Rev Neurosci 8:45-56.

Bateman A (1997) The structure of a domain common to archaebacteria and the homocystinuria disease protein. Trends Biochem Sci 22:12-13.

Bedford L, Walker R, Kondo T, van Cruchten I, King ER, Sablitzky F (2005) Id4 is required for the correct timing of neural differentiation. Dev Biol 280:386-395.

Ben-Ari Y (2002) Excitatory actions of gaba during development: the nature of the nurture. Nat Rev Neurosci 3:728-739.

Ben-Ari Y, Cherubini E, Corradetti R, Gaiarsa JL (1989) Giant synaptic potentials in immature rat CA3 hippocampal neurones. The Journal of physiology 416:303-325.

Ben-Ari Y, Gaiarsa JL, Tyzio R, Khazipov R (2007) GABA: a pioneer transmitter that excites immature neurons and generates primitive oscillations. Physiological reviews 87:1215-1284.

Bettler B, Kaupmann K, Mosbacher J, Gassmann M (2004) Molecular structure and physiological functions of GABA(B) receptors. Physiological reviews 84:835-867.

Birkenhager R, Otto E, Schurmann MJ, Vollmer M, Ruf EM, Maier-Lutz I, Beekmann F, Fekete A, Omran H, Feldmann D, Milford DV, Jeck N, Konrad M, Landau D, Knoers NV, Antignac C, Sudbrak R, Kispert A, Hildebrandt F (2001) Mutation of BSND causes Bartter syndrome with sensorineural deafness and kidney failure. Nature genetics 29:310-314.

Blaesse P, Airaksinen MS, Rivera C, Kaila K (2009) Cation-chloride cotransporters and neuronal function. Neuron 61:820-838.

Blanz J, Schweizer M, Auberson M, Maier H, Muenscher A, Hubner CA, Jentsch TJ (2007) Leukoencephalopathy upon disruption of the chloride channel ClC-2. J Neurosci 27:6581-6589.

Blatz AL, Magleby KL (1985) Single chloride-selective channels active at resting membrane potentials in cultured rat skeletal muscle. Biophysical journal 47:119-123.

Blatz AL, Magleby KL (1989) Adjacent interval analysis distinguishes among gating mechanisms for the fast chloride channel from rat skeletal muscle. The Journal of physiology 410:561-585.

Bormann J, Hamill OP, Sakmann B (1987) Mechanism of anion permeation through channels gated by glycine and gamma-aminobutyric acid in mouse cultured spinal neurones. The Journal of physiology 385:243-286.

Bosl MR, Stein V, Hubner C, Zdebik AA, Jordt SE, Mukhopadhyay AK, Davidoff MS, Holstein AF, Jentsch TJ (2001) Male germ cells and photoreceptors, both dependent on close cell-cell interactions, degenerate upon ClC-2 Cl(-) channel disruption. Embo J 20:1289-1299.

Bowery NG, Brown DA (1997) The cloning of GABA(B) receptors. Nature 386:223-224.

Brager DH, Johnston D (2007) Plasticity of intrinsic excitability during long-term depression is mediated through mGluR-dependent changes in I(h) in hippocampal CA1 pyramidal neurons. J Neurosci 27:13926-13937.

Bretag AH (1987) Muscle chloride channels. Physiological reviews 67:618-724.

Brumback AC, Staley KJ (2008) Thermodynamic regulation of NKCC1-mediated Cl- cotransport underlies plasticity of GABA(A) signaling in neonatal neurons. J Neurosci 28:1301-1312.

Burrone J, O'Byrne M, Murthy VN (2002) Multiple forms of synaptic plasticity triggered by selective suppression of activity in individual neurons. Nature 420:414-418.

Buzsaki G, Horvath Z, Urioste R, Hetke J, Wise K (1992) High-frequency network oscillation in the hippocampus. Science (New York, NY 256:1025-1027.

Cancedda L, Fiumelli H, Chen K, Poo MM (2007) Excitatory GABA action is essential for morphological maturation of cortical neurons in vivo. J Neurosci 27:5224-5235.

Caputo A, Caci E, Ferrera L, Pedemonte N, Barsanti C, Sondo E, Pfeffer U, Ravazzolo R, Zegarra-Moran O, Galietta LJ (2008) TMEM16A, a membrane protein associated with calcium-dependent chloride channel activity. Science (New York, NY 322:590-594.

Carvalho TP, Buonomano DV (2009) Differential effects of excitatory and inhibitory plasticity on synaptically driven neuronal input-output functions. Neuron 61:774-785.

Chenoy-Marchais D (1982) A Cl- conductance activated by hyperpolarization in Aplysia neurones. Nature 299:359-361.

Chesnoy-Marchais D (1983) Characterization of a chloride conductance activated by hyperpolarization in Aplysia neurones. The Journal of physiology 342:277-308.

Chub N, Mentis GZ, O'Donovan M J (2006) Chloride-sensitive MEQ fluorescence in chick embryo motoneurons following manipulations of chloride and during spontaneous network activity. J Neurophysiol 95:323-330.

Clayton GH, Owens GC, Wolff JS, Smith RL (1998a) Ontogeny of cation-Cl- cotransporter expression in rat neocortex. Brain research 109:281-292.

Clayton GH, Staley KJ, Wilcox CL, Owens GC, Smith RL (1998b) Developmental expression of C1C-2 in the rat nervous system. Brain research 108:307-318.

Cohen I, Navarro V, Clemenceau S, Baulac M, Miles R (2002) On the origin of interictal activity in human temporal lobe epilepsy in vitro. Science (New York, NY 298:1418-1421.

Combi R, Grioni D, Contri M, Redaelli S, Redaelli F, Bassi MT, Barisani D, Lavitrano ML, Tredici G, Tenchini ML, Bertolini M, Dalpra L (2009) Clinical and genetic familial study of a large cohort of Italian children with idiopathic epilepsy. Brain Res Bull 79:89-96.

Cossart R, Dinocourt C, Hirsch JC, Merchan-Perez A, De Felipe J, Ben-Ari Y, Esclapez M, Bernard C (2001) Dendritic but not somatic GABAergic inhibition is decreased in experimental epilepsy. Nat Neurosci 4:52-62.

Crepel V, Aronov D, Jorquera I, Represa A, Ben-Ari Y, Cossart R (2007) A parturition-associated nonsynaptic coherent activity pattern in the developing hippocampus. Neuron 54:105-120.

Crill WE (1996) Persistent sodium current in mammalian central neurons. Annu Rev Physiol 58:349-362.

Cuppoletti J, Tewari KP, Sherry AM, Ferrante CJ, Malinowska DH (2004) Sites of protein kinase A activation of the human ClC-2 Cl(-) channel. The Journal of biological chemistry 279:21849-21856.

D'Agostino D, Bertelli M, Gallo S, Cecchin S, Albiero E, Garofalo PG, Gambardella A, St Hilaire JM, Kwiecinski H, Andermann E, Pandolfo M (2004) Mutations and polymorphisms of the CLCN2 gene in idiopathic epilepsy. Neurology 63:1500-1502.

Daoudal G, Debanne D (2003) Long-term plasticity of intrinsic excitability: learning rules and mechanisms. Learn Mem 10:456-465.

Delpire E, Rauchman MI, Beier DR, Hebert SC, Gullans SR (1994) Molecular cloning and chromosome localization of a putative basolateral Na(+)-K(+)-2Cl- cotransporter from mouse inner medullary collecting duct (mIMCD-3) cells. The Journal of biological chemistry 269:25677-25683.

Denton J, Nehrke K, Yin X, Morrison R, Strange K (2005) GCK-3, a newly identified Ste20 kinase, binds to and regulates the activity of a cell cycle-dependent ClC anion channel. The Journal of general physiology 125:113-125.

Dhani SU, Mohammad-Panah R, Ahmed N, Ackerley C, Ramjeesingh M, Bear CE (2003) Evidence for a functional interaction between the ClC-2 chloride channel and the retrograde motor dynein complex. The Journal of biological chemistry 278:16262-16270.

Durand GM, Kovalchuk Y, Konnerth A (1996) Long-term potentiation and functional synapse induction in developing hippocampus. Nature 381:71-75.

Dutar P, Nicoll RA (1988) A physiological role for GABAB receptors in the central nervous system. Nature 332:156-158.

Dutzler R, Campbell EB, MacKinnon R (2003) Gating the selectivity filter in ClC chloride channels. Science (New York, NY 300:108-112.

Dutzler R, Campbell EB, Cadene M, Chait BT, MacKinnon R (2002) X-ray structure of a ClC chloride channel at 3.0 A reveals the molecular basis of anion selectivity. Nature 415:287-294.

Dzhala VI, Talos DM, Sdrulla DA, Brumback AC, Mathews GC, Benke TA, Delpire E, Jensen FE, Staley KJ (2005) NKCC1 transporter facilitates seizures in the developing brain. Nat Med 11:1205-1213.

Eilers J, Plant TD, Marandi N, Konnerth A (2001) GABA-mediated Ca2+ signalling in developing rat cerebellar Purkinje neurones. The Journal of physiology 536:429-437.

Esteban JA, Shi SH, Wilson C, Nuriya M, Huganir RL, Malinow R (2003) PKA phosphorylation of AMPA receptor subunits controls synaptic trafficking underlying plasticity. Nat Neurosci 6:136-143.

Estevez R, Pusch M, Ferrer-Costa C, Orozco M, Jentsch TJ (2004) Functional and structural conservation of CBS domains from CLC chloride channels. The Journal of physiology 557:363-378.

Estevez R, Boettger T, Stein V, Birkenhager R, Otto E, Hildebrandt F, Jentsch TJ (2001) Barttin is a Cl- channel beta-subunit crucial for renal Cl- reabsorption and inner ear K+ secretion. Nature 414:558-561.

Everett K et al. (2007) Linkage and mutational analysis of CLCN2 in childhood absence epilepsy. Epilepsy research 75:145-153.

Fisher SE, Black GC, Lloyd SE, Hatchwell E, Wrong O, Thakker RV, Craig IW (1994) Isolation and partial characterization of a chloride channel gene which is expressed in kidney and is a

candidate for Dent's disease (an X-linked hereditary nephrolithiasis). Human molecular genetics 3:2053-2059.

Foldy C, Lee SH, Morgan RJ, Soltesz I (2010) Regulation of fast-spiking basket cell synapses by the chloride channel ClC-2. Nat Neurosci 13:1047-1049.

Franciolini F, Nonner W (1987) Anion and cation permeability of a chloride channel in rat hippocampal neurons. The Journal of general physiology 90:453-478.

Freund TF, Buzsaki G (1996) Interneurons of the hippocampus. Hippocampus 6:347-470.

Fricker D, Verheugen JA, Miles R (1999) Cell-attached measurements of the firing threshold of rat hippocampal neurones. The Journal of physiology 517 (Pt 3):791-804.

Fritsch J, Edelman A (1996) Modulation of the hyperpolarization-activated Cl- current in human intestinal T84 epithelial cells by phosphorylation. The Journal of physiology 490 (Pt 1):115-128.

Fritschy JM (2008) Epilepsy, E/I Balance and GABA(A) Receptor Plasticity. Front Mol Neurosci 1:5.

Fukuda A, Tanaka M, Yamada Y, Muramatsu K, Shimano Y, Nishino H (1998a) Simultaneous optical imaging of intracellular Cl- in neurons in different layers of rat neocortical slices: advantages and limitations. Neuroscience research 32:363-371.

Fukuda A, Muramatsu K, Okabe A, Shimano Y, Hida H, Fujimoto I, Nishino H (1998b) Changes in intracellular Ca2+ induced by GABAA receptor activation and reduction in Cl- gradient in neonatal rat neocortex. J Neurophysiol 79:439-446.

Furukawa T, Ogura T, Katayama Y, Hiraoka M (1998) Characteristics of rabbit ClC-2 current expressed in Xenopus oocytes and its contribution to volume regulation. The American journal of physiology 274:C500-512.

Furukawa T, Ogura T, Zheng YJ, Tsuchiya H, Nakaya H, Katayama Y, Inagaki N (2002) Phosphorylation and functional regulation of ClC-2 chloride channels expressed in Xenopus oocytes by M cyclin-dependent protein kinase. The Journal of physiology 540:883-893.

Gadsby DC, Nairn AC (1999) Control of CFTR channel gating by phosphorylation and nucleotide hydrolysis. Physiological reviews 79:S77-S107.

Galietta LJ, Haggie PM, Verkman AS (2001) Green fluorescent protein-based halide indicators with improved chloride and iodide affinities. FEBS letters 499:220-224.

Galindo BE, Vacquier VD (2005) Phylogeny of the TMEM16 protein family: some members are overexpressed in cancer. Int J Mol Med 16:919-924.

Gamba G (2005) Molecular physiology and pathophysiology of electroneutral cation-chloride cotransporters. Physiological reviews 85:423-493.

Ganguly K, Schinder AF, Wong ST, Poo M (2001) GABA itself promotes the developmental switch of neuronal GABAergic responses from excitation to inhibition. Cell 105:521-532.

Garaschuk O, Hanse E, Konnerth A (1998) Developmental profile and synaptic origin of early network oscillations in the CA1 region of rat neonatal hippocampus. J Physiol 507 219-236.

Garaschuk O, Linn J, Eilers J, Konnerth A (2000) Large-scale oscillatory calcium waves in the immature cortex. Nat Neurosci 3:452-459.

Ge S, Goh EL, Sailor KA, Kitabatake Y, Ming GL, Song H (2006) GABA regulates synaptic integration of newly generated neurons in the adult brain. Nature 439:589-593.

Goldstein SA, Bockenhauer D, O'Kelly I, Zilberberg N (2001) Potassium leak channels and the KCNK family of two-P-domain subunits. Nat Rev Neurosci 2:175-184.

Grunder S, Thiemann A, Pusch M, Jentsch TJ (1992) Regions involved in the opening of ClC-2 chloride channel by voltage and cell volume. Nature 360:759-762.

Gulledge AT, Stuart GJ (2003) Excitatory actions of GABA in the cortex. Neuron 37:299-309.

Gulyas AI, Sik A, Payne JA, Kaila K, Freund TF (2001) The KCl cotransporter, KCC2, is highly expressed in the vicinity of excitatory synapses in the rat hippocampus. Eur J Neurosci 13:2205-2217.

Gunther W, Luchow A, Cluzeaud F, Vandewalle A, Jentsch TJ (1998) ClC-5, the chloride channel mutated in Dent's disease, colocalizes with the proton pump in endocytotically active kidney cells. Proceedings of the National Academy of Sciences of the United States of America 95:8075-8080.

Hartzell HC, Qu Z, Yu K, Xiao Q, Chien LT (2008) Molecular physiology of bestrophins: multifunctional membrane proteins linked to best disease and other retinopathies. Physiological reviews 88:639-672.

Haug K et al. (2009) Retraction: Mutations in CLCN2 encoding a voltage-gated chloride channel are associated with idiopathic generalized epilepsies. Nature genetics 41:1043.

Haug K et al. (2003) Mutations in CLCN2 encoding a voltage-gated chloride channel are associated with idiopathic generalized epilepsies. Nature genetics 33:527-532.

Hentschke M, Wiemann M, Hentschke S, Kurth I, Hermans-Borgmeyer I, Seidenbecher T, Jentsch TJ, Gal A, Hübner CA (2006) Mice with a targeted disruption of the Cl^-/HCO_3^- exchanger AE3 display a reduced seizure threshold. Mol Cell Biol 26:182-191.

Hille B. Ion channels of excitable membranes, third edition. Sinauer Associates, Inc. (2001)

Hinzpeter A, Lipecka J, Brouillard F, Baudoin-Legros M, Dadlez M, Edelman A, Fritsch J (2006) Association between Hsp90 and the ClC-2 chloride channel upregulates channel function. American journal of physiology 290:C45-56.

Hinzpeter A, Fritsch J, Borot F, Trudel S, Vieu DL, Brouillard F, Baudouin-Legros M, Clain J, Edelman A, Ollero M (2007) Membrane cholesterol content modulates ClC-2 gating and sensitivity to oxidative stress. The Journal of biological chemistry 282:2423-2432.

Hodgkin AL, Huxley AF (1952) A quantitative description of membrane current and its application to conduction and excitation in nerve. The Journal of physiology 117:500-544.

Honore E (2007) The neuronal background K2P channels: focus on TREK1. Nat Rev Neurosci 8:251-261.

Huber SM, Duranton C, Henke G, Van De Sand C, Heussler V, Shumilina E, Sandu CD, Tanneur V, Brand V, Kasinathan RS, Lang KS, Kremsner PG, Hubner CA, Rust MB, Dedek K, Jentsch TJ, Lang F (2004) Plasmodium induces swelling-activated ClC-2 anion channels in the host erythrocyte. The Journal of biological chemistry 279:41444-41452.

Huberfeld G, Wittner L, Clemenceau S, Baulac M, Kaila K, Miles R, Rivera C (2007) Perturbed chloride homeostasis and GABAergic signaling in human temporal lobe epilepsy. J Neurosci 27:9866-9873.

Hubner CA, Lorke DE, Hermans-Borgmeyer I (2001a) Expression of the Na-K-2Cl-cotransporter NKCC1 during mouse development. Mech Dev 102:267-269.

Hubner CA, Stein V, Hermans-Borgmeyer I, Meyer T, Ballanyi K, Jentsch TJ (2001b) Disruption of KCC2 reveals an essential role of K-Cl cotransport already in early synaptic inhibition. Neuron 30:515-524.

Hübner CA, Lorke DE, Hermans-Borgmeyer I (2001a) Expression of the Na-K-2Cl-cotransporter NKCC1 during mouse development. Mech Dev 102:267-269.

Hübner CA, Stein V, Hermans-Borgmeyer I, Meyer T, Ballanyi K, Jentsch TJ (2001b) Disruption of KCC2 reveals an essential role of K-Cl cotransport already in early synaptic inhibition. Neuron 30:515-524.

Huguenard JR, Alger BE (1986) Whole-cell voltage-clamp study of the fading of GABA-activated currents in acutely dissociated hippocampal neurons. J Neurophysiol 56:1-18.

Ibañez-Tallon I, Miwa JM, Wang HL, Adams NC, Crabtree GW, Sine SM, Heintz N (2002) Novel modulation of neuronal nicotinic acetylcholine receptors by association with the endogenous prototoxin lynx1. Neuron 33:893-903.

Inglefield JR, Schwartz-Bloom RD (1999) Fluorescence imaging of changes in intracellular chloride in living brain slices. Methods 18:197-203.

Inoue I (1988) Anion conductances of the giant axon of squid Sepioteuthis. Biophysical journal 54:489-494.

Iwasato T, Datwani A, Wolf AM, Nishiyama H, Taguchi Y, Tonegawa S, Knopfel T, Erzurumlu RS, Itohara S (2000) Cortex-restricted disruption of NMDAR1 impairs neuronal patterns in the barrel cortex. Nature 406:726-731.

Jacob TC, Moss SJ, Jurd R (2008) GABA(A) receptor trafficking and its role in the dynamic modulation of neuronal inhibition. Nat Rev Neurosci 9:331-343.

Jentsch TJ (2000) Neuronal KCNQ potassium channels: physiology and role in disease. Nat Rev Neurosci 1:21-30.

Jentsch TJ (2008) CLC chloride channels and transporters: from genes to protein structure, pathology and physiology. Crit Rev Biochem Mol Biol 43:3-36.

Jentsch TJ, Stein V, Weinreich F, Zdebik AA (2002) Molecular structure and physiological function of chloride channels. Physiological reviews 82:503-568.

Jia Y, Mathews CJ, Hanrahan JW (1997) Phosphorylation by protein kinase C is required for acute activation of cystic fibrosis transmembrane conductance regulator by protein kinase A. The Journal of biological chemistry 272:4978-4984.

Jordt SE, Jentsch TJ (1997) Molecular dissection of gating in the ClC-2 chloride channel. The EMBO journal 16:1582-1592.

Kahle KT, Staley KJ, Nahed BV, Gamba G, Hebert SC, Lifton RP, Mount DB (2008) Roles of the cation-chloride cotransporters in neurological disease. Nat Clin Pract Neurol 4:490-503.

Kasper D, Planells-Cases R, Fuhrmann JC, Scheel O, Zeitz O, Ruether K, Schmitt A, Poet M, Steinfeld R, Schweizer M, Kornak U, Jentsch TJ (2005) Loss of the chloride channel ClC-7 leads to lysosomal storage disease and neurodegeneration. The EMBO journal 24:1079-1091.

Kaupmann K, Huggel K, Heid J, Flor PJ, Bischoff S, Mickel SJ, McMaster G, Angst C, Bittiger H, Froestl W, Bettler B (1997) Expression cloning of GABA(B) receptors uncovers similarity to metabotropic glutamate receptors. Nature 386:239-246.

Kerem B, Rommens JM, Buchanan JA, Markiewicz D, Cox TK, Chakravarti A, Buchwald M, Tsui LC (1989) Identification of the cystic fibrosis gene: genetic analysis. Science (New York, NY 245:1073-1080.

Khazipov R, Leinekugel X, Khalilov I, Gaiarsa JL, Ben-Ari Y (1997a) Synchronization of GABAergic interneuronal network in CA3 subfield of neonatal rat hippocampal slices. The Journal of physiology 498 (Pt 3):763-772.

Khazipov R, Leinekugel X, Khalilov I, Gaiarsa JL, Ben-Ari Y (1997b) Synchronization of GABAergic interneuronal network in CA3 subfield of neonatal rat hippocampal slices. J Physiol 498 763-772.

Khirug S, Yamada J, Afzalov R, Voipio J, Khiroug L, Kaila K (2008) GABAergic depolarization of the axon initial segment in cortical principal neurons is caused by the Na-K-2Cl cotransporter NKCC1. J Neurosci 28:4635-4639.

Khirug S, Huttu K, Ludwig A, Smirnov S, Voipio J, Rivera C, Kaila K, Khiroug L (2005) Distinct properties of functional KCC2 expression in immature mouse hippocampal neurons in culture and in acute slices. Eur J Neurosci 21:899-904.

Klaus F, Laufer J, Czarkowski K, Strutz-Seebohm N, Seebohm G, Lang F (2009) PIKfyve-dependent regulation of the Cl- channel ClC-2. Biochem Biophys Res Commun 381:407-411.

Klausberger T (2009) GABAergic interneurons targeting dendrites of pyramidal cells in the CA1 area of the hippocampus. Eur J Neurosci 30:947-957.

Klausberger T, Somogyi P (2008) Neuronal diversity and temporal dynamics: the unity of hippocampal circuit operations. Science 321:53-57.

Koch MC, Steinmeyer K, Lorenz C, Ricker K, Wolf F, Otto M, Zoll B, Lehmann-Horn F, Grzeschik KH, Jentsch TJ (1992) The skeletal muscle chloride channel in dominant and recessive human myotonia. Science (New York, NY 257:797-800.

Kohling R, Lucke A, Straub H, Speckmann EJ, Tuxhorn I, Wolf P, Pannek H, Oppel F (1998) Spontaneous sharp waves in human neocortical slices excised from epileptic patients. Brain 121 (Pt 6):1073-1087.

Komuro H, Rakic P (1998) Orchestration of neuronal migration by activity of ion channels, neurotransmitter receptors, and intracellular Ca^{2+} fluctuations. J Neurobiol 37:110-130.

Kornak U, Kasper D, Bosl MR, Kaiser E, Schweizer M, Schulz A, Friedrich W, Delling G, Jentsch TJ (2001) Loss of the ClC-7 chloride channel leads to osteopetrosis in mice and man. Cell 104:205-215.

Krapivinsky G, Gordon EA, Wickman K, Velimirovic B, Krapivinsky L, Clapham DE (1995) The G-protein-gated atrial K+ channel IKACh is a heteromultimer of two inwardly rectifying K(+)-channel proteins. Nature 374:135-141.

Kullmann DM, Lamsa KP (2007) Long-term synaptic plasticity in hippocampal interneurons. Nat Rev Neurosci 8:687-699.

Kuner T, Augustine GJ (2000) A genetically encoded ratiometric indicator for chloride: capturing chloride transients in cultured hippocampal neurons. Neuron 27:447-459.

Kyrozis A, Reichling DB (1995) Perforated-patch recording with gramicidin avoids artifactual changes in intracellular chloride concentration. J Neurosci Methods 57:27-35.

Lacaille JC, Mueller AL, Kunkel DD, Schwartzkroin PA (1987) Local circuit interactions between oriens/alveus interneurons and CA1 pyramidal cells in hippocampal slices: electrophysiology and morphology. J Neurosci 7:1979-1993.

Lamsa K, Palva JM, Ruusuvuori E, Kaila K, Taira T (2000) Synaptic GABA(A) activation inhibits AMPA-kainate receptor-mediated bursting in the newborn (P0-P2) rat hippocampus. J Neurophysiol 83:359-366.

Leinekugel X, Tseeb V, Ben-Ari Y, Bregestovski P (1995) Synaptic GABAA activation induces Ca2+ rise in pyramidal cells and interneurons from rat neonatal hippocampal slices. The Journal of physiology 487 (Pt 2):319-329.

Leinekugel X, Khalilov I, Ben-Ari Y, Khazipov R (1998) Giant depolarizing potentials: the septal pole of the hippocampus paces the activity of the developing intact septohippocampal complex in vitro. J Neurosci 18:6349-6357.

Leinekugel X, Medina I, Khalilov I, Ben-Ari Y, Khazipov R (1997) Ca2+ oscillations mediated by the synergistic excitatory actions of GABA(A) and NMDA receptors in the neonatal hippocampus. Neuron 18:243-255.

Leinekugel X, Khazipov R, Cannon R, Hirase H, Ben-Ari Y, Buzsaki G (2002) Correlated bursts of activity in the neonatal hippocampus in vivo. Science (New York, NY 296:2049-2052.

Li H, Tornberg J, Kaila K, Airaksinen MS, Rivera C (2002) Patterns of cation-chloride cotransporter expression during embryonic rodent CNS development. Eur J Neurosci 16:2358-2370.

Li H, Khirug S, Cai C, Ludwig A, Blaesse P, Kolikova J, Afzalov R, Coleman SK, Lauri S, Airaksinen MS, Keinanen K, Khiroug L, Saarma M, Kaila K, Rivera C (2007) KCC2 interacts with the dendritic cytoskeleton to promote spine development. Neuron 56:1019-1033.

Ling DS, Benardo LS (1995) Activity-dependent depression of monosynaptic fast IPSCs in hippocampus: contributions from reductions in chloride driving force and conductance. Brain research 670:142-146.

Lloyd SE, Pearce SH, Fisher SE, Steinmeyer K, Schwappach B, Scheinman SJ, Harding B, Bolino A, Devoto M, Goodyer P, Rigden SP, Wrong O, Jentsch TJ, Craig IW, Thakker RV (1996) A common molecular basis for three inherited kidney stone diseases. Nature 379:445-449.

Lobet S, Dutzler R (2006) Ion-binding properties of the ClC chloride selectivity filter. The EMBO journal 25:24-33.

Lorenz C, Pusch M, Jentsch TJ (1996) Heteromultimeric CLC chloride channels with novel properties. Proceedings of the National Academy of Sciences of the United States of America 93:13362-13366.

Lu B, Su Y, Das S, Liu J, Xia J, Ren D (2007) The neuronal channel NALCN contributes resting sodium permeability and is required for normal respiratory rhythm. Cell 129:371-383.

Lu HC, She WC, Plas DT, Neumann PE, Janz R, Crair MC (2003) Adenylyl cyclase I regulates AMPA receptor trafficking during mouse cortical 'barrel' map development. Nat Neurosci 6:939-947.

Ludwig A, Li H, Saarma M, Kaila K, Rivera C (2003) Developmental up-regulation of KCC2 in the absence of GABAergic and glutamatergic transmission. Eur J Neurosci 18:3199-3206.

Luscher C, Jan LY, Stoffel M, Malenka RC, Nicoll RA (1997) G protein-coupled inwardly rectifying K+ channels (GIRKs) mediate postsynaptic but not presynaptic transmitter actions in hippocampal neurons. Neuron 19:687-695.

Lytle C, McManus TJ, Haas M (1998) A model of Na-K-2Cl cotransport based on ordered ion binding and glide symmetry. The American journal of physiology 274:C299-309.

Maccaferri G, Lacaille JC (2003) Interneuron Diversity series: Hippocampal interneuron classifications--making things as simple as possible, not simpler. Trends Neurosci 26:564-571.

Madison DV, Malenka RC, Nicoll RA (1986) Phorbol esters block a voltage-sensitive chloride current in hippocampal pyramidal cells. Nature 321:695-697.

Malenka RC, Bear MF (2004) LTP and LTD: an embarrassment of riches. Neuron 44:5-21.

Mansoura MK, Biwersi J, Ashlock MA, Verkman AS (1999) Fluorescent chloride indicators to assess the efficacy of CFTR cDNA delivery. Hum Gene Ther 10:861-875.

Marder CP, Buonomano DV (2003) Differential effects of short- and long-term potentiation on cell firing in the CA1 region of the hippocampus. J Neurosci 23:112-121.

Markova O, Mukhtarov M, Real E, Jacob Y, Bregestovski P (2008) Genetically encoded chloride indicator with improved sensitivity. J Neurosci Methods 170:67-76.

McBain CJ, Fisahn A (2001) Interneurons unbound. Nat Rev Neurosci 2:11-23.

McCarren M, Alger BE (1985) Use-dependent depression of IPSPs in rat hippocampal pyramidal cells in vitro. J Neurophysiol 53:557-571.

McCormick DA (1989) GABA as an inhibitory neurotransmitter in human cerebral cortex. J Neurophysiol 62:1018-1027.

McKernan RM, Whiting PJ (1996) Which GABAA-receptor subtypes really occur in the brain? Trends Neurosci 19:139-143.

Menendez de la Prida L, Bolea S, Sanchez-Andres JV (1998) Origin of the synchronized network activity in the rabbit developing hippocampus. Eur J Neurosci 10:899-906.

Mikawa S, Wang C, Shu F, Wang T, Fukuda A, Sato K (2002) Developmental changes in KCC1, KCC2 and NKCC1 mRNAs in the rat cerebellum. Brain research 136:93-100.

Miles R, Wong RK (1983) Single neurones can initiate synchronized population discharge in the hippocampus. Nature 306:371-373.

Miller C, White MM (1980) A voltage-dependent chloride conductance channel from Torpedo electroplax membrane. Annals of the New York Academy of Sciences 341:534-551.

Mintz IM, Bean BP (1993) GABAB receptor inhibition of P-type Ca2+ channels in central neurons. Neuron 10:889-898.

Misgeld U, Bijak M, Jarolimek W (1995) A physiological role for GABAB receptors and the effects of baclofen in the mammalian central nervous system. Prog Neurobiol 46:423-462.

Misgeld U, Deisz RA, Dodt HU, Lux HD (1986) The role of chloride transport in postsynaptic inhibition of hippocampal neurons. Science (New York, NY 232:1413-1415.

Miwa JM, Stevens TR, King SL, Caldarone BJ, Ibañez-Tallon I, Xiao C, Fitzsimonds RM, Pavlides C, Lester HA, Picciotto MR, Heintz N (2006) The prototoxin lynx1 acts on nicotinic acetylcholine receptors to balance neuronal activity and survival in vivo. Neuron 51:587-600.

Mladinic M, Becchetti A, Didelon F, Bradbury A, Cherubini E (1999) Low expression of the ClC-2 chloride channel during postnatal development: a mechanism for the paradoxical

depolarizing action of GABA and glycine in the hippocampus. Proc Biol Sci 266:1207-1213.

Mohajerani MH, Sivakumaran S, Zacchi P, Aguilera P, Cherubini E (2007) Correlated network activity enhances synaptic efficacy via BDNF and the ERK pathway at immature CA3 CA1 connections in the hippocampus. Proc Natl Acad Sci U S A 104:13176-13181.

Munoz A, Mendez P, DeFelipe J, Alvarez-Leefmans FJ (2007) Cation-chloride cotransporters and GABA-ergic innervation in the human epileptic hippocampus. Epilepsia 48:663-673.

Nehrke K, Arreola J, Nguyen HV, Pilato J, Richardson L, Okunade G, Baggs R, Shull GE, Melvin JE (2002) Loss of hyperpolarization-activated Cl(-) current in salivary acinar cells from Clcn2 knockout mice. The Journal of biological chemistry 277:23604-23611.

Niemeyer MI, Cid LP, Zuniga L, Catalan M, Sepulveda FV (2003) A conserved pore-lining glutamate as a voltage- and chloride-dependent gate in the ClC-2 chloride channel. The Journal of physiology 553:873-879.

Niemeyer MI, Yusef YR, Cornejo I, Flores CA, Sepulveda FV, Cid LP (2004) Functional evaluation of human ClC-2 chloride channel mutations associated with idiopathic generalized epilepsies. Physiological genomics 19:74-83.

O'Keefe J, Dostrovsky J (1971) The hippocampus as a spatial map. Preliminary evidence from unit activity in the freely-moving rat. Brain research 34:171-175.

Obata K, Oide M, Tanaka H (1978) Excitatory and inhibitory actions of GABA and glycine on embryonic chick spinal neurons in culture. Brain research 144:179-184.

Owens DF, Kriegstein AR (2002) Is there more to GABA than synaptic inhibition? Nat Rev Neurosci 3:715-727.

Owens DF, Boyce LH, Davis MB, Kriegstein AR (1996) Excitatory GABA responses in embryonic and neonatal cortical slices demonstrated by gramicidin perforated-patch recordings and calcium imaging. J Neurosci 16:6414-6423.

Pace AJ, Lee E, Athirakul K, Coffman TM, O'Brien DA, Koller BH (2000) Failure of spermatogenesis in mouse lines deficient in the Na(+)-K(+)-2Cl(-) cotransporter. J Clin Invest 105:441-450.

Painter RG, Wang G (2006) Direct measurement of free chloride concentrations in the phagolysosomes of human neutrophils. Anal Chem 78:3133-3137.

Palmada M, Dieter M, Boehmer C, Waldegger S, Lang F (2004) Serum and glucocorticoid inducible kinases functionally regulate ClC-2 channels. Biochem Biophys Res Commun 321:1001-1006.

Payne JA, Stevenson TJ, Donaldson LF (1996) Molecular characterization of a putative K-Cl cotransporter in rat brain. A neuronal-specific isoform. The Journal of biological chemistry 271:16245-16252.

Payne JA, Rivera C, Voipio J, Kaila K (2003) Cation-chloride co-transporters in neuronal communication, development and trauma. Trends Neurosci 26:199-206.

Pfaff T, Malitschek B, Kaupmann K, Prezeau L, Pin JP, Bettler B, Karschin A (1999) Alternative splicing generates a novel isoform of the rat metabotropic GABA(B)R1 receptor. Eur J Neurosci 11:2874-2882.

Pfeffer CK, Stein V, Keating DJ, Maier H, Rinke I, Rudhard Y, Hentschke M, Rune GM, Jentsch TJ, Hubner CA (2009) NKCC1-dependent GABAergic excitation drives synaptic network maturation during early hippocampal development. J Neurosci 29:3419-3430.

Picollo A, Pusch M (2005) Chloride/proton antiporter activity of mammalian CLC proteins ClC-4 and ClC-5. Nature 436:420-423.

Poet M, Kornak U, Schweizer M, Zdebik AA, Scheel O, Hoelter S, Wurst W, Schmitt A, Fuhrmann JC, Planells-Cases R, Mole SE, Hubner CA, Jentsch TJ (2006) Lysosomal storage disease upon disruption of the neuronal chloride transport protein ClC-6. Proceedings of the National Academy of Sciences of the United States of America 103:13854-13859.

Poncer JC, McKinney RA, Gahwiler BH, Thompson SM (1997) Either N- or P-type calcium channels mediate GABA release at distinct hippocampal inhibitory synapses. Neuron 18:463-472.

Ponting CP (1997) CBS domains in ClC chloride channels implicated in myotonia and nephrolithiasis (kidney stones). J Mol Med 75:160-163.

Prange-Kiel J, Rune GM, Leranth C (2004) Median raphe mediates estrogenic effects to the hippocampus in female rats. Eur J Neurosci 19:309-317.

Pusch M, Zifarelli G (2009) It's the proton also in ClC-2. The Journal of physiology 587:1379-1380.

Pusch M, Jordt SE, Stein V, Jentsch TJ (1999) Chloride dependence of hyperpolarization-activated chloride channel gates. The Journal of physiology 515 (Pt 2):341-353.

Quinton PM (1983) Chloride impermeability in cystic fibrosis. Nature 301:421-422.

Raley-Susman KM, Sapolsky RM, Kopito RR (1993) Cl-/HCO3- exchange function differs in adult and fetal rat hippocampal neurons. Brain research 614:308-314.

Riekki R, Pavlov I, Tornberg J, Lauri SE, Airaksinen MS, Taira T (2008) Altered synaptic dynamics and hippocampal excitability but normal long-term plasticity in mice lacking hyperpolarizing GABA A receptor-mediated inhibition in CA1 pyramidal neurons. J Neurophysiol 99:3075-3089.

Rinke I, Artmann J, Stein V (2010) ClC-2 voltage-gated channels constitute part of the background conductance and assist chloride extrusion. J Neurosci 30:4776-4786.

Rivera C, Voipio J, Payne JA, Ruusuvuori E, Lahtinen H, Lamsa K, Pirvola U, Saarma M, Kaila K (1999) The K+/Cl- co-transporter KCC2 renders GABA hyperpolarizing during neuronal maturation. Nature 397:251-255.

Robinson RB, Siegelbaum SA (2003) Hyperpolarization-activated cation currents: from molecules to physiological function. Annu Rev Physiol 65:453-480.

Rohrbough J, Spitzer NC (1996) Regulation of intracellular Cl- levels by Na(+)-dependent Cl- cotransport distinguishes depolarizing from hyperpolarizing GABAA receptor-mediated responses in spinal neurons. J Neurosci 16:82-91.

Ross SE, Greenberg ME, Stiles CD (2003) Basic helix-loop-helix factors in cortical development. Neuron 39:13-25.

Russell JM (2000) Sodium-potassium-chloride cotransport. Physiological reviews 80:211-276.

Russell L, Forsdyke DR (1991) A human putative lymphocyte G0/G1 switch gene containing a CpG-rich island encodes a small basic protein with the potential to be phosphorylated. DNA Cell Biol 10:581-591.

Rychkov GY, Pusch M, Roberts ML, Jentsch TJ, Bretag AH (1998) Permeation and block of the skeletal muscle chloride channel, ClC-1, by foreign anions. The Journal of general physiology 111:653-665.

Saint-Martin C, Gauvain G, Teodorescu G, Gourfinkel-An I, Fedirko E, Weber YG, Maljevic S, Ernst JP, Garcia-Olivares J, Fahlke C, Nabbout R, LeGuern E, Lerche H, Christophe Poncer J, Depienne C (2009) Two novel CLCN2 mutations accelerating chloride channel deactivation are associated with idiopathic generalized epilepsy. Hum Mutat 30:397-405.

Scheel O, Zdebik AA, Lourdel S, Jentsch TJ (2005) Voltage-dependent electrogenic chloride/proton exchange by endosomal CLC proteins. Nature 436:424-427.

Scholl U, Hebeisen S, Janssen AG, Muller-Newen G, Alekov A, Fahlke C (2006) Barttin modulates trafficking and function of ClC-K channels. Proceedings of the National Academy of Sciences of the United States of America 103:11411-11416.

Scholz KP, Miller RJ (1991) GABAB receptor-mediated inhibition of Ca2+ currents and synaptic transmission in cultured rat hippocampal neurones. The Journal of physiology 444:669-686.

Schroeder BC, Cheng T, Jan YN, Jan LY (2008) Expression cloning of TMEM16A as a calcium-activated chloride channel subunit. Cell 134:1019-1029.

Schwappach B, Stobrawa S, Hechenberger M, Steinmeyer K, Jentsch TJ (1998) Golgi localization and functionally important domains in the NH2 and COOH terminus of the yeast CLC putative chloride channel Gef1p. The Journal of biological chemistry 273:15110-15118.

Schwartz TH, Rabinowitz D, Unni V, Kumar VS, Smetters DK, Tsiola A, Yuste R (1998) Networks of coactive neurons in developing layer 1. Neuron 20:541-552.

Schwarz DA, Barry G, Eliasof SD, Petroski RE, Conlon PJ, Maki RA (2000) Characterization of gamma-aminobutyric acid receptor GABAB(1e), a GABAB(1) splice variant encoding a truncated receptor. The Journal of biological chemistry 275:32174-32181.

Scoville WB, Milner B (1957) Loss of recent memory after bilateral hippocampal lesions. J Neurol Neurosurg Psychiatry 20:11-21.

Seely J, Crotty P (2010) Optimization of the leak conductance in the squid giant axon. Phys Rev E Stat Nonlin Soft Matter Phys 82:021906.

Seibert FS, Chang XB, Aleksandrov AA, Clarke DM, Hanrahan JW, Riordan JR (1999) Influence of phosphorylation by protein kinase A on CFTR at the cell surface and endoplasmic reticulum. Biochimica et biophysica acta 1461:275-283.

Sholl DA (1953) Dendritic organization in the neurons of the visual and motor cortices of the cat. Journal of anatomy 87:387-406.

Sik A, Smith RL, Freund TF (2000) Distribution of chloride channel-2-immunoreactive neuronal and astrocytic processes in the hippocampus. Neuroscience 101:51-65.

Simon DB et al. (1997) Mutations in the chloride channel gene, CLCNKB, cause Bartter's syndrome type III. Nature genetics 17:171-178.

Simonds WF (1999) G protein regulation of adenylate cyclase. Trends Pharmacol Sci 20:66-73.

Sipila ST, Schuchmann S, Voipio J, Yamada J, Kaila K (2006) The cation-chloride cotransporter NKCC1 promotes sharp waves in the neonatal rat hippocampus. The Journal of physiology 573:765-773.

Sipilä ST, Huttu K, Soltesz I, Voipio J, Kaila K (2005) Depolarizing GABA acts on intrinsically bursting pyramidal neurons to drive giant depolarizing potentials in the immature hippocampus. J Neurosci 25:5280-5289.

Sipilä ST, Schuchmann S, Voipio J, Yamada J, Kaila K (2006) The cation-chloride cotransporter NKCC1 promotes sharp waves in the neonatal rat hippocampus. J Physiol 573:765-773.

Smith RL, Clayton GH, Wilcox CL, Escudero KW, Staley KJ (1995) Differential expression of an inwardly rectifying chloride conductance in rat brain neurons: a potential mechanism for cell-specific modulation of postsynaptic inhibition. J Neurosci 15:4057-4067.

Spruston N, Johnston D (1992) Perforated patch-clamp analysis of the passive membrane properties of three classes of hippocampal neurons. J Neurophysiol 67:508-529.

Staff NP, Spruston N (2003) Intracellular correlate of EPSP-spike potentiation in CA1 pyramidal neurons is controlled by GABAergic modulation. Hippocampus 13:801-805.

Staley K (1994) The role of an inwardly rectifying chloride conductance in postsynaptic inhibition. J Neurophysiol 72:273-284.

Staley K, Smith R, Schaack J, Wilcox C, Jentsch TJ (1996) Alteration of GABAA receptor function following gene transfer of the CLC-2 chloride channel. Neuron 17:543-551.

Staley KJ, Mody I (1992) Shunting of excitatory input to dentate gyrus granule cells by a depolarizing GABAA receptor-mediated postsynaptic conductance. J Neurophysiol 68:197-212.

Staley KJ, Soldo BL, Proctor WR (1995) Ionic mechanisms of neuronal excitation by inhibitory GABAA receptors. Science (New York, NY 269:977-981.

Stein V, Nicoll RA (2003) GABA generates excitement. Neuron 37:375-378.

Stein V, Hermans-Borgmeyer I, Jentsch TJ, Hubner CA (2004a) Expression of the KCl cotransporter KCC2 parallels neuronal maturation and the emergence of low intracellular chloride. The Journal of comparative neurology 468:57-64.

Stein V, Hermans-Borgmeyer I, Jentsch TJ, Hübner CA (2004b) Expression of the KCl cotransporter KCC2 parallels neuronal maturation and the emergence of low intracellular chloride. J Comp Neurol 468:57-64.

Steinmeyer K, Ortland C, Jentsch TJ (1991a) Primary structure and functional expression of a developmentally regulated skeletal muscle chloride channel. Nature 354:301-304.

Steinmeyer K, Klocke R, Ortland C, Gronemeier M, Jockusch H, Grunder S, Jentsch TJ (1991b) Inactivation of muscle chloride channel by transposon insertion in myotonic mice. Nature 354:304-308.

Sterio DC (1984) The unbiased estimation of number and sizes of arbitrary particles using the disector. J Microsc 134:127-136.

Stobrawa SM, Breiderhoff T, Takamori S, Engel D, Schweizer M, Zdebik AA, Bosl MR, Ruether K, Jahn H, Draguhn A, Jahn R, Jentsch TJ (2001) Disruption of ClC-3, a chloride channel expressed on synaptic vesicles, leads to a loss of the hippocampus. Neuron 29:185-196.

Stogmann E, Lichtner P, Baumgartner C, Schmied M, Hotzy C, Asmus F, Leutmezer F, Bonelli S, Assem-Hilger E, Vass K, Hatala K, Strom TM, Meitinger T, Zimprich F, Zimprich A (2006) Mutations in the CLCN2 gene are a rare cause of idiopathic generalized epilepsy syndromes. Neurogenetics 7:265-268.

Storm JF (1987) Action potential repolarization and a fast after-hyperpolarization in rat hippocampal pyramidal cells. The Journal of physiology 385:733-759.

Sun H, Tsunenari T, Yau KW, Nathans J (2002) The vitelliform macular dystrophy protein defines a new family of chloride channels. Proceedings of the National Academy of Sciences of the United States of America 99:4008-4013.

Swann JW, Brady RJ, Martin DL (1989) Postnatal development of GABA-mediated synaptic inhibition in rat hippocampus. Neuroscience 28:551-561.

Thiemann A, Grunder S, Pusch M, Jentsch TJ (1992) A chloride channel widely expressed in epithelial and non-epithelial cells. Nature 356:57-60.

Thompson SM, Gahwiler BH (1989a) Activity-dependent disinhibition. I. Repetitive stimulation reduces IPSP driving force and conductance in the hippocampus in vitro. J Neurophysiol 61:501-511.

Thompson SM, Gahwiler BH (1989b) Activity-dependent disinhibition. II. Effects of extracellular potassium, furosemide, and membrane potential on ECl- in hippocampal CA3 neurons. J Neurophysiol 61:512-523.

Titz S, Hans M, Kelsch W, Lewen A, Swandulla D, Misgeld U (2003) Hyperpolarizing inhibition develops without trophic support by GABA in cultured rat midbrain neurons. J Physiol 550:719-730.

Tyzio R, Represa A, Jorquera I, Ben-Ari Y, Gozlan H, Aniksztejn L (1999) The establishment of GABAergic and glutamatergic synapses on CA1 pyramidal neurons is sequential and correlates with the development of the apical dendrite. J Neurosci 19:10372-10382.

Tyzio R, Ivanov A, Bernard C, Holmes GL, Ben-Ari Y, Khazipov R (2003) Membrane potential of CA3 hippocampal pyramidal cells during postnatal development. J Neurophysiol 90:2964-2972.

Tyzio R, Cossart R, Khalilov I, Minlebaev M, Hubner CA, Represa A, Ben-Ari Y, Khazipov R (2006) Maternal oxytocin triggers a transient inhibitory switch in GABA signaling in the fetal brain during delivery. Science (New York, NY 314:1788-1792.

Tyzio R, Minlebaev M, Rheims S, Ivanov A, Jorquera I, Holmes GL, Zilberter Y, Ben-Ari Y, Khazipov R (2008) Postnatal changes in somatic gamma-aminobutyric acid signalling in the rat hippocampus. The European journal of neuroscience 27:2515-2528.

Ulrich D, Huguenard JR (1997) Nucleus-specific chloride homeostasis in rat thalamus. J Neurosci 17:2348-2354.

Verheugen JA, Fricker D, Miles R (1999) Noninvasive measurements of the membrane potential and GABAergic action in hippocampal interneurons. J Neurosci 19:2546-2555.

Wang C, Shimizu-Okabe C, Watanabe K, Okabe A, Matsuzaki H, Ogawa T, Mori N, Fukuda A, Sato K (2002) Developmental changes in KCC1, KCC2, and NKCC1 mRNA expressions in the rat brain. Brain research 139:59-66.

Wang DD, Kriegstein AR (2008) GABA regulates excitatory synapse formation in the neocortex via NMDA receptor activation. J Neurosci 28:5547-5558.

Weinreich F, Jentsch TJ (2001) Pores formed by single subunits in mixed dimers of different CLC chloride channels. The Journal of biological chemistry 276:2347-2353.

Wojcik SM, Katsurabayashi S, Guillemin I, Friauf E, Rosenmund C, Brose N, Rhee JS (2006) A shared vesicular carrier allows synaptic corelease of GABA and glycine. Neuron 50:575-587.

Wrong OM, Norden AG, Feest TG (1994) Dent's disease; a familial proximal renal tubular syndrome with low-molecular-weight proteinuria, hypercalciuria, nephrocalcinosis, metabolic bone disease, progressive renal failure and a marked male predominance. QJM 87:473-493.

Xu JC, Lytle C, Zhu TT, Payne JA, Benz E, Jr., Forbush B, 3rd (1994) Molecular cloning and functional expression of the bumetanide-sensitive Na-K-Cl cotransporter. Proceedings of the National Academy of Sciences of the United States of America 91:2201-2205.

Yamada J, Okabe A, Toyoda H, Kilb W, Luhmann HJ, Fukuda A (2004) Cl- uptake promoting depolarizing GABA actions in immature rat neocortical neurones is mediated by NKCC1. The Journal of physiology 557:829-841.

Yamazaki J, Britton F, Collier ML, Horowitz B, Hume JR (1999) Regulation of recombinant cardiac cystic fibrosis transmembrane conductance regulator chloride channels by protein kinase C. Biophysical journal 76:1972-1987.

Yang YD, Cho H, Koo JY, Tak MH, Cho Y, Shim WS, Park SP, Lee J, Lee B, Kim BM, Raouf R, Shin YK, Oh U (2008) TMEM16A confers receptor-activated calcium-dependent chloride conductance. Nature 455:1210-1215.

Yun K, Mantani A, Garel S, Rubenstein J, Israel MA (2004) Id4 regulates neural progenitor proliferation and differentiation in vivo. Development 131:5441-5448.

Yusef YR, Zuniga L, Catalan M, Niemeyer MI, Cid LP, Sepulveda FV (2006) Removal of gating in voltage-dependent ClC-2 chloride channel by point mutations affecting the pore and C-terminus CBS-2 domain. The Journal of physiology 572:173-181.

Yuste R, Katz LC (1991) Control of postsynaptic Ca2+ influx in developing neocortex by excitatory and inhibitory neurotransmitters. Neuron 6:333-344.

Zhang L, Spigelman I, Carlen PL (1991) Development of GABA-mediated, chloride-dependent inhibition in CA1 pyramidal neurones of immature rat hippocampal slices. The Journal of physiology 444:25-49.

Zheng YJ, Furukawa T, Ogura T, Tajimi K, Inagaki N (2002) M phase-specific expression and phosphorylation-dependent ubiquitination of the ClC-2 channel. J Biol Chem 277:32268-32273.

Zhu JJ, Esteban JA, Hayashi Y, Malinow R (2000) Postnatal synaptic potentiation: delivery of GluR4-containing AMPA receptors by spontaneous activity. Nat Neurosci 3:1098-1106.

Zhu L, Lovinger D, Delpire E (2005) Cortical neurons lacking KCC2 expression show impaired regulation of intracellular chloride. J Neurophysiol 93:1557-1568.

Zifarelli G, Pusch M (2009) Conversion of the 2 Cl(-)/1 H+ antiporter ClC-5 in a NO3(-)/H+ antiporter by a single point mutation. The EMBO journal 28:175-182.

Zifarelli G, Pusch M (2010) The role of protons in fast and slow gating of the Torpedo chloride channel ClC-0. Eur Biophys J 39:869-875.

Zuniga L, Niemeyer MI, Varela D, Catalan M, Cid LP, Sepulveda FV (2004) The voltage-dependent ClC-2 chloride channel has a dual gating mechanism. The Journal of physiology 555:671-682.

ACKNOWLEDGEMENTS

CURRICULUM VITAE

Ilka Rinke

Dipl. Biol.

Personal information

Date of birth: 17. February 1983
Place of birth: Schkeuditz, Germany
Citizenship: German

Contact details

Max-Planck-Institute of Neurobiology
Synaptic Receptor Trafficking Group
Am Klopferspitz 18
82152 Munich-Martinsried
Germany
fon: +49 89 8578 3622
fax: +49 89 8578 3690
email: rinke@neuro.mpg.de

Education

July 2007 – present   **PhD Thesis**: *"Chloride regulatory mechanisms and their influence on neuronal excitability"*
Max-Planck-Institute of Neurobiology, Munich-Martinsried

2006 – 2007   **Diploma Thesis**: *"Characterization of Purinergic P2-receptors in Spherical Bushy Cells of the Anterior Ventral Cochlea Nucleus in Mongolian Gerbil"*
Research Group of Neurobiology, University of Leipzig, Germany

2001 – 2006   **graduated Biologist** equal to Master of Science in Biology
University of Leipzig, Germany

2001   **Abitur**
Ehrenberg-Gymnasium, Delitzsch, Germany

Funding

2008 – present   Funding for *„Untersuchung des spannungsabhängigen Chloridekanals ClC-2 in Neuronen – Ursache für Epilepsy?"* by the Deutsche Forschungsgesellschaft (DFG STE1062/2-1 to VS)

2007 – 2008   Stipend of the Max-Planck Society

Publications:

1. Wierenga CJ, Müllner FE, <u>Rinke I</u>, Keck T, Stein V and Bonhoeffer T (accepted 2010) Molecular and electrophysiological characterization of GFP-expressing CA1 interneurons in GAD65-GFP mice. PLoS ONE

2. <u>Rinke I</u>, Artmann J, Stein V (2010) ClC-2 voltage-gated channels constitute part of the background conductance and assist chloride extrusion. J Neurosci 30:4776-4786.

3. Pfeffer CK, Stein V, Keating DJ, Maier H, <u>Rinke I</u>, Rudhard Y, Hentschke M, Rune GM, Jentsch TJ, Hubner CA (2009) NKCC1-dependent GABAergic excitation drives synaptic network maturation during early hippocampal development. J Neurosci 29:3419-3430.

4. Milenkovic I, <u>Rinke I</u>, Witte M, Dietz B, Rubsamen R (2009) P2 receptor-mediated signaling in spherical bushy cells of the mammalian cochlear nucleus. J Neurophysiol 102:1821-1833.